VOL. 24 • NO. 9 • JUNE 1984

IGM83-000-383
CNRC 26449

# Polymer

## ENGINEERING AND SCIENCE

### Modeling—83
### National Research Council of Canada
### Industrial Materials Research Institute

CONTENTS

623 Guest Editor's Note/L. A. Utracki

624 G. L. BATA/The Archimedean Screw as an Extruder; Historical Note

626 C. I. CHUNG/On the Scale-up of Plasticating Extruder Screws

633 V. L. LeNIR/Computerization of Wire Insulating Lines—An Industrial Approach

645 S. V. KAO and G. R. ALLISON/Residence Time Distribution in a Twin Screw Extruder

652 Y. KUO/Mathematical Modeling of Squashing Flows of Heated Polymer Particles

662 Y. KUO/Roll Fusing of Toner Particles on Rough Papers in the Xerographic Process

673 M. GRMELA/Common Structure, Compatibility and Complementarity of Mathematical Models of Injection Molding

686 M. R. KAMAL, W. I. PATTERSON, D. A. FARA, and A. HABER/A Study in Injection Molding Dynamics

692 M. R. KAMAL and P. G. LAFLEUR/Heat Transfer in Injection Molding of Crystallizable Polymers

698 M. E. RYAN/Rheological and Heat-Transfer Considerations for the Processing of Reactive Systems

707 E. MITSOULIS, J. VLACHOPOULOS, and F. A. MIRZA/Numerical Simulation of Entry and Exit Flows in Slit Dies

716 General Discussion on the Role of Computer Aided Engineering

PUBLISHED BY THE SOCIETY OF PLASTICS ENGINEERS, INC.

# Polymer ENGINEERING AND SCIENCE

*Published by the Society of Plastics Engineers*



**EDITOR—ROGER S. PORTER**

*% Polymer Science and Engineering*
*University of Massachusetts*
*Amherst, Mass. 01003*

**GUEST EDITOR—L. A. UTRACKI**

*% Industrial Materials Research Institute*
*National Research Council of Canada*
*75, Boul. De Mortagne*
*Boucherville, Quebec*
*Canada J4B 6Y4*

**ASSOCIATE EDITOR—RICHARD E. BALL**

*% Western New England College*
*Springfield, Mass. 01119*

## ADVISORY BOARD

E. BAER
*Case Institute of Technology*

J. A. BIESENBERGER
*Stevens Institute of Technology*

D. M. BIGG
*Battelle Columbus Laboratories*

L. L. BLYLER, JR.
*Bell Laboratories*

L. J. BROUTMAN
*Illinois Institute of Technology*

E. S. CLARK
*University of Tennessee*

A. N. GENT
*University of Akron*

H. B. HOPFENBERG
*North Carolina State University*

J. F. JOHNSON
*University of Connecticut*

M. R. KAMAL
*McGill University*

R. P. KAMBOUR
*General Electric Company*

J. R. KNOX
*Amoco Chemicals Corporation*

S. MATSUOKA
*Bell Telephone Laboratories*

B. MAXWELL
*Princeton University*

C. L. MCCORMICK
*University of Southern Mississippi*

D. R. PAUL
*University of Texas*

J. R. A. PEARSON
*Imperial College of Science & Technology*

D. H. RENEKER
*National Bureau of Standards*

C. E. ROGERS
*Case Western Reserve University*

R. SALOVEY
*University of Southern California*

N. S. SCHNEIDER
*Army Materials and Mechanics Research Center*

T. L. SMITH
*IBM Research Center*

Z. TADMOR
*Israel Institute of Technology*

M. TAKAYANAGI
*Kyushu University*

## PUBLICATIONS COMMITTEE

D. W. RILEY, Chairman
*Extrusion Engineers*

R. P. BRADDICKS, JR.
*Plastics Consultant*

R. D. FORGER
*Society of Plastics Engineers*

J. C. HAARSMA
*S/C Electric Co.*

J. L. HULL
*Hull Corporation*

D. JESIOLOWSKI
*Owens Illinois*

M. A. MENDELSOHN
*Westinghouse Electric Corp.*

R. S. PORTER
*University of Massachusetts*

A. A. SCHOENGOOD
*Society of Plastics Engineers*

R. F. STAATS-WESTOVER
*Bell Telephone Labs*

G. R. THOM
*Regal Plastics Company*

A. M. VARNER
*Moldflow USA, Inc.*

A. E. WHITNEY, JR.
*Goodyear Chemical*



Copyright by the Society of Plastics Engineers, Inc., 1984. Reproduction in whole or in part without written permission is strictly prohibited.



**Polymer Engineering and Science** (ISSN 0032-3888) is printed at Waverly Press, Easton, MD 21601. Address changes, undeliverable copies and orders for subscriptions should be sent to Circulation Manager, Society of Plastics Engineers, 14 Fairfield Dr., Brookfield Center, Conn. 06805. Published monthly except for February, April, June, August, October, and December when published semi-monthly. Second-class postage paid at Brookfield Center, Conn., and additional entry offices. Accepted at special postal rate provided in P.M. Sec. 132.122.



Neither the Society of Plastics Engineers, Inc., nor **Polymer Engineering and Science** is responsible for the views expressed by individual contributors either in articles published in **Polymer Engineering and Science** or in technical papers presented at meetings of the Society.



Subscription rates for 1984. SPE members, 1 year—$70, 2 years—$125, 3 years—$175. Nonmembers (U.S. and North America), 1 year—$95, 2 years—$170, 3 years—$225. Corporate, Institutional or library, 1 year—$250. Postage charge for all subscriptions outside North America—$18 per year. Air delivery outside North America—$50 per year.

**SOCIETY OF PLASTICS ENGINEERS, INC.**

*Business and Executive Offices, 14 Fairfield Dr., Brookfield Center, Conn. 06805*

ROBERT D. FORGER
*Publisher*

MICHAEL R. CAPPELLETTI
*Circulation Manager*

JANICE E. ALEXANDER
*Production Manager*

JOSEPH M. CASTAGNO
*Copy Editor*



## OFFICERS OF THE SOCIETY

WILLIAM C. KUHLKE
*President*

RICHARD G. JOHNSON
*President-elect*

GREG R. THOM
*First Vice President*

JOHN R. KRETZCHMAR
*Second Vice President*

JACQUES DE CRAENE
*Vice President for International Affairs*

BRUCE A. PETERSEN
*Secretary*

VIVIAN E. MALPASS
*Treasurer*

ROBERT D. FORGER
*Executive Director*



**POLYMER ENGINEERING & SCIENCE is indexed by:—Chemical Abstracts—Engineering Index, Inc.**

## GUEST EDITOR'S NOTE

The present mini-symposium, "Modeling-'83", was held on February 9th, 1983, in Montreal. It was the seventh mini-symposium in the field of polymer engineering and science, organized and sponsored by the Industrial Materials Research Institute of the National Research Council of Canada (IMRI-NRCC). Thematically, this was the second conference on "Mathematical Modeling of Plastics Processing and Properties" (viz. *Polym. Eng. Sci.*, 22, No. 17, (1982)).

Mathematical Modeling is closely associated with the broad field of activities labeled either CAD/CAM (computer aided design and manufacture) or CAE (computer aided engineering). CAE is one of the main area of activity at IMRI. It constitutes a vital part of program to aid the Canadian plastics industry.

During the last decade, computer simulation of important plastics manufacturing operations, like extrusion and injection molding, has become an important field of activity among polymer engineers and scientists. Such interest is not surprising, since process simulation finds many applications in process optimization and control, in addition to the optimization of resin selection and die and mold design, in order to improve production economics and product quality. It is expected that computer simulation will continue to gain prominence during the present decade as a result of the expanded use of microprocessors and computers in conjunction with the control and supervision of plastics operations. Other incentives include material and energy-saving applications in computer-aided die and mold design, the availability of powerful finite-element schemes and visco-elastic constitutive equations that permit the treatment of the processing behavior of complex materials in complicated dies and molds, and the development of procedures to relate the thermomechanical history of the resin during processing to microstructure and ultimate properties of the final product.

Since the early days of its foundation, IMRI has established three priority areas in the field of polymeric materials: blends, composites, and CAD/CAM. The activities of the Institute in mathematical modeling and computer simulation represent a link in the chain of activities, including: the development of a data bank for polymer and plastics properties; modeling and simulation; studies of the microstructure and performance of manufactured articles; computer packages for the basic design parameters for molds, dies, screws, etc.; and computer packages for controlled manufacturing capabilities. The task is vast, beyond the capabilities and competence of a single institution or group of people. It is expected that a number of interested organizations, including IMRI, will coordinate efforts to maximize benefits to the plastics industry. Communication and the exchange of ideas in symposia such as the present one play a significant role in this coordination effort.

The issue opens with a brief historical note (Bata) on the extrusion process. The next three papers (Chung, LeNir and Kao) relate to extrusion analysis, scale-up and control. Dr. Kuo's articles provide an engineering basis for the treatment of squashing flows and roll fusing of toner particles, which are an important aspect of copying processes. The following three contributions (Grmela and Kamal and coworkers) update our knowledge regarding various aspects of injection molding modeling and process dynamics. The paper on injection-molding dynamics, which won the Best Paper Award of the Injection Molding Division at ANTEC 1983 in Chicago, was not presented at the IMRI Symposium, but it was felt that publication in this special issue would be most appropriate. The final papers (Ryan and Mitsoulis and coworkers) summarize recent developments in the analysis of reactive processing and the application of finite element analysis to isothermal and non-isothermal melt flow problems.

Comparison of this "Modeling-'83" issue with the previous one "Modeling-'82" reflects some advances in various areas of plastics processing and, particularly, the expansion in the scope and significance of the IMRI Mini-symposium series on Mathematical Modeling of Plastics Processing and Properties. The papers selected for this issue deal with a cross-section of important commercial plastics manufacturing operations: extrusion, injection molding, wire coating, calendering, thermoset processing, CAD/CAM, mathematical techniques, and process dynamics. Moreover, a quick glance at the contents of the various papers shows that they involve a broad range of polymer engineering and science subjects; e.g., rheology, thermodynamics, fluid mechanics, heat transfer, crystallization kinetics, etc. It is hoped that the readers of the JOURNAL will find the material interesting and useful.

L.A. Utracki, Guest Editor
M.R. Kamal
and
R.E. Ryan, Symposium co-chairmen

# The Archimedean Screw as an Extruder; Historical Note

GEORGE L. BATA

*Industrial Materials Research Institute National Research Council Canada 75 De Mortagne, Boucherville, Quebec, Canada J4B 6Y4*

The extruder screw—or as the ancients called it—the *Cochlea Archimedis* was reputedly invented by Archimedes in Syracuse, during the 2nd Punic War. It was built for King Hiero, the employer of Archimedes, to pump out the water from the hold of a giant ship recently constructed, and leaking. This was around 225 BC, some 22 centuries ago.

The Archimedean screw was later applied to irrigation projects in Egypt, using the current of the river to drive the screw (*Fig. 1*).

Marcus Vitruvius Pollio, who was the superintendent of the Roman aqueducts during the time of the Emperor Augustus, describes the use of this machine in one of his installations for lifting water. His writings were lost, but rediscovered in a manuscript collection of the Abbey of St. Gall in Switzerland in the 15*th* century. This was a copy written down in the middle of the 10*th* century. It was copied around the time when the Saracens, the Magyars, and the Vikings were raiding the cities and monasteries of Europe.

Shortly after, probably based on the description of Vitruvius, Galeaz de Rubeis, a Swiss ironsmith, constructed a new prototype of the machine to draw water from the Ticino River (1). This screw-pump, called the *Machina Augustana* was still functioning 70 years later, in 1582, when Jean-Jacques Wecker wrote a description of it (*Fig. 2*).

It was only 10 generations later, that the hydraulic principles controlling the operation of the Archimedean screw became understood. Navier (1822), Poiseuille (1842), Boussinesq (1868), and Reynolds (1886) initiated systematic analyses of problems involving fluid flow near a flat plate, viscosity and turbulent flow (2–5). In the meantime, however, applications multiplied. The helical screw was not used anymore for lifting water but for screw conveyors, the making of briquettes and sausages, and the processing of spaghetti, rubber, and plastics. Perry's *Chemical Engineering Handbook* in 1950 states that "the process of extrusion has been regarded inevitably as an art rather than as a science, because the complexity of the conditions involved has made it impossible to analyze by any accurate mathematical treatment" (6). It is interesting to look at the illustration and the production capacities listed there, only 33 years ago (*Fig. 3* and *Table 1*).

Three years later that "inevitability" and "impossibility" had vanished, and the art became engineering science. Carley, Mallouk, McKelvey, and Strub, working as a team at Du Pont, established the basic principles of plastics extrusion as an engineering unit operation which were published in a

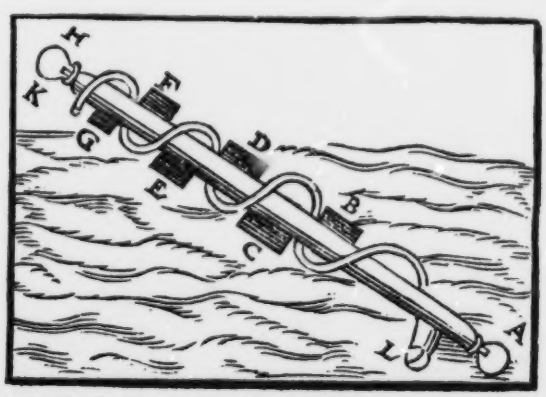


*Fig. 1. The Cochlea Archimedis on the Nile.*

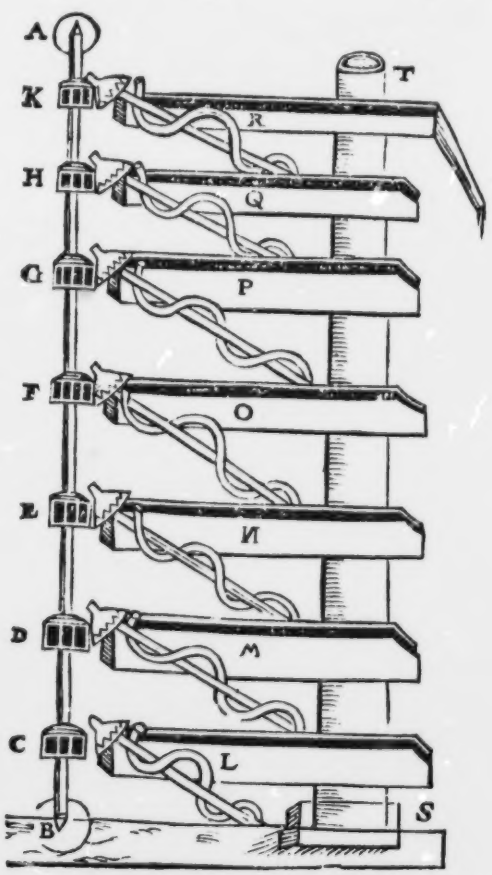


*Fig. 2. The Machina Augustana as used on the Ticino River in the 15th century.*

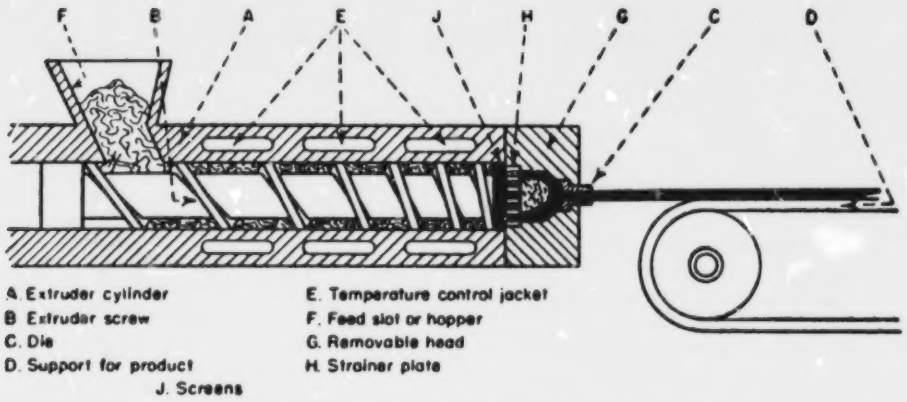


*Fig. 3. A screw extruder for plastics in the 1940s.*

**Table 1. Extruder output rates in the 1940s**

| Average productive capacities of screw extrusion machines for 0.25-inch rod of PVC. (Sp. Gr. 135)[6] | |
|---|---|
| **Diameter of screw, inches** | **Productive capacity, pounds per hour** |
| 2 | 30–50 |
| 2.5 | 40–75 |
| 3.25 | 75–125 |
| 3.5 | 95–150 |
| 4.5 | 150–200 |
| 6. | 250–300 |

symposium issue of *Industrial and Engineering Chemistry* (7–12). Within a few years the scientific approach became well established (13–15).

The emphasis and the challenge are different at this time. The quantitative parameters of extrusion and of many other plastics processing operations are now well understood. Our current concern is the quality, homogeneity, and the performance of the finished product and their dependence on the variables of the extrusion process. This challenge is no less than that faced by the Du Pont team, and it is the challenge facing the participants in this mini-symposium.

It took 60 generations to reinvent the Archimedean screw, 10 more generations to understand the underlying scientific parameters, and two more generations to lay down the engineering principles of this unit operation. We will have to do better than that: we have to accelerate our progression.

## REFERENCES

1. J. J. Wecker, DeSecretis, Basel (1582), p. 547.
2. C. L. M. Navier, *Mém. Acad. Sci. (Paris)*, **6**, (1822).
3. M. J. Boussinesq, *Math. Pures Appl. (2nd Ser.)*, **13**, 377 (1868).
4. J. L. M. Poiseuille, *Compt. Rend.*, **15**, 1167 (1842).
5. O. Reynolds, *Trans. Roy. Soc.*, **A177**, 157 (1886).
6. J. H. Perry, Ed., "Chemical Engineers Handbook," pp. 1180–1183, McGraw-Hill, New York (1950).
7. J. F. Carley and R. A. Strub, *Ind. Eng. Chem.*, **45**, 970 (1953).
8. J. F. Carley and R. S. Mallouk, J. M. McKelvey, *Ind. Eng. Chem.*, **45**, 974 (1953).
9. J. F. Carley and R. A. Strub, *Ind. Eng. Chem.*, **45**, 978 (1953).
10. J. F. Carley and R. A. Strub, *Ind. Eng. Chem.*, **45**, 982 (1953).
11. R. S. Mallouk and J. M. McKelvey, *Ind. Eng. Chem.*, **45**, 987 (1953).
12. J. F. Carley and J. M. McKelvey, *Ind. Eng. Chem.*, **45**, 989 (1953).
13. G. L. Bata, *Can. J. Chem. Eng.*, **35**, 159 (1957).
14. E. C. Beruhardt, "Processing of Thermoplastic Materials," Van Nostrand Reinhold Company, New York (1959).
15. J. M. McKelvey, "Polymer Processing," John Wiley and Sons, New York (1962).

# On the Scale-Up of Plasticating Extruder Screws

CHAN I. CHUNG

*Rensselaer Polytechnic Institute,*
*School of Engineering,*
*Troy, New York 12181*

In the most commonly used scale-up method of plasticating extruder screws, the screw channel depth is increased by the square root of the diameter ratio while the screw RPM is decreased by the square root of the diameter ratio such that the output rate increases proportionally to the square of the diameter ratio. This scale-up method, largely based on the pumping function of the screw, often leads to a higher melt temperature, a higher screw horsepower consumption per unit output rate and an inferior melt quality from the larger diameter screw. Analysis of the common scale-up method reveals that, although the shear rate in the melt is kept constant, the average residence time and the peripheral screw speed are increased for the larger diameter screw. Our recent study on the melting mechanism also reveals that the melting capacity increases less than the pumping capacity. A detailed examination of the common scale-up method in this paper shows that the pumping capacity and the solid conveying capacity increase more than necessary while the melting capacity increases insufficiently.

## INTRODUCTION

Plasticating extruders perform three functions: solid conveying, plasticating or melting, and pumping. All three functions must be considered and balanced properly in a scale-up of plasticating extruder screws. Therefore, a clear understanding of the three functions is a prerequisite of any scale-up theory. The pumping function has been clearly understood since the pioneering work of Carley, *et al.* (1) in 1953. The solid conveying function is also understood fairly well due to the contributions of Darnell and Mol (2) in 1956 and later Chung (3) in 1970. The melting function, however, was not clearly understood, at least analytically, until the contribution of Tadmor in 1966 (4).

Scale-up theory was first proposed by Carley and McKelvey (5) in 1953. Based solely on the pumping function, they showed that both the output rate and the power consumption would increase by the cubic power of the diameter ratio of the screws if the channel depth and width were increased in proportion to the diameter ratio and the screw RPM was kept constant. Their scale-up method is applicable to extruders used only as a melt pump, but it cannot be applied to plasticating extruders operating at high speeds, the output rates of which are limited by the melting capacity rather than the pumping capacity. Recognition of the melting capacity limitation and understanding of the melting mechanism, that melting occurs primarily on the barrel surface, have led to the scale-up method most commonly used today. In the common scale-up method, the output rate is increased by the square of the diameter ratio, exactly proportional to the ratio of the barrel surface areas, while maintaining a constant shear in the molten material by increasing the channel width proportional to the diameter ratio and the channel depth proportional to the square root of the diameter ratio but decreasing the screw RPM proportional to the square root of the diameter ratio. However, such scale-up often leads to a higher melt temperature, a higher specific screw HP (screw HP consumption per unit output rate), and an inferior melt quality from the larger diameter screw.

Our recent experimental and theoretical research on the melting mechanism (6–8) has provided a better understanding for the dependence of melting rate and power consumption during melting on barrel surface temperature, screw speed, channel width and pressure, as well as polymer properties. This paper examines the details of the common scale-up method considering all three functions of a screw and offers explanations for the problems encountered in the common scale-up.

## THEORETICAL ANALYSIS OF THE COMMON SCALE-UP

The basis for the common scale-up method is that the barrel surface area, where melting takes place by both heat conduction from the barrel and viscous heat generation of the screw power, increases by $(D/d)^2$ as barrel diameter is increased from $d$ to $D$ in a scale-up, and therefore the output rate, i.e., the pumping capacity should also be increased by $(D/d)^2$. Furthermore, the shear rate in the screw

channel should be kept constant in order to maintain the same degree of mixing and temperature build-up. Neglecting pressure flow and flight width, the pumping capacity ($G_p$) can be expressed as follows (1),

$$G_p = \frac{\pi}{2}\,\rho_m \cdot N \cdot D \cdot W \cdot H \cdot \cos^2\phi \qquad (1)$$

where
$\rho_m$ = melt density
$N$ = rotational screw speed
$W$ = channel width measured along the screw axis
$H$ = channel depth
$\phi$ = flight helix angle

The shear rate ($\dot\gamma$) in the screw channel can be approximated by

$$\dot\gamma = \frac{N\pi D}{H} \qquad (2)$$

If we let $H = \left(\frac{D}{d}\right)^{1/2} \cdot h$, $W = \left(\frac{D}{d}\right) \cdot w$ and $N = \left(\frac{d}{D}\right)^{1/2} \cdot \bar n$, then the requirements for the common scale-up mentioned above are satisfied as shown below

$$\left(G_p\right)_D = \left(\frac{D}{d}\right)^2 \cdot \left(\frac{\pi}{2}\,\rho_m \cdot \bar n \cdot d \cdot w \cdot h \cdot \cos^2\phi\right) = \left(\frac{D}{d}\right)^2 \cdot (G_p)_d \qquad (3)$$

$$(\dot\gamma)_D = \frac{N\pi D}{H} = \frac{\bar n \pi d}{h} = (\dot\gamma)_d \qquad (4)$$

Lower case characters are used to denote the variables of the smaller extruder of diameter $d$.

A detailed analysis of the common scale-up method reveals that the residence time and the peripheral screw speed increase in a scale-up although the shear rate in the screw channel remains constant as snown in *Table 1*. Increased residence time and increased peripheral screw speed obviously result in a higher specific screw HP and consequently a higher melt temperature. The common scale-up method is carefully examined here with respect to the predictions of the present extrusion theories.

## Pumping Capacity

Polymer melts are highly pseudoplastic and the pumping capacity of a screw cannot be correctly predicted by a simple equation developed for Newtonian fluids (1). Kroesser and Middleman (9) developed a method of calculating the pumping capacity by approximating polymer melts as power-law fluids. According to their work, the pumping capacity can be expressed by

$$G_p = F[(NDWH),\ \bar\alpha^n,\ n] \qquad (5)$$

where $\bar\alpha^n = \left(\frac{H}{V_Z}\right)^n \cdot \left(\frac{H}{K} \cdot \frac{\Delta P}{\Delta Z}\right)$, reduced pressure gradient. $n$ and $K$ are the constants in the power-law equation, $\eta = K \cdot \dot\gamma^{n-1}$

$\eta$ = viscosity of polymer melt
$V_Z = N\pi D \cdot \cos\phi$, the component of peripheral screw speed along the screw channel
$(\Delta P/\Delta Z)$ = pressure gradient along the screw channel (note that $\Delta P$ is related to the head pressure at the end of the screw)

The term, $(NDWH)$ is increased in proportion to $(D/d)^2$ in the common scale-up, and the pumping capacity is also increased by $(D/d)^2$ provided $\bar\alpha^n$ remains constant. $\bar\alpha^n$ causes pressure flow reducing the pumping capacity. However, $\bar\alpha^n$ is decreased if $\Delta P$ is kept constant as shown below and thus the pumping capacity will be increased more than $(D/d)^2$ times due to a less significant pressure flow.

$$\frac{(\bar\alpha^n)_D}{(\bar\alpha^n)_d} = \left[\frac{(D/d)^{1/2}}{(D/d)^{-1/2} \cdot (D/d)}\right]^n \cdot \left[\frac{(D/d)^{1/2}}{(D/d)}\right] = \left(\frac{d}{D}\right)^{1/2} \qquad (6)$$

The scale-up factors listed in *Table 1*, and $(\Delta P)_D = (\Delta P)_d$ and $|(\Delta Z)_D/(\Delta Z)_d| = (D/d)$ were used in the above relationship. *Equation 6* suggests that the length of the pumping section may be decreased by a factor of $(D/d)^{1/2}$ in the common scale-up as long as $\Delta P$ (i.e. the head pressure) is kept constant.

**Table 1. Scale-Up Factors in the Common Scale Up Method**

| | Small Extruder | Large Extruder |
|---|---|---|
| Diameter | $d$ | $D$ |
| Channel Width | $w$ | $W = \left(\frac{D}{d}\right) \cdot w$ |
| Channel Depth | $h$ | $H = \left(\frac{D}{d}\right)^{1/2} \cdot h$ |
| Screw RPM | rpm | RPM $= \left(\frac{d}{D}\right)^{1/2} \cdot$ rpm |
| Output Rate | $(G)_d$ | $(G)_D = \left(\frac{D}{d}\right)^2 \cdot (G)_d$ |
| Shear Rate | $(\dot\gamma)_d$ | $(\dot\gamma)_D = (\dot\gamma)_d$ |
| Peripheral Screw Speed | $v$ | $V = \left(\frac{D}{d}\right)^{1/2} \cdot v$ |
| Residence Time | $t$ | $T = \left(\frac{D}{d}\right)^{1/2} \cdot t$ |
| Melting Capacity | $(G_m)_d$ | $(G_m)_D = \left(\frac{D}{d}\right)^{1.75} \cdot (G_m)_d$ |
| Screw HP | $(HP)_d$ | $(HP)_D = \left(\frac{D}{d}\right)^{2.5} \cdot (HP)_d$ |

## Melting Capacity

The common scale-up method implicitly assumes that the melting rate per unit area of barrel surface, $\Omega$, remains constant in the scale-up and therefore the melting capacity increases in proportion to the increase in barrel surface area. However, such an assumption is not satisfied. $\Omega$ depends on channel width ($W$) and peripheral screw speed ($V$) as well as on barrel temperature (6, 7). $\Omega$ increases with

increasing $V$ but decreases with increasing $W$ according to the following approximate expression.

$$\Omega \propto \left(\frac{V}{W}\right)^{1/2} \tag{7}$$

Since $V$ increases by $(D/d)^{1/2}$ but $W$ increases by $(D/d)$ in the common scale-up, $\Omega$ is decreased approximately by the ratio $(D/d)^{1/4}$. The melting capacity ($G_m$) is obtained by multiplying $\Omega$ by the barrel surface area ($A_m$) available for melting, and it is increased only by $(D/d)^{1.75}$ times as seen below even though the barrel surface area increases by $(D/d)^2$ times.

$$\frac{(G_m)_D}{(G_m)_d} = \frac{(A_m)_D}{(A_m)_d}\cdot\frac{(\Omega)_D}{(\Omega)_d} = \left(\frac{D}{d}\right)^2\cdot\left(\frac{d}{D}\right)^{1/4} = \left(\frac{D}{d}\right)^{1.75} \tag{8}$$

It is seen that the melting capacity is increased less than the pumping capacity in the common scale-up. Inferior melt quality often observed from the larger diameter extruder is a consequence of the reduced melting capacity to pumping capacity ratio.

## Solid Conveying Capacity

The solid conveying function has been virtually ignored in scale-ups, and the common scale-up method is no exception in this regard. This paper examines the appropriateness of the solid conveying capacity in the common scale-up method.

Once feed polymer pellets or particles are compacted into a solid bed and the solid bed makes contact with the surrounding hot metal surfaces of the barrel and screw, the solid bed movement along the screw channel (i.e. the solid conveying mechanism) is controlled by the viscous shearing forces acting around the solid bed. This mechanism applies over most of the screw length. However, the solid bed movement, near the hopper where the metal surfaces are kept below the melting point of the polymer, will be controlled by the frictional forces acting around the solid bed. Predictions of both the viscous shearing theory (3) and the friction theory (2) will be examined here.

The solid conveying capacity is calculated from

$$G_S = \rho_b\cdot\pi^2\cdot N\cdot D\cdot H\cdot(D-H)\cdot\frac{\tan\theta\cdot\tan\phi}{\tan\theta+\tan\phi} \tag{9}$$

where

$\rho_b$ = bulk density of solid bed
$\theta$ = solid conveying angie which is the angle between the direction of screw rotation and the direction of solid bed movement relative to the barrel surface

$\rho_b$ is a strong function of internal pressure, $P$, especially at low pressures below about 1000 psi. $\theta$ is the only unknown in *Eq. 9* and the solid conveying theories (2, 3) are concerned with the calculation of $\theta$. $G_S$ increases with increasing $\theta$. If $\theta$ is unchanged and $D$ is much greater than $H$ in the common scale-up, it can be shown using *Eq. 9* that

$$\frac{(G_S)_D}{(G_S)_d} = \left(\frac{D}{d}\right)^2 \tag{10}$$

Therefore, $\theta$ must remain constant in the common scale-up since the solid conveying capacity, which must be the same as the output rate, increases by $(D/d)^2$.

### Viscous Shearing Theory

The angle $\theta$ can be related to screw geometry, operating conditions and the material properties of the polymer as follows (3, 10),

$$\begin{aligned}\frac{(P_2-P_1)}{S_n\cdot V^\alpha}\cdot\frac{H}{D} = {}& \frac{\pi}{\cos\phi}\cdot\frac{C}{B}\cdot\left[\frac{\sin\phi}{\sin(\theta+\phi)}\right]^\alpha \\ & \cdot\left(\frac{\cos\theta\cdot\sin\phi}{B}-\sin\theta\cdot\sin\phi\right) \\ & -C\cdot\left[\frac{\sin\theta}{\sin(\theta+\phi)}\right]^\alpha \\ & \cdot\left[\frac{A^{1+\alpha}}{B}\left(\sin^2\phi+\frac{A}{B}\cos^2\phi\right)+\frac{H}{D}\cdot\frac{2B^\alpha}{\pi\sin\phi}\right]\end{aligned} \tag{11}$$

where

$A = 1-2(H/D)$
$B = 1-(H/D)$
$S_n$ = number of the flight turns in solid conveying section
$P_1$ = pressure at the start of solid conveying section
$P_2$ = pressure at the end of solid conveying section.

$C$ and $\alpha$ are the constants in the expression of the shear stress ($\tau$) required for sliding a polymer solid on a hot metal surface, $\tau = C\cdot V^\alpha\cdot C$ and $\alpha$ depend on polymer and barrel temperature. The value of $\alpha$ is about 0.3 for many polymers in the usual temperature range of extrusion. *Equation 11* shows that $\theta$ will remain constant if $(H/D)$ and $[(P_2-P_1)/(S_n\cdot V^\alpha)]$ are kept constant in a scale-up. However, $(H/D)$ decreases in the common scale-up, causing $\theta$ to increase (3). Also, $(S_n\cdot V^\alpha)$ increases due to increased $V$ although $S_n$ remains constant, causing $[(P_2-P_1)/(S_n\cdot V^\alpha)]$ to decrease if the pressure rise, $(P_2-P_1)$ stays constant, and again causing $\theta$ to increase. The tendency to increase $\theta$, i.e., excessive solid conveying capability in the common scale-up, is usually counter-balanced by increased pressure rise, $(P_2-P_1)$. This analysis suggests that the length of the solid conveying section can be reduced for the larger diameter extruder in the common scale-up by the following approximate relationship.

$$\begin{aligned}&\frac{P_2-P_1}{S_n\cdot V^\alpha}\cdot\frac{H}{D} = \text{constant for constant } \theta \\ &\frac{1}{S_n\cdot V^\alpha}\cdot\frac{H}{D} = \text{constant if } (P_2-P_1) = \text{constant} \\ &S_n \propto \frac{1}{V^\alpha}\cdot\frac{H}{D} \\ &\frac{(S_n)_D}{(S_n)_d} = \left(\frac{d}{D}\right)^{0.5(1+\alpha)} \simeq \left(\frac{d}{D}\right)^{0.65} \quad \text{for} \quad \alpha = 0.3\end{aligned} \tag{12}$$

### Friction Theory

The angle $\theta$ can be related to screw geometry, operating conditions, and the frictional properties of the polymer as follows (2),

$$\cos\theta = K\cdot\sin\theta + A\,(K\cdot\sin\phi + A\cdot\cos\phi) + \left(\frac{H}{D}\right)\left[\frac{2}{\pi}\left(K\cdot A + \frac{B^2}{\tan\phi}\right) + \frac{B}{\mu\pi}\cdot\cos\phi \cdot(B\cdot\cos\phi + K\cdot\sin\phi)\cdot\frac{1}{S_n}\cdot ln\left(\frac{P_2}{P_1}\right)\right] \quad (13)$$

where

$K = B\,(\sin\phi + \mu\cdot\cos\phi)/(\cos\phi - \mu\cdot\sin\phi)$

$\mu$ = friction coefficient of polymer

*Equation 13* shows that $\theta$ will remain constant if $(H/D)$ and $[(1/S_n)\cdot ln(P_2/P_1)]$ are kept constant in a scale-up. $[(1/S_n)\cdot ln(P_2/P_1)]$ stays constant as long as pressure ratio, $(P_2/P_1)$ stays constant, but $(H/D)$ decreases in the common scale-up, causing $\theta$ to increase. Therefore, the friction theory also predicts excessive solid conveying capability in the common scale-up. The length of solid conveying section can be reduced, still maintaining the required solid conveying capacity, by the following approximate relationship.

$$\frac{H}{D}\cdot\frac{1}{S_n}\cdot ln\left(\frac{P_2}{P_1}\right) = \text{constant}$$

$$\frac{H}{D}\cdot\frac{1}{S_n} = \text{constant if } \left(\frac{P_2}{P_1}\right) = \text{constant} \quad (14)$$

$$S_n \propto \frac{H}{D}$$

$$\frac{(S_n)_D}{(S_n)_d} = \left(\frac{d}{D}\right)^{0.5}$$

### Screw HP Consumption

Although the common scale-up method implicitly assumes that screw HP increases proportionally to output rate by the ratio $(D/d)^2$, screw HP will increase by more than this $(D/d)^2$ ratio due mainly to increased peripheral screw speed. Thus,

$$\text{HP} \propto A\cdot\tau\cdot V$$

$A$ = barrel area

$\tau$ = shear stress acting on barrel

Noting that $A$ is proportional to $D^2$ and $V$ is equal to $N\pi D$, the above equation becomes

$$\text{HP} \propto \tau\cdot N\cdot D^3 \quad (15)$$

If $\tau$ is assumed to remain constant, for the common scale-up in which $N$ is proportional to $D^{-0.5}$, *Eq. 15* becomes

$$\text{HP} \propto D^{2.5}$$

$$\frac{(\text{HP})_D}{(\text{HP})_d} = \left(\frac{D}{d}\right)^{2.5} \quad (16)$$

*Equation 16* assumes an equal barrel surface temperature in the scale-up, but the actual barrel surface temperature of the larger-diameter extruder usually becomes higher than that of the smaller diameter extruder due to higher melt temperature and thus the actual screw HP consumption increases less than $(D/d)^{2.5}$ times due to reduced melt viscosity. According to *Eq. 15*, $N$ must be decreased inversely to $D$ in a scale-up in order to make the screw HP just proportional to the barrel area. That is, both $\tau$ and the peripheral screw speed must be kept constant in order to maintain a constant specific screw HP in a scale-up.

$\tau$ for pumping depends on the shear rate $(\dot{\gamma})$ in the screw channel and remains constant in the common scale-up. $\tau$ for melting, however, depends on peripheral screw speed $(V)$ and channel width $(W)$ rather than $\dot{\gamma}$ by the following approximate relationship (8),

$$\tau \propto \frac{V^{1.5n}}{W^{0.5n}} \quad \text{for melting} \quad (17)$$

where $n$ is the power-law exponent for viscosity. Noting that $V$ is proportional to $D^{0.5}$ and $W$ is proportional to $D$ in the common scale-up, *Eq. 17* becomes

$$\tau \propto D^{0.25n} \quad \text{for melting}$$

$$\frac{(\tau)_D}{(\tau)_d} = \left(\frac{D}{d}\right)^{0.25n} \quad \text{for melting} \quad (18)$$

Thus, $\tau$ for melting increases only slightly in the common scale-up. According to *Eq. 17*, $\tau$ for melting will remain constant if $W$ is increased proportionally to $D$ and $V$ is increased proportionally to $D^{0.33}$ in a scale-up. Such scale-up requires the screw RPM to decrease by $(D/d)^{0.67}$ and the channel depth to increase by $(D/d)^{0.67}$.

## CONCLUSION

It is seen that the common scale-up method leads to an imbalance in the solid conveying, melting, and pumping capacities. The melting capacity increases insufficiently, i.e., less than proportional to the square of the diameter ratio but the solid conveying and pumping capacities increase more than necessary. The peripheral screw speed and the specific screw HP are also found to increase. Increased peripheral screw speed and deficient melting capacity are mainly responsible for the problems experienced in the common scale-up. The analysis presented in this paper suggests that deficiency in the melting capacity may be compensated for by increasing the barrel surface area devoted to melting while decreasing the solid conveying and pumping areas. Peripheral screw speed is the most important factor for controlling screw HP and thus melt temperature. A reduced peripheral screw speed is desirable to reduce the screw HP in the common scale-up but this also reduces the melting capacity which is already deficient.

There appears to be no simple solution to an ideal scale-up. However, a satisfactory scale-up can be accomplished by a careful analysis of all three functions of a screw such as presented in this paper.

## REFERENCES


1. J. F. Carley, R. A. Strub, R. S. Mallouk, J. M. McKelvey, and C. H. Jepson, *Ind. Eng. Chem.*, **45**, 969 (1953).
2. W. H. Darnell and E. A. J. Mol., *SPE J.*, **12**, 20 (1956).
3. C. I. Chung, *SPE J.*, **26**, 32 (1970).
4. Z. Tadmor, *Polym. Eng. Sci.*, **6**, 185 (1966).
5. J. F. Carley and J. M. McKelvey, *Ind. Eng. Chem.*, **45**, 985 (1953).
6. E. M. Mount, III and C. I. Chung, *Polym. Eng. Sci.*, **18**, 711 (1978).
7. E. M. Mount, III, J. G. Watson, III and C. I. Chung, *Polym. Eng. Sci.*, **22**, 729 (1982).
8. K. H. Chung and C. I. Chung, *Polym. Eng. Sci.*, **23**, 191 (1983).
9. F. W. Kroesser and S. Middleman, *Polym. Eng. Sci.*, **5**, 230 (1965).
10. C. I. Chung, *Polym. Eng. Sci.*, **15**, 29 (1975).


## DISCUSSION

*V. L. LeNir:* Our methods engineers, when they run foam skin on a 2½ inch, 24 to 1, like a very long metering zone, 0.1 inch in depth, typically 21 inches in metering zone. They feel that gives them good mixing to get a good foam compound. Your analysis didn't really deal with mixing.

*C. I. Chung:* No, but you are speaking of a particular situation. In foam extrusion you inject a foaming agent, usually physical, like Freon or pentane, and that reduces the viscosity of the polymer greatly. The length of the so-called "cooling extruder" which is the second stage extruder that you are talking about, I assume, has many objectives and one is to cool the temperature of the melt. The temperature of the melt must be kept very low. Otherwise, when you extrude the polymer with a foaming agent through the die, it will have premature foaming inside the die. So you really have to keep the temperature low. The most important objective is cooling of the mixture. The second is pumping against the head pressure. You must have a certain head pressure to avoid premature foaming. A foaming die is usually converging so as to maintain the critical pressure up to the lip of the die and you must maintain that pressure. Pumping very low viscosity polymer against such a pressure takes a long metering section. So you are talking of a very special case and there again the main purpose is cooling. You need a long extruder screw or large barrel area in order to achieve the necessary cooling almost down to the melting point of the polymer.

*M. R. Kamal:* I noticed that in the melting treatment you used the Newtonian fluid model and not the power-law fluid as you did in the pumping treatment. What would be the effect of using a power-law fluid on the melting characteristics of the extruder or the scale-up?

*C. I. Chung:* Excuse me, Musa, probably I didn't make it clear. The approximate relationship that I presented here, the melting rate, $\Omega$, per unit area per unit time is only a function of velocity and channel width which is more important in scale-up. I didn't talk about the details but in our analysis we consider the pseudoplastic nature of the polymer and that's how we obtain the exponent "$n$" where $n$ denotes the pseudoplasticity of the material. So we do consider non-Newtonian characteristics. All of our analysis is based on the power-law fluid for melting.

*M. R. Kamal:* But the 1.75 power scale-up ratio remains the same for both Newtonian and power-law fluids.

*C. I. Chung:* No. The non-Newtonian characteristics are already contained there.

*Y. Kuo:* I have several questions. Firstly, your theory is developed for a constant barrel temperature.

*C. I. Chung:* Yes. Not constant along the screw or along the machine but the same temperature profile between two different sized machines.

*Y. Kuo:* So you assume that beyond the same maximum barrel temperature, in other words, in a scale-up situation, you cannot increase the temperature any further. Suppose you included a different barrel temperature in your scale-up, will this complicate your theory?

*C. I. Chung:* It certainly will. The implicit assumption is that when you run a small extruder, you have found the optimum operating conditions and the maximum. You crank up the extruder as much as possible and you raise the temperature of the barrel as much as possible or lower it as much as possible to cool, and the condition is assumed to stay the same in the large diameter extruder.

*Y. Kuo:* I have another question regarding the residence time. I noticed that your residence times do not include the channel depth as a variable.

*C. I. Chung:* I think I commented on residence time. That is, when you scale-up the residence time increases.

*Y. Kuo:* But the depth is not involved.

*C. I. Chung:* It is involved. The channel depth determines the volume of the screw and that determines the residence time. I was pointing out that you must consider residence time which is normally neglected or not discussed. One of the reasons that we have higher melt temperature is because we have higher residence time. But as far as horsepower is concerned, maybe that's your question, the way I treat it you don't have to worry about channel depth because I was only talking about stress on the barrel surface.

*Y. Kuo:* Is your theory limited to certain kinds of screws or certain configurations?

*C. I. Chung:* I don't think so. This is a gross overall analysis.

*Y. Kuo:* Is it applicable to twin screws?

*C. I. Chung:* Twin screws present an entirely different situation, but the analysis can apply to all single screws.

*Y. Kuo:* I am not working in this field but I noticed that there exists in the literature in-depth mathematical analyses of extrusion. Are there commercially available computer programs that can be used

which give results as opposed to this simplified analysis?

*C. I. Chung:* To my knowledge there is only one commercially available program. You feed in the required input data and you obtain the output predictions. This is offered by Scientific Process and Research by Dr. Klein in Highland Park, New Jersey. This has been the only commercial program available to my knowledge. At the current stage, I don't think the computer program is so good. If you really understand the theory you don't need to run the program. If you don't understand the theory or what is going on in the program and you run the program and believe in it, the program does more harm than good. Our extrusion research at RPI is directed toward eventually developing a simple program.

*Y. Kuo:* Thank you. I think you already answered my next question, which is, are you going to develop a complete model of the extruder?

*C. I. Chung:* Hopefully yes, and when we do, we will publish.

*M. E. Ryan:* I am going to prevail on Dr. Chung because I am interested in some of these calculations. Two very quick questions; one is: what is the commonly used thermal boundary condition at the screw/polymer interface?

*C. I. Chung:* The commonly used boundary condition is adiabatic. That is, no heat exchange between the screw and the polymer. That is the common assumption.

*M. E. Ryan:* The other question I have is the following. You talked about the sensitivity of the calculations using the Darnell and Mol analysis because of the problem associated with $P_1$. Various people have tried to calculate $P_1$ based on the solid height in the hopper. Does that really resolve the difficulty or does a problem still reside in modeling the pressure profile?

*C. I. Chung:* It does not. First of all, if indeed the solid conveying capacity were to depend on the level of polymer in the hopper, then a lot of problems would be encountered in operation but in most operations this problem is not encountered. You can load up the hopper, or almost empty it. The performance is the same. Second of all, we do know from experiments reported by other people that the polymer pellets are packed in the hopper and the pressure at the bottom of the hopper is virtually atmospheric and independent of the hopper level.

*L. Schmidt:* I would like to follow up on Professor Ryan's question. You mentioned that you don't get a good prediction using essentially the gravity or hopper loading for materials. If you use a crammer feeder so that you have a very definite force or pressure on the material, do you get a reasonable prediction?

*C. I. Chung:* I think you do, yes. When you use a crammer feeder, then you do have a definite pressure although it is usually low, less than 100 psi as you know, only 20 to 50 psi.

*L. Schmidt:* But you should be able to keep it relatively constant which is what you need.

*C. I. Chung:* The benefit of that is not just the 20 to 50 psi developed at the feed end of the screw, which is very low compared to thousands of psi which we are talking about. But the benefit is in the friction model. The pressure increases along the screw exponentially. If you have already 20 to 50 psi, you have that much pressure to begin with so that the pressure can increase very quickly. As you know, the so-called "water-cooled, grooved feed section" of German invention is to capitalize on the fact that if you really maintain friction mechanism by forced cooling and grooved geometry of the barrel, then you can increase the pressure exponentially so that over 5 turns or 7 turns you can reach 10,000 to 20,000 psi. So when you use a hopper feeder you have this pressure to begin with. Otherwise at the entrance to the screw, there is virtually no pressure even though there may be lots of material in the hopper. The screw channel will be partially empty and the pressure is essentially atmospheric. In fact, the material feeds like a grain feeder with the screw flight pushing the material in until it packs up. So when you use hopper feeder or crammer feeder, it is like having more turns of feeding section. Now this is the reason why I don't think it is necessary to use a hopper feeder for all polymers that feed well. They drop into the screw easily enough and there is no need to have a hopper feeder. You only need a hopper feeder for those materials which don't flow into the screw easily enough such as powders or flakes.

*L. Utracki:* Professor Chung, I somehow don't feel the physical reason for the reduction of the melting capacity. Is it the heat transfer which is responsible here?

*C. I. Chung:* Let's talk about the melting rate per unit area per unit time per unit sliding distance. If we double the speed, the time the cold solid polymer is exposed to the hot metal surface per unit distance is reduced by half. This is the reason.

*L. Utracki:* So, there are two possible solutions to this problem. Which one can you suggest immediately? First of all, preheating of the feed which is what is being done by industry, and second, to change the depth of the channel in the melting zone.

*C. I. Chung:* Changing the depth of the channel is not going to have any influence at the solid-barrel interface where melting occurs because the compacted solid rubs on the barrel surface and that interface does not see the depth of solid. So, it doesn't make any difference. The first suggestion you made is done by people, sometimes by necessity, like with nylon and polycarbonate which are hygroscopic polymers and must be dried before extrusion. Otherwise you are going to have moisture bubbles. However, the extruder is one of the most efficient heat exchangers. The energy efficiency of the extruder is 60 to 70 percent. If you were to use another piece of equipment it would

mean extra cost, extra handling, and the energy efficiency of a hot air heater is not as good. As much as can be done without additional equipment is desirable. This is the reason why we are using larger and longer extruders. Ten or fifteen years ago the extruder was only of 20 to 24 L/D ratio. Now 30 to 1 is common practice. 24 to 1 is the minimum, and I often see 36 to 1, 40 to 1, and more. So we use the more efficient extruder as a heat exchanger and it is less expensive than having another piece of equipment.

*V. L. LeNir:* What about the influence of the flights on the heat transfer? Surely if you have a very small clearance between the tip of the flight and the inside of the barrel, that would tend to wipe the barrel clean each time. You get good heat transfer.

*C. I. Chung:* That is a very good question. Heat exchange between the polymer and the barrel surface depends on the wiping frequency: Thus, one way to really increase the melting capacity or heat transfer is to use a smaller or narrower channel width. Instead of using an 8 inch channel width you can use a double flight so that the channel width is only 4 inches. This really increases melting capacity. However, if you do this, it will generate much more heat and the melt temperature increases. There are lots of advantages of using more flights. Typical flight widths that are used now are about 10 percent of the screw diameter. This has evolved from considerations of wear and horsepower. For a large extruder, a small reduction in flight width can have some reduction in horsepower which can reduce the melt temperature substantially. For a small extruder there is not much influence but for a large machine, such as a 10 or 12 inch machine or larger, you look at every aspect of the design.

# Computerization of Wire Insulating Lines—An Industrial Approach

V. L. LeNIR

*Northern Telecom Canada Limited*
*150 Montreal-Toronto Blvd*
*Lachine, Quebec*
*Canada*

The two main materials used for insulating wire are plastic and pulp. With the introduction of digital transmission techniques, there has been an increasing demand for improved cable quality, thereby stimulating an investigation of the insulating process in order to improve quality. The increasing availability of digital computers enabled mathematical models of the insulating process to be constructed, which together with experimental work, provided a basis for the installation of computerized control systems. This paper reviews three such models which were developed and are being used. These comprise a model for screw extrusion, a model for melt flow in the wire coating die, and a model for the subsequent cooling of the insulated wire (or cable). Relatively little work was done in the area of dynamic simulation of the insulating process and we found computer control systems could be relatively easily installed in production provided high level software process modules with interfaces to a high level programming language were available on the system. It was found that simplified control schemes were usually the most effective in production. Two computer control installations to illustrate this viewpoint are described—a multiline central computerized control system, and a single-line microprocessor-based system.

## INTRODUCTION

The two main materials used for insulating wire are pulp and plastic. Since 1965, there has been a rapidly increasing availability of high-speed digital computers for both scientific and control purposes—in addition there has been an increasing demand for upgrading cable quality. A development project (called "Process Simulation" was started in 1979 with the objective of introducing computerized control of the wire insulating lines (for both plastic and pulp insulations). The "computerization" of these lines has now been achieved and further improvements now seem to be possible and practicable.

In this paper three of the simulation programs will be discussed:

a. Screw design program (1978)
b. Die design program (1974)
c. Cable cooling program (1971)

Two computer control installations will also be discussed:

a. Multiline central computerized control system (for plastic insulated wire). (1976)
b. Single-line microprocessor-based system (for plastic insulated wire). (1980)

A discussion of a pulp insulating line distributed process control system can be found in *Ref. 6.*

## SIMULATION PROGRAMS

### Screw Design

*Figure 1* shows a diagram of a (conventional) extruder screw.

The analysis was divided into three parts—

a. feeding
b. transition (or melting)
c. metering.

The feeding and transition sections were modelled in a similar way to the approach outlined in *Ref. 1* (chapts. 4 and 5). Some small modifications were made. The metering section was analyzed using a finite difference method across the channel. This analysis takes into account the temperature gradient at the barrel wall—melt interface and the screw root temperature gradient, and introduces a term for convection. The nonisothermal one-dimensional power law model was used to solve the flow equations. The equations used to develop the solution are (a list of symbols is available at the end of the paper):

$$\tau_{yz} = m_0 e^{-b(T-T_{ref})} \left(\frac{dv_z}{dy}\right)^n \qquad (1)$$

(power law)

$$P_z = \frac{d\tau_{yz}}{dy} \tag{2}$$

(pressure gradient)

$$Jk\frac{d^2T}{dy^2} = -\tau_{yz}\frac{dv_z}{dy} + JpC_p\frac{DT}{Dt} \tag{3}$$

(viscous dissipation and thermal convection)

$$Q = W\int_0^H v_z dy \tag{4}$$

(flow rate)

Cross channel effects and the influence of the flights were neglected. *Equation 3* can be rewritten as

$$\frac{d^2T}{dy^2} = -\frac{\tau_{yz}}{Jk}\frac{dv_z}{dy} + \frac{\rho C_p}{k}\frac{DT}{Dt} \tag{5}$$

An expression for $\frac{dv_z}{dy}$ in terms of $\tau_{yz}$ and $T$ can be obtained from *Eq. 1*.
Substituting in *Eq. 5*, the following expression is derived:

$$\frac{d^2T}{dy^2} = -\frac{\frac{n+1}{n}\frac{b}{e^n}(T-T_{wl})}{Jkm_0^{1/n}} + \frac{\rho C_p}{k}\frac{DT}{Dt} \tag{6}$$

This equation provides the basis for obtaining solutions for melt temperature and flow down the channel. The solution method utilizing dimensionless parameters (*Ref. 2*) is given in *Appendix 1*. Non-Newtonian shape factors ("$F_d$" and "$F_p$") were used to modify results for "deep channels". A computer program written for the total system allows the user to specify an extruder and a compound and to predict extruder behavior (such as melt pressure and temperature rise, melting rate, and power dissipated) for different operating conditions. Different rates of screw cooling can also be investigated (in a similar manner as outlined in *Ref. 2*, chapt. 7).

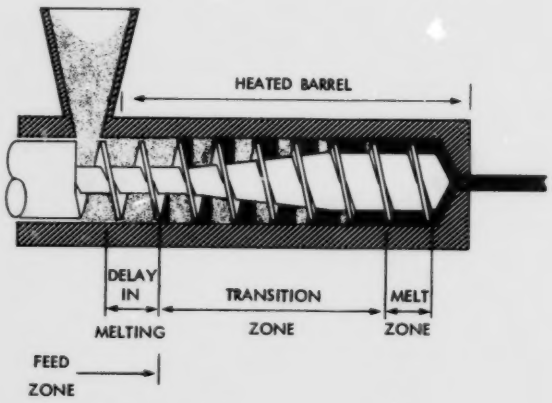


*Fig. 1. Single screw extruder.*

## RESULTS

*Reference 1* was used to compare melting rates and pressure rise (for a 2.5 inch, 24 to 1 screw)—excellent agreement (10 to 15 percent) was obtained (pages 155 to 162 and pages 366 to 371). An "in-house" comparison of results was made for a 6 inch, 24 to 1 jacketing screw (using a medium-density polyethylene) for both the neutral and cooled cases. Excellent agreement (10 percent) was obtained for pressure rise and power consumed and good agreement was found for temperature rise (*Table 1*) especially for the neutral screw.

## DIE DESIGN

*Figure 2* shows a diagram of a conventional high-speed wire coating die. Both single and dual extrusion can be handled by the program. The capability of the program is limited to an isothermal treatment of melt flow, and is based on concepts outlined in *Ref. 2* (chapt. 11) with some modifications (3). The method is based on interpolation from tables of dimensionless flow pressure characteristics and dimensionless stress characteristics. These were developed using a finite difference method (*Fig. 3*).

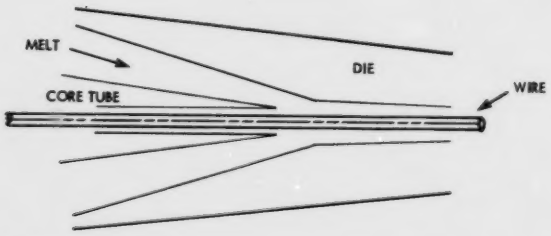


*Fig. 2. Wire coating die.*

**Table 1. Comparison of Simulated and Experimental Runs On a 6 inch, 24 to 1 Metering Screw**

| | | | OUPPUT LB/HOUR | | MELT TEMP. °F | | HORSEPOWER (HP) | |
|---|---|---|---|---|---|---|---|---|
| | SCREW RPM | PRESSURE PSI | PREDICTED | MEASURED | PREDICTED | MEASURED | PRE-DICTED | MEASURED |
| NEUTRAL | 10 | 1000 | 230 | 210 | 437 | 416 | 14.1 | 16.7 |
| | 20 | 1300 | 445 | 435 | 448 | 430 | 41.0 | 46.7 |
| | 28.8 | 1500 | 630 | 660 | 456 | 430 | 72.2 | 82.8 |
| | 39.6 | 1800 | 895 | 877.5 | 467 | 445 | 117 | 123 |
| COOLED | 30 | 1600 | 440 | 470 | 442 | 450 | 81.8 | 80.7 |
| | 40 | 1650 | 662 | 653 | 461 | 465 | 121.3 | 121.9 |
| | 50 | 1800 | 880 | 819 | 480 | 470 | 166 | 158.3 |
| | 60 | 2000 | 1115 | 1058 | 490 | 470 | 220 | 203 |

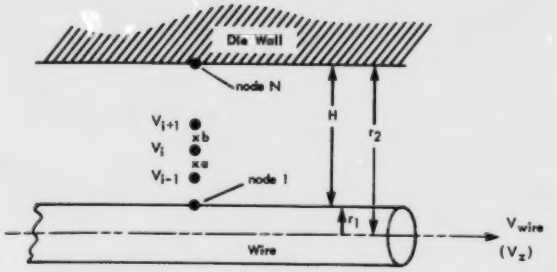


*Fig. 3. Finite difference mesh across annulus formed by die and wire.*

$$\beta = \frac{r_2}{r_1} \tag{7}$$

$$H = r_2 - r_1 \tag{8}$$

$$\Pi_Q = \frac{Q}{\Pi(r_1 + r_2)HV_z} \tag{9}$$

(dimensionless flow rate)

$$\Pi_P = -\frac{P_z H}{\tau_m} \tag{10}$$

(dimensionless pressure gradient)

$$\tau_m = m_0 \left(\frac{V_z}{H}\right)^n \tag{11}$$

(drag shear stress)

$$\Pi_{SU} = \frac{\tau_{\text{(die-melt interface)}}}{\tau_m} \tag{12}$$

(dimensionless shear stress)

The axisymmetric momentum equation is

$$P_z = \frac{1}{r}\frac{d}{dr}(r\tau_{rz}) \tag{13}$$

This equation can be integrated from any radius $r_a$ to $r_b$:

$$\tfrac{1}{2}P_z(r_b^2 - r_a^2) = r_b\tau_{bz} - r_a\tau_{az} \tag{14}$$

If $P_z$ is defined together with the shear rate at the upper (starting) boundary, the stress (and resulting shear rate) may be progressively computed to the lower boundary jumping from node to node. This gives the melt velocity for each node ($v_i$) and from this a value of flow ($Q_{i+1/2} = 2\Pi \int_{r_i}^{r_{i+1}} v_z r dr$) can be determined. Therefore the $\Pi_Q$, $\Pi_P$ curve can be found for any $n$. In a similar manner the $\Pi_Q$, $\Pi_{SU}$ curves can also be determined. These two sets of characteristics can be stored in the computer in tabulated form for $n = 0.1$ in steps of 0.1 up to $n = 1$ and for $\beta = 1.1$, 2, 4, and 8 for values of $\Pi_Q$ from 0 to 1.5 in increments of 0.02. Thus in a practical wire coating problem, the annulus formed by the die wall and wire surface is divided axially into small increments, the flow between each increment is treated as a flow between parallel cylindrical boundaries (lubrication approximation) and, for the known value of $\Pi_Q$, $n$, and $\beta$, values of $\Pi_P$ and $\Pi_{SU}$ are extracted, giving the pressure gradient and upper boundary shear stress values. By dividing the space radially into equally spaced nodes, the velocity at each node is progressively computed across the radius. Dual extrudates may be considered to be two concentric cylinders of melt with defined flow rates but an unknown interface velocity and position. The method used to solve this was an iterative method which automatically adjusts the interface velocity and position until the computed interface stress and pressure gradient $P_z$ are equal for both melts.

The method is computationally very efficient and gives practical and useful results. Its main disadvantage is that it does not involve viscous dissipation or convection effects and relies on the power law model (it cannot be readily adapted to any other model). The computer program written follows a similar method as for the EXTRUDE program—the user simply enters a specification for a die and a product, and then for different operating conditions a printout of pressure rise and shear stresses is provided. The wire drag, which is important for smaller wire gages, is also computed.

## RESULTS

Theoretical solutions for isothermal flow are available for a power-law index of $n = \frac{1}{2}$ for different $\Pi_Q$, $\Pi_P$ values. In addition, drag flow ($\Pi_p = 0$) values can be analytically solved for various values of the power law index. *Table 2* shows a comparison of the analytical results to the present (numerical) results from the program for any given increment in the wire coating die. Comparison of results with an available finite element program for wire coating shows good agreement (10 to 15 percent) in the wire carrying die section (for isothermal flow). Viscous dissipation and convection effects play significant roles in wire coating and therefore the present program is used to make a preliminary (and rapid) analysis of a die design.

## CABLE COOLING PROGRAM

*Figure 4* shows a cross section of a cable divided into radial increments. The finite difference method was used to solve the cooling problem—only radial heat flow was assumed.

The one-dimensional (radial) heat flow equation is

**Table 2. Numerical Versus Analytical Results For a Wire Carrying Die Axial Increment**

| | | | $\pi_Q$ | |
|---|---|---|---|---|
| $\eta$ | $\beta$ | $\pi_P$ | NUMERICAL | ANALYTICAL |
| 0.5 | 2 | −0.988 | 0.201 | 0.201 |
| 0.5 | 2 | 2.53 | 0.176 | 0.172 |
| 0.5 | 8 | −0.235 | 0.0893 | 0.0887 |
| 0.5 | 8 | 2.64 | 0.562 | 0.561 |
| 0.25 | 2 | 0.0 | 0.238 | 0.239 |
| 0.75 | 2 | 0.0 | 0.3695 | 0.371 |
| 0.25 | 4 | 0.0 | 0.0857 | 0.0857 |
| 0.75 | 4 | 0.0 | 0.2605 | 0.260 |

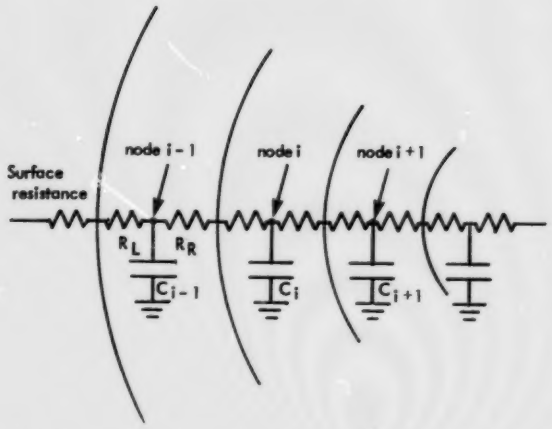


*Fig. 4. Cable formed into finite sections for heat flow analysis.*

$$\rho C_p \frac{\partial T}{\partial t} = k \frac{1}{r} \frac{\partial}{\partial r} \left( r \frac{\partial T}{\partial r} \right) \tag{15}$$

It is convenient to develop the finite difference formula in terms of an electrical analog (*Fig. 5*).

At time $j$ the following equation can be written for node $i$; time $j$:

$$I_{ij} + P_{ij} = I_{i+1j} + C_{ij} \frac{\partial u_i}{\partial t} \bigg|_j \tag{16}$$

where $P_{ij}$ represents a power source, $I_{ij}$ represents the heat flow, $R_{ij}$ is thermal resistance, $C_{ij}$ is thermal capacitance, and $U_{ij}$ is temperature. At time $j + 1$:

$$I_{ij+1} + P_{ij+1} = I_{i+1j+1} + C_{ij+1} \frac{\partial u_i}{\partial t} \bigg|_{j+1} \tag{17}$$

When the equations are combined an average value of $\frac{\partial u}{\partial t}$ at time $j + \frac{1}{2}$ was used—in finite difference form this becomes $\frac{u_{ij+1} - u_{ij}}{\Delta t}$.

The Crank Nicholson implicit method was used to solve the equation. One problem arising was to obtain a reasonable value for $R_{ij+1}$ and $C_{ij+1}$ (thermal resistance and capacitance), since they are dependent on the predicted temperature at time $j + 1$. Therefore a first approximation for $R_{ij}$, $C_{ij}$ was used and once a first estimate of temperature $U_{ij+1}$ was available an actual value for $R_{ij+1}$, $C_{ij+1}$ could be calculated (from temperature dependent curves for thermal conductivity and specific heat). This procedure is carried out iteratively. The values for $R_{ij}$ and $R_{ij+1}$ are usually adequate over reasonable time increments since the thermal conductivity changes slowly with temperature, but $C_{ij}$ (involving specific heat) changes very rapidly around the melting point—therefore the time increment is (or can be) made much smaller when the melt is solidifying.

In an actual cable, the program allows the user to subdivide segments into as many nodes as required and in addition the user can enter estimates of contact thermal resistances between cable segments. The cable exits from the head of the extruder usually into a short section of "air" and then into a water trough. The heat transfer coefficient at the surface is computed from a radiative and convective component in air, and on entering the water trough, the convective component is used.

Program users have the option of entering a cable identifier if they can construct their own "cable" and temperature profile can be generated for different operating or cooling conditions.

## RESULTS

Cooling curves for wires insulated with different compounds can be found in *Refs. 4* and *10*. The program results were tested against the curves and agreed to within 10 percent when referred against the "start" temperature.

## INPUT DATA REQUIREMENTS

- Shear viscosity: shear rate—temperature curves
- Melt density: as a function of pressure and temperature
- Thermal data: conductivity, specific heat, and heat of fusion
- Melting point (as a function of pressure)
- Solid pellet density as a function of pressure
- Friction coefficient of pellets against steel surface as a function of steel surface temperature
- Dimensional data (screw, barrel, die, cable)

In general the shear viscosity is measured at three temperatures (eg., 190°C, 210°C, 230°C) up to about 1000 $sec^{-1}$ in a capillary viscometer. The specific heat is also available from a differential scanning calorimetric analysis (DSC). Melt density as a function of pressure and temperature can also be determined in a capillary viscometer. The rest of the data can be found in the literature (1, 7, 8, 9).

## APPLICATIONS

The programs have been available in essentially finished form since 1974. Some work has been done since then to make them more user oriented such that they can gain wider usage:

a. Extrude:

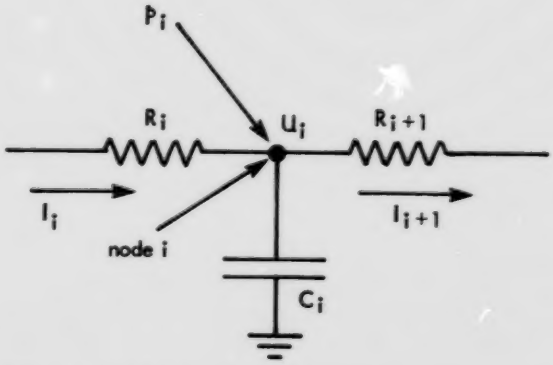


*Fig. 5. Electrical analog for heat flow.*

Applications have mainly focused on providing output *vs* pressure and melting rate characteristics for different screw designs. The program has enabled process engineers to assess (and purchase) screws for different tasks without undue dependence on the supplier.

b. Die:

Application has been more extensive—simulations have highlighted the direction in which improvements could be made to die geometry, for small gage dual layer insulation products where reductions of wire drag and pressure in the die were made possible.

c. Cool:

A number of cable cooling studies have been carried out. For high-speed insulating, the study has focused on the finished insulated conductor temperature prior to take-up in order to reduce insulation distortion. For heavier cables, interest concentrated mainly on the heating of the multiconductor core and the degree of protection offered by the core wrap tape.

## COMPUTERIZED PROCESS CONTROL

### Introduction

Simulation programs were used to provide a "background" against which a computer control system could be installed. The objective was to provide a stimulus for evaluating the process to enable critical parameters to be monitored and controlled. The application of what might be called "dynamic simulation" was minimal—it mainly concentrated on the provision of an "automatic tuning" program which would enable the control engineer to tune up the process in digital mode as opposed to analog mode. Again, this particular program was rarely used.

The following (major) installations were made:

a. Multiline central computerized control for high-speed plastic insulating lines.
b. Single-line microprocessor-based system (for a high-speed plastic insulating line).
c. Pulp insulating line distributed process control.

This paper will review installations (a) and (b)

## MULTI-LINE COMPUTER CONTROL FOR HIGH-SPEED WIRE INSULATING LINES

The reason for installing the control system was to improve the characteristics of the final cable. This can be achieved by controlling the coaxial capacitance and diameter of each single insulated wire and thereby improving the "capacitance unbalance to ground" of the final cable—which translates to an improvement of the cross talk level. The first installation on an experimental line was carried out at the Lachine Cable Division (1975) and the subsequent multiline control system was installed in the Kingston Cable Division in 1977 (5).

The system is based on a Foxboro Control computer—Fox 2/30—comprising a 32K 16 bit core memory with a fixed head storage of 1/2 MWord. There are 2 CRT's and 2 teletypes. In the field there is a control communication module for each "dual insulation" line (foam skin) and there is one for the six "solid" insulation lines—where control requirements are less demanding. *Figure 6* shows a schematic of a high speed wire coating line. *Figure 7* provides an overview of the computer process interface modules. *Figure 8* shows the inputs and outputs specified.

The software available consists of the control language IMPAC ("Industrial Multi-level Process Analysis and Control") and FORTRAN, which interfaces with it by system subroutines. IMPAC allows control blocks to be easily built and linked (for example PEID blocks, SCAN blocks, SWITCH

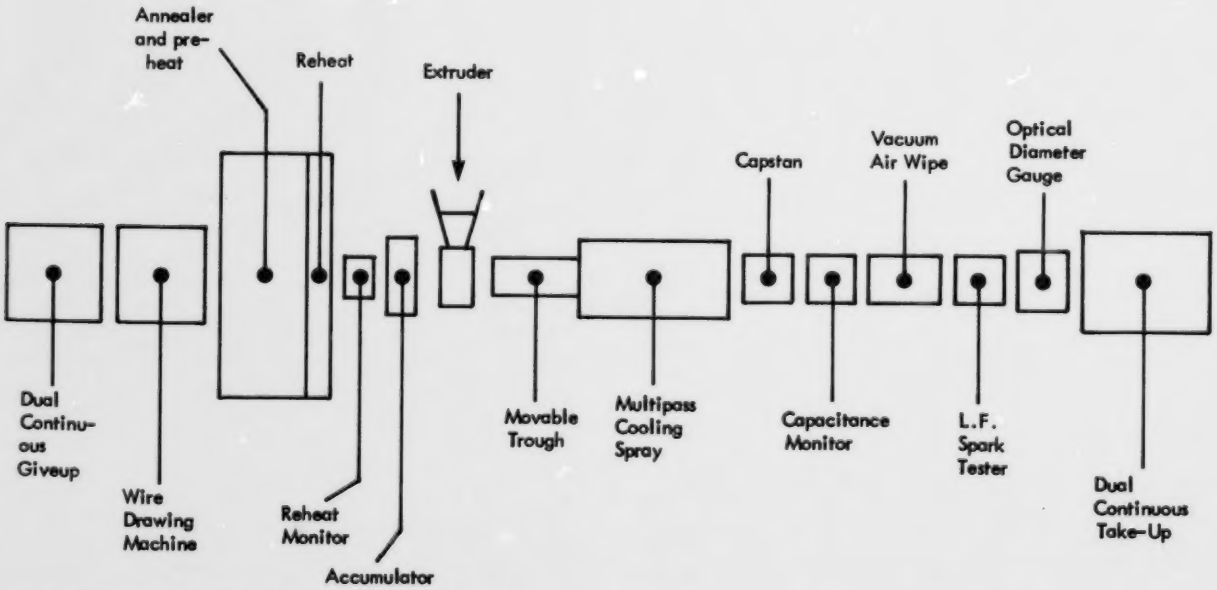


*Fig. 6. High-speed plastic-insulated wire coating line.*

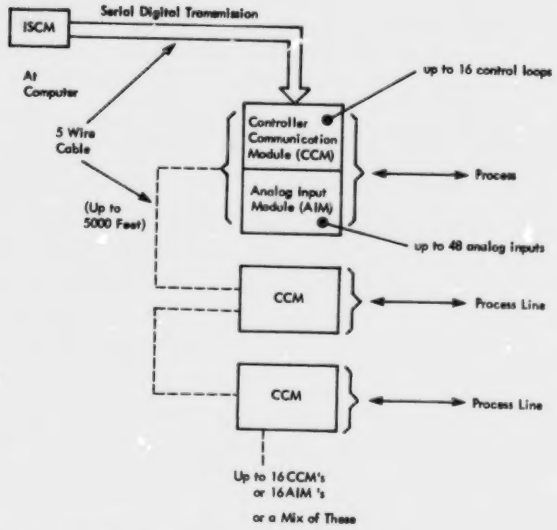


*Fig. 7. Multi-line process-computer communication.*

| PARAMETER | INPUTS PROCESS TO COMPUTER | OUTPUTS COMPUTER TO PROCESS |
|---|---|---|
| Analog Points | | |
| Diameter | X | - |
| Capacitance | X | - |
| Preheat | X | - |
| Melt Temperature | X | - |
| Main Screw RPM | X | X |
| Secondary Screw RPM | X | X |
| Line Speed | X | X |
| Movable Trough | X | X |
| Zone Temperature 1 - 5 | X | X |
| Head Temperature | X | X |
| Worm Water | X | X |
| Annealer, preheat current | X | - |
| Reheat Current | X | - |
| Digital States (on/off) | | |
| Product Type | X | - |
| Start/Stop | X | X |
| Line Reset | X | - |
| Reel Changeover | X | X |
| Line Reset | X | - |
| Line Status Lights | - | X |
| (Plus) Spark Count | X | - |

*Fig. 8. Plastic-insulating process-computer inputs and outputs.*

blocks, etc.), and the FORTRAN system routines allow the blocks to be switched on or off, and different control schemes to be tried. *Figure* 9 shows, as an example, the control scheme for such a line.

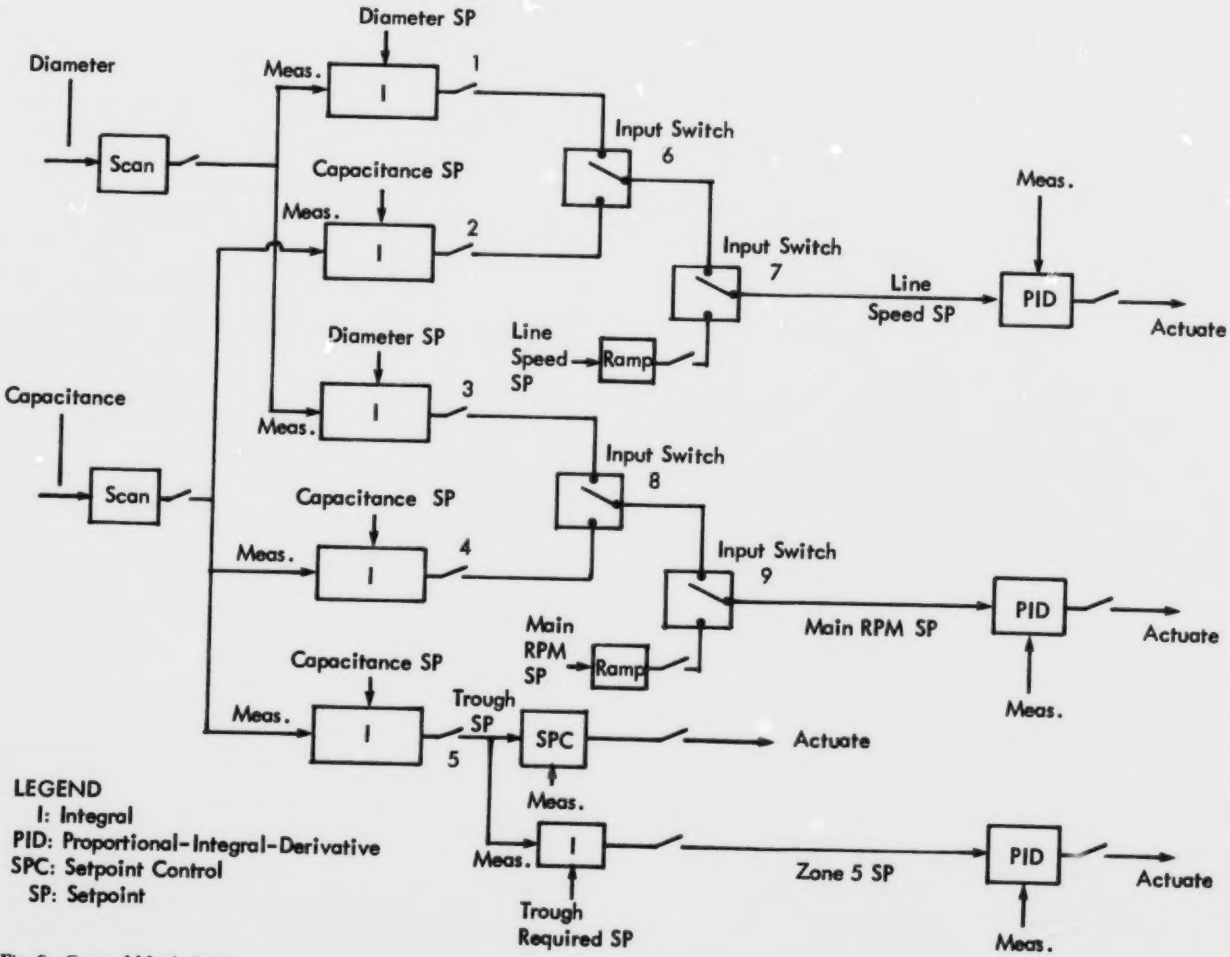


*Fig. 9. Control block diagram.*

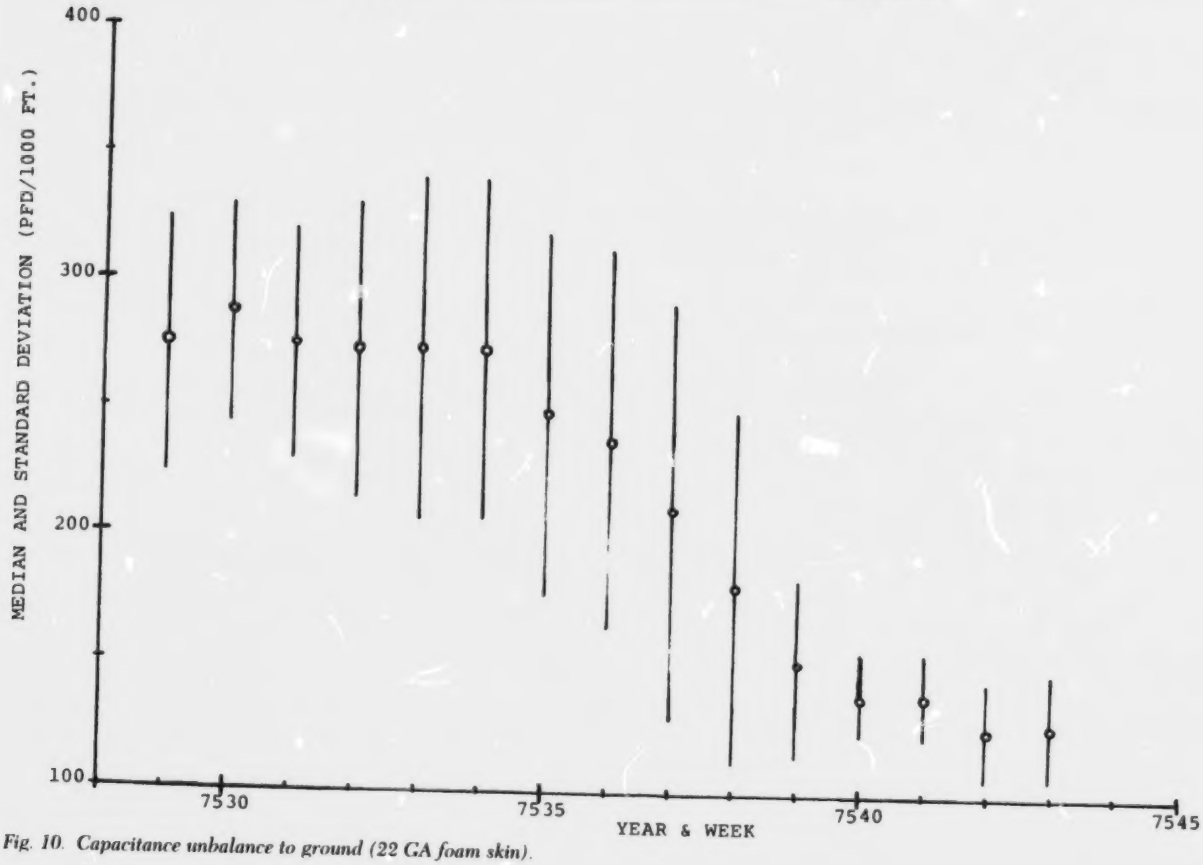


*Fig. 10. Capacitance unbalance to ground (22 GA foam skin).*

The start-up procedure for a foam skin product would follow the following steps:

a. Select product—checks product data files and gives permission to start
b. Line run—line ramps to speed for the product selected
c. Control on—computer switched to required control automatically
d. Line Stop.

For foam skin insulation switches 3 and 5 would be closed and switch 8 would be up, and for solid insulation switch 4 would be closed and switch 8 would be down.

In addition to control, other advantages of having a computer system are sophisticated trending capability and product reports (quality and number of reels being manufactured).

The advantages of such a centralized system are ease of programming and centralized control of all the lines. The disadvantages are reliability (when the computer goes down, all the lines go down), and resulting maintenance problems (the system tends to be more complex).

## RESULTS

The installation was successful and all objectives in terms of control capability and production reports were achieved—and the final product meets system noise level requirements. Capacitance unbalance to ground levels (which cause system noise) were substantially reduced, as shown in *Fig. 10.*

## SINGLE LINE MICROPROCESSOR CONTROL SYSTEM FOR HIGH SPEED WIRE COATING LINE

A decision was made to embark on a single-line control system in 1977. The objective of this was to provide similar capability in "remote" cable plants—those plants having only a single high-speed line. It was important to be able to produce the same quality of cable in any of our plants and a large (and expensive) computer control system was not feasible for such a plant.

The system was constructed around an Intel Single Board Computer (SBC) 80/20. *Figure 11* shows the boards used in the system with their function. *Figure 12* shows the control panel used by the operator. Digital and analog input/output channels were similar to those in the previous section.

Development of the system was undertaken using an Intellec MDS 230 with an In-Circuit Emulator (ICE-80)—peripherals consisted of a CRT terminal, dual double density diskette drive, a line printer, cassette unit and PROM programmer. The operating system was ISIS-11 and programming languages available were PLM/80 and 8080 Macro assembler. A real time executive RMS/80 enabled time oriented tasks to be developed. The system allowed a

BOARD CONFIGURATION

| | | | |
|---|---|---|---|
| SBC 80/20 | Processor with 8K bytes EPROM, digital I/O | SBC 310 | High speed mathematics unit |
| SBC 464 | 64K byte EPROM expansion | RTI 1201 | Analog outputs (4 channel) |
| SBC 032 | 32K byte RAM memory | RTI 1201 | Analog outputs (4 channel) |
| RTI 1200 | Analog inputs (16 channel) | SBC 534 | 4 channel communication expansion |

*Fig. 11. Microprocessor system boards.*

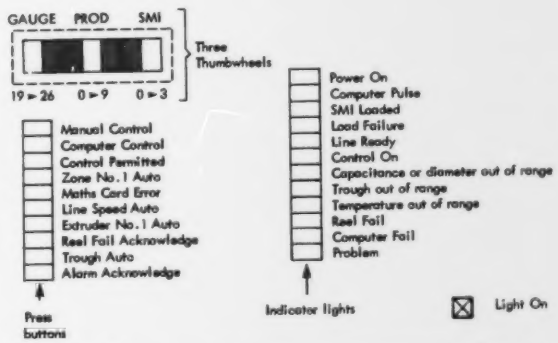


*Fig. 12. Operator panel for microprocessor control system.*

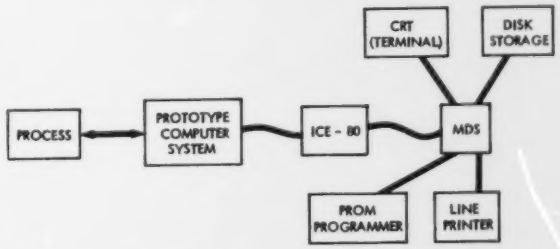


*Fig. 13. In circuit emulation.*

considerable amount of software to be written off-line (in a simulated mode). In the circuit emulation mode (*Fig. 13*), on line testing of the prototype system was carried out utilizing the debugging facilities of the ICE-80 software resident in the MDS. In the final stages of on-line testing the PROM programmer was used to "burn-in" the final program onto chips for locating on the SBC 80/20 board. The final program required 13 such chips (each chip had a capacity of 2048 bytes). The different product SMI's (shop manufacturing instruction) were stored on cassette tape which was activated when the product was selected. The amount of software development required for the system was considerably more than that for the previous system (Fox 2/30) and, even so, the final system did not provide any production reporting capability and had only limited parameter trending. However the hardware cost was also much less. In such a system there is extremely limited capability for experimenting or adjusting control modes other than by the use of tuning constants. Maintenance of the system is problematic (especially in a remote location), and the reliability of the system is heavily dependent on the installation and grounding. Improvements made in insulating line equipment and materials in the remote plant permitted a much simpler control system scheme to be adopted, obviating the need for a computerized control system—which would have necessitated the development of more sophisticated maintenance and diagnostic procedures. Therefore the system was not implemented in a production mode.

Today there are a number of small inexpensive systems which provide process control modules and more sophisticated software, permitting a small scale control system to be implemented. This should allow the installation of a per-line computerized control with much lower development and maintenance costs.

## CONCLUSION

We have not found it necessary to produce "dynamic simulation" models of the wire coating process, although "steady state" simulations have provided useful results in their own right. The dynamic behavior of a process can be rapidly (and practically) diagnosed by an on-line computer system with some process software modules (such as a variety of PID's, switch, summer and other modules) which are interfaceable to a high level language such as FORTRAN—such systems are on the market at a reasonable cost. The user should only ensure that adequate (and significant) process inputs and outputs are interfaced. From this point

experiments can rapidly indicate an adequate control strategy.

Steady state simulations have proved valuable and can be made as accurate as available input data. The main benefit has occurred in a relative sense rather than in the absolute sense—where the user compares the results of an experiment to the results of a simulation—the simulation can rapidly indicate in which direction design changes should be made and this reduces commissioning/experimental time in the factory.

## APPENDIX 1

*Figure 14* shows the node distribution across the extruder metering channel. The differential equation which is to be solved at each node is

$$\frac{d^2T}{dy^2} = -\frac{\tau^{\frac{n+1}{n}} e^{\frac{b}{n}(T-T_{ref})}}{J\ km_0^{1/n}} + \frac{\rho C_p}{k}\frac{DT}{Dt} \qquad \text{(A1)}$$

Neglecting the second (convection) term for the time being (this will be discussed later), the equation can be written in dimensionless form:

$$\frac{d^2T^*}{dy^{*2}} = -2\tau^{*\frac{n+1}{n}} e^{\frac{b}{n}T^*} \qquad \text{(A2)}$$

where

$$T^* = \frac{T - T_b}{\Delta T}$$

$$\Delta T = \frac{\tau_m \gamma_m H^2}{2Jk}$$

$$\tau_m = m_0 e^{-b(T_b - T_{ref})} \gamma_m{}^n$$

$$\gamma_m = \frac{V_z}{H}$$

$$y^* = \frac{y}{H}$$

$$b^* = b\Delta T$$

$$\tau^* = \frac{\tau}{\tau_m}$$

Thus

$$d^2T^* = -2\tau^{*\frac{n+1}{n}} e^{\frac{b^*}{n}T^*}\, dy^{*2} \qquad \text{(A3)}$$

At node $i$, this equation can be converted to finite difference form:

$$T^*_{i+1} - 2T_i^* + T^*_{i-1} = K_i^*\, e^{\frac{b^*}{n}T_i^*} \qquad \text{(A4)}$$

where

$$K_i^* = -2\tau_i^{*\frac{n+1}{n}} (\Delta y^*)^2$$

When the equations are expanded over the channel, the resulting vector $T_i^*$ can be solved provided $K_i^*$ is known (which itself is a function of $T_i^*$ and $\tau_i^*$).

A value for $\tau_i^*$ is available from $\tau^*_{i-1}\left(\tau_i^* = \Pi_p \Delta y^*\right.$ $\left. + \tau^*_{i-1}\right.$ where $\Pi_p$ is the dimensionless pressure gradient $\left.\frac{HP_z}{\tau_m}\right)$, and therefore if $\tau_1{}^*$ is guessed or known, all $\tau_i^*$ are available. The equations are solved iteratively:

$$\bar{T}^*_{(n+1)} = A^{-1}\bar{b}\ (\bar{T}^*_{(n)}), \quad \text{where} \quad \bar{T}^*_{(n+1)}$$

is the new set of temperatures at the $n + 1$ th iteration, and $\bar{b}$ is the right hand vector containing terms $T(n)^*$ available from the nth iteration. Once a solution for $T_i^*$ is available, the velocity vector $v_i{}^*$ can be immediately found:

$$v^*_{i+1} - v^*_{i-1} = -\left(\frac{T^*_{i+1} - 2T_i^* + T^*_{i-1}}{\Delta y^* \tau_i^*}\right) \qquad \text{(A5)}$$

A term for $v_i{}^*$ can be found from the equation

$$P_z = \frac{d\tau}{dy}.$$

Differentiating the term for $\tau$

$$\left[\frac{d}{dy}\left(m_0\, e^{-b(T\ -\ T_{ref})}\left(\frac{dv_z}{dy}\right)^n\right)\right]$$

the following expression can be derived

$$\frac{d^2v_z(i)}{dy^2} = \left(\frac{P_z}{n\tau_i} + \frac{b}{n}\frac{dT_i}{dy}\right)\frac{dv_z(i)}{dy} \qquad \text{(A6)}$$

When this equation is written in finite difference form and in dimensionless form, a term for $v_i{}^*$ can be found. The system algorithm proceeds as follows:

1: Define $\Pi_p$
2: Define $\tau_1{}^*$
3: Solve $\tau_i^*$
4: Solve $K_i^*$ (first iteration with $T_i = T_b$)
5: Solve $T_i^*$
6: Solve $v_i^*$ ($v_1{}^* = 0$)
7: $v_n{}^* = 1$?
8: If yes go to 10
9: go to step 2 and redefine $\tau_1{}^*$
10: compute $\Pi_q$ (dimensionless flow rate)
11: $\Pi_q$ = predefined $\Pi_q$?
12: If yes, this is a solution
13: If no, return to 1 and redefine $\Pi_p$

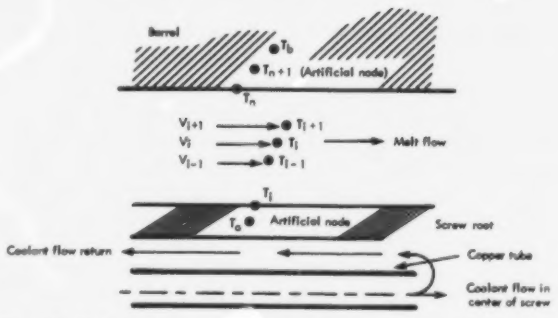


*Fig. 14. Node distribution across extruder metering channel.*

Although this system appears computationally excessive, acceleration methods can be employed which enable quite rapid convergence to be obtained. Furthermore as one proceeds helically along the extruder screw, the previous increment's solution can be used to define a new set of temperatures.

The temperature gradients at the screw root and barrel-melt interface may be readily introduced into the equation system by the use of "artificial" nodes.

**Screw Root**

$$T_{ys}^{\circ} = \frac{T_2^{\circ} - T_a^{\circ}}{2\Delta y^{\circ}}$$

or

$$T_a^{\circ} = T_2^{\circ} - 2\Delta y^{\circ} T_{ys}^{\circ}$$

The equation at $i = 1$ becomes

$$-2T_1^{\circ} + 2T_2^{\circ} = K_1^{\circ} e^{\frac{b^{\circ}}{n} T_1^{\circ}} + 2\Delta y^{\circ} T_{ys}^{\circ} \quad \text{(A7)}$$

Note that a value for $T_{ys}$ can be found from the coolant temperature and flow rate in a cooling tube in the centre of the screw (*Ref. 2*).

**Barrel-melt Interface**

At node $N$

$$k_b \left.\frac{dT}{dy}\right|_{\text{barrel}} = k_m \left.\frac{dT}{dy}\right|_{\text{melt}} \quad \text{(A8)}$$

Therefore

$$k_b \frac{T_b - T_N}{d} = k_m \frac{T_{N+1} - T_{N-1}}{2\Delta y} \quad \text{(A9)}$$

from which $T_{N+1}$ can be found. The equation at $i = N$ is

$$T_{N+1} - 2T_N + 2T_{N-1} = K_N e^{\frac{b}{n}(T_N - T_{md})} \quad \text{(A10)}$$

and the term for $T_{N+1}$ can be replaced with the value found from (A9) above. Then the equation is rewritten in dimensionless form.

**Convection Term**

The convection term $\frac{DT}{Dt}$ can be easily introduced into the system. $\frac{DT}{Dt}$ can be rewritten as $\frac{\partial T}{\partial t} + v_z \frac{\partial T}{\partial z}$ which in finite difference form at node $i$ can be written

$$\frac{T_i - T_i'}{\Delta t} + v_i \frac{T_i - T_i'}{\Delta z}$$

where $T_i'$ is the temperature at node $i$ in the previous increment, $\Delta z$ is the helical increment, and $\Delta t$ is given by the value for $\Delta z$ and average melt flow velocity. The equation set may readily be modified to incorporate this modification.

## NOMENCLATURE

| | |
|---|---|
| $b$ | Temperature coefficient of viscosity at constant shear rate |
| $C_p$ | Specific heat of melt |
| $H$ | Screw channel depth |
| $J$ | Mechanical equivalent of heat |
| $k$ | Thermal conductivity of melt |
| $m_0$ | Viscosity at reference temperature $T_{ref}$ and shear rate of 1 $sec^{-1}$ |
| $n$ | Power law index |
| $P_z$ | Pressure gradient (in downstream Z direction) (or axially in wire coating die) |
| $Q$ | Volumetric flow rate (in screw channel or in wire coating die) |
| $T$ | Temperature |
| $U$ | Temperature |
| $V_z$ | Relative velocity of parallel plates, or velocity of wire in die |
| $v_z$ | Velocity of melt in downstream ($z$) direction |
| $x$ | cross channel axis |
| $y$ | channel depth axis |
| $z$ | down channel (or die) axis |
| $\gamma_m$ | Drag shear rate ($V_z/H$) |
| $\rho$ | Melt density |
| $\tau_m$ | Shear stress at drag shear rate |
| $\tau_{yz}$ | Shear stress in $z$ direction at shear rate $\frac{dv_z}{dy}$ |

## REFERENCES


1. Z. Tadmor and I. Klein, "Engineering Principles of Plasticating Extrusion," Van Nostrand Reinhold Co. (1970).
2. R. T. Fenner, "Extruder Screw Design," ILIFFE Books, London, 1970.
3. V. L. LeNir, *Wire Journal*, pp. 59–64 (June 1974).
4. J. Calhoun and W. M. Flegal, WECo., Proc. 23rd International Wire and Cable Symposium, pp. 330–336 (1974).
5. V. L. LeNir, Proc. 25th International Wire and Cable Symposium, pp. 380–386 (1976).
6. V. L. LeNir, W. A. Cascarano, M. A. Shannon, Proc. 31st International Wire and Cable Symposium. pp. 38–44 (1982).
7. R. B. Gregory, SPE Proceedings pp. 114–118 (1969).
8. J. C. Ramsey, III, A. L. Fricke, and J. A. Caskey, *J. Appl. Polym. Sci.*, **17**, 1597 (1973).
9. N. M. Smith, J. Parnaby, *Polym. Eng. Sci.* **20**, 830 (1980).
10. R. D. Briggs and R. P. Guenther, *Mod. Plast.* from p. 126 (May 1963).


## DISCUSSION

*J. Vlachopoulos:* I would like to ask you about your steady-state simulation model. I notice that you have very good agreement between your predictions and the results that are given in Tadmor's book. In your model you were using the Darnell and Mol model for the solids conveying zone which requires the use of friction coefficients. You have taken the friction coefficients from the literature. A simple calculation using the Darnell and Mol model gives a pressure prediction which is very sensitive to the values of the friction coefficients

which means that the pressure values may be higher or lower by at least 50 percent depending on the values that you choose. Why do you have such good agreement?

*V. LeNir:* As I mentioned, I used the Chung modification for the solids conveying analysis. We used a finite difference method across the film to determine the temperature. The pressure rise was computed before and after melting at the solids barrel interface.

*J. Vlachopoulos:* When you start from the solids conveying zone with a small difference in the friction coefficient, no matter what else you do or what equations you solve, the pressure variation is exponential. This is true whether you see a value of 0.4 or 0.45, and who is going to measure the value that accurately in any case. The pressure may vary by 50 or even 100 percent.

*V. LeNir:* I found that as the pressure increased, melting occurred very rapidly. As the pressure builds up (and the time increment is made very small), a film of melt develops between the solid and the inside of the barrel. Therefore the whole picture changes and the pressure goes up and suddenly collapses as melting occurs.

*J. Vlachopoulos:* Do you mean that the model predicts all of that well?

*V. LeNir:* I don't know how good the actual values of the prediction are. We do see a rise and fall of pressure.

*J. Vlachopoulos:* However, you showed some results and the agreement was excellent between the results and your prediction.

*V. LeNir:* Well, I don't want to give that impression because we don't use the model in an absolute sense. I haven't done as much verification as I would like but when I obtained the verifications which I showed, I felt this was adequate for our needs. The program is used in a relative sense to show trends of behavior rather than to provide absolute results.

*M. R. Kamal:* I would like to follow up on that point. Suppose you start with experimental data and determine your friction factors from experimental fitting and then proceed. Would this be a better approach?

*J. Vlachopoulos:* The only thing which I am questioning is the absolute values. Now on a relative basis the pressure will go up and down. I even question the data in Tadmor's book since it looks too good to be right on. If you make a sensitivity analysis you will conclude that nobody can measure the friction coefficients that well. However, I suppose that the model is useful in a relative sense.

*V. LeNir:* It is important for us to see what the relative effects are. It is useful to know that there is an increase, then decrease of pressure in the feed zone.

*J. Vlachopoulos:* For relative comparison I accept that.

*I. Paterson:* I would like you to say a few more words on why you don't see the need for dynamic simulations, particularly for your control systems.

*V. LeNir:* We started a program to do dynamic simulations, after the extrusion steady-state simulation, but coincidentally we introduced the control computer, the Foxboro system (Fox 2/30), and the amount of time that we felt would be required for developing a control model did not seem to be justifiable. We were able to rapidly determine what control system would be suitable for a foam skin product without the need to go to dynamic simulation. Most projects in industry do require a measurable payback to justify an investment and this was a problem at the time.

*I. Paterson:* I think you have the same problem as you had for the steady-state simulation.

*V. LeNir:* We did the first work on the steady-state simulation model between 1971 and 1973. We did some updates to it in 1977 which lasted around 2 to 3 months. However since then, there has been a real problem of obtaining an adequate time frame (or about 6 to 9 months) to work on this sort of model. There is a requirement for rapid results. I don't know how a dynamic simulation could be justified or how long it would take to do a control model for the insulating process. I am sure dynamic stimulation is relevant in other industries, but in the wire coating industry we do not feel we have had the need.

*I. Paterson:* I don't think you know that at this point. As someone who is involved with control I would say that the dynamic simulation is going to do the same thing for your control and your control strategies as your steady-state simulation has done for your design problem.

*V. LeNir:* I've never gone into the control model but from your experience, how long would it take to do a control model?

*I. Paterson:* I don't want to turn the discussion into one on control models but essentially there is either a theoretical approach or an empirical approach, and if you want results quickly the one to use is the empirical approach. With that you will develop models and play with the models. It is almost always cheaper to play with the models then to play with the real production line to find out if there are other strategies that will give better production and tighter control. Maybe you can run the line faster.

*V. LeNir:* Unless you already have an experimental line available with a process control computer on it, in which case that is the way you would go. It is then very easy to look at the sensitivity of different parameters and link them together in a control mode.

*I. Paterson:* Yes, but you still need this in a dynamic sense.

*V. LeNir:* Yes. It still comes down to whether it is justifiable.

*I. Paterson:* My suspicion is that it probably would be. At least to the same extent as your steady-state

simulations.

*Y. Kuo:* I assume that your control system ultimately controls the coating thickness on the wire.

*V. LeNir:* Yes, the diameter and capacitance of the insulation.

*Y. Kuo:* I was surprised not to see any simulation of the die swell as related to all of the controllable variables which you have.

*V. LeNir:* No, we haven't gotten that far. We have a project at the moment that we hope will lead us to extensional viscosity and extensional effects in the process.

*G. Bata:* My question was somewhat similar. You do have all kinds of other variables on this process such as surface roughness, pinholing adhesion to the wire, ability to strip the telephone singles, and the like. How do you control those and how do you assure yourself that by only controlling some of the parameters you don't throw other parameters out of the process. In summary, how practical is your approach and how is it operating in practice.

*V. LeNir:* You mentioned pinholes, adhesion to the wire, surface roughness. We have not looked at surface roughness from a theoretical viewpoint nor from a control viewpoint. We would rely on a process engineer to make whatever changes he feels are necessary to the die in order to overcome a surface roughness problem. Sticking is a preheat type of problem. He would test the final wire, and make appropriate adjustments to the preheat.

*G. Bata:* You used to have a certain rejection rate because of quality problems per million feet, etc., beforehand. How does it compare after?

*V. LeNir:* I don't have any numbers but those problems can usually be solved acceptably by empirical changes.

*M. R. Kamal:* Could you give us more of an idea about the method for measuring the diameter of the fine wires?

*V. LeNir:* We use a laser mike. It is a typical diameter monitor and was purchased commercially.

*M. R. Kamal:* How accurate is the measurement?

*V. LeNir:* To about 0.0001 inch.

*M. E. Ryan:* You mentioned that in the wire coating die itself the shear rates might typically be in the order of $10^5$ or $5 \times 10^5$ sec. or higher. I presume that your characterization of the rheology of the materials is at much lower shear rates probably in the order to $10^3$ to $10^4$ $sec^{-1}$. Do you simply extrapolate the rheological behavior out to the higher shear rates?

*V. LeNir:* Yes.

# Residence Time Distribution in a Twin Screw Extruder

S. V. KAO *and* G. R. ALLISON

*Xerox Research Centre of Canada*
*2660 Speakman Drive*
*Mississauga, Ontario*

The residence time distribution (RTD) in a fully intermeshing, corotating twin screw extruder was determined with a stimulus-response technique. In addition to varying three process parameters (i.e. throughput, screw rotational speed, and barrel temperature), two screw configurations were also studied: one containing four kneading block mixing sections, and the other consisting only of regular screw bushings. Although screw configuration was an important variable, it was found that for both configurations the throughput had the largest effect on RTD. The screw rotational speed was second in importance, and the barrel temperature change produced no effect.

A fluid mechanical model based on the fluid flow in a partially-filled rectangular channel was used to explain the experimentally observed dependence of RTD on the process parameters. Reaction engineering approaches were adopted to compare the RTD results of two screw configurations with two idealized flows.

## INTRODUCTION

In recent years, due to their excellent conveying and compounding capabilities, twin screw extruders have gradually gained popularity in the polymer industry. Although all twin screw extruders have two screws, in most cases side-by-side, in a figure-8-shaped barrel their principles of operation can be very different, depending on whether the screws are corotating or counter-rotating, and on the degree of intermeshing between the two screws. For example, in a fully intermeshing, counter-rotating twin screw extruder material is enclosed in a C-shaped closed chamber and pushed forward in a positive displacement fashion, whereas in a fully intermeshing, corotating twin screw extruder material flows in a continuous channel as a result of the relative movement between the barrel and the screws. The work presented in this paper deals only with the latter case, i.e., a fully intermeshing, corotating twin screw extruder. A very good discussion on the characteristics of various twin screw extruders can be found in a recent publication by Rauwendaal (1).

The residence time distribution (RTD) in an extruder is a useful tool in determining optimal processing conditions for blending, dispersing, and polymerization applications. This is particularly true in the case of twin screw extruders where the complex geometry has so far prevented us from reaching the same state of knowledge that we have with the single screw extruders. Investigations of RTD in twin screw type equipment have been carried out by Todd (2) in a twin-rotor reactor and by Janssen *et al.* (3) in counter-rotating twin screw extruders. More recently, Rauwendaal (1) made comparisons between a corotating and a counter-rotating twin screw extruder by measuring the residence time distribution and Walk (4) did an extensive RTD study using a non-intermeshing, counter-rotating, twin screw extruder. Unquestionably, these studies have improved our understanding of the twin screw extrusion operations. In our RTD study on a corotating twin screw extruder, in addition to examining the effects of process parameters, i.e. throughput, screw rotational speed, and barrel temperature, on the residence time the role of screw configuration was also investigated. One of the screw configurations used in the study employed a large number of kneading blocks in four separate mixing sections, representing the case where extensive compounding was required. Another screw configuration consisted entirely of regular screw bushings, representing the other extreme where no additional mixing was needed.

Corotating twin screw extruders are often operated under starved-feeding conditions. The throughput in this case is determined solely by the rate the material is fed to the extruder. The fully filled zone stretches upstream from the die for several turns. A large length of the screw channel is only partially filled. Theoretical analysis of fluid flow in a partially filled screw channel was attempted by Werner (5) and Booy (6). Werner analyzed the fluid motion using the actual channel geometry. Because of the irregular shape of the boundary a numerical scheme had to be used. As a result, no explicit analytical form for the down channel velocity was available. Booy, on the other

hand, used a simplified geometry valid for a very small degree of fill and obtained only the average velocity of the liquid. In order to explain the experimental observations made during our RTD experiments, we tried a very simple model: the fluid flow in a partially filled rectangular channel. Calculations of average residence time based on this model correctly predicted the experimental results. Because of the availability of analytical solutions, it is hoped that this model will be helpful when one tries to understand what happens in a corotating twin screw extruder.

## EXPERIMENTAL

The fully intermeshing, corotating twin screw extruder, ZSK-30, is made by Werner & Pfleiderer. The diameter of the screw is 30.7 mm and the effective screw length is 870 mm. The ZSK-30 extruder has two-flighted screw elements, thus generating three parallel flow streams during operation. The drive power at the maximum rotational speed of 500 rpm is 9.0 kw. Six temperature control zones cover the barrel sections and the two-strand die.

In the RTD experiments a styrene-based copolymer was fed to the ZSK-30 extruder by a K-Tron loss-in-weight feeder. At steady state, tracer particles were added as a "pulse" through a side opening on the extruder feed hopper. Two types of tracers were used; one is a yellow dye soluble in the polymer and another a carbon black. Extrudate samples were collected every 10 seconds after tracer injection and the concentrations of tracer were determined with a UV spectrophotometer. For each processing condition, four RTD measurements were made. No significant difference between the two tracers was found.

The screws of the ZSK-30 extruder are assembled from individual screw elements. This building block design offers enormous flexibility in arranging different types of screw elements to suit any particular material or application. The regular helical-shaped screw bushings are used for conveying and pressure buildup. For blending and dispersing purposes, kneading blocks are employed. These kneading blocks are stacks of discs staggered by a certain angle. Usually several different kneading blocks are placed in series to form a kneading section. Several kneading sections are used during compounding operations to enhance polymer melting, additive dispersion and distribution. To examine the effect of screw configurations on the residence time distribution, two configurations (*Fig. 1*) were used. The first screw configuration has four kneading sections consisting of various kneading blocks. Reversed-flight (left-handed) screw bushings or kneading blocks are placed at the end of the kneading sections to keep material there for a longer period of time. The second screw configuration used in the experiment is a screw made completely of screw bushings. Since the channel depth is kept constant for self-wiping screws, the design of screw bushings has to rely on the changing pitch length to account for compression effect.

Three major process parameters, throughput, screw rotational speed, and barrel temperature, were varied at two levels to form a matrix of eight processing conditions. The experimental design for each screw configuration is shown in *Table 1*. Two barrel temperature profiles were used for the plasticating extrusion of the styrene-based copolymer. The set points of the *"high"* barrel temperature profile were respectively 180, 170, 170, 170, 170, and 200 for each of the six temperature control zones of the ZSK-30 extruder and those for the "low" barrel temperature profile were respectively 130, 120, 120, 120, 120, and 150. All temperature readings are in Celsius. In addition to these 8 processing conditions, several runs at a screw speed of 300 rpm were conducted.

## RESULTS AND DISCUSSION

The residence time distribution data are first examined in typical exit age distribution versus time plots (7). The discrete exit age distribution function is defined as:

$$E_i = \frac{C_i}{\sum_{i=1}^{n} c_i \Delta t} \tag{1}$$

where $C_i$ is the concentration of tracer in each sample and $\Delta t$ is the time span between successive samplings. In *Fig. 2*, the exit age distributions for two screw configurations are compared. The screw configuration 1, which has four kneading sections, kept material in the extruder for a longer period of time. This observation is true at all processing conditions. To examine the dependence of RTD on extrusion process parameters one quantitative means for characterizing the RTD curve, the mean residence time, is used. It is calculated according

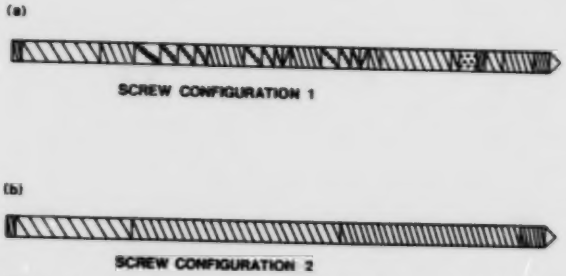


*Fig. 1. Screw configurations: a) screw configuration 1, b) screw configuration 2.*

**Table 1. Experimental Design.**

| | Throughput | Screw Speed | Barrel Temperature |
|---|---|---|---|
| 1 | L (4.54 kg/hr) | L (115 rpm) | L |
| 2 | H (13.6 kg/hr) | L | L |
| 3 | L | H (492 rpm) | L |
| 4 | H | H | L |
| 5 | L | L | H |
| 6 | H | L | H |
| 7 | L | H | H |
| 8 | H | H | H |

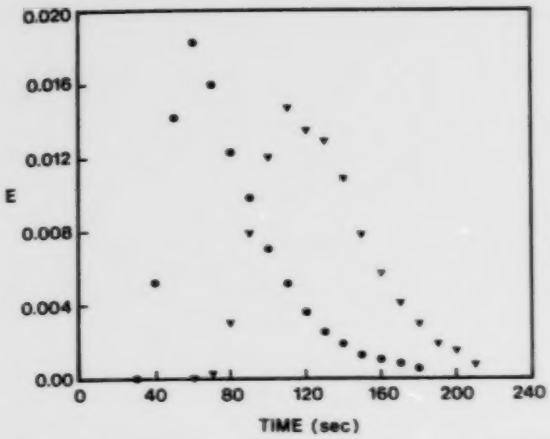


*Fig. 2. Exit age distributions for screw configuration 1 (▼) and screw configuration 2 (●) at 4.54 kg/hr, 492 rpm, and low barrel temperatures.*

to the relation:

$$\bar{t} = \frac{\sum_{i=1}^{n} t_i C_i \Delta t}{\sum_{i=1}^{n} C_i \Delta t} \qquad (2)$$

In *Fig.* 3, the dependence of the mean residence time on screw speed, throughput, barrel temperature profile, and screw configuration is shown. From this plot, the following observations were derived:

a) The throughput has by far the largest effect on the mean residence time. For screw configuration 1, the increase in throughput from 4.54 kg/hr to 13.6 kg/hr reduced the mean residence time by about 70 secs. For screw configuration 2 the reduction is about 40 secs.
b) The screw rotational speed also affects the mean residence time. Both screw configurations showed a reduction of approximately 30 secs. in the mean residence time, when the screw speed changed from 115 rpm to 492 rpm.
c) The screw configuration also affects the mean residence time. The all-screw bushing screw configuration 2 conveyed material faster than the kneading block loaded screw configuration 1. The reduction is larger at low throughput.
d) The barrel temperature profile has almost no effect on the mean residence time.
e) There is very little or no interaction among the three process parameters: throughput, screw speed, and barrel temperature profile.
f) There is interaction between throughput and the screw configuration.

The large dependence of the mean residence time upon the throughput was unexpected. We were feeding the ZSK-30 extruder at the low end of its capacity. (The ZSK-30 extruder is capable of extruding the styrene-based copolymer at a rate of 45.4 kg/hr or higher.) There was certainly more than enough space in the screw channel to accommodate the small increase in throughput from 4.54 to 13.6 kg/hr. In other words, a proportional increase in the filled volume in the partially filled channel when one increases the throughput, i.e. $Q$ = (constant) $f$, should not change the mean residence time. This can be easily shown by examining the relationship:

$$\tau = \frac{Vf}{Q} \qquad (3)$$

where $\tau$ is the average residence time or hold-up time, $f$ the degree of fill in the screw channel, and $Q$ the volumetric flow rate. However, the RTD results indicated that as more polymer was fed to the extruder the material inside the extruder channel actually moved faster. In order to explain this experimental observation, the relationship between the volumetric flow rate and the degree of fill needs to be established. A mathematical model of fluid flow in a partially filled rectangular channel was adopted. The theoretical development is described below.

Although the fluid flow in a fully intermeshing, corotating twin screw extruder is much more complicated than that in a single screw extruder, the bulk of the melt flow is still the drag flow (5, 6, 8). Therefore, drag flow in the screw channel bounded by the inner barrel surface, two screw flights, and the root of the screw, is considered here. In order to simplify the mathematical treatment, the cross-section of a screw channel is represented by a rectangle as shown in *Fig.* 4. The channel is partially

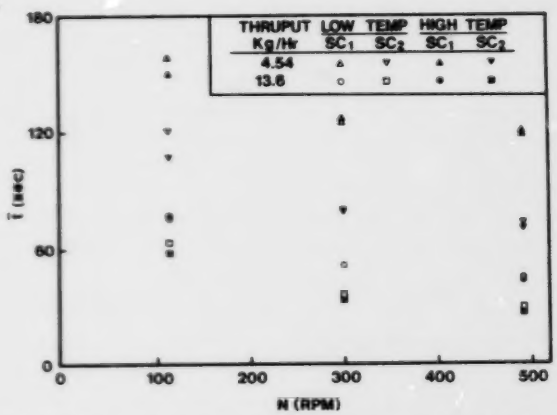


*Fig. 3. Mean residence time versus screw rotational speed, etc.*

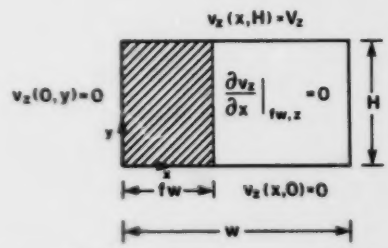


*Fig. 4. A partially filled rectangular screw channel.*

filled with fluid and the inner barrel surface is moving, in accordance with the practice commonly used in modelling a single screw extruder. This fluid mechanical problem is defined by the following set of partial differential equations and boundary conditions:

$$\mu\left(\frac{\partial^2 v_z}{\partial x^2}+\frac{\partial^2 v_z}{\partial y^2}\right)=0 \tag{4a}$$

$$\frac{\partial^2 v_x}{\partial y^2}=0 \tag{4b}$$

$$v_z = V_{bz} \quad \text{at} \quad y = H$$

$$v_z = 0 \quad \text{at} \quad x = 0$$

$$v_z = 0 \quad \text{at} \quad y = 0$$

$$\partial v_z/\partial x = 0 \quad \text{at} \quad x = fW$$

$$v_x = 0 \quad \text{at} \quad y = 0$$

$$v_x = V_{bx} \quad \text{at} \quad y = H$$

Note that the pressure gradient term vanishes in the case of a partially filled channel. Because the throughput is determined by the flow in the down channel direction (i.e., Z axis) only the Z component of the velocity vector, $v_z$, will be considered. In adopting the above equation, the underlying assumptions include: incompressible Newtonian fluid, no inertia effect, and steady isothermal operation. The solution of the above differential equation for the velocity component $v_z$ is:

$$v_z=\sum_{n=1,3..}^{\infty}\frac{4V_{bz}}{n\pi}\sin\left(\frac{n\pi}{2fw}\right)\times\frac{\sinh(n\pi/2fwy)}{\sinh(n\pi/2fwH)} \tag{5}$$

The volumetric flow rate per channel can then be calculated as:

$$\begin{aligned}Q&=\int_0^{fw}\int_0^{H}v_z\,dy\,dx\\&=\frac{16V_{bz}f^2w^2}{\pi^3}\sum_{n=1,3..}^{\infty}\frac{1}{n^3}\tanh\left(\frac{n\pi H}{4fw}\right)\\&=\frac{V_{bz}}{2}WHF_d\\&=\frac{\pi D\cos\varphi WH}{2}NF_d\\&=\alpha NF_d\end{aligned} \tag{6}$$

where

$\varphi$ = helical angle of screws

$N$ = screw rotational speed (in rpm)

$$F_d=\frac{32f^2w}{\pi^3H}\sum_{n=1,3..}^{\infty}\frac{1}{n^3}\tanh\left(\frac{n\pi H}{4fw}\right) \tag{7}$$

$$\alpha = \tfrac{1}{2}\pi D\cos\varphi WH \tag{8}$$

The same problem as described above has been treated by Squires (9) albeit for a different situation, i.e. a volatile extracting screw for the single screw extruder. To illustrate how we used the fluid mechanical model to explain the dependence of the mean residence time on the process parameters, we assume a hypothetical ZSK-30 whose screws are made completely of 28 mm pitch screw bushings. The characteristics of this extruder are:

free volume per channel (870 mm screws),

$V = 130\ \text{cm}^3$

$H = 0.478$ cm

$W = 1.18$ cm

$\varphi = 16.2°$

The average residence time in the extruder can be computed from the equation:

$$\begin{aligned}\tau&=\frac{Vf}{Q}\\&=\frac{Vf}{\alpha NF_d}\end{aligned} \tag{9}$$

Here, we use the term "*average residence time*" to differentiate it from the experimentally determined "*mean residence time*".

In the following, the average residence time as affected by each of the three process parameters will be discussed:

(a) The Dependence of Average Residence Time on the Throughput

Since $F_d$ is a complicated function of $f$ a plot of $F_d$ versus $f$ as shown in *Fig. 5* was prepared according to *Eq. 7* so that $f$ can be determined from the plot once $F_d$ is known. To examine the effect of $Q$ at a constant $N$, the value of $F_d$ is obtained from *Eq. 6* for a given $Q$. Then $f$ is obtained with the aid of *Fig. 5*. At $N$ = 115 rpm, the average residence time (*Eq. 9*) was calculated at various throughputs as shown in *Table 2*. In *Fig. 6* the average resi-

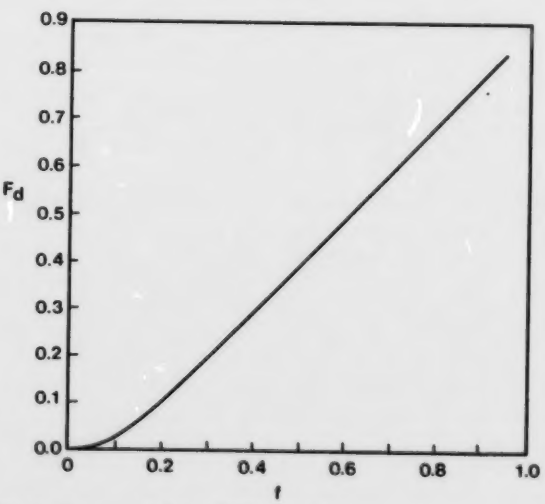


*Fig. 5. $F_d$ versus $f$ plot at $H/W = 0.405$.*

**Table 2. Average Residence Time *vs* Throughput at a Constant Screw Speed.**

| Throughput (kg/hr) | Q ($cm^3$/sec) | $F_d$ | f | $\tau$ (sec) |
|---|---|---|---|---|
| 4.54 | 0.4 | 0.0795 | 0.180 | 58.5 |
| 13.6 | 1.2 | 0.239 | 0.349 | 37.8 |
| 22.7 | 2.0 | 0.398 | 0.509 | 33.1 |
| 45.4 | 4.0 | 0.795 | 0.910 | 29.6 |

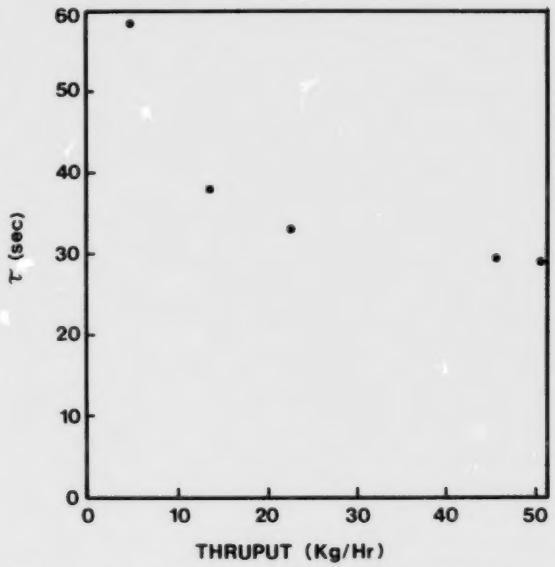


*Fig. 6. Average residence time versus throughput at 115 rpm.*

dence time is plotted against the throughput. Indeed, it shows a decrease with increasing throughput, as was observed experimentally for the mean residence time. Another point worth noting is the variation of the volumetric flow rate $Q$ (or throughput) with the degree of fill $f$. In *Table 2* it is seen that the throughput triples from 4.54 to 13.6 kg/hr when the degree of fill is approximately doubled. According to the fluid mechanical model, this extra capacity is possible because the fluid-air boundary moves away from the stationary rear flight as the degree of fill increases. As a result, the fluid moves faster and the conveying capability of the screw increases.

(b) The Dependence of Average Residence Time on the Screw RPM

At a constant throughput, the degree of fill varies with the screw rotational speed $N$. This relationship can be obtained from *Eq. 6* and *Fig. 5*. Once $f$ is known, the average residence time is simply $(V/Q)f$. As can be seen from the equation $Q = \alpha N F_d$ when $N$ increases, $F_d$ will decrease. Consequently, the degree of fill, and the average residence time, will all decrease, in agreement with the experimental observations. In *Table 3*, the variation of $f$ and $\tau$ with $N$ was calculated at a throughput of 13.6 kg/hr. *Figure 7* shows the decrease of the average residence time with increasing screw speed.

(c) The Dependence of Average Residence Time on the Barrel Temperature Profile

In the equation calculating the average residence time $\tau = Vf/\alpha N F_d$, none of the quantities is temperature dependent. Therefore, the average residence time should be independent of the barrel temperature. This is what we observed experimentally when the barrel temperature profile was raised by 50°C.

The treatment carried out above has shown that a simple fluid mechanical model is capable of explaining the dependence of the mean residence time on the process parameters. It should be noted, however, that we have made a number of assumptions and simplifications along the way. In addition to the assumptions imposed in writing down the Navier-Stokes equation, we have neglected the leakage flow, the curvature of the screw channel, and the curvature of the screw root. We have also implied that the dependence of the mean residence time on the process parameters came mainly as a result of the difference in conveying capacity in the partially filled sections. The solid conveying zone, melting zone, and the completely filled metering zone (which is very short, probably one or two $D$ in length for the particular polymer used) either behaved similarly to the partially filled section or

**Table 3. Average Residence Time *vs* Screw Speed at a Constant Throughput.**

| N (rpm) | $F_d$ | f | $\tau$ (sec) |
|---|---|---|---|
| 115 | 0.239 | 0.349 | 37.8 |
| 200 | 0.137 | 0.244 | 26.4 |
| 300 | 0.0915 | 0.194 | 21.0 |
| 400 | 0.0686 | 0.165 | 17.9 |
| 500 | 0.0549 | 0.146 | 15.8 |

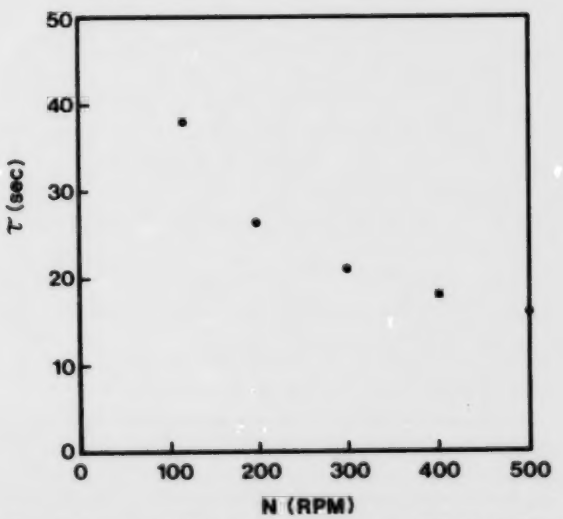


*Fig. 7. Average residence time versus screw rotational speed at 13.6 kg/hr.*

did not make any contribution to the difference in residence time.

Experimentally, it is observed that the screw configuration also had a major effect on the mean residence time. This is understandable, because of the low conveying capability of the kneading blocks as compared with the screw bushings. To explain the experimental observations by a mathematical model of fluid flow in the kneading section, however, is very difficult. Instead, we shall examine the two screw configurations with a different approach.

In chemical reaction engineering, models are used to characterize non-ideal flow within reaction vessels. Two basic models for ideal flow are often used to build up more complicated models. One of the two models is the plug flow model in which a flat velocity profile is assumed. The necessary and sufficient condition for plug flow is for the residence time in the reactor to be the same for all elements of fluid. The other ideal flow model is the so called mixed flow model. As the name suggests, the contents inside the vessel are well mixed and uniform throughout. Thus, the exit stream from the vessel has the same composition as the fluid within the vessel.

To compare our experimental results with the two ideal flow models, the cumulative exit age distribution function $F(\theta)$ is calculated using the following equation:

$$F_j(\theta) = \frac{\sum_{1}^{j} C_i}{\sum_{1}^{n} C_i} \qquad (10)$$

where $\theta = t/\bar{t}$ is the dimensionless time. In *Fig. 8*, the cumulative exit age distribution function for two screw configurations at identical processing conditions, i.e. 492 rpm screw speed, 4.54 kg/hr throughput, and low barrel temperatures, and those of the ideal flow models are plotted.

A similar plot of data obtained at a different processing condition (i.e. 115 rpm, 4.54 kg/hr, and high barrel temperatures) is shown in *Fig. 9*. Both plots and others not shown here indicate that the screw configuration 1, which has four kneading sections to improve mixing, actually has an exit age distribution function closer to that of the plug flow than the screw configuration 2 does. Very similar findings were also reported recently by Walk (4) using a different twin screw extruder, the non-intermeshing counter-rotating twin screw extruder, and three different screw configurations: a low work screw containing no mixing elements and relatively deep channels, a medium work screw containing some mixing elements, and a high work screw containing reversed-flight mixing elements.

The reason why a screw configuration with a large number of mixing sections (SC1) should have a cumulative exit age distribution more characteristic of the plug flow than a plain screw (SC2) is still not clear. One thing worth noting is that, when the extruder is being starved-fed, the kneading sections due to their low conveying capability will tend to accumulate material, thus behaving more or less like a series of holding tanks. This may have influenced the residence time distribution, in addition to slowing down the tracer flow rate. Lacking a complete picture of how material flows in the kneading section, our recommendation is to interpret the $F(\theta)$ information from a twin screw extruder with caution. Further RTD study focussing on the kneading sections is, therefore, warranted.

## CONCLUSIONS

The residence time distribution in a fully intermeshing, corotating twin screw extruder was studied using a stimulus-response technique for two different screw configurations, one with four kneading sections and another with no kneading sections, at various processing conditions (i.e. throughput, screw rotational speed, and barrel temperature profile). The mean residence time was then calculated from the RTD curve.

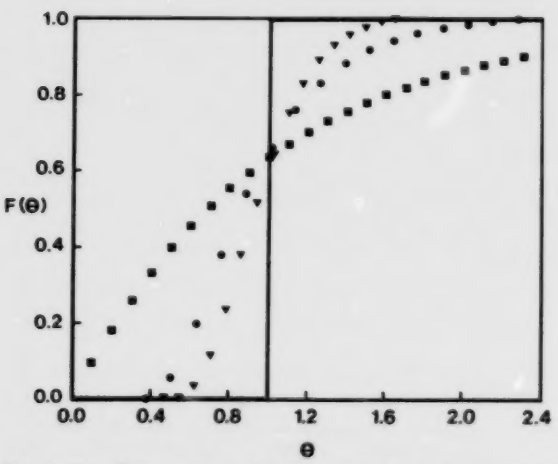


*Fig. 8. Cumulative exit age distribution functions for screw configuration 1 (▼), screw configuration 2 (●), perfect mixed flow (■), and plug flow (—) at 4.54 kg/hr, 492 rpm, and low barrel temperatures.*

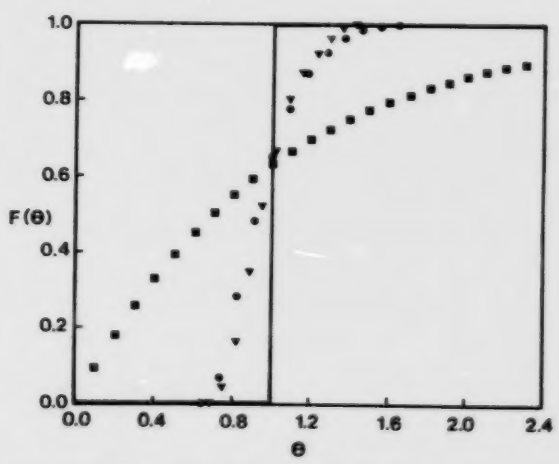


*Fig. 9. Cumulative exit age distribution functions for screw configuration 1 (▼), screw configuration 2 (●), perfect mixed flow (■), and plug flow (—) at 4.54 kg/hr, 115 rpm, and high barrel temperatures.*

The throughput has the largest effect on the mean residence time. Increasing the throughput reduces the mean residence time. The dependence of the mean residence time upon the throughput was explained in terms of a simple mathematical model of fluid flow in a partially filled rectangular channel. According to the model, the decrease in the mean residence time is the result of the increase in down-channel velocity when the degree of fill is increased. The model also predicts the decrease of the mean residence time with increasing screw rotational speed and the independence of mean residence time on the barrel temperature change. One can thus conclude that the model, although quite simple, has correctly predicted the variation of the mean residence time with the throughput, screw speed and barrel temperature. Therefore, it is felt that this model offers a convenient tool in studying various processes taking place in a corotating twin screw extruder.

An approach borrowed from reaction vessel characterization, i.e. the cumulative exit age distribution of ideal and real flows, was adopted to compare the two screw configurations. Surprisingly, the screw configuration with four kneading sections showed a flow characteristic closer to the plug flow model than the plain screw. So far, we haven't been able to offer a satisfactory explanation for this observation. Further RTD study focussing on the kneading sections is, therefore, warranted.

## NOMENCLATURE

$C_i$ = tracer concentration
$D$ = diameter of screw
$E_i$ = cumulative exit age distributions
$F_d$ = $\dfrac{32f^2w}{\pi^3 H} \sum_{n=1,3..}^{\infty} \dfrac{1}{n^3} \tanh\left(\dfrac{n\pi H}{4fw}\right)$
$f$ = degree of fill
$H$ = height of screw channel
$L$ = length of screw
$N$ = screw rotational speed
$Q$ = volumetric flow rate
$t$ = time
$\bar{t}$ = mean residence time
$V$ = free volume in the extruder barrel
$V_{bz}, V_{bx}$ = velocity components of a moving barrel
$v_x, v_y$ = velocity components of fluid in the screw channel
$W$ = width of screw channel
$x, y$ = Cartesian co-ordinate system
$\alpha$ = $\pi D \cos\varphi WH/2$
$\tau$ = average residence time
$\varphi$ = screw helical angle
$\theta$ = dimensionless time, $\theta = t/\bar{t}$

## REFERENCES


1. C. J. Rauwendaal, *Polym. Eng. Sci.*, **21**, 1092 (1981).
2. D. B. Todd, *Polym. Eng. Sci.*, **15**, 437 (1975).
3. L. P. B. M. Janssen, R. W. Hollander, M. W. Spoor, and J. M. Smith, *AIChE J.*, **25**, 345 (1979).
4. C. J. Walk, *SPE ANTEC Tech. Papers*, **28**, 423 (1982).
5. H. P. Werner, Ph.D. Dissertation, University of Technology of Munchen, West Germany (1976).
6. M. L. Booy, *Polym. Eng. Sci.*, **20**, 1220 (1980).
7. O. Levenspiel, "Chemical Reaction Engineering", Ch. 9, John Wiley, New York (1972).
8. K. Burkhardt, H. Hermann, and S. Jakopin. *SPE ANTEC Tech. Papers*, **24**, 498 (1978).
9. P. H. Squires, *SPE Journal*, **14**, 5, 24 (1958).


## DISCUSSION

*C. I. Chung:* I would like to offer some constructive comments and suggestions. First of all, you stated that your main theoretical contribution is the calculation of pumping efficiency of partially filled channels. I believe that the pumping efficiency of partly filled channels for Newtonian fluids was analyzed and published before. If you cannot find the reference I can perhaps help you, but it was done to the best of my recollection.

*S. V. Kao:* It was pointed out in our paper that a similar calculation was carried out by Squires. He analyzed the vacuum extraction section of a single screw extruder where the channel was partially filled with melt.

*C. I. Chung:* I checked your references and that particular paper. I don't recall exactly but I don't think it was listed. However, I do remember seeing it. The partially filled channel has a higher pumping efficiency than the completely filled channel. Physically this is easy to understand because each screw flight face serves as a dead space so that if it is partially filled you have only one dead space while if it is completely filled you have two dead spaces. So I feel that your main contribution is probably on the experimental side. Furthermore, in your boundary condition regarding velocity $V_z$, the derivative with respect to $X$ is zero at the free boundary, which is correct, but it seems that you kept that boundary condition until the completely filled condition as shown in the figure where $F_D$ increases linearly to $F_W = 1$, which shouldn't be.

*S. V. Kao:* Yes. There is a discontinuity in this boundary condition. (The authors would like to thank Dr. C. I. Chung for pointing out this mistake in the drawing).

*C. I. Chung:* When $F_W$ becomes unity the boundary condition should be such that $V_z = 0$, that is, wetted perimeter. I think you'll find that the curve is not linear; it has to drop off. Also, you use a mean residence time and average residence time.

*S. V. Kao:* What I meant there was that mean residence time was calculated from experimental data whereas the average residence time represented a theoretically obtained value, that is, volume divided by the volumetric flow rate.

*C. I. Chung:* I don't think the use of mean residence time and average residence time was distinctly clear to me and I don't think that the use of mean follows the usual definition of mean in a mathematical sense.

*S. V. Kao:* The use of mean residence time to characterize a residence time distribution curve and the equation for calculating it can be found in a popular book, "Chemical Reaction Engineering", written by Levenspiel.

# Mathematical Modeling of Squashing Flows of Heated Polymer Particles

YOUTI KUO

*Xerox Corporation*
*Joseph C. Wilson Center for Technology*
*Rochester, New York 14580*

A combination of shear and extension is encountered in the squashing flows of heated polymer particles. Extensional rate affects the non-Newtonian viscosity in determining the flow field in the squashing of cylindrical particles, but both the extensional and shear rates are equally important for disc-like particles.

A viscous-type constitutive equation is used for simplicity. The solution of the momentum equations satisfying no-slip boundary conditions leads to a particle flattening equation that can predict flattening ratios of nonisothermal particles in terms of rheological parameters and dimensionless groups of process variables. Application of this analysis to roll fusing of toner particles in copiers is described in a companion article in this issue.

## INTRODUCTION

The squeezing flows of viscoelastic films have been analyzed by many investigators (1), but there has been no analysis of the squashing flow of viscoelastic particles. The most notable application of squashing flow analysis is in the roll fusing of dry toners in the xerographic processes of copier machines. In evaluating the quality of xerographic copies, the deformation of toner particles on papers can be used as a measure of the fix level of xerographic images; the deformation can also be used for evaluating the rheological properties of toner materials.

This paper is the first of two on the mathematical modeling of roll fusing of toner particles in xerographic copiers. This paper analyzes the kinematics of particle deformation to capture the dominant rheological parameters. Some sacrifices in secondary factors have been made in order to simplify the mathematics and to make the complex problem tractable.

The second paper (2) applies the analysis to the squashing of particles under various contact conditions on rough papers in a simulation of the roll fusing process. In addition to the theoretical description, the second paper compares model predictions and gives experimental results from analyses of a large number of toner particles.

Technically, the squashing flow of heated polymer particles is a combination of extension and shear and involves thermal gradients. Since the particles are, in general, viscoelastic, rigorous analyses using constitutive equations and satisfying the momentum equations and boundary conditions are extremely difficult. Simplifications are needed to deal effectively with the problem.

Many of the previous analyses (1, 3) have approximated the flow kinematics of squeezing flows. These approximations may be valid for the geometry of films but not for particles whose shapes are more cylindrical.

Most of the studies regarded the squeezing flow field as a shear flow. Consequently, the contribution of the extensional element of the flows was not considered. At the other extreme, the importance of the extensional element was recognized (4) but emphasized using an elaborate nonlinear constitutive equation which limited itself to pure extension, thus neglecting the effects of no-slip boundary conditions and shear.

This analysis is more realistic in modeling the flattening of polymer particles (aspect ratios close to unity) in that it first analyzes the compound nature of shear and extension in squashing flows and identifies the two modes of deformation and their effects on the velocity and pressure fields.

For simplicity and to make specifying rheological properties feasible, the model uses a separable functional form at the outset to approximate the dependency of the non-Newtonian viscosity on temperature and strain rate. Furthermore, instead of using a steady state value, an average of transient viscosity over dwell time period will be used. It will be shown that for a power-law extensional viscosity, the particle flattening equation can produce master curves for indicating flattening ratios in terms of rheological parameters and a dimensionless group of process variables.

## SQUASHING FLOWS OF CYLINDRICAL PARTICLES

The flow characteristics and approaches used in the analysis are as follows:

1. The particle shapes are treated as right-circular cylinders;
2. The velocity has axial and radial components (see *Fig. 1*), and the particle deformation is a combination of shear and extension (in the radial direction);
3. One contact surface has uniform compressive velocity relative to the other in parallel, and no-slip conditions prevail on both contact surfaces;
4. Surface tension has little effect in restricting spreading compared to the dominant effect of pressure gradients;
5. Flow is nonisothermal and non-Newtonian; and
6. Particles are liquid-like rather than solid-like at elevated temperatures.

To simplify the mathematics, some specific approximations are used in the following analysis.

## Governing Equations

With respect to the cylindrical coordinate system defined in *Fig. 1*, the equations of motion expressed by the balance of stress components are

$$\frac{\partial \tau_{rr}}{\partial r} + \frac{\partial \tau_{rz}}{\partial z} + \frac{\tau_{rr} - \tau_{\phi\phi}}{r} = 0, \tag{1}$$

and

$$\frac{\partial \tau_{rz}}{\partial r} + \frac{\partial \tau_{zz}}{\partial z} + \frac{1}{r}\tau_{rz} = 0. \tag{2}$$

The equation for the angular direction is ignored because of the axisymmetric condition of the flow. Because of the high melt viscosity, the contribution of flow inertia is also neglected in the above equations. Explicit forms of the stress components relating the deformation gradients and rheological properties will be used to find the velocity components.

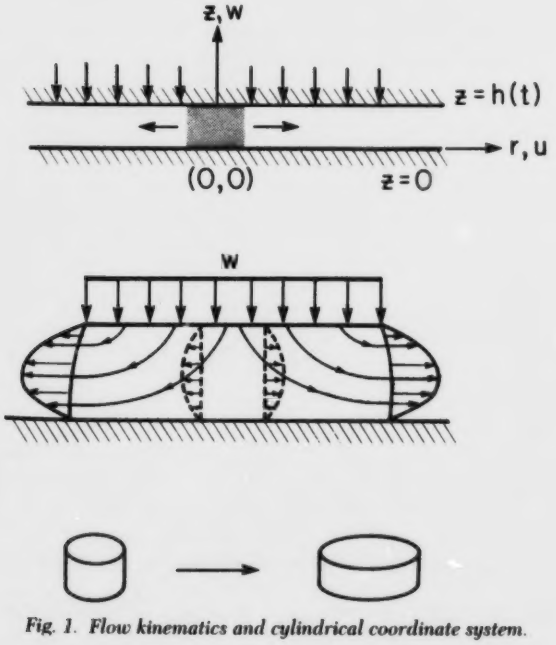


*Fig. 1. Flow kinematics and cylindrical coordinate system.*

The flow should satisfy the continuity equation,

$$\frac{\partial u}{\partial r} + \frac{u}{r} + \frac{\partial w}{\partial z} = 0, \tag{3}$$

where $u$ and $w$ are the radial and axial components, respectively (see *Fig. 1*). The solution of $u$ in terms of $w$ is

$$u = -\frac{1}{r}\int_0^r r\frac{\partial w}{\partial z}\,dr. \tag{4}$$

In addition to the prior assumptions of parallel contact surfaces and uniform surface velocity, we further assume that the first-order solution of the axial velocity, $w$, is independent of $r$. By neglecting the second-order and higher terms that would depend on $r$, we choose to use the velocity, $w$, of the following form throughout the analysis:

$$w = w(z, t). \tag{5}$$

Then, from *Eq. 4* we can obtain the first-order solution of $u$ as follows:

$$u = -\frac{r}{2}\frac{\partial w}{\partial z}. \tag{6}$$

The radial velocity increases linearly with both the radius and the axial velocity gradient (extensional strain rate). The latter is determined through the use of momentum equations (*Eqs. 1* and *2*) in conjunction with a constitutive equation of the stress and strain rate. The simple form above enables finding an analytical solution of the complex flow situation being dealt with.

## Working Constitutive Equation

### *Viscous-type Equation*

To determine the velocity components, explicit forms for the stress tensor are needed for solving momentum equations (*Eqs. 1* and *2*). There are a number of constitutive equations in the literature which describe behaviors of viscoelastic fluids. Generally, they can be used for simple flow situations such as pure shear or pure extension, but their mathematics for the case of combined shear and extension are too complex to be used in the momentum equations.

For practical purposes, a "viscous-type" constitutive equation is constructed here. Instead of fitting stress and strain data at steady state as in the case of a viscous constitutive equation, the viscous-type equation is for fitting transient data (of viscoelastic fluids) in process ranges. By using the effective viscosity within the dwell time region, the viscous-type constitutive equation can be written as:

$$\boldsymbol{\tau} = -p\boldsymbol{I} + \tfrac{1}{2}\,\eta_{eff}(T, \mathrm{II}_D)\boldsymbol{D} \tag{7}$$

where $\boldsymbol{I}$ and $\boldsymbol{D}$ are the unit tensor and deformation tensor, respectively, and $p$ is the hydrostatic pressure. The effective viscosity, $\eta_{eff}$, is expressed as a function of temperature, $T$, and the second invar-

iant, $\Pi_D$, of $D$. The explicit forms of the above equation are given in *Appendix I*.

For the squashing flow, as indicated in *Appendix I*, the viscosity depends on the combined shear and extensional rates:

$$\eta_{eff}(T, \Pi_D) = \eta_{eff}\left[T, \frac{3}{4}\left(\frac{\partial w}{\partial z}\right)^2 + \frac{r^2}{16}\left(\frac{\partial^2 w}{\partial z^2}\right)^2\right] \quad (8)$$

↑ extensional rate ↑ shear rate

*Viscosity at Dominant Strain Rate*

Because of the complexity of the functional dependency as shown above, there has been no experimental method available to measure this type of viscosity. Nevertheless, by examining the order of magnitudes of the two types of strain rates, the above form reveals that the shear rate dominates the deformation in the region of large radius, whereas the extensional rate dominates in the region of small radius. These two extreme conditions can be expressed as

$$\eta_{eff} \to \tilde{\eta}\left[T, \frac{r^2}{16}\left(\frac{\partial^2 w}{\partial z^2}\right)^2\right], \quad \text{as} \quad \frac{r}{h} \gg 1, \quad (9a)$$

(shear viscosity)

and

$$\eta_{eff} \to \tilde{\eta}_e\left[T, \frac{3}{4}\left(\frac{\partial w}{\partial z}\right)^2\right], \quad \text{as} \quad \frac{r}{h} \ll 1, \quad (9b)$$

(extensional viscosity)

where $\tilde{\eta}$ and $\tilde{\eta}_e$ denote, respectively, the effective shear and extensional viscosities within the dwell time.

The above are characteristic of the deformation gradients of squashing flows. It is shown in later sections that the velocity components are primarily affected by the extensional viscosity, and the pressure distribution at large radii is also additionally affected by the shear viscosity.

*Viscosity Model—Shear and Extension*

For simplifying computations, a power-law functional form is used to represent the effective viscosity data in the time region of interest:

$$\tilde{\eta}_e = \lambda(T)\Pi_D^{m/2} \quad (10)$$

Based on the above form and according to *Eqs. 8* and *9b*, the effective viscosity encountered in the flow field close to the center of the cylinder is

$$\tilde{\eta}_e = \alpha(T)\left|\frac{\partial w}{\partial z}\right|^m, \quad \frac{r}{h} \ll 1 \quad (11)$$

in which $\alpha(T)$ is $\lambda(T)\,(3/4)^{m/2}$, whereas the effective viscosity of the flow field far away from the center becomes

$$\tilde{\eta}_e = \alpha(T)\left(\frac{1}{3}\right)^{m/2}\left[\frac{r}{2}\left|\frac{\partial^2 w}{\partial z^2}\right|\right]^m, \quad \frac{r}{h} \gg 1 \quad (12)$$

When the power-law form is used to fit extensional viscosity data, the same power-law index should be used in *Eq. 2*, even though the flow field ($r/h \gg 1$) is predominantly shear. This is in conflict with the fact that the power-law index of shear flow of a real fluid may differ from the index of its extensional flow. This indicates the deficiency of the single power-law index model. In engineering applications, if we regard the power-law index as dependent on the range of strain rate, then different index values can be used: extensional viscosity index for the flow near the cylinder axis and shear viscosity index for the flow in large radius. This argument is interesting from the viewpoint that the viscosity curve of squashing flows may have a behavior as illustrated in *Fig. 2*.

Apart from the single power-law index model of *Eq. 10*, in practice one may use the shear viscosity for large radius. The shear viscosity has different power-law index, as denoted by $-n$ as

$$\tilde{\eta}_e = \beta(T)\,\frac{r}{2}\left|\frac{\partial^2 w}{\partial z^2}\right|^{-n}, \quad \frac{r}{h} \gg 1 \quad (13)$$

The above formulation is a violation of *Eq. 10*, but it suggests that the power-law model should be replaced by a model that can satisfy both extreme cases as given in *Eqs. 11* and *13*.

## Determinations of the Velocity Field

As stated previously, the first-order solution of the axial velocity is independent of the radius. With this approximation plus the fact that the extensional viscosity is the principal rheological property to be considered in the small radius region, the velocity field can be derived by first determining the axial velocity at small radius which involves only the extensional viscosity.

By substituting the stress components in (I-1), (I-2), and (I-3) into the momentum Equation (*Eq. 1*), one obtains

$$\frac{\partial p}{\partial r} + \frac{r}{2}\frac{\partial}{\partial z}\left[\tilde{\eta}_e \frac{\partial^2 w}{\partial z^2}\right] = 0 \quad (14)$$

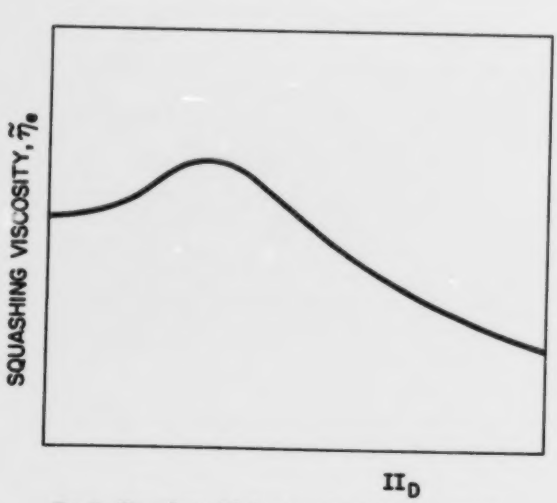


*Fig. 2. Hypothetical behavior of squashing viscosity.*

The boundary conditions to be satisfied by the solution of the axial velocity, $w$, are:

$$w = 0, \quad \text{at} \quad z = 0; \tag{15a}$$

$$w = W(t), \quad \text{at} \quad z = h(t); \tag{15b}$$

and

$$\frac{\partial w}{\partial z} = 0 \ (u = 0) \quad \text{at} \quad z = 0 \quad \text{and} \quad z = h(t); \tag{15c}$$

where the last condition obtained through the use of *Eq. 6* implies no-slip on contact surfaces. The surface velocity, $W(t)$, is to be related to contact pressure. Assuming no temperature gradient in the radial direction, the change of the extensional viscosity, $\tilde{\eta}_e$, is mainly in the axial or $z$ direction. To satisfy the above equation, it is clear that the pressure, $p$, may have the following form (3):

$$p = a(t)r^2 + f(z, t), \tag{16}$$

where $a$ and $f$ are to be determined.

Substituting *Eqs. 16* and *10* into *Eq. 14* and integrating the latter with respect to $z$, one finds the local extensional rate occurring in the squashing of a cylindrical particle to be:

$$\frac{\partial w}{\partial z} = -(m+1)^{\frac{1}{m+1}} \cdot \left\{-4a(t)\int_0^z \frac{z}{\alpha(T)}\,dz + q_1(t)\int_0^z \frac{dz}{\alpha(T)}\right\}^{\frac{1}{m+1}} \tag{17a}$$

The above form satisfies the no-slip boundary condition, $u = 0$, at $z = 0$. For $q_1(t)$ to satisfy a similar condition at $z = h$, it should be

$$q_1(t) = \frac{4a(t)\displaystyle\int_0^h \frac{z}{\alpha(T)}\,dz}{\displaystyle\int_0^h \frac{dz}{\alpha(T)}} \tag{17b}$$

It should be pointed out that because of no-slip conditions, the extensional rates on both contact surfaces are zero [see *Eq. 6*].

To find the axial velocity, $w$, an integration of *Eq. 17* with respect to $z$ leads to the following solutions:

$$w(z, t) = W(t)\frac{Q(z, t)}{Q(h, t)}, \tag{18}$$

where

$$Q(z, t) = \int_0^z \left[-\int_0^{z'} \frac{z''}{\alpha(T)}\,dz'' + \frac{\displaystyle\int_0^h \frac{z'}{\alpha(T)}\,dz'}{\displaystyle\int_0^h \frac{dz'}{\alpha(T)}}\int_0^{z'} \frac{dz''}{\alpha(T)}\right]^{\frac{1}{m+1}} dz', \tag{19}$$

in which $\alpha(T)$ depends upon the temperature. The radial velocity, $u$, can be determined simply by *Eq. 6*.

### Determination of Pressure Distributions

The surface velocity, $W(t)$, of the particle cylinder, which is the interfacial velocity of the contact surface, is related to the contact force (varying with the local pressure). The relationship can be found by solving the momentum Equation (*Eq. 2*) to determine the pressure distribution inside the particle in spreading.

After using (I-2) and (I-3), *Eq. 2* can be rewritten as

$$\frac{1}{r}\frac{\partial}{\partial r}\left(r\tilde{\eta}_e\frac{\partial u}{\partial z}\right) - \frac{\partial p}{\partial z} + 2\frac{\partial}{\partial z}\left(\tilde{\eta}_e\frac{\partial w}{\partial z}\right) = 0. \tag{20}$$

In a squashing situation, although the particle cylinder is under pressure, no pressure is on the spreading front (free surface, see *Fig. 3*).

Thus, one can select the boundary condition for *Eq. 20* to be:

$$p = 0 \quad \text{at} \quad z = h(t), \qquad r = R(t). \tag{21}$$

The profile of the flow front is curved due to nonuniform radial velocity. However, the particle during flow will be treated as a right circular cylinder. The neighborhood at the edges of wall/fluid interface is filled in by "fountain flow," accelerated from the center of the gap. Rigorously, a free surface condition should be used. An attempt to improve the boundary conditions, *Eq. 21*, by forcing the average of the radial stress at the flow front be zero was discussed (5) for compressive Newtonian flow between parallel disks.

By using the form used in *Eq. 16* for $p$, the solution for the pressure can be expressed in terms of $w$ as

$$p = a(t)(r^2 - R^2(h)) + \int_z^h \tilde{\eta}_e\frac{\partial^2 w}{\partial z^2}\,dz + 2\tilde{\eta}_e\frac{\partial w}{\partial z} \tag{22}$$

The complete solution is obtainable by using the explicit form of $\tilde{\eta}_e$ and the solution $\partial w/\partial z$. Despite the complexity of the above solution, the contact pressure of interest here is

$$p(z = h) = a(t)(r^2 - R^2), \tag{23}$$

which is parabolic.

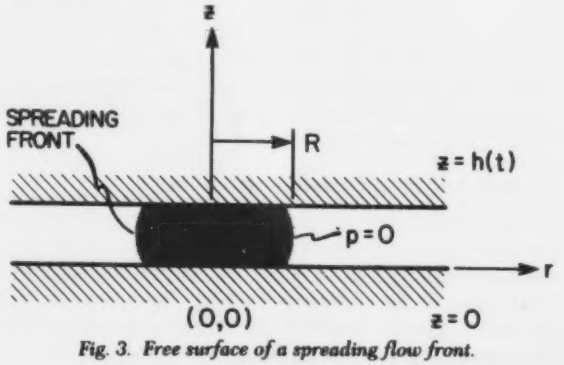


*Fig. 3. Free surface of a spreading flow front.*

The contact force, $F$, can then be evaluated as:

$$F = \int_0^R \tau_{zz}(z = h) \cdot 2\pi r \cdot dr$$

$$= -\int_0^R p(z = h) \cdot 2\pi r \, dr \qquad (24)$$

$$= -\frac{1}{2} \pi a R^4$$

Note that according to (I-3) $\tau_{zz}$ is equal to $-p$ at the contact surface because of the zero extensional rate. Thus, from *Eq. 24* one obtains

$$a(t) = \frac{-2F(t)}{\pi R^4(t)}. \qquad (25)$$

Consequently, by substituting *Eq. 25* into *Eq. 16* and by using the solution form given in *Eq. 18* the following relationship can be derived:

$$W(t) = -(m + 1)^{\frac{1}{m+1}} \left(\frac{8F(t)}{\pi R^4(t)}\right)^{\frac{1}{m+1}} Q(h(t), t). \qquad (26)$$

Note that the above relation between $W$ and $F$ is derived based on the dominant role of the extensional viscosity in the range of small radius.

For a large radius, as a particle cylinder is sufficiently flattened, the squashing flow is increasingly affected by the shear viscosity. In that situation, by using *Eqs. 1* and *14*, the pressure distribution in the region of large radius is

$$p = \frac{(R^{2-n} - r^{2-n})}{(2 - n) \cdot 2^{1-n}} \frac{\partial}{\partial z} \left[\beta(T) \left(\frac{\partial^2 w}{\partial z^2}\right)^{1-n}\right], \frac{r}{h} \gg 1 \qquad (27)$$

in which the shear viscosity index has been used. If the single power-law model is to be followed, then $n = -m$ and $\beta(t) = \alpha(T)(1/3)^{-n/2}$. Instead of a parabolic profile for cylinder particles, the contact pressure for disks ($r/h \gg 1$) has a more complicated form, since $\partial^2 w/\partial z^2$ depends on the extensional viscosity. The above equation involves both the power-law indexes of extensional and shear viscosities.

The pressure profile in the median radius, which cannot be described by close form solutions, can be calculated provided the whole viscosity curve expressed in *Fig. 2* is given. Unfortunately, lack of such experimental data and theory prevents such an effort. In engineering applications, however, the contact pressure between the two extremes can be approximated by interpolation. Since this paper is limited to the squashing of cylindrical particles, the subject of squashing disks of large radius is not further explored here.

### Flow Front Progression—Spreading

The progression of the flow front of a flattening particle can be determined by the equation for the surface velocity given in *Eq. 26*, which governs the decrease of the particle height. To convert the equation into an ordinary differential equation for $h(t)$, one may use the following substitution:

$$w = \frac{dh}{dt}, \qquad (28)$$

$$F(t) = P(t) \cdot \pi R^2(t), \qquad (29)$$

and

$$R(t) = R_0 \sqrt{\frac{h_0}{h(t)}}. \qquad (30)$$

where $P(t)$ is the pressure experienced by the particle. The relationship given, *Eq. 30*, comes from the condition of equal volume in which the initial height and radius are $h_0$ and $R_0$, respectively. Thus, *Eq. 26* becomes

$$\frac{dh}{dt} = -(m + 1)^{\frac{1}{m+1}} \left(\frac{8P(t)h}{R_0^2 h_0}\right)^{\frac{1}{m+1}} Q(h, t). \qquad (31)$$

The above equation is a nonlinear ordinary differential equation coupled with $P(t)$ and $Q$, which is dependent upon the temperature profile. When $h$ is solved, the radius of the flow front, $R$, can be determined from *Eq. 30*.

### DIMENSIONLESS FLATTENING EQUATION

For computing particle spreadings, *Eq. 31* can be rewritten in the following nondimensional form:

$$\frac{dh'}{dt'} = -\left[(m + 1)8P_h' \frac{\bar{p}\theta}{\bar{\eta}_0(T_R)}\right]^{\frac{1}{m+1}} \cdot Q'(h', t') \left[\frac{h_0^2}{R_0^2}\right]^{\frac{1}{m+1}} \qquad (32)$$

where the normalized variables are defined as

$$h' = \frac{h}{h_0}, \qquad (32a)$$

$$t' = \frac{t}{\theta}, \qquad (32b)$$

and

$$p' = \frac{P}{\bar{p}}, \qquad (32c)$$

in which $h_0$, $\theta$, and $P$ are the initial height, dwell time, and average pressure, respectively.

The dimensionless function, $Q'$, which involves transient local temperature distribution, is

$$Q'(h', t') = \int_0^{h'} \left[ -\int_0^{z'} \frac{z''}{\alpha_T'} dz'' + \frac{\int_0^{h'} \frac{z''}{\alpha_T'} dz''}{\int_0^{h'} \frac{dz''}{\alpha_T'}} \int_0^{z'} \frac{dz''}{\alpha_T'} \right]^{\frac{1}{m+1}} dz' \qquad (32d)$$

in which

$$\alpha_T' = \frac{\alpha(T)}{\alpha(T_R)} \qquad (32e)$$

Note that $\bar{\eta}_0(T_R)$ is the effective viscosity at a reference temperature, $T_R$, at the strain rate of $1/\theta$. The nonlinear ordinary differential equation can be solved numerically by the Runge-Kutta method. The formulation of *Eq. 32* also enables computations that treat the power-law index to be varying with strain rate. In that case, more general extensional viscosity curves can be followed in every time increment in computation.

To proceed with computation, the pressure variation as seen by a particle should be given. Owing to a particle's small size, the temperature reaches the interfacial temperature rapidly. A typical case computed from an analytical solution (6) is shown in *Fig. 4*. The use of more rigorous boundary conditions in computing the temperature rises in particles would not improve predictions of spreadings significantly.

As a result, the particle squashing model can be greatly simplified by assuming an isothermal condition. In that case, using a contact temperature as the particle temperature, the governing equation given in *Eq. 32* can be integrated over the dwell time to obtain the final cylinder height as:

$$\int_{h'}^{h_f'} \frac{dh'}{\underbrace{\frac{1}{m+1}\int_0^{h'} (h'z' - z'^2)^{\frac{1}{m+1}} dz'}_{S_1}} = \underbrace{\int_0^1 p'^{\frac{1}{m+1}}\, dt' X}_{S_2} \cdot \underbrace{X\left[4(m+1)\frac{h_0^2}{R_0^2}\frac{\bar{p}\vartheta}{\eta_0(T)}\right]^{\frac{1}{m+1}}}_{S_3} \qquad (33)$$

where $h_f'$ is the final height (dimensionless) of the particle. As a special case for $m = 0$ for Newtonian fluids, the equation can be reduced to a simple form which is identical to the equation obtained by Stefan (7).

The above equation can be separated into three dimensionless groups as shown: $S_1$ involves the final cylinder height, $S_2$ involves the pressure profile, and $S_3$ involves process variables. Being dependent on the parameter $m$, they all can be plotted to form coupled master curves for determining the spreading of particles at a variety of conditions. It is of interest that the partical size, the process, and the viscosity form a dimensionless group as:

$$G_1 = \left(\frac{h_0}{R_0}\right)^2 \frac{\bar{p}\vartheta}{\bar{\eta}_0(T)} \qquad (34)$$

## COMPUTATIONAL RESULTS AND DISCUSSIONS

*Figures 5* and *6* show the effects of pressure and dwell time, respectively. As expected, spreading increases with pressure and dwell time, but these influences level off at higher values. It is also shown that particles having higher aspect ratios are more sensitive to the changes. This phenomenon agrees with the observation of less spreading found in repeated squashings. *Figure 7* shows the effect of temperature. Because of the nonlinear dependency of the viscosity on temperature, the spreading does not increase proportionately at higher temperatures at which particles become much softer. On the other hand, sharp interceptions of the curves at lower temperatures with the zero-spreading line ($R_f/R_0 = 1$) indicate that very little spreading is possible below a critical temperature below which the viscoelastic particle behaves more like a solid than a liquid.

The analysis of squashing flow can be applied to the area of roll fusing of xerographic toner images. The quality of the adhesion of the toner particles

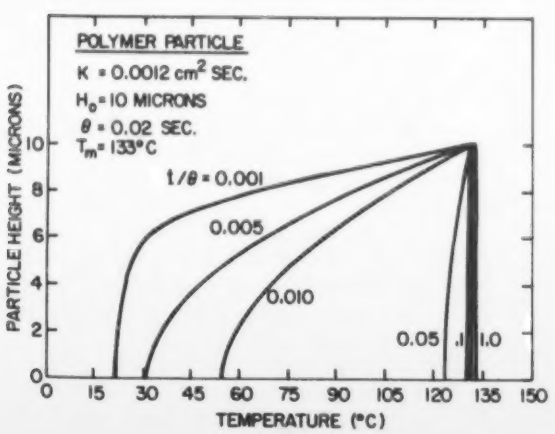


*Fig. 4. Typical temperature rise in a polymer particle.*

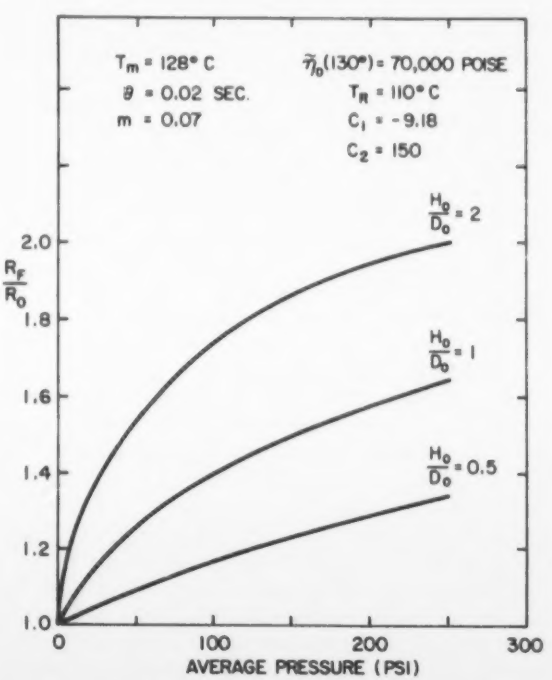


*Fig. 5. Effects of average pressure on particle squashing.*

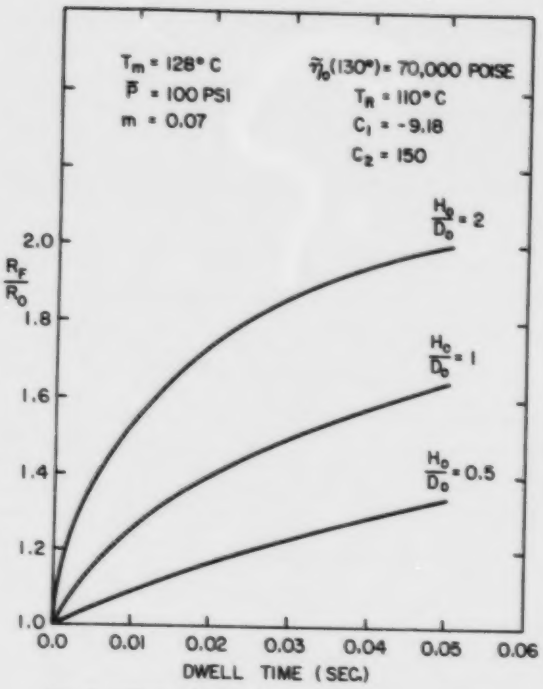


*Fig. 6. Effects of dwell time on particle squashing.*

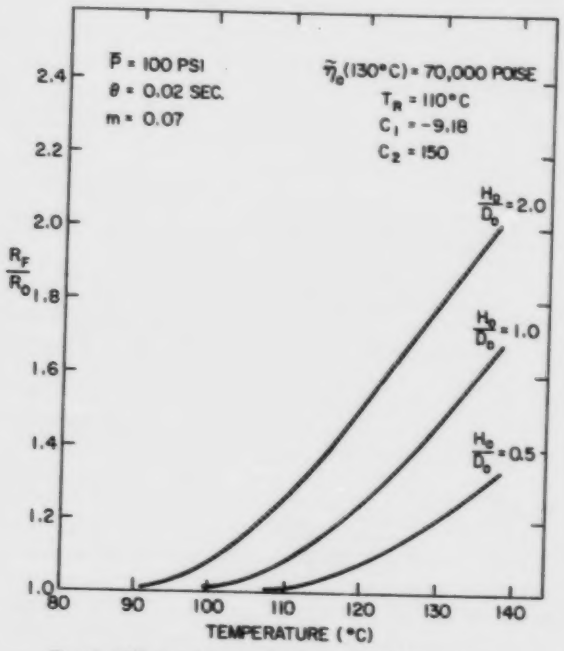


*Fig. 7. Effects of temperature on particle squashing.*

on papers can be evaluated by the degree of flattening of the particles. An extension of this analysis to include the effect of paper roughness along with some experimental results is described in a separate paper. Based on these analyses, one can determine the rheological properties required and the fusing conditions for achieving a desirable fix level.

## CONCLUSIONS

1. The squashing viscosity is affected by both the extensional and shearing rates. It cannot be adequately represented by a single power-law model. To satisfy two extreme cases of the predominantly extensional effect on particles and the shearing effect on disks and films suggests that the squashing viscosity is not a monotonically increasing or decreasing function with deformation rate.
2. Extensional effect dominates the non-Newtonian viscosity and the velocity field of particle squashing, and both the extensional and shearing rates affect the pressure distribution in highly flattened particles and disks.
3. Squashing of small particles with a heated platen usually can be approximated by isothermal conditions because of fast temperature rise in attaining uniform temperatures.
4. In addition to the viscosity parameter represented by the power-law index, particle squashing is governed by the dimensionless group: $(h_0/R_0)^2 r\theta/\tilde{\eta}_0(T)$.

## ACKNOWLEDGMENTS

The author is grateful to J. Elter for many stimulating thoughts and encouragement during the course of this work. Special thanks are due to R. Karz, S. Ahuja, and V. Lobe for providing rheological properties of the particle materials being studied.

## REFERENCES

1. R. J. Grimm, *AIChE J.*, **24**, 3 (1978).
2. Y. Kuo, *Polymer Eng Sci.*, this issue.
3. G. Brindley, M. Davis and K. Walters, *J. NonNewt. Fluid Mech.*, 1 (1976).
4. C. W. Macosko and Sh. Chatraei, *J. Rheology*, **25**, 4 (1981).
5. S. J. Lee, M. M. Denn, M. J. Crochet and A. B. Metzner, *J. NonNewt. Fluid Mech.*, **10**, 3 (1982).
6. H. S. Carslaw, and J. C. Jaeger, "Conduction of Heat in Solids," Oxford, (1959).
7. R. B. Bird, R. C. Armstrong and O. Hassager, "Dynamics of Polymeric Liquids," Vol. 1, J. Wiley, New York, (1977).

## NOMENCLATURE

| | |
|---|---|
| $D$ | : Diameter of a particle cylinder. |
| $D_0$ | : Original particle diameter. |
| $\boldsymbol{D}$ | : Deformation tensor given in *Appendix I.* |
| $F$ | : Contact force. |
| $h, H$ | : Height of a particle cylinder. |
| $h_0, H_0$ | : Original particle height. |
| $h_F, H_F$ | : Final particle height after squashing. |
| $\boldsymbol{I}$ | : Unit tensor. |
| $m$ | : Power-law index defined in *Eq. 10.* |
| $n$ | : Power-law index, defined in the effective shear viscosity model, see *Eq. 13.* |
| $p$ | : Local pressure in the flow field. |
| $\bar{p}$ | : Average pressure. |
| $Q$ | : An integration function given in *Eq. 19.* |

$r$ : Radial coordinate, see *Fig. 1.*
$R$ : Radius of particle in spreading.
$R_0$ : Original particle radius.
$R_F$ : Final particle radius after squashing.
$S_1, S_2, S_3$ : Dimensionless groups defined in *Eq. 33.*
$T$ : Temperature distribution in a toner.
$T_R$ : Reference temperature (used in obtaining WLF coefficients).
$u$ : Radial velocity.
$t$ : Time.
$W$ : Axial velocity at contact surface.
$w$ : Axial velocity.
$\tau_{rr}, \tau_{rz}, \tau_{\theta\theta}, \tau_{zz}$ : Stress components in the cylindrical coordinate system.
$z$ : Axial coordinate, see *Fig. 1.*
$\dot{\eta}_{eff}$ : Effective viscosity in the dwell time range.
$\eta_0$ : Effective viscosity at the characteristic strain rate, $1/\theta$.
$\alpha(T)$ : Temperature-dependent function of extensional viscosity, see *Eq. 11.*
$\beta(T)$ : Temperature-dependent function of shear viscosity, see *Eq. 13.*
$\mathrm{II}_D$ : The second invariant of $D$, see *Eq. I-8.*
$\tau$ : Stress tensor.
$\theta$ : Dwell time.

## APPENDIX I

### Viscous-Type Constitutive Equations and Effective Viscosity

The "viscous-type" constitutive equations for stress components, in cylindrical coordinates are

$$\tau_{rr} = -p + 2\eta \frac{\partial u}{\partial r}, \tag{I-1}$$

$$\tau_{rz} = \eta \left( \frac{\partial w}{\partial r} + \frac{\partial u}{\partial z} \right), \tag{I-2}$$

$$\tau_{zz} = -p + 2\eta \frac{\partial w}{\partial z}, \tag{I-3}$$

$$\tau_{\phi\phi} = -p + 2\eta \left( \frac{u}{r} + \frac{1}{r} \frac{\partial v}{\partial \phi} \right). \tag{I-4}$$

where

$$\eta = \eta(\mathrm{II}_D, T,) \tag{I-5}$$

Instead of using the viscosity (function) at steady state, viscous-type constitutive equations use a transient viscosity (function) which is averaged over the duration of the flow. The less the transient viscosity varies in the flow period, the more the viscous-type equations can represent the actual relationships of the components of the stress and strain rate.

By definition, the rate of deformation tensor, $D$, is

$$D = \tfrac{1}{2} (L + L^T) \tag{I-6}$$

where $L^T$ is the transpose of the velocity gradient, $L$. Using a standard form of $L$ in cylindrical coordinates the using *Eq. 6* given in the text, one can obtain an explicit form for $D$ in terms of one velocity component only:

$$D = \begin{pmatrix} -\frac{1}{2}\frac{\partial w}{\partial z} & 0 & -\frac{r}{4}\frac{\partial^2 w}{\partial z^2} \\ 0 & -\frac{1}{2}\frac{\partial w}{\partial z} & 0 \\ -\frac{r}{4}\frac{\partial^2 w}{\partial z^2} & 0 & \frac{\partial w}{\partial z} \end{pmatrix} \tag{I-7}$$

where

$$\begin{aligned} \mathrm{II}_D &= \frac{1}{2} \{2D_{11}D_{22} - 2D_{12}^2 + 2D_{11}D_{33} \\ &\quad - 2D_{13}^2 + 2D_{22}D_{33} - 2D_{23}^2\} \\ &= -\left[ \frac{3}{4} \left( \frac{\partial w}{\partial z} \right)^2 + \frac{r^2}{16} \left( \frac{\partial^2 w}{\partial z^2} \right)^2 \right] \end{aligned} \tag{I-8}$$

Or, in terms of $u$,

$$\mathrm{II}_D = -\left[ 3 \left( \frac{\partial u}{\partial r} \right)^2 + \frac{1}{4} \left( \frac{\partial u}{\partial z} \right)^2 \right]$$

↑ extensional rate ↑ shear rate

## DISCUSSION

*L. A. Utracki:* Youti, first of all, elongational viscosity as such doesn't exist. You must define what you mean: uniaxial, biaxial, planar or other. It is not clear to me which elongational viscosity you claim to incorporate in these equations. In the squeezing flow the biaxial viscosity should be important. The biaxial extensional viscosity at the very low rates of extension should be proportional to the zero shear viscosity. Recently we demonstrated that for low viscosity liquids even at high rate of straining the uniaxial elongational viscosity can be taken as three-times the shear viscosity. In addition, only for some polymers the elongational viscosity increases steeply, as you indicated, with the extension rate, but this increase occurs only at low rates of deformation. I believe that this is not true in the case of squeezing flow. I didn't see numerical values of extensional rate, but I believe that these values are rather high. In the higher range of deformation the extensional viscosity actually goes down with the rate. Thus, you have a parallel trend between the shear dependence of shear viscosity and extensional rate dependence of elongational viscosity which cannot account for the stiffening of the pellet when you compress. What can account for this are the transient effects. Stress overshoot is usually observed in the rheological testing at high rates. This may provide an explanation, but I don't think that you can claim that this is due to the elongational viscosity effect.

*Y. Kuo:* The extensional viscosity I used is uniaxial extensional viscosity. I think that you have touched on some of the weak areas. In our application range the compression rate is typically above 10 $sec^{-1}$

which means that we do not have any viscosity data available at all. To avoid that kind of controversy we simply back-calculated the rheological parameters from experimental data. The power law index, $m$, was determined in that manner. We found that with that single adjustable parameter we can fit the results obtained. It is a weakness not only in this analysis but, also in this field; we don't have very accurate data to work with.

*L. A. Utracki:* But if you have $\tilde{\eta}_e$ versus $(\partial w/\partial z)$ as you showed, do you get $m$ from this graph?

*Y. Kuo:* Yes.

*L. A. Utracki:* Do you get negative $m$?

*Y. Kuo:* No. I get a very small positive value.

*L. A. Utracki:* What I am saying is that for $\eta_e$ at $\dot{\epsilon} > 10\ \text{sec}^{-1}$ you should be getting a negative slope.

*Y. Kuo:* We have used an analytical constitutive relation proposed by Prof. White which also provides time dependent behavior, but is not discussed here. Actually, the finalized computer program does not use this fixed "$m$" power law exponent; the numerical scheme permits $m$ to vary with the rate. It is like a finite difference method in dealing with transient parameters.

*J. M. Dealy:* Dr. Utracki's question was based on the assumption that the material is being treated as an elastic material whereas in fact in your model you treated the material as purely inelastic. This type of model, in which the stress is assumed to be a function of the second invariant of the rate of deformation times the rate of deformation tensor, has been explored for quite some time. Prof. Bird did a lot on this about 20 years ago and he called this a Generalized Newtonian Fluid. Now in a Generalized Newtonian Fluid you have, as you do in one of your equations, the stress or the effective viscosity as a function of the temperature and the second invariant of the rate of strain tensor times $\Delta$. In applying this to both shear and extension you used special cases in which you had $m$ and, in the case of extension, $n$. But this is not permitted, however, because if your material is isotropic and obeys the principle of material indifference there you can't change the functional dependence as you move from one kinematics to another. It must remain the same function whereas what you have done is to change the function as you went from one deformation to another. This is rheologically inconsistent. It is just not possible. In fact, I would have to agree with Dr. Utracki that if this function is a decreasing function of the rate of deformation or second invariant then this must also be a decreasing function. You cannot have one increase and the other decrease. Therefore, $m$ and $n$ cannot be independent. $m$ must depend on $n$ and in some very simple way. They cannot be independent. Now as soon as you say that you are going to let the material be elastic then, of course, none of these restrictions applies, but if you are going to say the material is inelastic then you must obey these restrictions. You mentioned Grimm's paper. Grimm was using elastic models to compare the data. It seems to me that he was trying to evaluate elastic models so he wasn't assuming that it was simply a shear deformation. In fact, he has got to be right no matter what since at a sufficiently high rate of deformation the Deborah number becomes so large that you must take elasticity into account. I think that to say that if he had just taken into account some extensional deformation there wouldn't have been any problem isn't quite fair since there is bound to be a problem if you go to high enough strain rate just because of the Deborah number effect. Now I don't know anything about the characteristic times of your fluids so I can't say anything about the Deborah numbers. But if the characteristic time of the deformation is 1/10 sec, then that is quite short, so to suggest that elasticity isn't coming in is to suggest that the characteristic time of your fluid is much smaller than that. I would be quite astonished if that were really so. I suspect that actually your material has relaxation times that are larger than this which means that your Deborah number must be greater than one which means that elasticity must be coming into the picture.

*Y. Kuo:* Your remarks have been considered during the course of all of this study and a lot of discussions have been undertaken with several rheologists that I work with. Grimm's paper reported findings of previous authors and I tried to offer my explanation based on the contribution of extensional rate in the viscosity. I emphasize that the effect of extensional rate in viscosity must be considered in the determination of axial velocity, which was ignored by most previous authors. As far as using the second invariant, initially I said I used effective viscosity. I distinguish it from steady state viscosity in the "viscous-type" equations. Suppose I have viscosity data valid in that short time, I will use the data and determine the viscosity parameters according to the generalized viscous-type model defined here, taking into account the combined deformation. When we apply this for solving a flow field in a small radius for a particle from the combined strain rate we find that extension predominates. In this case we simply use the extensional viscosity since there is no point in using the shear viscosity because there is not much shear deformation. Once the axial velocity field is determined at small radius with the extensional viscosity, and since the axial velocity is independent of radius, then the use of the momentum equation to solve the pressure field at larger radius will require the use of the shear viscosity because the dominance of the shear rate in that region. It does not mean violation of a constitutive relationship. As for the pressure field where both components are present, as I mentioned earlier, we just don't have rheological data in a combined flow field so we don't really know how to deal with it. What I presented is a middle step in which these two effects are considered together. This is really a no-slip boundary condition when you squash it. Another point that I mentioned earlier is that in later work we improved this with an expression for

the extensional viscosity derived from a viscoelastic model. Of course, that expression depends on time and extensional rate. For the computer program I used a separate subroutine just to simplify the calculations. This by no means is a substitute for a viscoelastic model. It simply says that in the absence of detailed quantitative data, this is the kind of analysis that enables us to analyze the problem. (The paper has later been revised according to some of Professor Dealy's suggestions.)

*L. R. Schmidt:* Are you at liberty to comment on the experimental technique that was used to get the rheological data on these toner particles?

*Y. Kuo:* No, because my colleague was working on this. Actually he used the same technique that Prof. White has been using to characterize his material. It is an extrusion technique. We have a Rheomatrics Mechanical Spectrometer, but we couldn't characterize at high shear rates. We do use the functional form I previously mentioned to fit the experimental data and that is why the curves increase with strain rate, but we can't get to sufficiently high rates to say whether it decreases or not.

*L. A. Utracki:* You said that you had 10 $sec^{-1}$ rate of deformation in biaxial extension. What is the order of the rate of deformation in shear?

*Y. Kuo:* That depends on radius, but we have only considered extension. We have virtually no shear at all.

*M. E. Ryan:* When you went through the analysis and developed the second scalar invariant you cast it in a form where one could explicitly see contributions due to shear deformation and extensional deformation and you talked about the dominance or significance of one over the other depending on radius. That, of course, is just the local radial position as opposed to the radius of the particle. So, depending on the radial position of interest, the shear or extensional component may be more dominant than the other.

*Y. Kuo:* For example, if you consider a disk, the velocity field is dominated more by the extensional viscosity effect in the neighborhood of the center of the disk.

# Roll Fusing of Toner Particles on Rough Papers in The Xerographic Process

YOUTI KUO

*Xerox Corporation*
*Joseph C. Wilson Center for Technology*
*Rochester, New York 14580*

This paper deals with squashing of toner particles in a variety of paper topographies in the roll fusing of toner images in xerographic machines. The model developed can be used for predicting the mean spreading ratio of toner particles related to fix level with given rheological properties and fusing temperature and pressure.

The deformation of toner particles is solved with respect to the asperity pressure encountered in the contact between the roll and the paper surfaces. Various contact situations are considered, among them: toners on smooth papers, on tops of paper asperities, and at valleys of a paper surface. In addition to rheological properties and fusing conditions, toner spreadings also depend on toner size, paper roughness, and the rubber modulus of the fuser roll.

Based on an integration algorithm, statistical averages of toner spreadings can be computed in terms of distribution functions of toner and paper asperity height. Comparisons of theoretical predictions with measurements show good agreement over a broad range of data.

## INTRODUCTION

In the contact fusing of a xerographic process, toner images are pressed on a paper substrate at an elevated temperature in the nip between a fuser and a pressure roll as illustrated in *Fig. 1*. The combination of heat and pressure causes toners to spread so as to achieve a desirable level of fix and enhancement of optical density.

In addition to depending on the process conditions (pressure, dwell time, and temperature) and on rheological properties, the degree of spreading also depends on the contact condition of an individual toner. This paper is the second of two papers that deal with the mathematical modeling of roll fusing of toner particles in xerographic machines. In the first paper (1), the mathematical analysis was limited to the case of isolated toners on smooth paper. In this paper, the effect of paper roughness on toner spreading is analyzed.

Physically, paper roughness affects the contact pressure between the roll surface and a toner particle, which can be at a variety of positions among paper asperities (fibers) as shown in *Fig. 2*. The higher the paper asperities, the less the toners at valleys can be flattened. Generally, the degree of toner flattening varies with the ratio of toner height to paper asperity, and, therefore, it differs with respect to toner position on a paper surface which has nonuniform roughness.

This paper begins with a derivation of the fundamental relationship between the asperity pressure (actual contact pressure) and local nip pressure (nominal pressure). Then, it relates toner spreading to the microdeformation of the rubber layer and the contact pressure at any time in the nip. The complexity of a particle's stability at a slope is not involved; the analyses only deal with toners either on the tops of or in the valleys of a paper surface.

In the latter part of this paper, a formulation is given for calculating the statistical average of spreadings of toner particles on rough papers in terms of the spreading function of a single particle and the distribution functions of toner size and paper roughness. Finally, for verifying the models, predictions are compared with experimental data obtained on a large number of individual toner particles whose projected diameters were measured before and after the fusing process.

## DERIVATION OF ASPERITY PRESSURE

The contact pressure of an isolated toner particle squashed in a fuser nip differs from local nip pressure, which, by definition, is an average pressure over a small area covering many paper asperities. For determining the deformation of a toner particle, the actual contact pressure should be used for calculation. In the following analysis, a relationship between the contact pressure and the nip pressure is first derived and then used in later sections in more complicated situations involving many interactions among paper, rubber, and toners. In the following first two sections, the concept of asperity pressure and conformability condition will be described in terms of spherical particles, but actual applications will be on cylindrical toners.

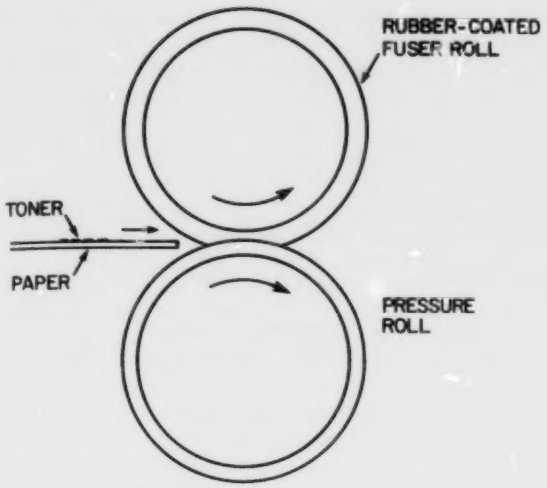


*Fig. 1. Roll fusing of toner image.*

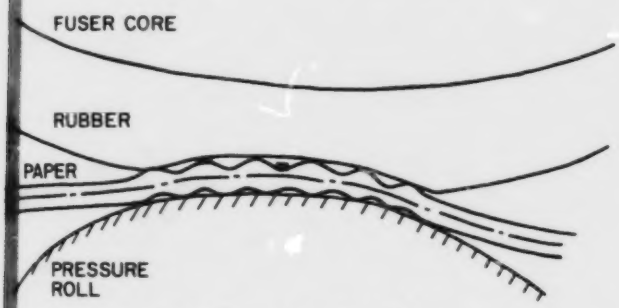


*Fig. 2. Contacts between roll surface and toners on rough paper.*

## Contact Pressure of an Array of Spherical Particles

For simplicity, first assume that indentation of a rigid particle on a rubber layer causes a depression surface that is spherical, as shown in *Fig. 3*. In a geometric relationship, the contact radius, $R_i$, can be expressed in terms of the maximum penetration, $\xi$, as

$$R_i = \sqrt{R^2 - (R - \xi)^2} \approx \sqrt{2R\xi}, \tag{1}$$

where $R$ is the radius of the assumed spherical surface. In terms of an average contact pressure, $P_i$, the maximum penetration, $\xi$, is given (2) as

$$\xi = 2(1 - \nu^2)\frac{P_i R_i}{E}, \tag{2}$$

where $\nu$ and $E$ are the Poisson ratio and Young's modulus of the rubber. Note that the above result is based on indentation of a single particle on a semi-infinite solid.

When the contacts of an array of identical particles are separated by a distance, $l$, as shown in *Fig. 4*, one can relate the contact pressure to the average pressure or nip pressure as follows:

$$n\pi R_i^2 P_i = A_o P_n, \tag{3}$$

where $A_o$ is the total area that encompasses $n$ particles. Considering $A_o = nl^2$, $P_i$ can be found through the above equation as

$$P_i = k(PnE^2)^{1/3}. \tag{4}$$

For spherical particles, the geometric parameter is

$$k = \left[\frac{1}{\pi}\left(\frac{l}{4R(1 - \nu^2)}\right)^2\right]^{1/3}. \tag{5}$$

It should be pointed out that the effect on the deformation of rubber due to indentations of neighboring particles has been ignored.

## Asperity Pressure on Paper Surface

To extend the preceding analysis to the contact between rubber and rough paper having a continuous surface profile, the algebra may be simplified by assuming that the contact pressure is equal to the nip pressure when the latter exceeds the conformable pressure required for the rubber to contact fully with the topography of the paper surface, as illustrated in *Fig. 5*. Thus, to meet the conformity condition, which is $P_i = P_n = P_c$, the parameter $k$ in *Eq 4* should be

$$k = \left(\frac{P_c}{E}\right)^{2/3} \tag{6}$$

where $P_c$ is the conformable pressure.

Note that the approach is satisfactory if the shapes of individual asperities can be reasonably matched by a spherical segment. If a paper surface is approximated by a sinusoidal profile, then by substituting in *Eqs. 4* and *6* the following explicit

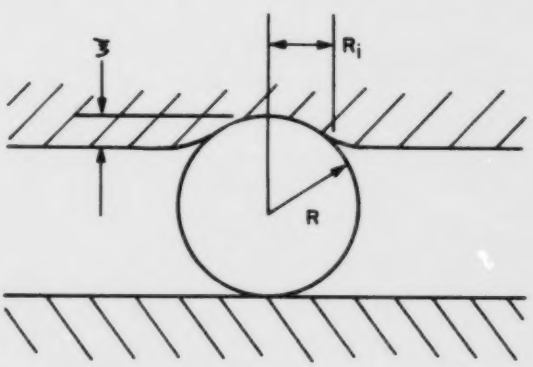


*Fig. 3. Indentation of a rigid sphere on a semi-infinite solid.*

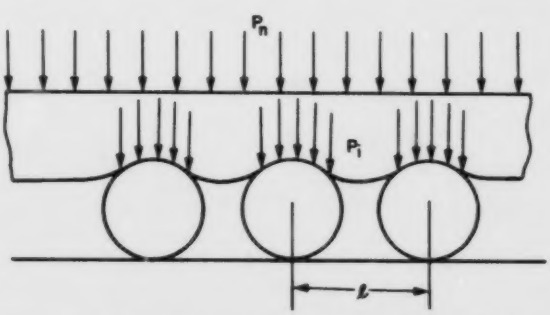


*Fig. 4. Contacts of an array of identical particles.*

expression for $P_c$, which is described in the *Appendix I*,

$$P_c = \frac{\sqrt{2\pi}}{3\nu} E \frac{\frac{h_p}{l}}{\tanh\left(2\sqrt{2\pi}\frac{H_r}{l}\right)}, \quad (7)$$

one obtains

$$P_i = \left[\frac{\sqrt{2\pi}}{3\nu}\frac{\frac{h_p}{l}}{\tanh\left(2\sqrt{2\pi}\frac{H_r}{l}\right)}\right]^{2/3} (P_n E^2)^{1/3}, \quad (8a)$$

$$P_i = P_n \quad (8b)$$

where $H_r$ is the thickness of the rubber layer. The amplitude and period of the paper roughness, respectively, are $h_p$ and $l$.

*Figure 6* shows a computed contact pressure (asperity pressure) on the asperity of a paper with its roughness represented by $h_p = 5$, $l = 70$ microns, which gives $k$ equal to 0.32 for a thick rubber layer ($H \gg l$). In this case, the contact is nonconformable,

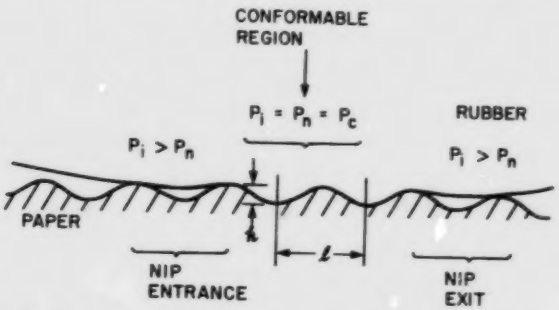


*Fig. 5. Conformable and nonconformable regions in a nip.*

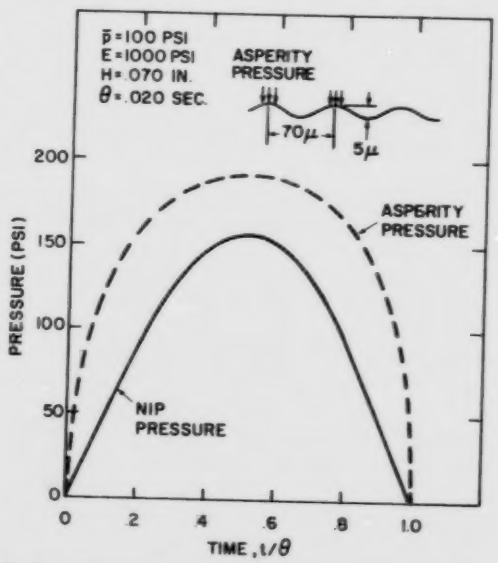


*Fig. 6. Asperity pressure in rough paper—nonconformable contact.*

and the asperity pressure is much higher than the nip pressure. A conformable case is illustrated in *Fig. 7* for a smoother paper of $h_p = 2$ and $l = 70$ microns. By following the conformity criterion given in *Eqs. 8a* and *8b*, the asperity pressure is equal to nip pressure at the central portion of the nip.

## CONTACT PRESSURE AND FLATTENING OF TONERS ON A ROUGH SURFACE

In the foregoing analysis, the contact pressure was derived on the basis of indentations of rigid bodies on a deformable semi-infinite body; the effect of mutual deformations of bodies in contact was not considered. The contact pressure does not obey the criterion given in *Eq. 8a* for toners in valleys of a rough paper surface. Owing to the presence of paper asperities, which shoulder the load over the nip, actual contact between the roll and the toner starts only when the local nip pressure equals the conformable pressure required for the rubber surface to reach the top of the toner particle. To determine the subsequent contact pressure, therefore, consideration needs to be given to the spatial constraint, conformability, and the deformation of rubber and toner spreading simultaneously.

### Spatial Relationships

The spatial relationships among dimensions and deformations of rubber, paper, and toner can be found by first considering the fact that the space between the rigid surfaces of two rolls is fixed. Then, locally, when the rubber and toner are in contact such that the space is fully occupied, their subsequent deformations should be confined to this space. The sum of the toner height and rubber displacement should be equal to the sum of their values at the time of initial contact. In the following sections, relationships and corresponding equations for $p_i$, $w_t$, and $w_p$ will be described.

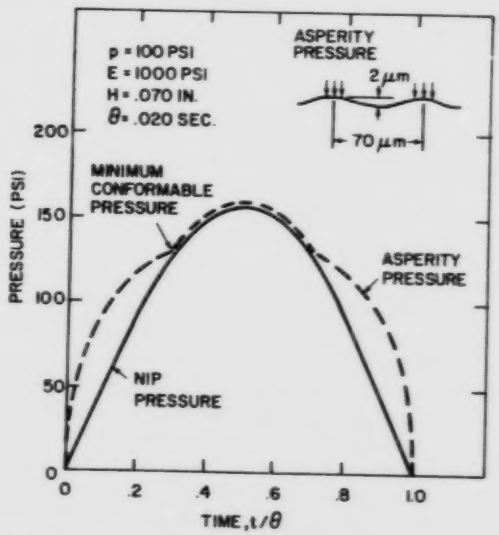


*Fig. 7. Asperity pressure in smooth paper—conformable contact.*

**Toners Higher Than Paper Asperities**

*Rubber—Toner Contact Only*

Two situations are considered: one is for toners on the tops of paper asperities as shown in *Fig. 8a* and the other is for toners at valleys but taller than asperities shown in *Fig. 8b*. In both cases, the rubber may not be in touch with paper asperities. For the contact involving only the rubber surface and an array of toner particles in a nip, the resultant nip pressure differs from the contact between two smooth surfaces. This difference in the nip pressure profile is affected by the flattening of toner particles and the local deformations of the rubber surface. A detailed analysis of this complex interaction is given in the *Appendix II*. Here a simplified approach is presented as it can well capture the key characteristic of the process.

If the deformation of paper asperities, which are much less than that of toners, is ignored, then a simplified equation relating the changes of rubber indentation and toner height under nip pressure can be expressed as:

$$(h_t - h_{t_o}) + (w_t - w_{t_o}) = 0 \tag{9}$$

where $h_{t_o}$ and $w_{t_o}$ are the initial values of toner height and local indentation of rubber surface, respectively. $h_t$ and $w_t$ are toner height and rubber indentation, which vary with the nip pressure.

Using a solution given by Timoshenko and Goodier (2) for the indentation of small area on a semi-infinite solid, an average value of the indentation of rubber surface can be approximated by the following equation*:

$$w_t = -\frac{2(2+\pi)(1-\nu^2)}{\pi E} R_t P_i, \tag{10}$$

where $R_t$ is the radius of a toner cylinder. Note that the contact radius at any time can be related to the toner height through the condition of constant volume as

$$R_t^2 h_t = R_{t_o}^2 h_{t_o}, \tag{11}$$

where $R_{t_o}$ is the initial radius. Accordingly, by using *Eqs. 9* and *10*, $P_i$ can be determined by the following differential equation:

$$\frac{dP_i}{dt} = \frac{dh_t}{dt}\left[\frac{h_t^{1/2}}{B_3} + B_2 P_n\right] \tag{12}$$

$$B_2 = \frac{l^2}{2\pi R_{t_o}^2 h_{t_o}} \tag{13a}$$

where

$$B_3 = \frac{2(2+\pi)(1-\nu^2) R_{t_o} h_{t_o}^{1/2}}{\pi E} \tag{13b}$$

*Equation 3* has been used to make the right-hand side of the above equation explicitly depend on the nip pressure.

On the other hand, $h_t$ at any time is governed by the equation obtained previously for the flattening of a toner (1).

$$\frac{dh_t}{dt} = -(m+1)^{\frac{1}{m+1}} \left(\frac{8P_i}{R_t^2}\right)^{\frac{1}{m+1}} Q(h_t, T), \tag{14a}$$

where $m$ is the power-law index of effective extensional viscosity. The function $Q$, which involves local viscosity $\eta_T$ and temperature distribution in the toner particles, is

$$Q(h_t, T) = \int_0^{h_t} \left[-\int_0^z \frac{z'}{\eta_T}\, dz' + \frac{\int_0^{h_t} \frac{z'}{\eta_T}\, dz'}{\int_0^{h_t} \frac{dz'}{\eta_T}} \int_0^z \frac{dz'}{\eta_T}\right]^{\frac{1}{m+1}} dz \tag{14b}$$

Based on *Eqs. 12* and *14b*, both $P_i$ and $h_t$ can be solved with the initial conditions given by *Eq. 8a*. Note that the spatial relationship given in *Eq. 9* applies up to the moment at which the rubber also touches paper asperities.

*Rubber in Contact with Toners and Paper Asperities*

Referring to *Fig. 9a*, while toners may be higher than paper asperities, the rubber may contact both simultaneously. In the presence of paper asperities, the spatial relationship becomes

$$(h_t - h_{t_o}) + (w_p + w_t - w_{t_o}) = 0 \tag{15}$$

which is similar to *Eq. 9* except that the additional rubber deformation, $w_p$, due to the presence of pressure asperities is included.

Let $P_n^*$ be the nip pressure at which the rubber starts touching paper asperities. Then, according to the concept of conformity (see *Appendix 1*), the nip pressure at which the threshold of conformity condition occurs coincides with the time that the transient nip pressure and the toner height meet the following condition:

$$P_n^* = \frac{\sqrt{2}\pi E}{3\nu l} \frac{(h_t^* - h_p)}{\tanh\left(2\sqrt{2}\pi \frac{H_r}{l}\right)} \tag{16}$$

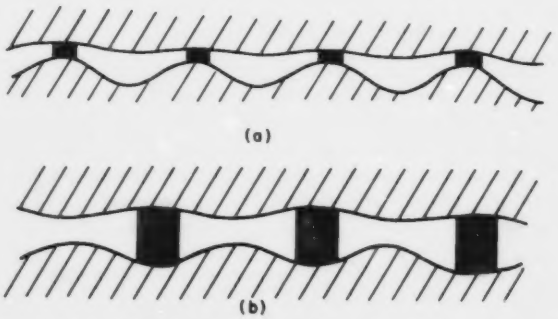


*Fig. 8. a) Rubber in contact with toners-toners on tops of paper asperities. b) Rubber in contact with toners-toners at valleys, but taller than paper asperities.*

* Instead of using *Eq. 2* based on spherical geometry, *Eq. 10* is used to be consistent with the approach used previously in modeling the spreading of cylindrical toners. In fact, contact geometry has little effect on the average displacement and pressure.

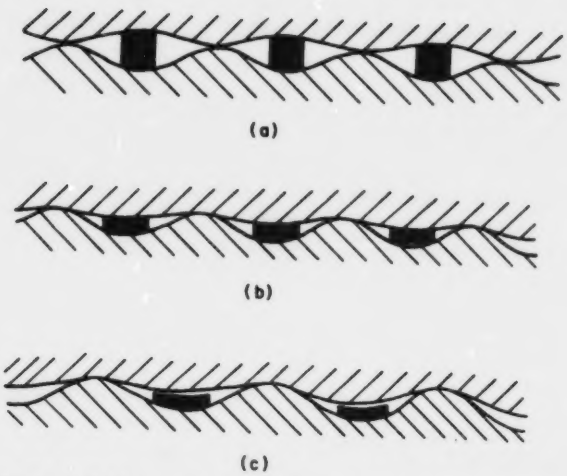


*Fig. 9. a) Rubber in contact with both toners and paper asperities—toners higher than paper asperities initially. b) Rubber in contact with both toners and paper asperities—toners flattened from higher position to lower position. c) Rubber in contact with both toners and paper asperities—toners lower than paper asperities initially.*

where $h_t^\circ$ denotes the corresponding value of the toner height which can be determined through the numerical calculation of *Eqs. 14a* and *16*.

Let $w_p$ be superimposed on the reference surface profile at which the rubber layer touches paper asperities. Then, similar to *Eq. A-8*, $w_p$ can be estimated by the following equation as

$$w_p = -B_1(P_n - P_n^\circ), \qquad P_n \geq P_n^\circ \tag{17}$$

where $B_1$ is given in *Eq. A-10*.

As for the relation between $w_t$ and $P_t$, *Eq. 10* is still applicable. To solve for $P_t$, *Eqs. 10* and *16* must be substituted into *Eq. 15* in order to obtain the following equation:

$$\frac{dP_t}{dt} = \frac{(h_t)^{1/2}}{B_3}\left\{B_1\frac{dP_n}{dt} + \frac{dh_t}{dt}\left[1 + \frac{B_3}{2}\frac{P_t}{(h_t)^{3/2}}\right]\right\}. \tag{18}$$

It is clear that *Eqs. 14a* and *18* are coupled differential equations for $P_t$ and $h_t$ and are to be solved simultaneously. The above equation should be used, instead of *Eq. 12*, after the nip pressure $P_n$ exceeds $P_n^\circ$ defined in *Eq. 16*.

### Toners Lower Than Paper Asperities

The equations given (*Eqs. 15–18*) are applicable to toners continuously flattened from an originally higher position to a position below neighboring paper asperities. For toners initially lower than paper asperities, as shown in *Fig. 9c*, the sum of the current toner height and the microscopic deflections of the rubber equals the original height of the paper asperity:

$$w_p + w_t + h_t = h_p, \qquad w_p \neq 0. \tag{19}$$

Besides, the initial contact pressure, $P_r$ should be zero and the minimum conformable pressure is

$$P_n^\circ = \frac{\sqrt{2}\pi E}{3\nu l}\frac{(h_p - h_{t_o})}{\tanh\left(2\sqrt{2}\pi\dfrac{H_r}{l}\right)}, \qquad h_p > h_{t_o}. \tag{20}$$

Since no contact exists for $P_n < P_n^\circ$, the effective dwell time (duration of actual contact) of the toner is less than the nominal dwell time (nip width/speed). It should be pointed out that the deformation of paper asperities has been assumed negligible in soft roll fusing (nip pressure about 150 psi). It should be considered, however, in cold roll fusing which uses high nip pressure in the order of 2000 psi.

## STATISTICAL EVALUATION OF TONER SPREADINGS

The preceding analyses of spreadings of toners in different paper topographies can be readily applied to compute the increase of area coverage in background at different fusing conditions.

Since in a nonimage area, toner particles of various sizes are randomly deposited on the tops and in the valleys of a paper surface which generally has variations in roughness, the area enhancement should be characterized by the statistical average of toner spreadings in all possible situations. An appropriate approach is to use distribution curves of toner diameters and heights as well as distribution of paper asperities to find joint probabilities of toner-asperity engagements. By this method, the product of a joint probability and the corresponding toner spreading is the percentage share in the area coverage.

Without much elaboration, the following equation for calculating the average fused area, $A_F$ for toners having the same projected areas, $\pi R_o^2$, before fusing may be written:

$$\bar{A}_F(R_o) = \pi\int_0^\infty\int_0^\infty R_F^2(R_o, h_t, h_p)q_p q_t dh_p dh_t, \tag{21}$$

for a fixed $l$, where

- $A_F$: average area coverage of toners after fusing,
- $R_o$: projected toner radius before fusing,
- $R_F$: projected toner radius after fusing,
- $q_t$: distribution function of toner height,
- $q_p$: distribution function of paper asperity height,
- $h_t$: toner height,
- $h_p$: paper asperity height, and
- $l$: period of paper roughness.

In the above formulation, the use of the product, $q_p q_t$, implies the assumption of independent events and equal weight on the probability of any toner-asperity engagement. For simplicity, an overall average of fused area coverage based on all sizes of toners can be formulated as follows:

$$\bar{A}_F = \int_0^\infty \bar{A}_F(R_o)g(R_o)dR_o \tag{22}$$

where $g(R_o)$ is the normalized distribution function of the projected toner radius before fusing.

Note that for brevity, instead of writing a general equation also covering the variation in the period of surface roughness, the above expressions are written only for a fixed roughness period, $l$.

## Computation and Discussion

### *Computed Contact Pressures and Toner Spreadings*

The results of computations for four typical cases are given here. *Figure 10*, for toners lying on a smooth paper, shows plots of the changes of nip pressure, contact pressure, and toner spreading in time.

The effect of the conformity of rubber is indicated in *Fig. 11* for toners at valleys and initially higher than the asperities. The rubber contacts toners first, but then touches the asperities as the local nip pressure exceeds the required conformable pressure. It is interesting to note the sharp drop of contact pressure that occurs as the rubber also touches the neighboring asperities—an indication that the load is shared by more contact areas.

*Figure 12* illustrates the contact pressure of a toner that is initially lower than the paper asperities. Because of lower nip pressure, the toner is not touched at regions near the nip entrance and exit so that the effective dwell time is less than the nominal dwell time. This kind of contact situation also exists for toners in a bottom layer of an image.

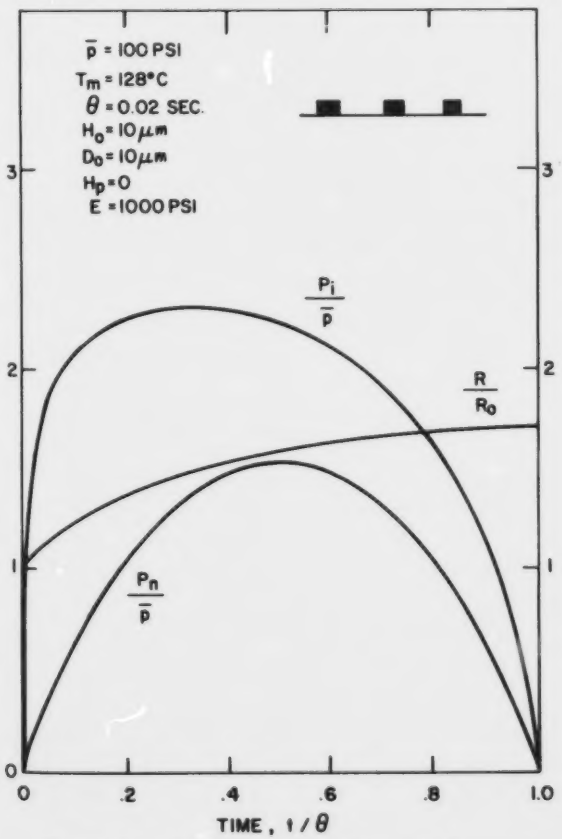


*Fig. 10. Spreading of a toner particle on smooth paper.*

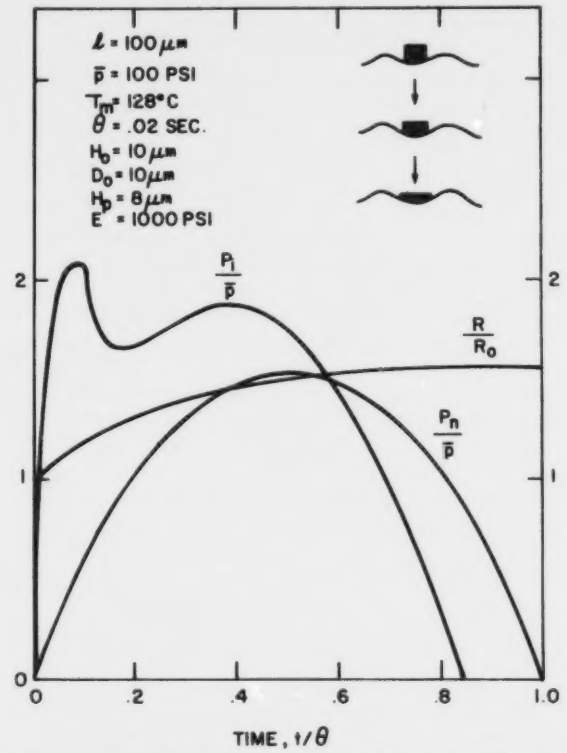


*Fig. 11. Spreading of a toner particle at valley—toner higher than paper asperities initially.*

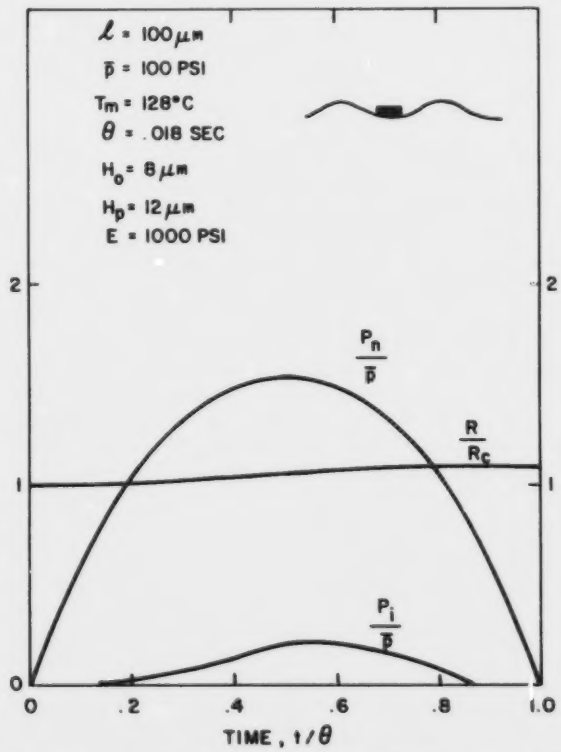


*Fig. 12. Spreading of a toner particle at valley—toner lower than paper asperities initially.*

## EXPERIMENTAL RESULTS AND MODEL VERIFICATION

Rigorous verifications of the theories developed here are not feasible because of the approximations by right circular cylinders, the idealized sinusoidal surface profile, and many other simplifications which enable mathematical analysis but are difficult to materialize as test conditions. Nevertheless, comparisons can be made on statistical averages between predicted and measured values over a wide range of toner size and paper asperities.

Here we use extensive experimental results (3, 4) of the spreading of toners in nonimage areas (called background) at different fusing conditions. In the experiments, apparent diameters (projected under a microscope) of identified toners were measured before and after fusing by using Quantimet equipment. (Note that at the nip exit, toners are cooled instantly to room temperature, and no further deformation is possible.)

*Figure 13* shows the data obtained from a fuser roll with the stated roll surface temperature at average pressure at 100 psi and dwell time at 0.020 second. The numbers on the figure indicate the numbers of toner particles being counted having the same apparent diameter before fusing and also having the same apparent diameters after fusing (they may differ in height). A total of 196 particles was counted. The scattering of data indicates different degrees of spreading among toners. For example, apparent diameters after fusing could range from 10 to 18 microns for the toners whose apparent diameters are 6 microns originally. The variation is due to differences in individual toner heights and positions in the topography of the paper. It is clear that we can obtain average spreadings from the data.

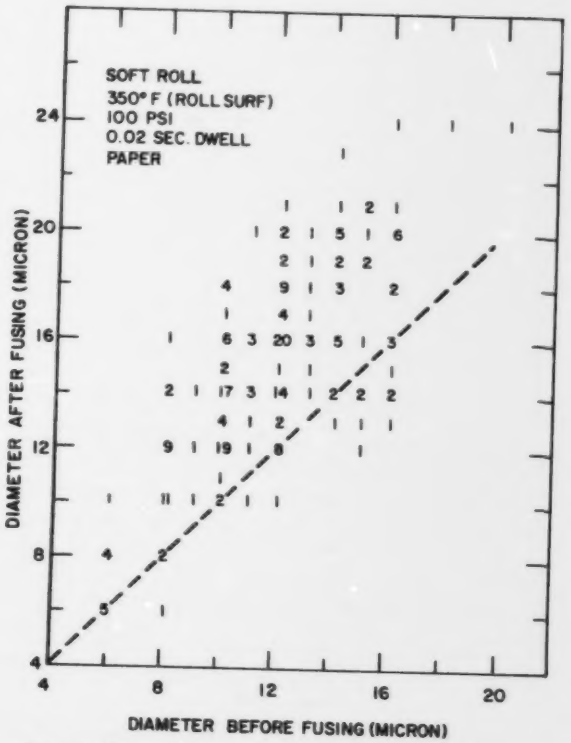


*Fig. 13. Measured toner diameter before and after fusing.*

So far, no data on the effective extension viscosity in the fusing ranges (strain rate about 10 $sec^{-1}$ and within a dwell time of about 0.04 sec) are available for straightforward computation for testing the model. The hindrance is due to experimental difficulty in acquiring the data in the desirable ranges. The alternative, however, is to use one data set to determine the viscosity parameters, $m$, defined in the model and then to use the values obtained to predict the other sets of experimental data. By this approach, self-consistency of the model is emphasized so that spreading of background toners of all sizes can be predicted on the basis of identical values of fusing variables and material parameters.

*Figure 14*, a summary of all possible spreadings, shows spreading curves of toners (before fusing) of the same projected radius but at different aspect ratios *vs* the height of paper asperity. The spreadings are highest on smooth surfaces and affected by paper asperities when they are much shorter. However, the degree of spreading decreases as the heights of neighboring asperities approach the toner height. Furthermore, a drastic decrease of spreading occurs when the toner height is less than the asperity height. This is due to reductions of both the contact pressure and the effective dwell time available for spreading flow. Such curves are useful for calculating the statistical average of spreadings of background toners.

To account for all possible toner-asperity engagements and toner sizes, the average spreading can be calculated according to *Eq. 21* in terms of distribution functions of toner and asperity height as well as the spreading function of toners, $R_F$. *Figures 15* and *16* show measured distributions of toner size and paper asperity height, respectively. In our computations, toner size data were fitted with the log

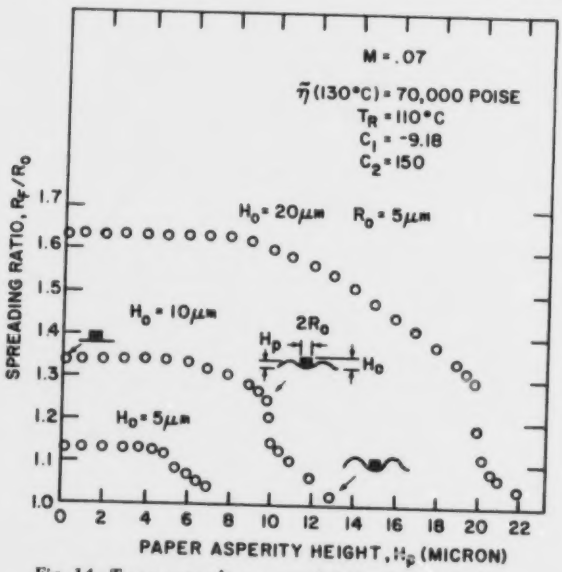


*Fig. 14. Toner spreading versus height of paper asperity.*

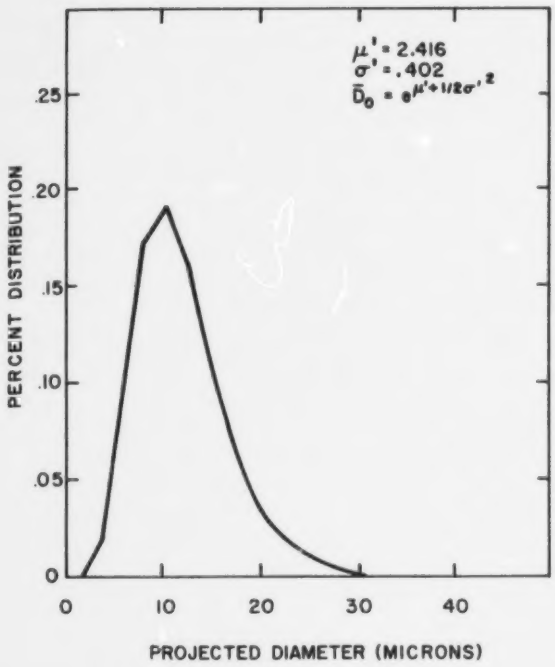


*Fig. 15. Toner diameter distribution.*

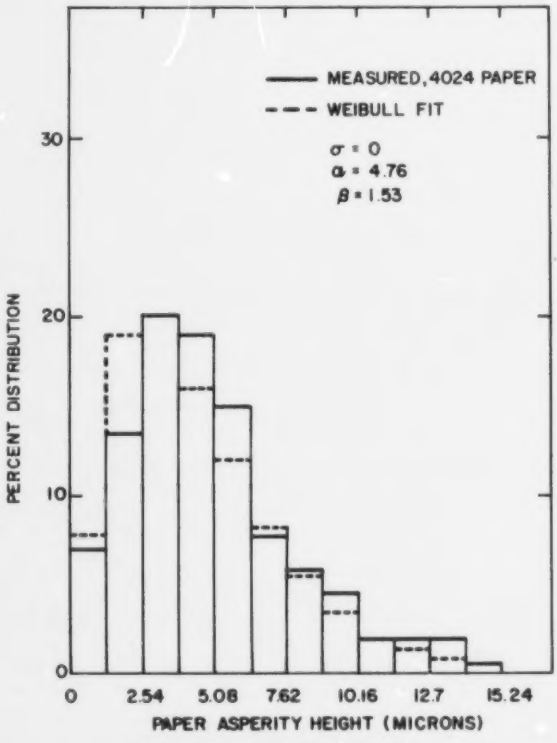


*Fig. 16. Paper asperity distribution.*

normal function and paper asperity with the Weibull function. A statistical average of height/diameter ratio of 8 to 12 was used in converting the toner size distribution to the height distribution.

*Figure 17* compares computational and experimental results at the fusing conditions indicated.

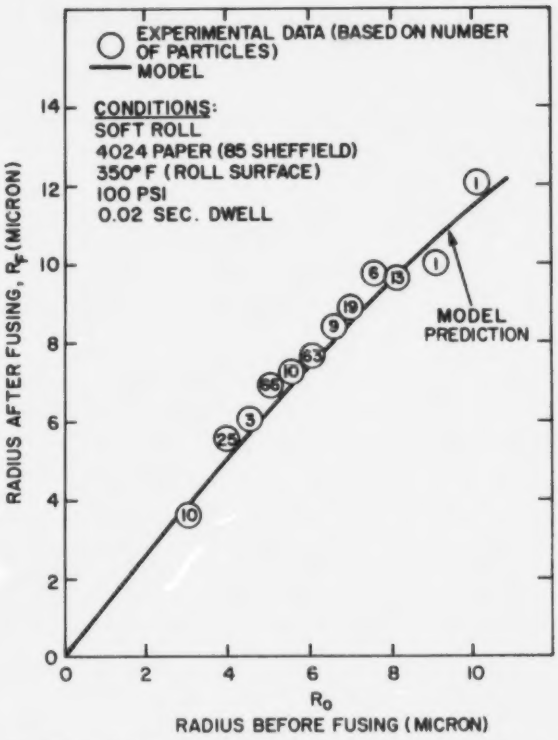


*Fig. 17. Statistical averages of toner spreadings—comparisons of theoretical predictions and experimental results.*

The spreading function was based on a wide spectrum of computed data, some of which are shown in *Fig. 14*. The predictions agree well with experimental data over a broad range of unfused toner radii.

## CONCLUSIONS

The deformations of toner particles on rough paper can be described by a system of two simultaneous ordinary differential equations. One of these is the particle flattening equation which involves rheological properties. The other is the particle pressure equation which is derived from the mechanics of particle contact.

Contact pressures on particles differ significantly from bulk or average pressures depending on their respective contact situations. As a result, different degrees of particle flattening occur on rough papers. Although particle deformations at the tops and valleys of a paper surface can be modeled and calculated, accurate predictions of individual particles are difficult because of assumptions of idealized geometry and contact conditions. However, the models can successfully predict trends and statistical averages of flattenings for various size groups of particles having a distribution of aspect ratios.

Despite some key assumptions, there is good agreement between model predictions and experimental results. With given toner and paper asperity size distributions, the mean spreading ratio (postfusing radius/prefusing radius) can be predicted if

the rheological properties are known along with the process temperature and pressure of the fusing system.

Many aspects of the models can be improved. Because a liquid state has been assumed, the model is not applicable to polymer particles heated below melting temperatures. The time-dependency of extension viscosity should be considered for long dwell times. Accurate data on viscosity variation with temperature is very important for larger particles, which may develop significant temperature gradients during the fusing process. Additionally the analysis of particle contact pressure based on the sinusoidal profile can be improved with a more realistic surface profile. Similar analyses can be done on rubber surfaces; these were ignored in the current analysis.

## ACKNOWLEDGMENTS

The author is grateful to H. Kocher without whose experimental support this study could not have been developed into the present scope. Special thanks are due to J. Elter for many stimulating thoughts and encouragement. The author also must acknowledge R. Karz, S. Ahuja, and V. Lobe for providing rheological properties of the toner materials being studied.

## REFERENCES

1. Kuo, Y., this issue.
2. Timoshenko, S. P. and J. N. Goodier, "Theory of Elasticity," p. 405 and p. 366, 3rd Edition (1970).
3. Soong, T. C. and C. Li, *Int. J. Mech. Sci.*, 23, 263 (1981).
4. Kocher, H. S., priv. commun.

## APPENDIX I

### Conformability Equation

Let the surface profile of the paper be represented by a sinusoidal function having spatial frequency $2\pi/l$ and amplitude $h$. With respect to the coordinate system shown in *Fig. 1*, the displacement of the conformable rubber layer has the following form:

$$w(x, y, z) = -\frac{h}{2}\cos\left(2\pi\frac{x}{l}\right)\cos\left(2\pi\frac{y}{l}\right)\frac{sh\left(2\sqrt{2}\pi\frac{z}{l}\right)}{sh\left(s\sqrt{2}\pi\frac{H}{l}\right)} \quad \text{(A-1)}$$

The components satisfy the Laplace equation and the continuity equation. Note that the problem is simplified by assuming that the finite deformation in the nip is locally uniform; therefore, it contributes to constant hydrostatic pressure in that local area.

From a given displacement field, the deformation gradient can be evaluated to determine the stress field. The normal stress, which is of interest here, is

$$\sigma_z = \frac{-3\nu}{1+\nu}P + \frac{E}{1+\nu}\frac{\partial w}{\partial z} \quad \text{(A-2)}$$

In the above equation, $\nu$ is the Poisson ratio and $E$ is Young's modulus. The normal stress $\sigma_z$ at any point has two components: one is due to the hydrostatic pressure, $p$, and the other, called extra stress, is due to the deformation gradient, $\partial w/\partial z$, which can be evaluated from *Eq. A-1*. For simplicity, only the above equation is used to derive the conformity condition.

In a nonconformable contact, the displacement profile of the rubber surface does not match the profile of the paper, as illustrated in *Fig. 2a*. In the contact area, the stress is finite, but in noncontact areas the surface traction is zero, which means that the extra stress balances the hydrostatic pressure. To achieve conformity, the rubber surface should deform more to reach the valley of the paper surface as shown in *Fig. 2b*. It is, therefore, clear that the conformity condition exists when the surface traction of the rubber layer is less than or equal to zero (by conventional definition the direction of normal stress is opposite to that of the pressure). It can be written as

$$\sigma_z \leq 0. \quad \text{(A-3)}$$

The above is a simplified condition.

To evaluate the conformability in this case, the above conformity condition can be applied to the lowest positions of the profile. By setting $x = l/2$ and $y = 0$ for evaluating the deformation gradient, the following conformity criteria are obtained:

*Fig. A-1. Coordinate system illustrating small displacements.*

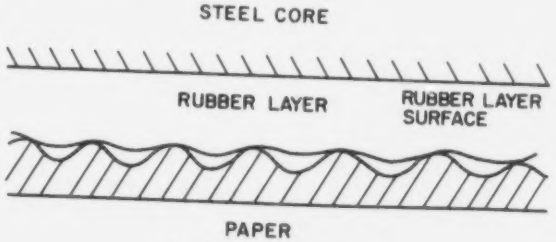


*Fig. A-2a. Partial contact.*

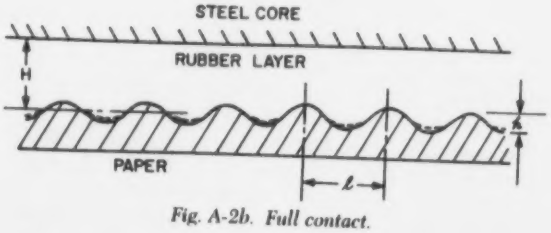


*Fig. A-2b. Full contact.*

$$\nu \frac{P}{E} \geq \frac{\sqrt{2}\pi}{3} \frac{\frac{h}{l}}{\tanh\left(2\sqrt{2}\pi \frac{H}{l}\right)} \qquad \text{(A-4)}$$

The above equation agrees well qualitatively with observations in practice.

## APPENDIX II

### Governing Equations for the Nip Pressure as Affected by the Presence of Particle Layers

The spatial relationships among dimensions and deformations of rubber, paper, and toner can be found by first considering the fact that the space between the rigid surfaces of two rolls is fixed. For simplicity, we may assume that the local distance between a paper's median plane and the interface between the rubber and the core of a fuser roll does not change with time. Let the distance be $S(x)$, which is a function of location in a nip in the process direction. Then locally, when the rubber and toner are in contact such that the space is fully occupied, their subsequent deformations should be confined to this space. Hence, we may write

$$S(x) = \left(\frac{H_p}{2} - h_p\right) + h_t \qquad \text{(A-5)}$$

$$= H_r + w_{n_t} + w_p + w_t,$$

where $H_p$ and $h_p$ are paper total thickness and asperity height, respectively. $h_t$ is the height of a toner. $H_r$ is the rubber thickness of a fuser roll. $w_{n_t}$ is the nip interference of the rubber surface under the effect of toner contacts. And, $w_p$, $w_t$ are components of microscopic deformation due, respectively, to paper roughness and toner. $h_t$, $w_{n_t}$, $w_p$ and $w_t$ are functions of time and other variables.

At the absence of toners, the above equation becomes

$$S(x) = \left(\frac{H_p}{2} - h_p\right) + H_r + w_n \qquad \text{(A-6)}$$

where $w_n$ is the nip interference of the rubber layer due to the nip formation by two rolls. Equating the above two equations in differential form, one has

$$\frac{d}{dt}(w_n - w_{n_t}) = \frac{dh_t}{dt} + \frac{dw_p}{dt} + \frac{dw_t}{dt} \qquad \text{(A-7)}$$

Each term in the right-hand side of *Eq.* A-7 is discussed in the text. The left-hand side can be related to the nip pressure profiles with and without toners by assuming that the rubber interference in the nip without toners can be linearly proportional to the local nip pressure as

$$w_n = -B_1 P_n \qquad \text{(A-8)}$$

By using the same proportionality, one can write a similar relationship for the nip interference affected by toner particles as

$$w_{n_t} = -B_1 P_{n_t} \qquad \text{(A-9)}$$

The proportionality constant $B_1$, can be derived from a nip geometric relationship.* It has the following form:

$$B_1 = \frac{L^2}{8}\left(\frac{1}{R_1} + \frac{1}{R_2}\right)\frac{1}{P_{n_{max}}} \qquad \text{(A-10)}$$

where $R_1$ and $R_2$ are the radii of two contact rolls. $l$ and $P_{n_{max}}$ are nip width and the maximum pressure at the center of the nip, respectively.

Substituting *Eqs. A-8* and *A-9* into *Eq. A-10* and neglecting $w_p$ (contribution is included in the text) here for the convenience of discussion, one obtains

$$\frac{dP_{n_t}}{dt} = \frac{dP_n}{dt} + \frac{1}{B_1}\left(\frac{dh_t}{dt} + \frac{dw_t}{dt}\right) \qquad \text{(A-11)}$$

In terms of $P_{n_t}$, the particle contact pressure can be calculated by

$$P_t = \left(\frac{l^2}{\pi R_{t_o}^2 h_{t_o}}\right) h_t P_{n_t} \qquad \text{(A-12)}$$

The indentation due to a toner particle can be calculated by *Eq. 10*, which is repeated as follows:

$$w_t = -\frac{2(2+\pi)(1-\nu^2)}{\pi E} R_t P_t \qquad \text{(A-13)}$$

The flattening of toners is given in *Eq. 14a*, which is also repeated here:

$$\frac{dh_t}{dt} = -(m+1)^{\frac{1}{m+1}}\left(\frac{8P_t}{R_t^2}\right)^{\frac{1}{m+1}} Q(h_t, T) \qquad \text{(A-14)}$$

It is clear that the *Eqs. A-11* through *A-14* are the governing equations to be solved simultaneously for the four unknowns, $P_{n_t}$, $P_t$, $w_t$ and $h_t$. The required inputs for these equations are the pressure profile in the nip in the absence of toners, viscosity of the toner material, rubber modulus and the initial particle size.

Owing to smaller toner heights in comparison with the rubber thickness, the difference between the nip pressure profiles with and without a layer of toner particles is assumed to be insignificant. This minor effect has been neglected in *Eqs. 9* and *15*.

## NOMENCLATURE

- $E$ : Young's modulus of rubber.
- $H_p$ : total thickness of paper.
- $H_r$ : rubber thickness.
- $h_p$ : height of paper asperity.
- $h_t$ : toner height.
- $h_{t_o}$ : initial toner height.
- $k$ : geometric parameter defined in *Eq. 4*.
- $l$ : period of paper roughness.
- $m$ : power-law index of extension viscosity.
- $P_c$ : minimum conformable pressure.
- $P_t$ : contact pressure or asperity pressure.
- $P_n$ : local nip pressure.
- $R$ : radius of a spherical particle.

* The geometric relationship is an oversimplification of complex rolling contact problems. An elaborate treatment on the subject was given by Soong and Li (3).

$R_i$ : radius of contact area.
$R_t$ : radius of a cylindrical toner.
$T$ : temperature.
$t$ : time.
$\xi$ : maximum penetration.
$w_n$ : displacement of rubber surface due to nip pressure.
$w_p$ : displacement of rubber surface due to contacting paper asperities.
$w_t$ : displacement of rubber surface due to contacting toners.
$w_{t_0}$ : initial displacement of rubber surface in contacting toners.
$\eta_t$ : extensional viscosity.
$\nu$ : Poisson ratio.

## DISCUSSION

(Continued discussion after questions and answers relating to the first paper, "Mathematical Modeling of Squashing Flows of Heated Polymer Particles")

*M. E. Ryan:* My question then is the following: The deformation of paper itself is not taken into account in the analysis, "Am I correct on this?"

*Y. Kuo:* Not in this analysis. However, I would like to say that in some small copiers they use cold pressure toners or cold pressure fix which doesn't involve heat at all. In that situation you are dealing with pressures of 1000 or even 2000 psi and in that case the paper will be deformed, but not for this case where the pressure is usually 100 or 150 psi.

*J. H. Walling:* The basic assumption is that there is no relative movement between the particle and the roller?

*Y. Kuo:* That is correct.

*J. H. Walling:* That assumption is wrong because as you change diameter you change the relative motion between the paper and the roll and you get a tremendously high shear between the paper and the roll and you get a smear effect.

*Y. Kuo:* I see what you mean. The spreading is similar to the injection molding's "fountain effect" that the fluid elements in the vicinity of the progressing front move upward toward the wall so that the material deposits on the wall in this manner and not due to the relative slippage between the media.

*J. H. Walling:* But here you get effectively a relative movement between the material and the roller, that is the same as steel rolling where you enter the rolling mill with a lower speed of the bar stock and you get one point in the roll gap where the speed is exactly equal to the circumferential roll speed and at the exit the material goes faster than the roll. You have exactly the same condition here also.

*Y. Kuo:* I think you are talking in greater depth than I originally thought you were. That is true if you are working on the calendaring of sheet for example. The mathematics indicates that you must have some kind of slippage between the substrate and the roll surface. It is true that there is slip. But if you consider this from a microscopic viewpoint you are almost talking about a single point and I doubt that it will affect the analysis.

*J. H. Walling:* I would agree with you that it doesn't affect your analysis, but it definitely affects your impact upon the hardness of the roll surface. You mentioned a tremendous impact of the surface on the quality of the product, sharpness of the image, and this is definitely influenced exclusively by this fact.

*Y. Kuo:* No, the contact pressure increases from zero to maximum in the nip.

# Common Structure, Compatibility and Complementarity of Mathematical Models of Injection Molding

MIROSLAV CRMELA

*Department of Chemical Engineering*
*Ecole Polytechnique of Montreal*
*Montreal, Quebec, Canada*
*and*
*NRCC—IMRI*
*Montréal, Québec, Canada H4C 2K3*

The hierarchy of mathematical models of injection molding is reviewed. Compatibility of the models of the hierarchy, usefulness of simultaneous applications of models formulated on several different levels of the hierarchy and compatability between physical approximations leading to the formulation of a model, and mathematical approximations used to solve numerically the governing equations of the model are discussed. This review is intended to facilitate the search for a model that is best suited to a given need and to indicate future research.

## INTRODUCTION

In the injection molding of thermoplastics, a hot polymer melt flows into an empty cold cavity and solidifies. The molded article is then removed and the whole process is repeated. Formally, we can represent the injection molding as a mapping

$$I^{(im)} \rightarrow O^{(im)} \tag{I.1}$$

where $I^{(im)}$ and $O^{(im)}$ denote, respectively, the input and the output data of the injection-molding process. In this paper, we do not consider the complete process of industrial production of injection-molded articles. Our attention will be focused only on the part of the complete production process for which the input data $I^{(im)}$ consist of $\{I_i^{(im)}, I_w^{(im)}, I_m^{(im)}\}$, where $I_i^{(im)} = \{P_i, Q_i, T_i\}$ are the inlet input data ($P_i$, $Q_i$, $T_i$ denote, respectively, the inlet pressure, the inlet flow rate, and the inlet temperature), $I_w^{(im)}$ includes all the necessary information about the walls of the mold (e.g., wall temperature, etc.), and $I_m^{(im)}$ denotes the thermoplastic material under consideration. The output data $O^{(im)}$ consist of the density flow, temperature, and microstructure of the melt inside the mold cavity during and after the molding cycle. Important quantities included in $O^{(im)}$ are, for example, the fill time $t_f$ (length of time between the instant the polymer begins moving into the mold cavity and the instant the mold become full), cooling time $t_c$ (time interval needed for solidification of the melt), clamp force $P_c$ (pressure on the clamp of the mold), position of weld lines if the melt flows into a cavity from more than one gate. In order to be able to design an efficient injection-molding system producing articles with required properties, it is important to develop a mathematical model of the injection molding that would allow us to obtain the mapping (I.1) theoretically. The mathematical model can then be used to optimize and control the injection-molding process. Formally, we can represent a mathematical model of the injection molding by a diagram

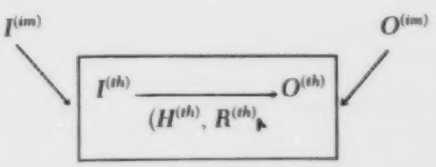


(I.2)

The box represents a theory of polymer melts; $I^{(th)}$, $O^{(th)}$, $H^{(th)}$, $R^{(th)}$ denote, respectively, input data, output data, state variables, and governing equations of the theory. The mapping $I^{(th)} \rightarrow O^{(th)}$ is obtained by solving the governing equations $R^{(th)}$ of the theory. All the mathematical models of injection molding that will be introduced in the next sections will be presented in the form (I.2).

The process of developing a mathematical model of injection molding can be divided into four stages. In the *first stage* the needs—questions expected to be answered by the model—have to be identified. In terms of the formal representation (I.1), subsets of $I^{(im)}$ and $O^{(im)}$ are identified. Depending on the outcome of the first stage, the theory needed in the mathematical model of injection molding (see (I.2)) is chosen or developed. This constitutes the *second stage*. We note that the larger the sets $I^{(im)}$ and $O^{(im)}$ are (i.e. more complete the model is) the more microscopic and consequently the more complex theory has to be chosen in (I.2). Mathematical models that only relate subsets of $I^{(im)}$ and $O^{(im)}$ are called partial models. All the models introduced in the next sections are partial models. In the *third*

*stage* the governing equations of the chosen theory are solved, i.e. the mapping $I^{(th)} \rightarrow O^{(th)}$ is obtained. The *fourth stage* involves a testing of the model. Two kinds of tests can be used. In the first, consequences of the model are compared with results of observations. The second kind of testing compares consequences of other models corresponding to different choices of theories.

In this paper we focus on testing of the models (i.e. the fourth stage) and in particular we concentrate on the second kind of testing. The object of our study is not a particular model of injection molding but a family of the models. Our objectives is to study compatibility and complementarity of the models in the family. We shall see that many practically important problems in mathematical modeling belong to this category. The existing mathematical modeling theory (e.g. Zeigler *et al.* [1, 2], Aris [3], Petrie [4], Middleman [5], Tadmor *et al.* [6], Pearson [7]) does not offer a covenient setting for the study of our problem. Its importance is pointed out and illustrated in Aris [3] and Van Deemter [8]. A list of models of injection molding that were developed in the last thirty years (the first model of injection molding was developed by Spencer and Gilmore [9] in 1951) can be found in recent reviews (e.g. Kamal *et al.* [10]).

## MODELS BASED ON FLUID MECHANICS WITH NO ADDITIONAL INTERNAL STATE VARIABLES

We start to build up a family of partial models of injection molding. In this section we concentrate only on the mass density, the flow velocity, and the temperature. Internal structures such as entanglements, crystallinity, orientation of fibers in filled thermoplastic materials, and internal stresses will be ignored. Due to this limitation, from the start we exclude from our considerations all aspects of injection molding associated with viscoelasticity and solidification of polymer melts. These aspects can, however, be included in the models of this section **a posteriori** as their empirical modifications. A systematic study of an internal structure begins in section III.

### Fluid Mechanics with No Additional Internal State Variables

Fluid mechanics with no additional internal state variables (hereafter simply called fluid mechanics) is chosen in this section to be the theory used in the mathematical model of injection molding (I.2). Fluid mechanics has been developed independently of other theories of macroscopic systems from the experience and intuition generated from hydrodynamic measurements $I^{(hydro)} \rightarrow O^{(hydro)}$ (see for example Lamb [11]). Relations of fluid mechanics to more microscopic theories such as kinetic theory can be established by using the method presented later in this section (see Grmela and Laidlaw [12] and references cited therein). The importance of this study will increase in the next section where additional internal state variables will be included.

We introduce fluid mechanics as an independent theory.

The space of state variables of fluid mechanics $H^{(fm)}$ is a space of five fields $\rho(\underline{r}, t)$, $\underline{v}(\underline{r}, t)$, $e(\underline{r}, t)$ denoting, respectively, the mass density, velocity and the specific internal energy; $\underline{r}$ denotes the position coordinate, $t$ denotes the time. The time evolution equations $R^{(fm)}$ are local expressions of the global conservations of the total mass, the total momentum and the total energy. Undetermined in these equations are the presence tensor $\Pi$, heat flux $\underline{Q}$, and the local equation of state relating the state variables to the local pressure $P(\underline{r}, t)$ and the local temperature $T(\underline{r}, t)$. A specification of these quantities, called constitutive relations, represents the material input data $I^{(fm)}{}_m$ of fluid mechanics. Freedom of choice of constitutive relations is limited by the requirement that the resulting theory be compatible with equilibrium thermodynamics in the sense of the method presented later in this section (see Grmela *et al.* [12, 13]), Wood [14], *Appendix I*).

The simple, commonly used constitutive relations are: (i) the power-law shear viscosity with the Arrhenius type temperature dependence

$$\Pi_{\alpha\beta}(\underline{r}, t) = P(\underline{r}, t)\delta_{\alpha\beta} + \tau_{\alpha\beta}(\underline{r}, t);$$

$$\tau_{\alpha\beta}(\underline{r}, t) = -\eta(\dot{\gamma}_1 T)\left(\dot{\gamma}_{\alpha\beta} - \frac{2}{3}\dot{\gamma}_{\epsilon\epsilon}\delta_{\alpha\beta}\right) - \kappa(\dot{\gamma}_1 T)\dot{\gamma}_{\epsilon\epsilon}\delta_{\alpha\beta}; \qquad \text{(II.1)}$$

$$\dot{\gamma}_{\alpha\beta}(\underline{r}, t) = \frac{\partial v_\alpha}{\partial r_\beta} + \frac{\partial v_\beta}{\partial r_\alpha}; \qquad \dot{\gamma} = \left(\frac{1}{2}\dot{\gamma}_{\alpha\beta}\dot{\gamma}_{\alpha\beta}\right)^{1/2};$$

$$\eta(\dot{\gamma}_1 T) = A \exp\left(\frac{T_a}{T}\right)\dot{\gamma}^{n-1},$$

($T_a$, $n$, $A$ are constants, the bulk viscosity $\kappa$ as well as dependence of $\eta$ on $\dot{\gamma}_{\epsilon\epsilon}$ is usually neglected, $\alpha$, $\beta$, $\epsilon \ldots = 1, 2, 3$, the summation convention is used); (ii) the Fourier law

$$Q_\alpha = -k\frac{\partial T}{\partial r_\alpha} \qquad \text{(II.2)}$$

(the coefficient of thermal conductivity $k$ is assumed to be a constant); (iii) the van der Waals type local equation of state (see e.g. *Eq. II.10* and Kamal *et al.* [10]).

The mathematical model of injection molding that adopts fluid mechanics as the theory used in the model is not, however, very useful. The task of solving the equations of fluid mechanics remains very difficult. Simpler partial models have to be developed. As a first example of a reduction—simplification—of the model we mention the modification that is needed if a computer is asked to assist in the process of solving the governing equations. Since computers can operate only in finite dimensional spaces, the modification must involve discretization, i.e. reduction of the infinite dimensional state space $H^{(fm)}$ to a finite dimensional one. The problem of the compatibility of the original

model and its discrete version is the problem of compatibility of solutions of the governing equations obtained with the help of computer and exact solutions of the governing equation of the original model.

A most general method that is used to discretize a model with infinite dimensional state space is the so-called method of weighted residuals (e.g. Finlayson [15]) or its more particular version known as finite element method (e.g. Zienkiewicz [16]). We have observed that other methods of reduction that were developed in the context of other theories (e.g. Chapman-Enskog method developed to relate kinetic and fluid mechanics theories—see Grmela *et al.* [12]), share with the method of weighted residuals the following common structure.

*Step 1. Guess of solutions to the governing equations of the original model—selection of trial functions*

We say that two models are compatible if the input—output relation obtained by passing through the theories corresponding to both models are identical. We can therefore expect that the governing equations of the reduced model are obtained by partially solving the governing equations of the original model. By using all possible information that is at our disposal about solutions of the original governing equations, we propose to look for them in a form that involves a chosen set of trial functions and state variables used in the reduced model.

*Step 2. Reduction—selection of weighting functions*

We say that an approximative solution to the governing equations of the original model is close to its exact solution if the input—output relation implied by both of these solutions is close. This meaning of closeness in the state space of the theory corresponding to the original model is then translated into a definition of an inner product in the state space. The inner product involves a set of weighting functions. The weighting functions are functions of the same set of independent variables as the trial functions. Governing equations of the reduced model are obtained by (i) inserting the suggested (guessed) solution of the original model obtained in Step 1 into the governing equations of the original model, (ii) multiplying the resulting equation by weighting functions, and (iii) integrating the equation obtained over the independent variables of the weighing (and thus according to our assumption also trial) functions.

## Creeping Flow, Filling, Packing and Cooling Stages of the Injection-Molding Cycle

By following the reduction method presented above we first try to guess some properties of the solution of the fluid mechanics model of injection molding and then use the guess to construct simpler models.

1. We anticipate that the velocity of the melt that flows into the cavity will be relatively small so that the quadratic term in the time evolution equation of $v(\underline{r}, t)$ will be neglected (so-called creeping flow approximation, see e.g. Langlois [17]).
2. We recognize three stages in the injection-molding process with three different characters of solutions to the fluid mechanics equations. During the *filling stage* the mold cavity is filled. After the filling comes to *packing stage* in which an additional amount of material is forced into the cavity to minimize the effect of shrinkage due to cooling. The last stage of the process is the *cooling stage* in which the polymer melt in the cavity solidifies.
3. Surface tension effects and gravitational forces are neglected.

We now consider separately the filling, packing, and cooling stages and we continue in our solution guesses.

*Filling Stage*:

1. We assume that the melt during the filling stage behaves as an incompressible fluid.
2. We assume that the flow is fully developed so that $\partial \underline{v}/\partial t$ will be neglected, so called quasi-stationary approximation.

The fluid mechanics equations reduce to:

$$\rho(\underline{r}, t) = \text{const.}$$

$$\frac{\partial u(\underline{r}, t)}{\partial x} + \frac{\partial v(\underline{r}, t)}{\partial y} + \frac{\partial w(\underline{r}, t)}{\partial z} = 0 \tag{II.3}$$

Hereafter we use the following notation: $\underline{r} = (x, y, t)$, $\underline{v}(y, z, t) = (u(x, y, z,t), v(x, y, z, t), w(x, y, z,t)$, the $x$-direction is the length direction, from the entrance of the cavity to its end, $z$-direction is the thickness direction, $y$-direction is the width direction),

$$\begin{aligned}
\frac{\partial P}{\partial x} &= -\frac{\partial}{\partial x}\tau_{xx} - \frac{\partial}{\partial y}\tau_{yx} - \frac{\partial}{\partial z}\tau_{zx} \\
\frac{\partial P}{\partial y} &= -\frac{\partial}{\partial x}\tau_{xy} - \frac{\partial}{\partial y}\tau_{yy} - \frac{\partial}{\partial z}\tau_{zx} \\
\frac{\partial P}{\partial z} &= -\frac{\partial}{\partial x}\tau_{xz} - \frac{\partial}{\partial y}\tau_{yz} - \frac{\partial}{\partial z}\tau_{zz},
\end{aligned} \tag{II.4}$$

$$\begin{aligned}
\frac{\partial e}{\partial t} = &- u\frac{\partial e}{\partial x} - v\frac{\partial e}{\partial y} - w\frac{\partial e}{\partial z} - \frac{1}{\rho}\left[\tau_{xy}\left(\frac{\partial v}{\partial x} + \frac{\partial u}{\partial y}\right)\right. \\
&\left. + \tau_{xz}\left(\frac{\partial w}{\partial x} + \frac{\partial u}{\partial z}\right) + \tau_{yz}\left(\frac{\partial w}{\partial y} + \frac{\partial v}{\partial z}\right)\right] \\
&- \frac{1}{\rho}\left(\frac{\partial Q_x}{\partial x} + \frac{\partial Q_y}{\partial y} + \frac{\partial Q_z}{\partial z}\right).
\end{aligned} \tag{II.5}$$

*Equation II.5* can be transformed into a time evolution equation for the local temperature $T$ by using the local equation of state (see more in Monin and Yaglom [18] and in *Appendix I*)

$$c_p\rho\left(\frac{\partial T}{\partial t}+u\frac{\partial T}{\partial x}+v\frac{\partial T}{\partial y}+w\frac{\partial T}{\partial z}\right)$$
$$=\frac{\partial P}{\partial t}+u\frac{\partial P}{\partial x}+v\frac{\partial P}{\partial y}+w\frac{\partial P}{\partial z}-\frac{\partial Q_x}{\partial x}-\frac{\partial Q_y}{\partial y}$$
$$-\frac{\partial Q_z}{\partial z}$$
$$-\left[\tau_{xy}\left(\frac{\partial v}{\partial x}+\frac{\partial u}{\partial y}\right)+\tau_{xz}\left(\frac{\partial w}{\partial x}+\frac{\partial u}{\partial z}\right)\right.$$
$$\left.+\tau_{yz}\left(\frac{\partial w}{\partial y}+\frac{\partial v}{\partial z}\right)\right], \qquad \text{(II.6)}$$

$c_p$ is the specific heat of the melt at constant pressure (this quantity is known if the local equation of state is known).

Still further reductions leading to simpler models are presented in the subsequent subsections. The packing and cooling stages cannot be studied by the model formulated in *Eqs. II.3 – II.6*. In the packing stage neither the incompressibility nor quasi-stationarity represent good guesses of solutions of the full set of fluid mechanics equations. Moreover, the importance of the internal structure of the melt increases in this stage. Some simple models that are presented later in this section have been, however, *a posteriori* extended to this stage. The internal structure and its evolution is clearly essential in the cooling stage. The fluid mechanics model of injection molding considered in this section is thus not applicable. We mention the cooling stage in section "Models based on fluid mechanics with additional internal state variables."

### Spencer and Gilmore [9]

The mold cavity is assumed to be a circular tube of radius $R$, the temperature is assumed to be a constant $T_0$. Solution of *Eqs. II.3* and *II.4* gives the Poiseuille flow. A state of the melt that is filling a circular tube is characterized in the Spencer-Gilmore model by two state variables $q$ and $x$. The quantity $q(t)$ denotes the instantaneous volume flow rate, and $x(t)$ denotes the position of the melt front at time $t$. The Poiseuille solution and the mass conservation imply the following two equations governing the time evolution of $q(t)$ and $x(t)$:

$$q(t)=\frac{\Pi R^3}{3+\frac{1}{n}}\left(\frac{R(P_i-P_{int})}{2B\times(t)}\right)^{1/n} \qquad \text{(II.7)}$$

$$\frac{dx}{dt}=\frac{1}{\Pi R^2}q(t), \qquad \text{(II.8)}$$

$P_i$ denotes the inlet pressure, $P_{int}$ is the pressure at the plastic-air interface, $B = A\exp)Ta/T)$; the meaning of other symbols has been explained in the text after the constitutive relation, *Eq. II.1*.

Spencer and Gilmore [9] have also extended their model to the packing stage. In this stage $x(t) = L$ ($L$ denotes the length of the tube), $q(t)$ remains a state variable, and the second state variable is $P(t)$ denoting the instantaneous pressure at the end of the tube. The equation governing the time evolution of $q(t)$ is *Eq. II.7*, where $x(t) = L$ and $P_{int}$ is replaced by $P(t)$. The equation governing the time evolution of $P(t)$ is obtained from the mass conservation

$$\frac{dM(t)}{dt}=\frac{q(t)M(t)}{V}, \qquad \text{(II.9)}$$

$M(t)$ is the mass of the melt inside the cavity at time $t$, $V$ is the volume of the cavity) and from a local equation of state. Spencer and Gilmore have used the van der Waals local equation of state

$$(P(t)+a)\left(\frac{V}{M(t)}+b\right)=cT(t), \qquad \text{(II.10)}$$

$a$, $b$, $c$ are material constants, $T(t)$ is assumed to be known.

The range of validity of the model can also be extended by empirically adjusting the constants introduced in the equations and/or by introducing new adjustable constants (see Spencer and Gilmore [9]). We also note that use of appropriate coordinate systems in the Spencer-Gilmore model can also yield other cavity shapes (e.g., end-gated strip and center-gated sector disk).

### Harry and Parrott [19]

The shape of the cavity allowed in this model is the same as in the Spencer-Gilmore model, but the temperature is not assumed to be constant. Various applications and developments of this model have been published [20, 28]. We write the governing equations only in Cartesian coordinates (i.e. the shape of the cavity is an end gated strip). A state of the melt is characterized in the Harry-Parrott model by $u(x, z, t)$, $P(x, t)$, $T(x, z, t)$. The equations governing the evolution of the state variables follow easily from *Eqs. II.4* and *II.6*. The first equation to be satisfied is the conservation of mass equation

$$q_i \equiv q(t) = q\int_0^{z_w} dz\,W(z)u(x, z, t), \qquad \text{(II.11)}$$

where $q_i$ is the inlet volume flow rate, $z_w$ is the half thickness of the strip, and $W(x)$ is its width. The second equation follows from *Eq. II.4*,

$$\frac{dP}{dx}=-\frac{\partial}{\partial z}\tau_{zx}. \qquad \text{(II.12)}$$

The last equation of the model follows from *Eq. II.6*,

$$\rho c_p\left(\frac{\partial T}{\partial t}+u\frac{\partial T}{\partial x}\right)=\frac{\partial}{\partial z}\left(k\frac{\partial T}{\partial z}\right)-\tau_{zx}\frac{\partial u}{\partial z}. \qquad \text{(II.13)}$$

The omission of $dP/dt$ in *Eq. II.13* is compatible with the quasi-stationary approximation.

Boundary conditions in $z$-direction are the no-slip boundary condition for $u$ and

$$\left[\frac{\partial T}{\partial z}\right]_{(x,0,t)} = 0$$
$$T(x, z_W, t) = T_W \qquad \text{(II.14)}$$

$T_W$ is the wall temperature. The $x$-direction boundary conditions are:

$$T(0, z, t) = T_i \qquad \text{(II.15)}$$

$$T(x_f, z, t_f) = \bar{T}(x_{\bar{f}}, t_f), \qquad \text{(II.16)}$$

$T_i$ is the in let temperature. *Equation II.16* defines the temperature of the volume element filled at time $t_f$ as equal to the bulk temperature of the fluid element slightly upstream, denoted in *Eq. II.16* as $x_{\bar{f}}$.

The initial boundary conditions are:

$$T(x, z, 0) = T_0 = \text{const.}$$
$$q(0) = q_0 = \text{const.} \qquad \text{(II.17)}$$

We note that if the temperature is assumed to be constant then the Harry-Parrott model reduces to the Spencer-Gilmore model. Summing up, we have $H^{(HP)} = (u(x, z, t), P(x, t), T(x, z, t))$, $I_i^{(HP)} = (q_0, T_i, T_0)$, $I_w^{(HP)} = (z_w, T_W, W(x), L)$, $I_m^{(HP)} = (k, A, T_a, n)$; by $L$ we denote the length of the strip, $(HP)$ denotes Harry-Parrott.

In order to solve the system of *Eqs. II.11–II.17* another reduction, preparing the model for application of a computer, is needed. The regularity of the shape of the mold cavity suggests the use of the finite difference method. This method of reduction is a particular case of the finite element method (see Zienkiewicz [16]) and thus also a particular case of the general reduction method introduced earlier. The Harry-Parrott model has been extended to include approximately the packing stage and effects arising due to the solidification (see Kamal *et al.* [20]).

### Pearson [29]

The Spencer-Gilmore model allows calculation of the progression of the melt front in the isothermal filling of an end-gated circular tube, an end-gated strip, or a center-gated disk; the Harry-Parrott model allows calculation of the progression of the melt front and the temperature in the filling of an end-gated circular tube, an end-gated strip, or a center-gated disk. Information about the shape of the melt front if the width of the gate is smaller than the width of the cavity is beyond the scope of these models. We turn our attention now to a model that allows calculation of the shape of the melt front. The mold cavity is assumed to be thin (i.e. its dimension in $z$-direction is much smaller than its dimensions in $x$ and $y$-directions). The gate is at $x = 0$ and its width is smaller than the width of the cavity. Pearson [17] has realized that in this case the filling may be described in terms of generalized Hele-Shaw flow (see [29], [33], [17]). A state of the melt is described by $u(x, y, z)$, $v(x, y, z)$, $P(x, y)$, $T(x, y, z,t)$. *Equation II.4* is further simplified by assuming that $\partial u/\partial x$ and $\partial u/\partial y$ is negligible with respect $\partial u/\partial z$, similarly, $\partial v/\partial x$ and $\partial v/\partial y$ is negligible with respect to $\partial v/\partial z$. We obtain

$$\frac{\partial P}{\partial x} = \frac{\partial}{\partial z}\left(\eta \frac{\partial u}{\partial z}\right)$$
$$\frac{\partial P}{\partial y} = \frac{\partial}{\partial z}\left(\eta \frac{\partial v}{\partial z}\right) \qquad \text{(II.18)}$$

*Equation II.3* is averaged over the thickness of the mold cavity,

$$\frac{\partial}{\partial x}(\bar{b}\bar{u}) + \frac{\partial}{\partial y}(\bar{b}\bar{v}) = 0, \qquad \text{(II.19)}$$

where $\bar{b}(x, y)$ is the thickness of the cavity at $(x, y)$, $\bar{u}(x, y) \overset{\text{def}}{=} \int_0^{\bar{z}^w} u(x, y, z)dz$, $v(x, y) \overset{\text{def}}{=} \int_0^{\bar{z}^w} v(x, y, z)dz$. *Equation II.6* reduces to

$$\rho c_p \left(\frac{\partial T}{\partial t} + u\frac{\partial T}{\partial x} + v\frac{\partial T}{\partial y}\right) = k\frac{\partial T}{\partial z^2} + \eta\dot{\gamma}^2 \qquad \text{(II.20)}$$

The terms $\partial^2 T/\partial x^2$ and $\partial^2 T/\partial y^2$ have been neglected in comparison with $\partial^2 T/\partial z^2$. Various modifications and applications of the Pearson model are studied in [34–39]. The model consisting of *Eqs. II.18–II.20* equipped with appropriate boundary and initial conditions (see e.g. Hieber and Shen [36, 37]) has to be further reduced to allow computer assistance. Hieber and Shen [37] have described an implementation of the finite element method. They have chosen quadratic trial functions for $P(x, y)$, linear trial functions for $T_{z,t}(x, y)$ and finite difference type approximation of $z$ and $t$ dependence of $T$. The special form of *Eqs. II.18* also allows a different approach to finding their solutions (see [30, 34, 35]). Possible extension of the Pearson model to include the packing stage and the evolution of microstructure will be discussed in the next section.

### Kamal [40]

An interesting flow pattern has been observed near advancing melt front. Rose [41] has called it a fountain type flow (see also Tadmor and Gogos [6]). In this flow the thickness component (i.e. $w$-component) of the velocity becomes important. Details of the flow near the melt front are important particularly for determining quality and morphology of the surface of the molded article. Neither of the models discussed in the previous three sections can be used to study the fountain flow. Kamal [40] has recently suggested a relatively simple model that allows calculation of it. The state variables in the Kamal model are $u(x, z)$, $w(x, z)$, $P(x, z)$, $T(x, z, t)$. Equations governing the evolution of these state variables can be readily obtained from *Eqs. II.3–II.6*. We shall return to this model in a later section.

### Mold Network

Applicability of the relatively simple models that were discussed so far is limited mainly by assuming simple shapes of mold cavities. Only the Pearson

model, appropriately modified by using the finite element method, can be used for complex geometries of the cavity provided, however, the cavity is thin. The full set of fluid mechanics equations can be modified by using the finite element method, and used to study general three dimensional cavities (see for example [16], [42]). However, the complexity of the resulting set of equations remains an essential obstacle even for the biggest contemporary computers. The question arises as to whether the models and results obtained for cavities of simple geometries can be used to deal with cavities of complex geometries. This question has been posed and analyzed by Stevenson, *et al.* [25–27], Kamal, preprint, Richardson *et al.* [43], Booy [44] and Hieber [45]. Only the principal ideas will be presented here.

The complex mold cavity is divided into basic units (also called primitive segments). Richardson *et al.* [43] suggest the following basic units: a circular pipe of a constant diameter, a rectangular channel of constant cross section, and an axisymmetric flat channel of constant depth. In all three cases the constant dimension can be replaced by dimensions linearly varying along the axis in the first two basic units and along the radius in the third basic unit. Hieber [45] suggests consideration of a circular tube, center-gated section of a disk, end-gated strip, and a center gated section of a disk with non-zero inner radius. Moreover, in cavities with branchings, all possible flow paths are identified. The complex mold cavity composed of the flow paths and the basic units is called a mold network. Let's consider first a single flow path composed of several basic units. The decomposition on basic units is in fact an appropriate choice of cavity adapted coordinate systems (the coordinate transformations vary in dependence on location in the flow path) so that the Harry-Parrott model (i.e. the one-dimensional analysis) can be applied to the whole flow path. In the case of several flow paths, the flow and the temperature in flow paths are coupled to each other. The coupling is determined by requiring that some properties of the total flow (e.g. the property that the pressure drop is the same along each flow path) are satisfied.

## MODELS BASED ON FLUID MECHANICS WITH ADDITIONAL INTERNAL STATE VARIABLES

In this section we introduce fluid mechanics theories with an enlarged set of state variables and we adopt them in mathematical models of injection molding (I.2). In additon to the fields $\rho$, $\underline{v}$, $e$ introduced by fluid mechanics we introduce new state variables characterizing internal structures of the thermoplastic materials under consideration. In general, the new additional state variables will be different for different thermoplastic materials. The choice will be determined by our experience from observations (see e.g. [46–56]) and by an intuitive insight into the nature of the internal structures of principal importance. In the context of the complete molecular characterization of thermoplastic materials the new state variable should collect the molecular properties that dominate the long time behavior of the molecular state variables. The mass, momentum, and energy conservation are insufficient for formulating the governing equations. A consideration of the generalized fluid mechanics theory in the context of other theories (that are either more microscopic such as quantum mechanics or kinetic theory or more macroscopic such as equilibrium thermodynamics) becomes therefore of fundamental importance.

### Viscoelastic Materials

The new state variable is proposed to be a symmetric tensor $\underline{\underline{c}}(\underline{r}, t)$ having the physical meaning of a measure of an internal strain. The internal structure of the thermoplastic material assumed to be responsible for viscoelastic behavior is a network of entangled molecular chains. The tensor $\underline{\underline{c}}(\underline{r}, t)$ denotes a deformation of the network. This point of view of viscoelastic materials has been developed by Hand [57], Leonov [58], Dashner and Vanarsdale [59], and Vanarsdale [60]. Several different points of view can be employed to investigate the possible forms of the equations governing the time evolution for the state variables $\rho(\underline{r}, t)$, $e(\underline{r}, t)$, $\underline{v}(\underline{r}, t)$, $\underline{\underline{c}}(\underline{r}, t)$.

(1) An analysis that takes its inspiration from the molecular point of view has been developed by the authors of references 61–67. A natural new state variable in kinetic theories is the phase space respectively configuration space distribution function. The time evolution of the distribution functions is governed by a kinetic equation.

(2) We shall see later that the requirement of the compatibility of the time evolution equations with equilibrium thermodynamics implies that the pressure tensor $\underline{\underline{\Pi}}(\underline{r}, t)$ is basically proportional to $\underline{\underline{c}}(\underline{r}, t)$ (see more in *Appendix I*). The new equation governing the time evolution of $\underline{\underline{c}}(\underline{r}, t)$ is therefore closely related to an equation governing the time evolution of the pressure tensor $\underline{\underline{\Pi}}(\underline{r}, t)$. A time evolution equation for $\underline{\underline{\Pi}}(\underline{r}, t)$ has been suggested by Maxwell and generalized by Oldroyd [68] (see also Schowalter [69]). However, most of the time evolution equations for $\underline{\underline{\Pi}}(\underline{r}, t)$ have been suggested for the case of constant temperature. Generalizations to include non-isothermal effects have been considered by Bird [70], and Gupta and Metzner [71]. These authors, however, do not consider the corresponding equations governing the time evolution of the temperature.

(3) A different point of view, in related context of micropolar fluids, has been developed by Eringen [72] (see also Martin *et al.* [73], where liquid crystals are considered).

(4) Let's assume that the equation governing the time evolution of $\underline{\underline{\Pi}}(\underline{r}, t)$ has been solved. The solution is the pressure tensor $\underline{\underline{\Pi}}(\underline{r}, t)$ depending in general on $\rho(\underline{r}', t')$, $e(\underline{r}', t')$, $\underline{v}(\underline{r}', t')$ where $\underline{r}' = \underline{r}$, $t' = t$. Now we can regard the set of generalized fluid mechanics equations as classical fluid mechanics equations governing the time evolution of $\rho$, $\underline{v}$,

$e$. The constitutive relations are, however, generalized to allow non-locality in time (in other words to allow a memory). This point of view of viscoelastic fluids has been developed by Coleman and Noll [74], Rivlin [75], and Crochet and Naghdi [76]. These authors have also considered restrictions on the constitutive relations implied by the requirement of the compatibility of the resulting set of the time evolution equations with equilibrium thermodynamics. It is however, far from obvious what is meant precisely by the compatibility of a dynamical theory with equilibrium thermodynamics. A wide disagreement exists on this point in the literature (see Grmela and Carreau [13], Woods [14]).

(5) A set of equations determining the time evolution of $\rho(\underline{r}, t)$, $e(\underline{r}, t)$, $\underline{v}(\underline{r}, t)$, $\underline{\underline{c}}(\underline{r}, t)$ that reduces to the standard set of equations of fluid mechanics if $\underline{\underline{c}}$ = identity and that is compatible with equilibrium thermodynamics in the sense of Grmela and Carreau [13] as introduced in *Appendix I*. Interesting new terms arise in the equation governing the time evolution of the internal energy (and consequently also in the equation governing the time evolution of the temperature). Their appearance is a consequence of the introduction of the internal energy $e = E_{tot} - (E_{kin} + E_{el})$, where $E_{tot}$, $E_{kin}$, $E_{el}$ are, respectively, the total energy, the kinetic energy, and the stored elastic energy. The necessity of new terms has been clearly recognized in the context of the explicit considerations of another type of internal structure, namely the structure that is associated with crystallinity. The new term in this context is the term accounting for the latent heat generation.

We now review several examples of a simplified set of equations governing the time evolution of viscoelastic fluids for which solutions have been studied.

*Kawahara and Takeuchi [77]*

A state of a viscoelastic fluid in this model is described by six state variables $u(x, y, t)$, $v(x, y, t)$, $P(x, y, t)$, $\tau_{xx}(x, y, t)$, $\tau_{xy}(x, y, t)$, $\tau_{yy}(x, y, t)$. The temperature $T$ and the density $\rho$ are assumed to be constant. The time evolution equations are:

(1) Incompressibility condition

$$\frac{\partial u}{\partial x} + \frac{\partial v}{\partial y} = 0, \tag{III.1}$$

(2) Momentum equations

$$\rho \frac{\partial u}{\partial t} + \rho u \frac{\partial u}{\partial x} + \rho v \frac{\partial u}{\partial y} = -\frac{\partial P}{\partial x} - \frac{\partial \tau_{xx}}{\partial x} - \frac{\partial \tau_{xy}}{\partial y}$$

$$\rho \frac{\partial v}{\partial t} + \rho u \frac{\partial v}{\partial x} + \rho v \frac{\partial v}{\partial y} = -\frac{\partial P}{\partial y} - \frac{\partial \tau_{xy}}{\partial x} - \frac{\partial \tau_{yy}}{\partial y} \tag{III.2}$$

(3) Maxwell-Oldroyd equations

$$\bar{a}\left(\frac{\partial \tau_{xx}}{\partial t} + u\frac{\partial \tau_{xx}}{\partial x} + v\frac{\partial \tau_{xx}}{\partial y} - q\frac{\partial u}{\partial x}\tau_{xx} - q\frac{\partial u}{\partial y}\tau_{xy}\right) + \tau_{xx} = -q\eta\frac{\partial u}{\partial x}$$

$$\bar{a}\left(\frac{\partial \tau_{yy}}{\partial t} + u\frac{\partial \tau_{yy}}{\partial x} + v\frac{\partial \tau_{yy}}{\partial y} - q\frac{\partial v}{\partial x}\tau_{xy} - q\frac{\partial v}{\partial y}\tau_{yy}\right) + \tau_{yy} = -q\eta\frac{\partial v}{\partial y} \tag{III.3}$$

$$\bar{a}\left(\frac{\partial \tau_{xy}}{\partial t} + u\frac{\partial \tau_{xy}}{\partial x} + v\frac{\partial \tau_{xy}}{\partial y} - \frac{\partial u}{\partial x}\tau_{xy} - \frac{\partial u}{\partial y}\tau_{yy} - \frac{\partial v}{\partial x}\tau_{xx} - \frac{\partial v}{\partial y}\tau_{xy}\right) + \tau_{xy} = -\eta\left(\frac{\partial u}{\partial y} + \frac{\partial v}{\partial x}\right),$$

$\bar{a}$ and $\eta$ are constants characterizing the material under consideration. Kawahara and Takeuchi reduce further *Eqs* III.1–III.3, equipped with appropriate boundary and initial conditions, by using the finite element method. The trial functions chosen by Kawahara and Takeuchi are quadratic for $u$, $v$, $\tau_{xx}$, $\tau_{xy}$, $\tau_{yy}$, and linear for $P$. The weighting functions are chosen to be the same as the trial functions (in this special case the weighted residual method is called the Galerkin method). The time dependence has been treated by using the finite difference method. It has been observed by Mandelson *et al.* [78] (see also Crochet and Walters [79]) that this type of model fails to give a reliable steady-state solution if the constant $\bar{a}$ is sufficiently large (i.e. if the elastic effects become comparable with viscous effects, in another words, if the Deborah number ~1). Mandelson *et al.* [78] suggest that the failure might be due to the unrealistic restriction to two dimensions.

*Isayev and Hieber [80]*

This model extends the Harry-Parrott model to viscoelastic fluids. A state of polymer melt is characterized by $u(z)$, $P(x, z)$, $c_{xx}(z, t)$, $c_{xz}(z, t)$, $c_{zz}(z, t)$, $T(z, t)$. Measures of the internal strain $\underline{\underline{c}}(z, t)$ appear as new additional state variables. The equations determining the state variables are:

i) *Eq II.11*
ii) *Eq II.13* (Isayev and Hieber however omit the term $\partial T/\partial x$, the term $-\tau_{xz}\partial u/\partial t$, and the terms arising due to stored elastic energy, (see *Appendix I*),
iii) *Eq III.12*
iv) $$\frac{\partial P}{\partial t} = -\frac{\partial}{\partial t}\tau_{zz}$$
v) Leonov's [58] time evolution equations for $c_{xx}(z, t)$, $c_{xz}(z, t)$, $c_{zz}(z, t)$

*Kamal [40]*

This model extends the Kamal model to viscoelastic fluids. A state of a polymer melt in the Kamal model is characterized by $u(x, z)$, $w(x, z)$, $P(x, z)$, $T(x, z, t)$, $\tau_{xx}(x, z, t)$, $\tau_{xz}(x, z, t)$, $\tau_{zz}(x, z, t)$. Equations determining $u$, $w$, $P$, $T$ are readily obtained from *Eqs II.3–II.6*, the stress tensor $\underline{\underline{\tau}}$ is determined by the Maxwell-Oldroyd-Gupta-Metzner [71] equation. The terms arising in the time evolution equation for temperature (see *Appendix I*) are not considered.

### Composites

Thermoplastic materials are often filled with reinforcing particles, particularly glass fibers (see e.g. Goettler [52]). A state of one fiber is described by the position of its center of mass $\underline{r}$ and by a unit vector $\underline{\kappa}$ denoting its orientation. A distribution function $\psi(\underline{r}, \underline{\kappa}, t)$ of the fibers appears to be a natural candidate for the new additional state variable. The problem of constructing equations governing the time evolution of the state variables $\rho$, $\underline{v}$, $e$, $\psi$ can be approached by following the strategy presented in *Appendix I* in the context of viscoelastic fluids. Some aspects of these equations have been studied by Leal *et al.* (81, 82), Takserman-Krozer *et al.* [53], Goettler [52], Christie *et al.* [54], Chung *et al.* [83]. Observations that are pertinent to injection molding of composites have been reported by the authors of Refs 46–50, 52, 55, and 56.

### Crystallizing Thermoplastic Materials

Solidification of some thermoplastic materials (e.g. polyethylene) is associated with creation of a crystalline structure. This structure then plays a very important role in the cooling stage and in determining properties of molded articles. An appropriate new additional state variable may be a degree of crystallinity $\psi_c = (V_a - V)/(V_a - V_c)$, where $V$, $V_a$, $V_c$ are specific volumes of the specimen, amorphous material, and crystallized material, respectively. The problem now is to construct equations governing the time evolution of $\rho$, $\underline{v}$, $e$, $\psi_c$. Again, the strategy presented in *Appendix I* can be followed. Some aspects of the full set of equations have been studied by Gordon and Hiller [84], Tadmor [51], Kamal [10] (see also references cited therein).

### Remarks

i) Models presented in the second section have been extended to take into account some aspects associated with internal structure by: (a) keeping the setting of the five state variable fluid mechanics presented in the second section, (b) adding new terms to the governing equations (e.g. the heat generation due to solidification—Kamal *et al.* [38], [10]) and modifying boundary conditions (Kamal *et al.* [38]). The approach presented in this section provides a more systematic method for including the influence of an internal structure.

ii) The flow equation (II.4) and the temperature equation (II.6) are coupled through the temperature dependence of viscosity. The flow-temperature coupling becomes much more complex in generalized fluid mechanics equations presented in this section (see Pearson and McIntire [85]).

iii) The quantities characterizing the individuality of the thermoplastic materials (material parameters) are represented in our notation by $I_m^{(th)}$. We note that these quantities are the quantities associated with the adopted theory. In general, different theories require different types of material parameters. The association $I_m^{(im)} \rightarrow I_m^{(th)}$ assigning material parameters to a given thermoplastic material is usually obtained as follows: (a) A separate observation (or observations) $i \rightarrow 0$ are conducted with the given thermoplastic material; (b) The results of the observations are calculated by using the chosen theory; (c) The values $i_m^{(th)}$ for which the theoretical and the experimental results coincide represent the material parameters $i_m^{(im)}$ corresponding to the thermoplastic material. We note that this procedure for measuring material parameters requires that: (i) the same theory (in its complete form) be used to analyze both injection molding and measurement experiments (i.e. in particular, that all the state variables relevant in the injection-molding process—e.g. an internal structure—be controlled in the measurement experiment), and (ii) both the injection-molding and the measurement experiment belong to the range of validity of the chosen theory. These conditions are rarely, if ever, satisfied.

iv) Instabilities in the flow of thermoplastic materials into mold cavities have been observed (e.g. pressure oscillation—see Utracki *et al.* [86]). A theoretical analysis of the stability of the injection molding is thus of considerable practical interest.

## CONCLUSION

Modeling of physical processes that take place during injection molding has been reviewed. We have concentrated on developing a unified point of view allowing a systematic study of relationships between models belonging to different levels of sophistication.

The first source of difficulty in formulating models that are simple (requiring relatively short computer time) and complete (providing answers to all practically important questions) is the necessity to include in the consideration an internal structure such as entanglements, crystallinity, and internal strains. A point of view leading to a systematic development of the corresponding generalized fluid mechanics that is compatible with both more microscopic theories (e.g. with a kinetic theory) and more macroscopic theories (e.g. equilibrium thermodynamics) has been suggested by the author [13] (see also *Appendix I*).

The second source of difficulty in meeting the requirement of simplicity and completeness in modeling of injection molding is the necessity to consider complex geometries of mold cavities. The finite element method in the case of thin cavities that are treated as two-dimensional or the generalized finite element method (generalizing the ideas on which the mold network concept is based) may provide a promising answer.

A useful model of injection molding will not likely be a single big model but rather a family of mutually compatible models providing answers of different degrees of completeness. For this reason, we have

discussed the concept of the compatibility of models in some detail.


## ACKNOWLEDGMENT

I would like to thank R. Gauvin, M. R. Kamal, G. Salloum and L. A. Utracki for stimulating discussions.


## APPENDIX I

### Energy Balance in Viscolastic Fluids

The analysis of fluids with internal strain developed by Leonov [58], Dashner *et al.* [59], and Vanarsdale [50] is incomplete since a complete analysis of the energy equation is missing. Our objective in this *Appendix* is to complete the Leonov analysis by constructing the time evolution equations for the mass density $\rho(\underline{r}, t)$ velocity $\underline{v}(\underline{r}, t)$, internal strain $\underline{\underline{c}}(\underline{r}, t)$ and the internal energy $e(\underline{r}, t)$ and by considering in a systematic way their compatibility with equilibrium thermodynamics. The method developed by Grmela *et al.* ([13] and references cited therein) is used. The energy equation contains new terms due to the consideration of the stored elastic energy. A detailed analysis of the new terms as well as a detailed consideration of generalized fluid mechanics equations involving the additional state variables previously suggested will be presented in a separate publication.

The equations governing the time evolution of mass density $\rho(\underline{r}, t)$, total energy density $E(\underline{r}, t)$ and the total momentum density $\underline{U}(\underline{r}, t)$ are

$$\begin{aligned} \frac{\partial \rho}{\partial t} &= -\frac{\partial}{\partial r_\gamma} \dot{\rho}_\gamma \\ \frac{\partial E}{\partial t} &= -\frac{\partial}{\partial r_\gamma} \dot{E}_\gamma \\ \frac{\partial U_\alpha}{\partial t} &= -\frac{\partial}{\partial r_\gamma} \dot{U}_{\alpha\gamma} \end{aligned} \tag{A.1}$$

expressing the conservation of the total mass

$$M = \int_V^{d\underline{r}} \rho(\underline{r}, t) \tag{A.2}$$

total energy

$$E = \int_V^{d\underline{r}} E(\underline{r}, t) \tag{A.3}$$

and the total momentum

$$\underline{U} = \int_V^{d\underline{r}} \underline{U}(\underline{r}, t) \tag{A.4}$$

The fluxes $\dot{\underline{\rho}}, \dot{\underline{E}}, \dot{\underline{U}}$ are left undetermined at this point. They are only assumed to be local, sufficiently regular, functionals of the state variables. A functional is said to be local if its value at $(\underline{r}, t)$ depends only on the state variables evaluated at $(\underline{r}, t)$. The equation governing the time evolution of the internal strain $\underline{\underline{c}}(\underline{r}, t)$ is assumed to be the form

$$\frac{\partial c_{\alpha\beta}}{\partial t} = -V_\gamma \frac{\partial}{\partial r_\gamma} c_{\alpha\beta} - R_{\alpha\beta} + d_{\alpha\beta} . \tag{A.5}$$

Both $\underline{\underline{R}}(\underline{r}, t)$ and $\underline{\underline{d}}(\underline{r}, t)$ are left undetermined; $v$ is introduced in (A.6). An independent physical insight allowing the suggestion of an appropriate form of $R\alpha\beta$ is provided by the concept of a codeformational derivative introduced by Oldroyd [68]. The term on the left-hand side of (A.5) together with the first two terms on the right-hand side of (A.5) can be regarded, for example, as the codeformational (Oldroyd) time derivative (see Leonov [58]). We introduce new state variables $\rho, e, \underline{v}, \underline{\underline{c}}$ denoting, respectively, mass density, specific internal energy density, velocity, and internal stress by

$$\begin{aligned} \rho &= \rho \\ U_\alpha &= \rho v_\alpha \\ E &= \frac{1}{2} \rho v_\gamma v_\gamma + \rho\epsilon + \rho e , \end{aligned} \tag{A.6}$$

$\epsilon$ denotes the density of the specific stored elastic energy. We assume (for the sake of simplicity) that $\epsilon$ is a local functional of only the internal strain $\underline{\underline{c}}$. Furthermore, we introduce new fluxes, $\underline{\underline{\Pi}}$, $\underline{\mathcal{F}}$, $\underline{Q}$, $\underline{\underline{R}}$, $\underline{\underline{d}}$ denoting, respectively, the total stress tensor, flux of the stored elastic energy, heat flux, and the tensors introduced in equation (A.5) by

$$\begin{aligned} \dot{\rho}_\alpha &= \rho v_\alpha \\ \dot{U}_{\alpha\gamma} &= \rho v_\alpha v_\gamma + \Pi_{\alpha\gamma} \\ \dot{E}_\alpha &= E v_\alpha + \Pi_{\gamma\alpha} v_\gamma + \mathcal{F}_\alpha + Q_\alpha \\ R_{\alpha\beta} &= R_{\alpha\beta} \\ d\alpha_\beta &= d\alpha_\beta . \end{aligned} \tag{A.7}$$

By inserting (A.6) and (A.7) into (A.1) and (A.5) we obtain

$$\begin{aligned} \frac{\partial \rho}{\partial t} &= -\frac{\partial}{\partial r_\gamma} (\rho v_\gamma) \\ \frac{\partial c_{\alpha\beta}}{\partial t} &= -v_\gamma \frac{\partial}{\partial r_\gamma} c_{\alpha\beta} - R_{\alpha\beta} + d_{\alpha\beta} \\ \frac{\partial v_\alpha}{\partial t} &= -v_\gamma \frac{\partial}{\partial r_\gamma} v_\alpha - \frac{1}{\rho} \frac{\partial}{\partial r_\gamma} \Pi_{\alpha\gamma} \\ \frac{\partial e}{\partial t} &= -v_\gamma \frac{\partial}{\partial r_\gamma} e - \frac{1}{\rho} \Pi_{\gamma_\alpha} \frac{\partial}{\partial r_\alpha} v_\gamma - \frac{1}{\rho} \frac{\partial}{\partial r_\gamma} \\ &\quad \cdot (\mathcal{F}_\gamma + Q_\gamma) - \epsilon_{c_{\alpha\beta}} (d_{\alpha_3} - R_{\alpha_\beta}) . \end{aligned} \tag{A.8}$$

By $\epsilon_{c_{\alpha\beta}}$ we denote the derivative of $\epsilon$ with respect to $c_{\alpha\beta}(\underline{r}, t)$. The equations (A.8) represent the equations governing the time evolution of the state variables $\rho, e, \underline{v}, \underline{\underline{c}}$. They involve, however, quantities $\{\epsilon, \underline{\underline{\Pi}}, Q, \underline{\mathcal{F}}, \underline{\underline{R}}, \underline{\underline{d}}\}$ that remain undetermined functionals of the state variables. The rest of this *Appendix* is devoted to comments concerning constitutive relations (i.e. specification of $\{\epsilon, \underline{\underline{\Pi}}, Q, \underline{\mathcal{F}}, \underline{\underline{R}}, \underline{\underline{d}}\}$ as functions of $\rho, e, \underline{v}, \underline{\underline{c}}$).

The constitutive relations can be obtained from considerations based on the requirement of the compatibility of (A.8) with more microscopic theories (as, e.g., with kinetic theory), with equilibrium

thermodynamics, and on the comparison of theoretical and experimental results. Here we only derive consequences of the requirement of the compatibility of (A.8) with equilibrium thermodynamics. Before this, however, we comment about the relation of *Eq A.8* with the equations introduced by Leonov [58], Dashner *et al.* [59] and Vanarsdale [60]. These authors have introduced particular forms of $\underline{\underline{R}}$, $\underline{q}$, and $\Pi$. They have also considered the entropy inequality (a part of a study of the compatibility of (A.8) with equilibrium—see Grmela *et al.* [13] and the rest of the *Appendix*; their discussion is, however, incomplete since the energy equation (the last equation in (A.8)) is absent in their considerations. The last two terms in the energy equation are new; they arise due to the introduction of the stored elastic energy. The coupling between the flow equation (the third equation in (A.8)) and the energy in (A.8) is much more complex than in the case of classical fluid mechanics.

We now turn our attention to a study of the compatibility of (A.8) with equilibrium thermodynamics. By following the general method of reduction presented previously, we arrive at the following understanding of this notion (see Grmela, *et al.* [13], [12]). We say that equations (A.8) are compatible with equilibrium thermodynamics if three functionals $M$, $E$, $S$ of the state variables $\rho$, $e$, $\underset{\sim}{v}$, $\underline{\underline{c}}$, exist that satisfy the following four properties:

(1)

$$\frac{dM}{dt} = 0 \tag{A.9}$$

$$\frac{dE}{dt} = 0 \tag{A.10}$$

$$\frac{dS}{dt} \geq 0 \tag{A.11}$$

(2) The state variables for which the functional

$$H(\rho, e, \underset{\sim}{v}, \underline{\underline{c}}, T_{th}, \mu_{th}, P_{th}) \stackrel{\text{def}}{=} - S(\rho, e, \underset{\sim}{v}, \underline{\underline{c}}) - \frac{\mu_{th}}{T_{th}} M(\rho, e, \underset{\sim}{v}, \underline{\underline{c}}) + \frac{1}{T_{th}} E(P, e, \underset{\sim}{v}, \underline{\underline{c}}) + \frac{P_{th}}{T_{th}} V \tag{A.12}$$

reaches its minimum are the state variables representing the states studied in equilibrium thermodynamics. They are called equilibrium states. In *Eq* A.12, $T_{th}$, $\mu_{th}$, $P_{th}$ are parameters, and $V$ is volume of the region confirming the system under consideration. The functionals $M$, $E$, $S$ evaluated at equilibrium states become the thermodynamic mass $M_{th}$, thermodynamic energy $E_{th}$ and the thermodynamic entropy $S_{th}$. They possess all the properties required of them in equilibrium thermodynamics. The quantities $T_{th}$, $\mu_{th}$, $P_{th}$ denote the temperature, chemical potential, and pressure, respectively.

(3) The equality in (A.11) holds only for solutions of $R^+(\rho, e, \underset{\sim}{v}, \underline{\underline{c}}) = 0$, where $R^+$ formally denotes the right-hand side of (A.8) that remains invariant if $\underset{\sim}{v}$ is changed into $-\underset{\sim}{v}$.

(4) The fourth property is a symmetry property of the equations (A.8) linearized around an equilibrium state (a generalization of the Onsager-Casimir symmetry). We are content here with the reference to Grmela *et al.* [13], [12] where its precise formulation can be found.

The functionals $M$ and $E$ that satisfy all the above requirements are the functionals (A.2) and (A.3). We look for the functional $S$ in the form

$$S = \int_V dr \rho(\underset{\sim}{r}, t) s(\underset{\sim}{r}, t) . \tag{A.13}$$

Without a loss of generality we assume that $\underline{\underline{R}}$ changes its sign and $\underline{q}$ does not change its sign if $\underset{\sim}{v} \to -\underset{\sim}{v}$. Morever, we assume that the part of $\underline{\underline{\Pi}}$ that changes its sign if $\underset{\sim}{v} \to -\underset{\sim}{v}$, denoted $\Pi$, is given by (II.1) (note that in general $\underline{\underline{\Pi}} = \underline{\underline{\Pi}}^+ + \underline{\underline{\Pi}}^-$, where $\underline{\underline{\Pi}}^+$ is invariant with respect to the transformation $\underset{\sim}{v} \to -\underset{\sim}{v}$), $Q$ is given by (II.2), and $\mathcal{L}$ is assumed to change its sign if $\underset{\sim}{v} \to -\underset{\sim}{v}$. By following the calculations presented in Grmela *et al.* [13] we find that (A.8) is compatible with equilibrium thermodynamics provided the following relations, restricting the freedom of choice of constitutive relations and relating $s(\underset{\sim}{r}, t)$ with the indetermined quantities [$\epsilon$, $\underline{\underline{\Pi}}$, $Q$, $\mathcal{L}$, $\underline{\underline{R}}$, $\underline{q}$], are satisfied.

$$\begin{aligned} &\zeta > 0 \\ &\varkappa > 0 \\ &k > 0 \\ &s_e = \frac{1}{T} > 0 \\ &\rho d_{\alpha\beta}(s_{c_{\alpha\beta}} - s_e \epsilon_{c_{\alpha\beta}}) \geq 0 , \\ &(- (\rho s)_\rho v_\gamma - \rho s_e \tilde{a}_{\partial_\gamma \rho}) d\rho \\ &+ (- \rho s_e v_\gamma - \rho s_e \tilde{a}_{\partial_\gamma e}) de \\ &+ (- \rho s_{c\alpha\beta} v_\gamma - \rho s_e \tilde{a}_{\partial_\gamma c_{\alpha\beta}}) dc_{\alpha\beta} \\ &+ (- \rho (\rho s)_{\rho_\alpha} \rho_{\gamma\alpha} - \rho s_{c\delta\beta} (R_{\beta\delta})_{\partial_\gamma u_\alpha} \\ &- \rho s_e \Pi^+_{\alpha\gamma} - \rho s_e \tilde{a}_{\partial_\gamma u_\alpha}) du_\alpha \end{aligned} \tag{A.14, A.15}$$

is an exact differential form for $\gamma = 1, 2, 3$. In (A.15) we used the following notation, $\tilde{a} = 1/\rho \partial_\beta \mathcal{L}_\beta - \epsilon_{c_{\alpha\beta}} R_{\alpha\beta}$, $\partial_\gamma \equiv \partial/\partial R_\gamma$, $s_e = \partial s/\partial e$, etc. We note that if $\underline{\underline{c}}$ = identity, $\underline{q} = 0$, $\underline{\underline{R}} = 0$, $\epsilon = 0$, $\mathcal{L} = 0$, $\Pi^+_{\alpha\beta} = P\delta_{\alpha\beta}$ then the equations (A.8) reduce to the classical fluid mechanics equations and the conditions (A.14) and (A.15) reduce to the well-known conditions. The condition (A.15) in this particular case is identical to the relation $s_e P + \rho^2 s_\rho = \text{constant}$ that, together with the relation $s_e = 1/T$ (see (A.14)), expresses the local equilibrium assumption. The energy equation (the last equation in (A.8)) can be transformed to an equation governing the time evolution of the local temperature (introduced in the Fourier constitutive relation (II.2)) by using $s_{e(\underset{\sim}{r}, t)} = 1/T(\underset{\sim}{r}, t)$.

## NOMENCLATURE

$A$ = material parameter introduced in *Eq. II.1.*
$E$ = total energy.
$\dot{E}$ = energy flux.
$H^{(th)}$ = set of state variables of a theory.
$I^{(im)}$ = input data of the injection molding process.
$I^{(th)}$ = input data of a theory.
$M$ = total mass.
$O^{(im)}$ = output data of the injection molding.
$O^{(th)}$ = output data of a theory.
$P$ = local pressure.
$P_{th}$ = thermodynamic pressure.
$Q$ = heat flux.
$R^{(th)}$ = time evolution equation of a theory.
$\underline{\underline{R}}$ = tensor introduced in *Eq. A.5.*
$S$ = total entropy.
$T$ = local temperature.
$T_{th}$ = thermodynamic temperature.
$T_a$ = material constant introduced in *Eq. II.1.*
$\underline{U}$ = total momentum.
$\underline{\underline{U}}$ = flux of the total momentum.
$V$ = volume.
$W$ = width of a strip.
$a$ = material parameter introduced in *Eq. II.10.*
$\dot{a}$ = quantity introduced in *Eq. A.15.*
$b$ = material parameter introduced in *Eq. II.10.*
$b$ = thickness of the cavity.
$c$ = material parameter introduced in *Eq. II.10.*
$\underline{\underline{c}}$ = field of internal strain.
$\underline{\underline{d}}$ = tensor introduced in *Eq. A.5.*
$h$ = is an element of $H^{(th)}$.
$i$ = is an element of $I$.
$k$ = coefficient of thermal conductivity (see *Eq. II.2*).
$n$ = material parameter introduced in *Eq. II.1.*
$o$ = is an element of $O$.
$q$ = volume flow rate.
$r$ = position vector, $r = (x, y, z)$.
$s$ = local entropy.
$t$ = time.
$\underline{v}$ = velocity field $\underline{v} = (u, v, w)$.
$\underline{\mathcal{E}}$ = flux of the stored elastic energy.
$\epsilon$ = stored elastic energy.
$\mu_{th}$ = thermodynamic chemical potential.
$\eta$ = viscosity, see (II.1).
$\dot{\gamma}$ = see (II.1).
$\varkappa$ = bulk viscosity.
$\underline{\varkappa}$ = unit vector denoting orientation of fibers.
$\rho$ = mass density.
$\dot{\rho}$ = mass flux.
$\underline{\underline{\Pi}}$ = total pressure tensor.
$\underline{\underline{\tau}}$ = pressure tensor.
$\Psi$ = a distribution function.

## REFERENCES


1. B. P. Zeigler, "Theory of Modeling and Simulation," John Wiley, New York, (1976).
2. B. P. Zeigler, M. S. Elzas, G. J. Klir and T. I. Oren, "Methodology in System Modeling and Simulations," North Holland, Amsterdam (1978).
3. R. Aris, "Mathematical Modeling Techniques," Pitman, London (1978).
4. C. J. S. Petrie, *Polym. Eng. Sci.*, **15**, (1975).
5. S. Middleman, "Fundamentals of Polymer Processing," McGraw Hill, New York (1977).
6. Z. Tadmor and C. G. Gogos, "Principles of Polymer Processing," John Wiley, New York (1979).
7. J. R. A. Pearson, "Mechanical Principles of Polymer Melt Processing," Pergamon Press, Oxford, England (1966).
8. J. J. Van Deemter, *Chem. Eng. Sci.*, **37**, 657 (1982).
9. R. S. Spencer and R. D. Gilmore, *J. Colloid Sci.*, **6**, 118 (1951).
10. M. R. Kamal and P. G. Lafleur, *Polym. Eng. Sci.*, **22**, (1982). M. R. Kamal, V. Tan and M. F. Ryan "Injection Molding: A Critical Profile," Science and Technology of Polymer Processing, Suh and Sung (Eds.), MIT Press (1979).
11. H. Lamb, *Hydrodynamics*, Cambridge Univ. Press (1932).
12. M. Grmela and W. G. Laidlaw, *J. Chem. Phys.*, **78**, 5151 (1983).
13. M. Grmela and P. J. Carreau, *Rheol. Acta*, **21**, 1 (1982).
14. L. C. Woods, *Quart. Appl. Math.*, **39**, 119 (1981).
15. B. A. Finlayson, "The Method of Weighted Residuals and Variational Principles," London, Academic Press (1972).
16. O. C. Zienkiewicz, "The Finite Element Method," McGraw Hill, New York, (1977).
17. W. E. Langlois, "Slow Viscous Flow," MacMillan, New York (1964).
18. A. S. Monin and A. M. Yaglom, "Statistical Fluid Mechanics," Mechanics of Turbulence, Vol. 1, The MIT Press (1971).
19. D. H. Harry and R. G. Parrott, *Polym. Eng. Sci.*, **10**, 209 (1970).
20. M. R. Kamal and S. Kenig, *Polym. Eng. Sci.*, **12**, 294 (1972).
21. J. L. Berger and C. G. Gogos, *Polym. Eng. Sci.*, **13**, 102 (1973).
22. G. Williams and H. A. Lord, *Polym. Eng. Sci.*, **15**, 553 (1975).
23. H. A. Lord and G. Williams, *Polym. Eng. Sci.*, **15**, 569 (1975).
24. G. Titomanlio, *Polym. Eng. Sci.*, **22**, 324 (1982).
25. J. F. Stevenson, *Polym. Eng. Sci.*, **18**, 577 (1978).
26. J. F. Stevenson and W. Chuck, *Polym. Eng. Sci.*, **19**, 849 (1979).
27. J. F. Stevenson, A. Galskoy, K. K. Wang, and D. H. Reber, *Polym. Eng. Sci.*, **17**, 706 (1977).
28. P. C. Wu, C. F. Huang and C. G. Gogos, *Polym. Eng. Sci.*, **14**, 223 (1974).
29. J. R. A. Pearson, "The Lubrication Approximation to Non-Newtonian Flow Problems: A Perturbation Approach," in "Nonlinear Partial Differential Equations: A Symposium on Methods of Solution," Ed. W. F. Ames, pp. 73–107, Academic Press, New York (1967).
30. S. Richardson, *J. Fluid Mech.*, **56**, 609 (1972).
31. W. E. Langlois, *Trans Soc. Rheol.*, **VII**, 75 (1963).
32. A. M. Benis, *Chem. Eng. Sci.*, **22**, 805 (1967).
33. H. Schlichting, "Boundary-Layer Theory," Sixth Ed., McGraw Hill, New York (1968).
34. I. Kuo and M. R. Kamal, *AIChE J.*, **22**, 661 (1976).
35. M. E. Ryan and T. S. Chung, *Polym. Eng. Sci.*, **20**, 642 (1980).
36. C. A. Hieber and S. F. Shen, *Isr. J. Technol.*, **16**, 248 (1978).
37. C. A. Hieber and S. F. Shen, *J. Non-Newt. Fluid Mech.*, **7**, 1 (1980).
38. M. R. Kamal, Y. Kuo and P. H. Doan, *Polym. Eng. Sci.*, **15**, 863 (1975).
39. J. L. White, *Polym. Eng. Sci.*, **15**, 44 (1975).
40. M. R. Kamal, priv. commun.
41. W. Rose, *Nature*, **191**, 242 (1961).
42. P. G. Ciarlet and P. Destynder, "Approximation of Three-Dimensional Models by Two-Dimensional Models" in Plate Theory, in "Energy Methods in Finite Element Analysis" R. Glowinski, E. Y. Rodin, and O. C. Zienkiewicz, Eds. John Wiley, New York (1979).
43. S. M. Richardson, H. J. Pearson and J. R. A. Pearson, *Plast. Rubber Process Appl.*, **5**, 55 (1980).
44. M. C. Booy, *Polym. Eng. Sci.*, **22**, 432 (1982).
45. C. A. Hieber, *SPEANTEC Tech. Papers*, **28**, 356 (1982).
46. B. Haworth, C. S. Hindle, G. J. Sandilands and J. R. White, *Plast. Rubber Process Appl.*, **2**, 59 (1982).
47. J. P. Trotignon, J. L. Lebrun, and Verdu J., *Plast. Rubber Process Appl.*, **2**, 247 (1982).

48. J. B. Shortall and D. Pennington, *Plast. Rubber Process Appl.*, **2**, 33 (1982).
49. R. J. Kent, K. E. Puttick, and J. G. Rider, *Plast. Rubber Process Appl.*, **1**, 111 (1981).
50. P. F. Bright and M. W. Darlington, *Plast. Rubber Process Appl.*, **1**, 139 (1981).
51. Z. Tadmor, *J. Appl. Polym. Sci.*, **18**, 1753 (1974).
52. L. A. Goettler, *Polym. Compos.*, **5**, 60 (1984).
53. R. Takserman-Krozer and A. Ziabicki, *J. Polym. Sci.*, **A1**, 491 (1963).
54. M. A. Christie, M. W. Darlington, D. McCammond and G. R. Smith, *Fibre Sci. Technol.*, **12**, 167 (1979).
55. A. T. Mutel and M. R. Kamal, *Polym. Compos.*, **5**, 29 (1984).
56. L. A. Utracki and J. Lara, *Polym. Compos.*, **5**, 36 (1984).
57. G. S. Hand, *J. Fluid Mech.*, **13**, 33 (1962).
58. A. I. Leonov, *Rheol. Acta*, **15**, 85 (1976).
59. P. A. Dashner and W. E. Vanarsdale, *J. Non-Newt. Fluid Mech.*, **8**, 59 (1981); **8**, 69 (1981).
60. W. E. Vanarsdale, *J. Rheol.*, **26**, 477 (1982).
61. M. S. Green and A. V. Tobolsky, *J. Chem. Phys.*, **14**, 80 (1946).
62. M. Yamamoto, *J. Phys. Soc. Japan*, **11**, 413 (1956); **12**, 1148 (1957); **13**, 1200 (1958).
63. A. S. Lodge, *Trans. Faraday Soc.*, **52**, 120 (1956).
64. G. Marruci, G. Titomanlio and G. C. Sarti, *Rheol. Acta*, **12**, 269 (1973).
65. D. Soong and M. Shen, *J. Rheol.*, **25**, 259 (1981).
66. I. Y. Liu, D. S. Soong and M. C. Williams, *Polym. Eng. Sci.*, **21**, 675 (1981).
67. M. Grmela and P. J. Carreau, *J. Chem. Phys.*, **78**, 5140 (1983).
68. J. G. Oldroyd, *Proc. R. Soc.*, (London), **A200**, 523 (1950).
69. W. R. Schowalter, "Mechanics of Non-Newtonian Fluids," Perganom Press, London, (1978).
70. R. Bird, *J. Non-Newt. Fluid Mech.*, **5**, 1 (1979).
71. R. K. Gupta and A. B. Metzner, *J. Rheol.*, **26**, 181 (1982).
72. E. C. Eringen, "Continuum Physics," Vol. IV, Pergamon Press, London (1976).
73. R. C. Martin, O. Parodi and P. S. Pershan, *Phys. Rev. A.*, **6**, 2401 (1972).
74. B. D. Coleman and W. Noll, *Arch. Rational Mech. Anal.*, **6**, 355 (1960).
75. R. S. Rivlin, "The Thermomechanics of Materials with Fading Memory in "Theortical Rheology," J. F. Huttou, J. R. A. Pearson, K. Walters, Eds. John Wiley, New York (1974).
76. M. J. Crochet and P. M. Naghdi, *Rheol. Acta*, **12**, 237 (1973).
77. M. Kawahara and N. Takeuchi, *Comp. Fluids*, **5**, 33 (1977).
78. M. A. Mandelson, P. W. Yeh, R. A. Brown and R. C. Armstrong, *J. Non-Newt. Fluid Mech.*, **10**, 31 (1982).
79. M. J. Crochet and K. Walters, *Ann. Rev. Fluid Mech.*, **15**, 241 (1983).
80. A. I. Isayev and C. A. Hieber, *Rheol. Acta*, **19**, 168 (1980).
81. E. J. Hinch and L. G. Leal, *J. Fluid Mech.*, **71**, 481 (1975), **76**, 187 (1976).
82. W. L. Olbricht, J. M. Rallison and L. G. Leal, *J. Non-Newt. Fluid Mech.*, **10**, 291 (1982).
83. B. Chung and C. Cohen, *SPEANTEC Tech. Papers*, **28**, 8 (1982).
84. M. Gordon and I. H. Hiller, *Phil. Mag.*, **11**, 31 (1965).
85. J. R. A. Pearson and L. V. McIntire, *J. Non-Newt. Fluid Mech.*, **6**, 81 (1979).
86. L. A. Utracki and M. M. Dumoulin, *SPEANTEC Tech. Papers*, **28**, 51 (1982).

## DISCUSSION

*M. R. Kamal:* Do I understand from your conclusions and presentation that three-dimensional complete models, or three-dimensional models of any level of completeness, are the last thing that we must look at?

*M. Grmela:* A discrete version of model equations (needed in order to be able to use the service of computers) represents just another reduced model. There is no fundamental problem in extending the standard methods leading to discrete equations in two-dimensional models to three-dimensional models. The problems arise in the study of compatibility of the original model and its discrete version (i.e. can we believe in results coming from the computer?) and in the computation time requirement. I would therefore always recommend first considering modifications of the methods leading to discrete equations (e.g., a special choice of large finite elements of the shape suggested, for example, by an insight into the physics of the process that is modeled) or a completely new reformulation of the original model before the standard methods are applied mechanically.

*V. L. LeNir:* You did not have a solution in the problem you quoted. Just what do you mean by not having a solution?

*M. Grmela:* Here again is the problem of compatibility of an original model and its discrete version. In this case the model under consideration is a model of a flow of a two-dimensional viscoelastic fluid. It has been reported by several authors (see e.g. Mandelson *et al.* [78] for a recent review) that for Deborah numbers larger than one the results coming from the computer are unstable and do not seem to be in agreement with observations. Does the disagreement arise due to the incompatibility of the discrete version of the model and the original model (the problem of numerical analysis), or because the original model itself is incompatible with observations (e.g. due to unrealistic restriction to two dimensions)? To the best of my knowledge there is no satisfactory answer to this question at present.

*J. Vlachopoulos:* I would like to make a comment on that. We have some results for convergence for Deborah numbers greater than one. We actually went up to a Deborah number of 1.77.

*M. E. Ryan:* I would also like to comment on that. This problem of instability at higher Deborah numbers is common. We encountered this problem in our blowmolding calculations and people report this problem no matter what type of viscoelastic fluid mechanical problem is considered. Perhaps we can have a more in-depth and free ranging discussion on this point later on. I think it is a most interesting problem which must somehow be resolved.

*L. A. Utracki:* The study of the hierarchy of models which you are proposing would require that the models be developed in house and that we do not use a "black box" commercially available model where one does not know the details. On the basis of conversations that I have had with a number of people, this is the approach which is being used by the most advanced companies and laboratories. It requires a large number of people who are knowledgeable about the theory and processing. On the other hand, there are a large number of models that are commercially available. Is there any practical justification in paying for these "black boxes"?

*M. Grmela:* The answer depends on objectives and economy. I would like to stress that important ad-

vantages of modeling (as, e.g., gain of an insight, a lead in the future research) are lost if only the service of "black boxes" is bought.

*G. Bata:* You have to put a time scale on this type of approach because the results we want are practical results. We would like to have our industrial partners use it. Can you comment on the amount of effort required for this approach compared to some other possible approaches?

*M. Grmela:* Most of the models that are commercially available now (let us call them first-generation models) are based on the Harry-Parrott one-dimensional analysis and on the concept of mold network. The industrial applicability of these models is limited. The first-generation models provide answers only to basic questions concerning processing operations. The models are unable, for example, to predict properties of the final product. Because of the incompleteness of the existing models, the widespread recognition of the usefulness of mathematical modeling of the injection molding and the large effort devoted to this task, I predict a rapid development in this field. Consequently, anyone who relies on commercially available models is unable to provide practical results to its industrial partners since the competing companies that develop or participate in developing their own models will have models always available providing a superior service. Having in mind precisely the practical usefulness of the service to our industrial partners, I do not see any other approach than in-house development of the models. As I have argued in my talk, the models that will be most useful will consist of a family of compatible and complementary models of various levels of sophistication. In particular, the first-generation models will always belong to these families. The process of creating in-house models cannot therefore be accelerated by buying a service of "black boxes." To the time scale, the first-generation models should be produced by a small group of competent people in less than one year. On the basis of the arguments presented in my talk, I would always recommend a simultaneous development of models on different levels of sophistication.

# A Study in Injection Molding Dynamics

M. R. KAMAL, W. IAN PATTERSON, D. ABU FARA *and* A. HABER

*Department of Chemical Engineering*
*McGill University, Montreal, Canada*
*H3A 2A7*

Some aspects of injection-molding dynamics were studied using a laboratory injection-molding machine operated under the control of a microprocessor-based servocontrol system. Two types of experiments were performed: deterministic tests which introduced step changes in the servovalve opening and stochastic tests using pseudo-random binary sequence (PRBS) perturbations of the servovalve. Deterministic models were written for the hydraulic and nozzle pressures which were in good agreement with the experimental data. A stochastic transfer function-noise model was obtained for the nozzle pressure, but an adequate model was not found for the hydraulic pressure. The agreement between the nozzle pressure stochastic model and the corresponding step test model was satisfactory.

## INTRODUCTION

Process modelling is a useful tool for the understanding of plastics manufacturing operations like extrusion, injection molding, blowmolding, etc. Injection-molding models may be employed to yield information regarding the moldability of the material, the thermo-mechanical history that it experiences, and the microstructure and ultimate properties of the molded article (1).

Another important application of process modelling is for the purposes of process optimization and control. Process control can be an important tool for achieving improved production economics, the minimization of waste and product variability, and the control of the quality of the molded article.

The present work deals with the study of the dynamics of the injection-molding process with the objective of obtaining dynamic models that would be useful for the purposes of injection-molding process control. Both step and stochastic input functions have been employed in the study.

## MODELLING TECHNIQUES

Mathematical models of the injection-molding process are generally based on solving the appropriate equations of continuity, momentum, and energy in conjunction with suitable initial and boundary conditions (2, 3). These models yield information regarding the relationships between resin properties, molding conditions, and the thermo-mechanical history experienced by the resin during the process. The models described above, although very useful, do not incorporate the effects that result when the process variables are changing in response to a time-variable forcing function. Dynamic models are required in such a case, and the mathematical solution of the problem is substantially more complex. Nonetheless, a dynamic model of the process is essential to achieve rational and effective process control strategies.

Much of control theory relies on dynamic models based on the experimental, or transfer function approach. According to this approach, a controlled variation is generated in a process input variable and the response to this input is measured. The transfer function is obtained as the ratio of the transformed input and output variables, as illustrated in *Fig. 1*. This approach suffers from two disadvantages: (a) the process must be physically tested to obtain the necessary data, and (b) the method involves the implicit assumption that the process is linear. It is therefore necessary to determine the limits of the validity of this assumption. On the other hand, the transfer function approach is significantly simpler than the transport phenomena approach previously mentioned. Moreover, transfer functions are better suited for process control applications because of their simpler mathematical structure.

The input or forcing functions used in early work were of the step or pulse type, yielding responses of the type indicated in *Fig. 2(a)*. A statistical approach has been developed recently (4, 5), which, after treatment of the measured response, permits the determination of the transfer function and the description of the noise (or random effects) associated with the process. This technique, using a pseudo-random binary sequence input, is illustrated in *Fig. 2(b)*. It is well-suited for application in conjunction with computers which generate the input function and measure the response at discrete time intervals.

The models obtained by this statistical approach often called "stochastic identification," are of the form:

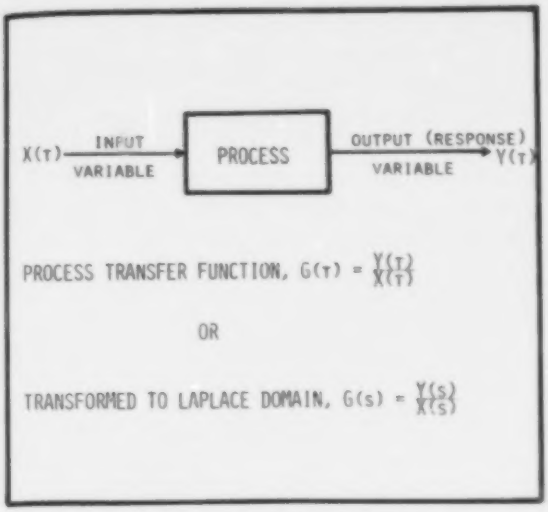


*Fig. 1. Transfer function representation of a process.*

$$y(k)\ (1 - \delta_1 B - \delta_2 B^2 \ldots) = (\omega_0 - \omega_1 B - \omega_2 B^2 \ldots)x(k-1)$$

where $y(k)$ = the output at the $k^{th}$ measurement
$x(k-1)$ = the input at the $(k-1)^{th}$ measurement
$B$ = the backwards operator: $By(k) = y(k-1)$

and $\delta_1, \delta_2, \ldots$ and $\omega_0, \omega_1, \omega_2, \ldots$ are coefficients to be determined by analysis of the experimental data.

The models presented in the following discussion have been obtained from both step inputs and stochastic identification applied to different injection-molding machine variables.

## EXPERIMENTAL

### Apparatus

This study was performed on a Danson Metalmec 2½ oz., model 60-SR, reciprocating screw injection-molding machine equipped for operation in automatic, semi-automatic, and manual modes. The hydraulic system of the machine was redesigned and refitted to be controlled by a microprocessor-driven servovalve.

The microprocessor control system is based on a Cromenco Single Card Computer (SCC). The facilities include 13$k$($k$ = 1024) bytes of random access memory (RAM) and 12$K$ bytes of read only memory (ROM); there are seven 8-bit parallel input and output ports, and four serial (RS232) ports. The ROM software has monitor and BASIC interpreter programs. The peripherals used are: a Hazeltine CRT terminal (model 1400), digital input and output modules (Opto 22), a Burr-Brown 12-bit analog to digital converter (SDM-856), and an 8-bit digital to analog converter. The system was programmed with subroutines for the machine sequencing, control algorithms, and data acquisition programs for examining the process variables during the injection phase of the molding cycle.

Two pressure transducers manufactured by Dynisco (model PT 435 A) were used for pressure measurements. One pressure transducer (0 to 1000 psi) was located in the line between the servovalve and the injection cylinder to measure the hydraulic pressure. The second pressure transducer (0 to 10,000 psi) was mounted in the nozzle. A linear displacement transducer, Markite model 4709, was used to obtain the ram position.

## MATERIAL

The resin used in this study was a DuPont of Canada Sclair 2908 high-density, injection-molding-grade polyethylene resin. It has a melt index of 7.4 g/10 min and a density of 0.962 g/cm$^3$.

## EXPERIMENTAL PROCEDURE

A number of deterministic (step) changes were made by suddenly opening or closing the servovalve during the injection phase. The hydraulic pressure, nozzle pressure, and linear displacement of the injection ram were measured throughout the phase. Tests with different step magnitudes of ±5, ±10, ±15, ±20 percent in the servovalve opening, (0 percent = valve closed; 100 percent = valve fully open) were performed to estimate the dynamic parameters of the process and to examine the system linearity. Several runs were performed for each step change to verify the reproducibility of the data.

A series of stochastic experiments were performed using a pseudo-random binary sequence

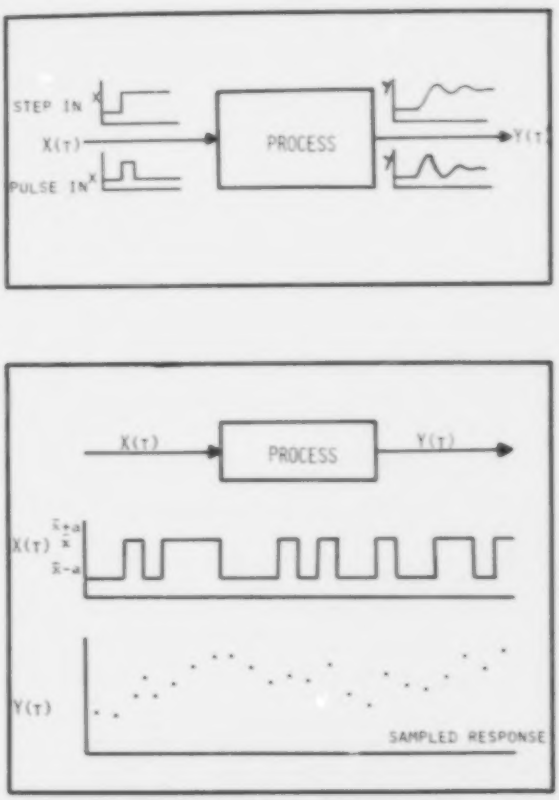


*Fig. 2. (a) Deterministic and (b) stochastic testing of a process to obtain the transfer function.*

(PRBS) to vary the servovalve opening about a mean value. The PRBS was begun 0.32 seconds after the commencement of injection and both hydraulic and nozzle pressure responses were recorded.

The barrel temperatures were held constant at 200 ± 2°C and 160 ± 2°C in the front and rear zones, respectively, for all tests. The data sampling intervals were 0.01 seconds for the PRBS tests and 0.005 seconds for the step tests.

## RESULTS AND DISCUSSION

### Step Tests

*Figures 3* and *4* show the responses of the hydraulic and nozzle pressures to the ±10, ±15, and ±20 percent step changes in the servovalve opening. The hydraulic pressure, shown in *Fig. 3*, suggests a noisy, over-damped second order response superimposed on a constantly increasing (ramp) pressure component. The constantly increasing pressure is found at constant valve opening and, for the purposes of dynamic behavior analysis, is ignored.

Although it is not immediately obvious from *Fig. 3*, the apparent noise, or random deviation from a second order response, actually has a damped oscillatory nature. This is probably due to servovalve overshoot and resonance (6). The combined response can be modelled by:

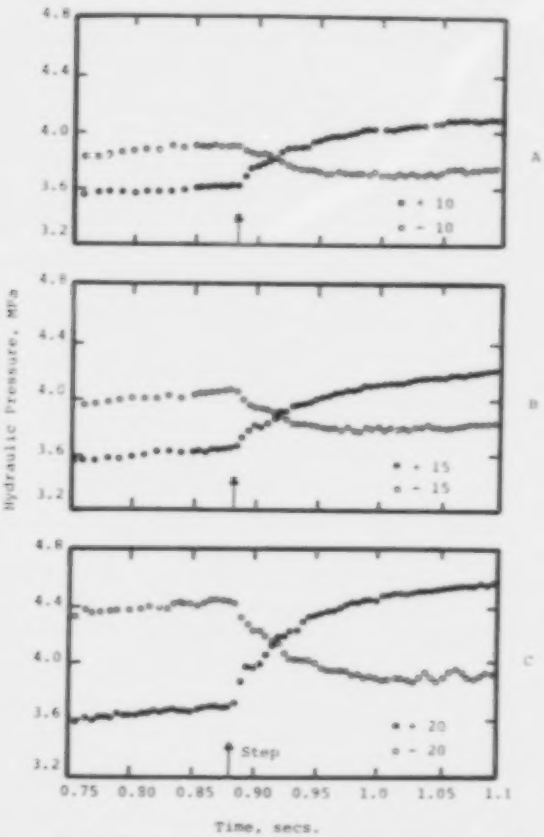


*Fig. 3. Hydraulic pressure responses to step changes in valve opening, (a) ±10 percent, (b) ±15 percent, (c) ±20 percent.*

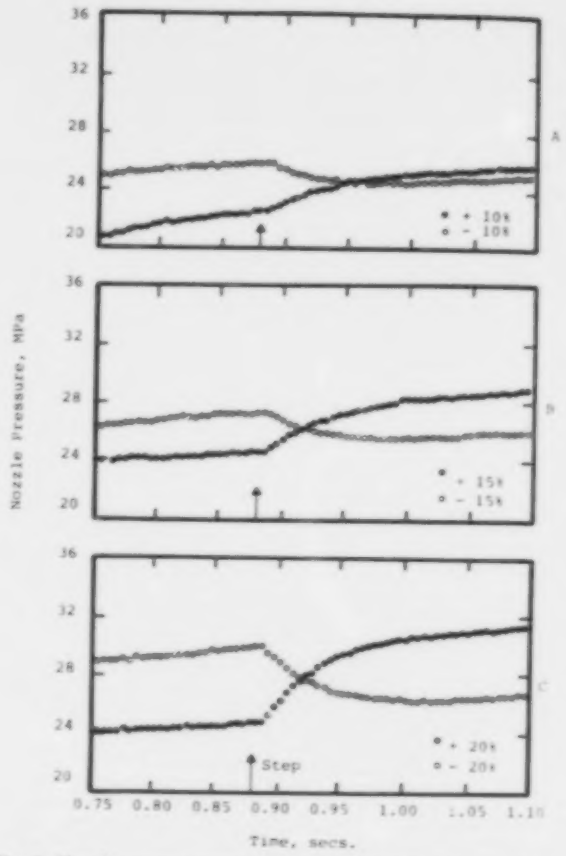


*Fig. 4. Nozzle pressure responses to step changes in valve opening, (a) ±10 percent, (b) ±15 percent, (c) ±20 percent.*

$$P_H = G\left[1 - \frac{\tau_1\tau_2}{\tau_1 - \tau_2}\left(\frac{1}{\tau_2}e^{-t/\tau_1} - \frac{1}{\tau_1}e^{-t/\tau_2}\right)\right] + G_1\left[\frac{1}{(1-\xi^2)^{1/2}\tau_3}e^{-t/\tau_3}\sin\left[(1-\xi^2)^{1/2}\frac{t}{\tau_3}\right]\right] \quad (1)$$

where $P_H$ = hydraulic pressure, Pa
$G$, $G_1$ = process gains, Pa/percent change in valve opening
$\tau_1$, $\tau_2$, $\tau_3$ = time constants, seconds
$\xi$ = damping factor, dimensionless

The first term of *Eq. 1* accounts for the second order part of the response while the second term is the oscillatory, valve induced, component. Although physical considerations support the use of *Eq. 1*, better fits to the data were obtained from a delayed first order plus oscillatory response model as given by *Eq. 2*:

$$P_H = G(1 - e^{-(t-D)/\tau}) + G_1\left[\frac{1}{(1-\xi^2)^{1/2}\tau_1}e^{-t/\tau_1}\sin\left[(1-\xi)^{1/2}\frac{t}{\tau_1}\right]\right] \quad (2)$$

where $D$ = time delay, seconds.

The fittings of the models were done using the NONLINWOOD (7) computer program. The best values of the parameters of *Eq. 2* are given in *Table 1*.

Table 1. Values of the Parameters for the Hydraulic Pressure Model, Equation 2

| First Order Model Parameters | | | Oscillatory Component | | |
|---|---|---|---|---|---|
| Change in Valve Opening, percent | Gain, G, kPa/percent | Time Constant, $\tau$ (sec.) × $10^2$ | Gain, G1, kPa/percent | Time Constant, $\tau_1$ secs. | Damping Factor, $\xi$ |
| +10 | 29.6 ± 1.9 | 4.0 ± 0.30 | 0.0262 | 0.005 | 0.16 |
| −10 | 32.2 ± 2.1 | 4.9 ± 0.48 | 0.0206 | 0.005 | 0.20 |
| +15 | 27.6 ± 2.0 | 4.8 ± 0.46 | 0.0193 | 0.005 | 0.16 |
| −15 | 27.6 ± 1.9 | 4.8 ± 0.44 | 0.0190 | 0.005 | 0.18 |
| +20 | 34.5 ± 1.5 | 4.1 ± 0.33 | 0.0248 | 0.005 | 0.13 |
| −20 | 33.1 ± 1.6 | 4.6 ± 0.39 | 0.0234 | 0.005 | 0.18 |

N.B.: The time delay for all cases is $D = 0.005$ seconds.

The nozzle pressure, shown in *Fig. 4*, has the appearance of an overdamped second order process. Again, there is the constantly increasing component that is ignored in our analysis, but the small oscillatory component that was present in the hydraulic pressure response has been absorbed by the hydraulic piston and ram system. The nozzle pressure response was modelled by an overdamped second order process as:

$$P_N = G\left[1 - \frac{\tau_1\tau_2}{\tau_1 - \tau_2}\left(\frac{1}{\tau_2}e^{-t/\tau_1} - \frac{1}{\tau_1}e^{-t/\tau_2}\right)\right] \quad (3)$$

where $P_N$ = nozzle pressure, Pa

The first order plus time delay model was also fitted to the nozzle pressure data using *Eq. 4* below:

$$P_N = G(1 - e^{-(t\ -\ D)/\tau}) \quad (4)$$

The best parameters for the fitted *Eqs. 3* and *4* are given in *Tables 2* and *3* respectively. *Figure 5(a)* shows the hydraulic pressure model, *Eq. 2*, together with the data from one test. *Figures 5(b)* and *5(c)* compare the two model *Eqs. 3* and *4*, for the nozzle pressure, to the data. The fits for both *Eqs. 3* and *4* appear to be equally good, but a comparison of the two models using the sum of squares of the residuals indicated that *Eq. 3* is a better fit and is physically more consistent with the process.

The change in hydraulic pressure versus the change in valve opening is shown in the upper part of *Fig. 6* and illustrates the linearity of the hydraulic pressure response for valve opening changes in the range of ±20 percent. The change in hydraulic pressure for a given change in valve opening is the hydraulic pressure process gain, G. This is plotted in the lower portion of *Fig. 6* and is seen to be independent of valve opening, a condition implied by the process linearity. Similar plots for the nozzle pressure versus the valve opening show a similar linearity, although the value of the process gain is considerably higher, as shown by *Tables 1* to *3*.

The ram displacement versus time for ±5 percent, ±10 percent and ±15 percent changes in valve opening are shown in *Fig. 7*. The change in valve opening is distinguished by the change in slope of the displacement curve. It can be seen that the data are confounded with considerable measurement noise, although the change in slope (ram velocity) is very rapid. The velocity, obtained by differentiating the displacement data, is plotted in

Table 2. Values of the Parameters for the Nozzle Pressure Model: Second-Order, Equation 3

| Changes in Valve Opening, percent | Gain kPa/percent | Time Constants, (sec) × $10^2$ | |
|---|---|---|---|
| | | $\tau_1$ | $\tau_2$ |
| +10 | 206 ± 24 | 3.6 ± 1.26 | 1.14 ± 0.40 |
| −10 | 191 ± 19 | 3.5 ± 1.04 | 1.00 ± 0.35 |
| +15 | 210 ± 23 | 4.0 ± 1.00 | 1.00 ± 0.20 |
| −15 | 194 ± 12 | 3.9 ± 0.70 | 0.99 ± 0.26 |
| +20 | 223 ± 13 | 3.5 ± 0.53 | 1.03 ± 0.25 |
| −20 | 218 ± 11 | 4.1 ± 0.42 | 0.90 ± 0.20 |

Table 3. Values of the Parameters for the Nozzle Pressure Model: First-Order Plus Time Delay, Equation 4

| Change in Valve Opening, percent | Gain, G, kPa/percent | Time Constant $\tau$, (sec) × $10^2$ | Time Delay D, sec. |
|---|---|---|---|
| +10 | 208 ± 11 | 4.50 ± 0.51 | 0.0046 |
| −10 | 210 ± 09 | 4.80 ± 0.45 | 0.0043 |
| +15 | 207 ± 10 | 5.20 ± 0.45 | 0.0046 |
| −15 | 195 ± 09 | 5.30 ± 0.40 | 0.0042 |
| +20 | 229 ± 09 | 4.70 ± 0.33 | 0.0043 |
| −20 | 220 ± 08 | 5.00 ± 0.28 | 0.0034 |

*Fig. 8*, where the measurement noise is obvious from the scatter of points. It was not possible to find a model for the ram velocity. The scatter evidenced in *Fig. 8* can be caused by displacement variations as small as 0.001 inch. It thus seems probable that machine vibration was the source of the noise in the data.

## STOCHASTIC EXPERIMENTS

The stochastic experiments exhibited responses similar to those observed during the step tests. *Figure 9* shows a typical input (PRBS) and the corresponding measured hydraulic and nozzle pressure responses. The data were treated by standard time series analysis procedures (5). The oscillatory valve response superimposed on main hydraulic pressure response required a seasonal type of time series model, and an adequate model could not be obtained. However, the nozzle pressure could be satisfactorily modelled as:

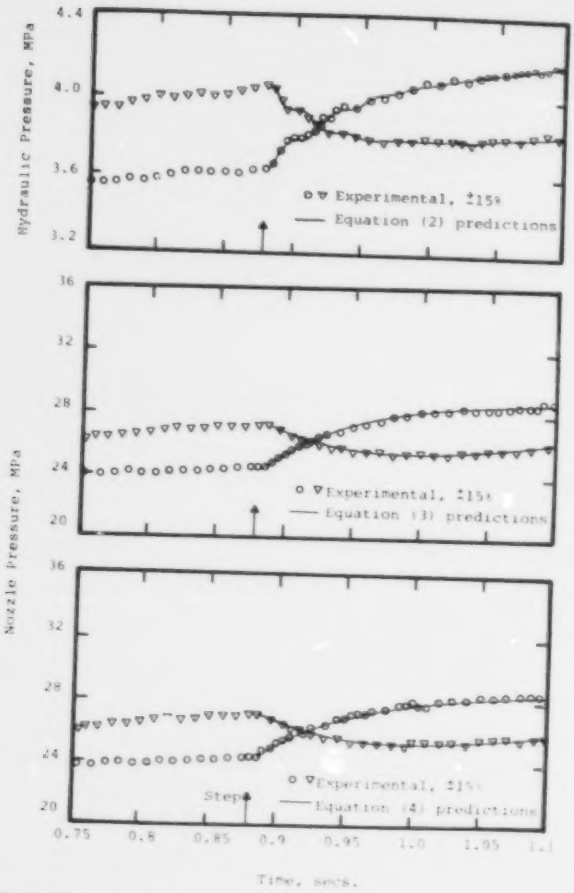


*Fig. 5. Comparison of experimental hydraulic and nozzle pressure responses to fitted models*

$$P_N(k) = \frac{\omega_0 - \omega_1 B}{1 - \delta_1 B} U(k-2) + \frac{1}{1 - \phi_1 B} a(k) \quad (5)$$

where $P_N(k)$ = nozzle pressure at discrete sampling instant, $k$
$U(k)$ = valve opening at sampling instant, $k$
$\delta_1 = 0.68$
$\omega_0 = 6.62$
$\omega_1 = -1.00$
$\phi_1 = 0.97$
$a(k)$ = random noise value at sample time, $k$
$B$ = backwards difference operator defined as $BU(k) = U(k-1)$

*Equation 5* distinguishes two components of the nozzle pressure response; the first term is the direct response defined in terms of previous values of $P_N$ and $U$, while the second term describes the noise inherent in the process and the measurement. A model of the form of *Eq. 5* can be compared to the continuous (step) test models by calculating the gain and time constant of the process that would produce *Eq. 5*. This calculation gives the following values:

$$G = 163 \text{ KPa/percent}$$
$$\tau = 0.03 \text{ seconds}$$

Both the gain and the time constant compare favorably with the values of *Tables 2* and *3*, although the gain is somewhat lower than that found from the step tests.

## CONCLUSIONS

Deterministic (step) and stochastic testing of the hydraulic and nozzle pressure responses to various servovalve openings were carried out. The nozzle pressure was best modelled as a second order overdamped process while the hydraulic pressure showed an oscillatory component superimposed on a delayed first order response. The damped oscillations were attributed to the servovalve.

Ram displacement was measured as a function of time, and an attempt to obtain the ram velocity by differentiation of the displacement-time data was unsuccessful, due to measurement noise. The source of this noise is probably machine vibration.

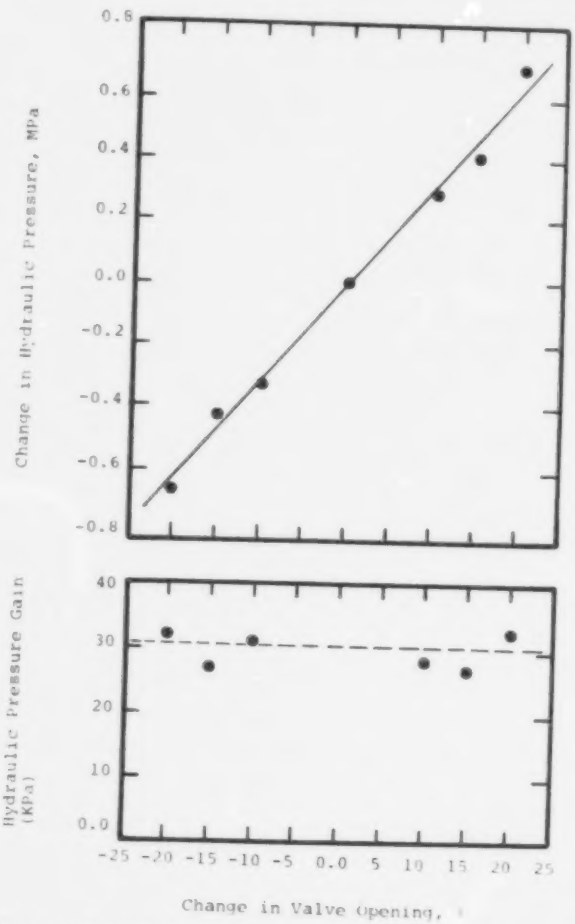


*Fig. 6. Gain for the hydraulic pressure (psi/percent) for different percent changes in valve opening*

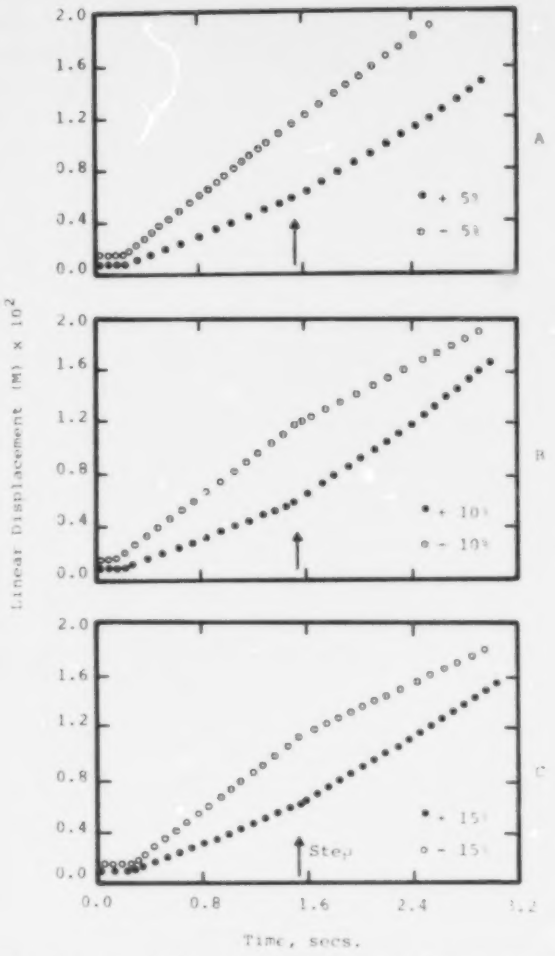


*Fig. 7. Linear displacement response to step changes in valve opening. (a) ±5 percent, (b) ±10 percent, (c) ±15 percent*

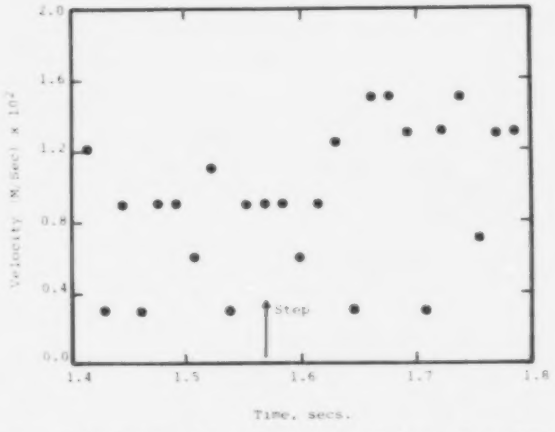


*Fig. 8. Velocity derived from the linear displacement data of Fig. 7(b) versus time for a +10 percent change in valve opening.*

Finally, a stochastic model of the nozzle pressure was obtained that compared favorably to those found from the step tests. It appears that, for pressure control of injection molding, it is preferable to use nozzle rather than hydraulic pressure. Responses of all the variables were extremely rapid and are thus possible candidates for manipulating the injection-molding process.

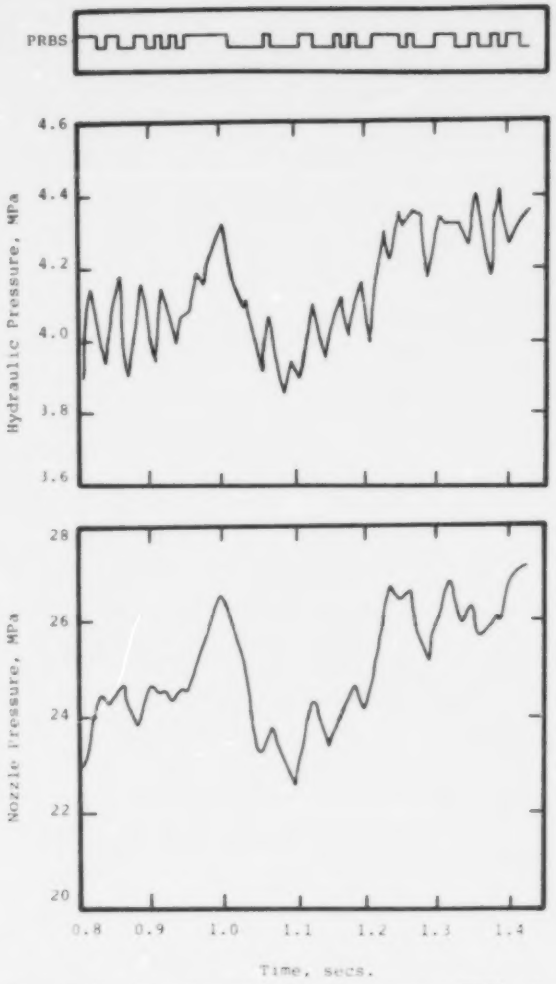


*Fig. 9. Hydraulic and nozzle pressure responses to PRBS valve signal (±10 percent) of 63 intervals of 10 ms duration.*

## REFERENCES

1. M. R. Kamal & P. G. Lafleur, "Computer Simulation of Thermoplastic Injection Molding," *Advances in Plastics Technology*, **1**, 8 (1981).
2. M. R. Kamal & S. Kenig, *Polym. Eng. Sci.*, **12**, 294 (1972).
3. H. A. Lord, *Polym. Eng. Sci.*, **19**, 469 (1979).
4. E. A. Robinson & M. T. Silvia, "Digital Signal Processing and Time Series Analysis," Holden-Day Inc., San Francisco (1978).
5. G. E. Box & G. M. Jenkins, "Time Series Analysis: Forecasting and Control," Holden-Day Inc., San Francisco (1976).
6. Anon, "Moog A076 Servovalve Technical Manual," Moog Inc., Industrial Division, New York.
7. C. Daniel & F. Wood, "Fitting Equations to Data," John Wiley, New York (1980).

# Heat Transfer in Injection Molding of Crystallizable Polymers

M. R. KAMAL *and* P. G. LAFLEUR

*Department of Chemical Engineering*
*McGill University*
*Montreal, Quebec*
*Canada*
*H3A 2A7*

A model is proposed for the treatment of heat transfer with crystallization during plastics processing in general, and injection molding in particular. The model incorporates experimentally determined crystallization kinetics parameters. It permits the calculation of the distribution of both temperature and crystallinity in the molding. Theoretical predictions are in good agreement with experimental measurements in both injection molding and a prototype apparatus.

## INTRODUCTION

In most of the plastics-processing operations, the polymer must flow in order to be shaped and then must solidify while retaining the desired shape. The thermomechanical history experienced by plastics melts during processing leads to the development of microstructure, which directly influences the ultimate properties of the plastics article. In the case of a crystallizing polymer, the morphology and crystallinity of the final product are strongly influenced by the cooling conditions. Thus, a transient heat transfer model, incorporating kinetics of crystallization, is essential for the analysis of the process.

In one of the first attempts to establish a cooling model for crystallizing polymers, Gloor (1) adapted a method used by Dusinberre (2) converting latent heat to an equivalent temperature. He assumed atmospheric pressure and constant average properties. Kenig and Kamal (3) calculated temperature profiles and pressure drop for pressurized HDPE undergoing solidification. Latent heat was taken into consideration by calculating a partial delay of the temperature based on the proportions of the crystalline and amorphous phases. They included in their solution the dependence of polymer properties both on temperature and pressure and the effects of pressure and rates of cooling on the solidification temperature. The model dealt with a two-phase system (solid and melt) with a moving boundary. Sifleet *et al.* (4) incorporated kinetics of crystallization by adding an internal heat-generation term to the heat-conduction equation. Thermal properties were considered constant, and comparisons with different methods of cooling calculations were presented. The unsteady-state heat-transfer model for plastics-processing operations presented by Dietz (5) took into account the effect of pressure drop in the energy equation and the dependence of thermal properties on temperature and pressure. A variable, specific heat, $C_p$, over the entire range of temperature was calculated from the P-V-T diagram, implicitly accounting for crystallization effects.

In the following sections, we outline the features of a model of the injection-molding process that incorporates the effects of crystallization kinetics during all stages of the process. Some of the predictions of this model are subsequently compared to experimental data relating to the injection molding of high-density polyethylene.

## INJECTION MOLDING MODEL

The injection-molding process can be fully described in terms of the equations of conservation of mass, momentum and energy, coupled with appropriate thermodynamic relationships and a set of constitutive relations which describe the behavior of the material under the influence of stress and thermal fields. In general tensorial formulation, the conservation equations are as follows:

Continuity:

$$\frac{D\rho}{Dt} = -\rho(\nabla \cdot \vec{v}) \tag{1}$$

Momentum:

$$\rho \frac{D\vec{v}}{Dt} = -\nabla P - (\nabla \cdot \vec{\vec{\tau}}) + \rho \vec{g} \tag{2}$$

Energy:

$$\rho C_v \frac{DT}{Dt} = -(\nabla \cdot \vec{q}) - T\left(\frac{\partial P}{\partial T}\right)_\rho (\nabla \cdot \vec{v}) - (\vec{\vec{\tau}} : \nabla \vec{v}) \tag{3}$$

Each stage of the process is governed by a set of initial and boundary conditions coupled with simplifying assumptions.

The filling stage is represented by the unsteady flow of a hot, non-Newtonian, compressible melt into an empty cold cavity, which is held at a temperature below the solidification temperature of the polymer. The problem has to do with simultaneous unsteady flow and heat transfer. Polymer

flow into the cavity does not cease when the melt reaches the outer boundaries of the cavity. It is desirable to introduce more polymer into the cavity during the packing stage. With regard to pressure variation in the cavity two factors compete during the packing stage. The first is the flow of the polymer into the mold, which leads to an increase of pressure corresponding to the increase of density of the polymer in the cavity. The second factor is the cooling of the polymer, which continues during the entire process. Cooling tends to reduce the pressure in the cavity. After filling and packing are complete, cooling of the plastic continues by virtue of the lower temperature of the mold. Cooling without flow continues until the plastic has reached a sufficient level of solidification.

In view of the above, injection molding involves unsteady state flow problems coupled with heat transfer; heat transfer being present during the three stages of the process.

In order to simplify the geometry of the system, a fan gate mold has been considered, and the analysis is restricted to two-dimensional motions in a plane. The fluid is assumed to be incompressible during the filling stage, and body forces are negligible. With these assumptions, the conservation equations take on the following forms.

Continuity:

$$(\nabla \cdot \vec{v}) = 0 \tag{4}$$

Momentum:

$$\rho \frac{D\vec{v}}{DT} = -\nabla P - (\nabla \cdot \bar{\bar{\tau}}) \tag{5}$$

Energy:

$$\rho C_P \frac{DT}{Dt} = -(\nabla \cdot \vec{q}) + \frac{T}{v}\left(\frac{\partial v}{\partial T}\right)_\rho \frac{dP}{dt} - (\bar{\nabla} \cdot \bar{\bar{\tau}}) \tag{6}$$

The momentum equations relate the velocity vector to the stress tensor and are valid for any fluid. The additional required information is embodied in the constitutive equations, which relate the stress field to the flow field, usually through the rate-of-deformation tensor, and thereby define the type of fluid for which a solution is being sought. There is no constitutive equation that can represent the full range of flow and deformation encountered in the injection-molding process. Thus, one must learn the art of constitutive compromise. It is necessary to examine the flow kinematics of the injection-molding process and judge which elements are most crucial to the predictive specifications of the model. In order to predict the development of normal stresses and transient phenomena, a viscoelastic model is essential. In the present work, the White-Metzner (6) modification of the Maxwell model, utilizing the Oldroyd derivative in contravariant form, has been employed:

$$\bar{\bar{\tau}} + \lambda(\mathrm{II})\frac{\partial \bar{\bar{\tau}}}{\partial t} = \eta(\mathrm{II})\bar{\bar{\nabla}} \tag{7}$$

where both $\lambda$ and $\eta$ are functions of the second invariant of the flow field.

Assuming that the specific heat of the melt and the solid are independent of the cooling process, within the solidification range, the latent heat of solidification is included in the specific heat as follows:

$$C_P = C_P' + \frac{d\lambda_c}{dT} = C_P' + \lambda_{pc}\frac{dX}{dT} \tag{8}$$

where $\lambda_c$ is the heat of crystallization released by the sample, $\lambda_{pc}$ is the heat of fusion of the pure crystal, and $X$ is the degree of crystallinity. Thus, it is essential to follow the development of crystallinity in order to calculate the specific heat at any desired temperature.

Nakamura *et al.* (7) developed a model based on the Avrami equation, which was modified to apply to the nonisothermal process under certain assumptions. The fundamental equation was written on the basis of isokinetic conditions in the following form

$$X(t) = 1 - \exp\left[-\left(\int_0^t K(T)d\tau\right)^n\right] \tag{9}$$

$X(t)$: degree of phase transformation at time $t$

$n$: Avrami index determined in the isothermal experiments

$K(T) = \{k(T)\}^{1/n}$: Rate constant related to the Avrami isothermal crystallization rate constant, $k(T)$.

From this model, non-isothermal crystallization can be analysed in terms of data from isothermal crystallization.

The Avrami equation has the form

$$X(t) = X(\infty)\,[1 - \exp(k(T)t^n)] \tag{10}$$

where $X(\infty)$ refers to the fact that a sample will reach a limiting crystallinity level. $X(\infty)$ will depend on temperature, and is below 1.0.

For the resin under consideration, Sclair 2908 high-density polyethylene supplied by Du Pont of Canada Ltd., $X(\infty)$ was determined experimentally by quenching small samples in a large constant-temperature bath. The value of $X(\infty)$ was obtained by heating the sample in the differential scanning calorimeter (DSC). The values obtained are shown in *Fig. 1*. For these data, quenching experiments were carried out in the DSC above 110°C and in a thermostating bath below 110°C.

## STATIC COOLING EXPERIMENT

In order to test some of the above concepts in a simple heat-transfer situation, a cooling experiment was designed to permit cooling of the polymer from the melt in the absence of flow and under only a slight pressure. Besides the simplifications resulting from the no-flow condition, the experiment avoided complications resulting from the effects of pressure and shear on crystallization kinetics.

A premolded disc-shaped sample of the resin was introduced into a circular mold equipped with heaters and cooling channels, as shown in *Fig. 2*. A

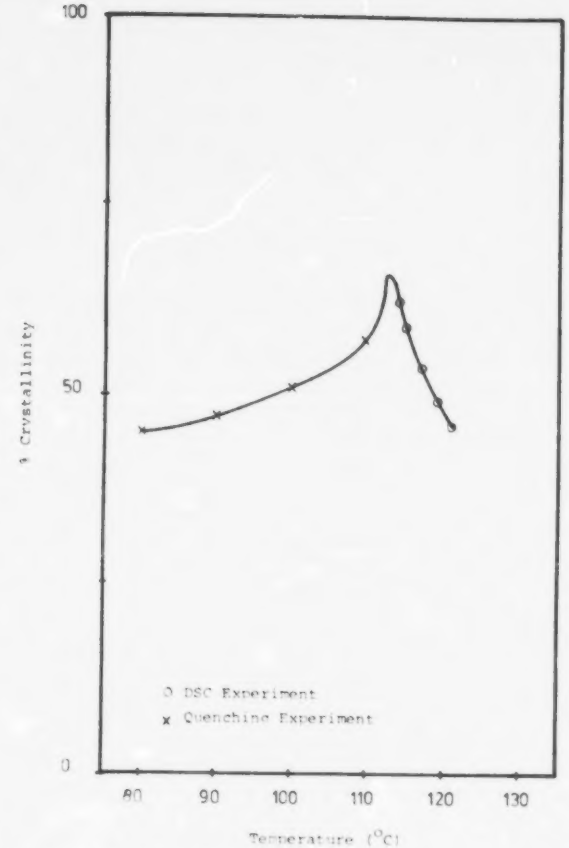


*Fig. 1. Ultimate crystallinity versus temperature.*

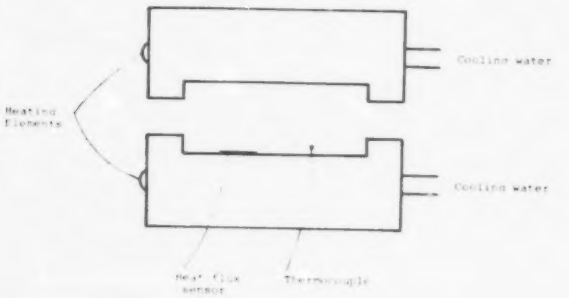


*Fig. 2. Static cooling experiment.*

heat flux sensor was squeezed between the sample and the mold wall to measure the heat flux and the contact temperature. A thermocouple was embedded into the sample to determine the temperature near the centerline of the molding. The heat flux sensor (Type 20455 manufactured by RDF Co.) was employed to supply the boundary conditions for the system, while the thermocouple gave the temperature profile near the center of the cavity during the cooling process.

During a typical experiment, the premolded Sclair 2908 high-density polyethylene disc with the thermocouple was placed in the apparatus, which was then heated to 180°C. When stable thermal conditions were established, as indicated by a stable reading of 180°C both in the molten sample and at the cavity wall, cooling was started. Water cooling was employed, and a slight pressure was applied to the polymer in order to assure good contact between the polymer and metal surface. A continuous record was obtained of the heat flux, contact temperature, and melt temperature.

Typical experimental data relating to the variation of the melt temperature at the center of the cavity during cooling are shown in *Fig. 3*. *Figure 3* also shows the results of model predictions for the case under study. It is apparent that the proposed model gives results in very good agreement with experimental data.

In addition to testing the capacity of the model to predict temperature variations in the sample, an attempt was made to evaluate its potential for predicting the resulting distribution of crystallinity. For this purpose, the solid polyethylene piece, after cooling, was microtomed in the depth direction. The microtomed sections were then analayzed using differential scanning calorimetry, to obtain the crystallinity distribution in the depth direction.

*Figure 4* shows a comparison between the measured and calculated crystallinity distributions in the solid piece after cooling. These results indicate that the level of agreement between experimental and predicted crystallinity values is very good.

## INJECTION MOLDING RESULTS

For the filling stage of the injection-molding process, the continuity, momentum, and energy equations are solved simultaneously, coupled with rheological and crystallization kinetics equations to obtain the distributions of pressure, velocities, temperature, stresses, and crystallinity in the mold. The same set of equations, with the assumption of a no-flow situation, is used for the cooling stage.

Moldings were obtained employing a reciprocating screw 2⅓ oz., Metalmec injection-molding ma-

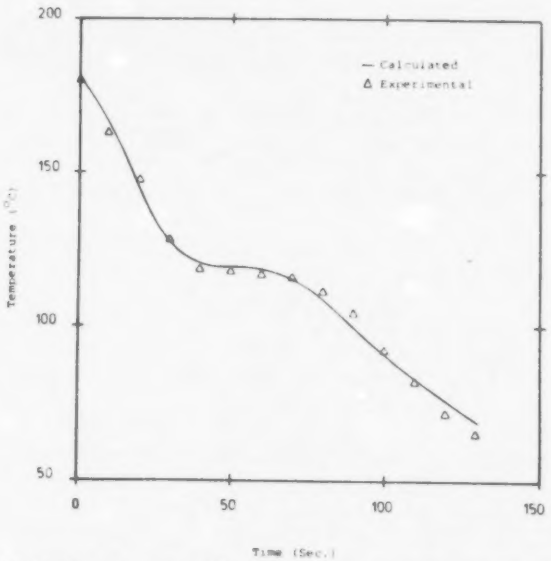


*Fig. 3. Temperature profile during static cooling experiment.*

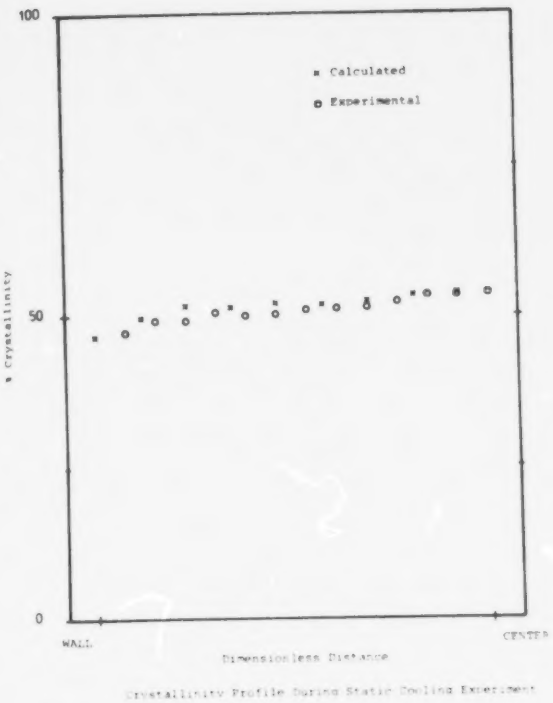


*Fig. 4 Crystallinity profile during static cooling experiment*

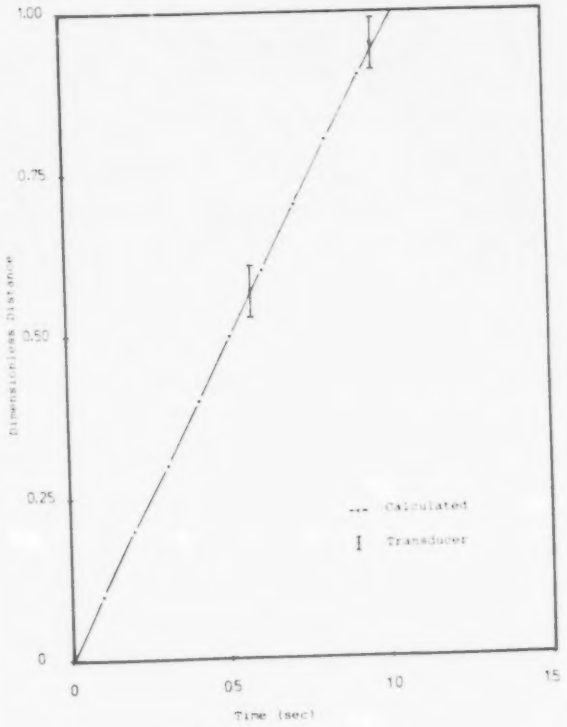


*Fig. 5 Progression of the melt front*

chine in conjunction with a fan-gated mold cavity with dimensions: 9.1 cm x 6.35 cm x 3.18 mm. Rheological data were obtained using a Rheometrics Mechanical Spectrometer and the Instron Capillary Rheometer. The crystallization kinetics data were based on differential scanning calorimetry.

The thermomechanical history of the resin during the various stages of the process influences the ultimate properties of the plastics article. Thus, a generalized integrated model of the injection-molding process should be helpful in the prediction of both moldability and product quality. Experimental and calculated curves are shown in *Figs. 5* and *6* for the progression of the melt front and the variation of pressure with time at the entrance of the mold. Predictions of the pressure and melt front positions show that the model can predict very well the moldability parameters such as the filling time or the maximum pressure during filling. However, in order to calculate ultimate properties of the final product, the development of the stress, temperature, and pressure fields during filling, packing and cooling should be considered. Based on the evaluation of the stress and temperature fields, the model can predict birefringence distribution and crystallinity profiles. The combination of these two properties can be used to calculate ultimate properties.

In this paper, oriented towards heat transfer, only results related to temperature and crystallinity profiles are discussed. *Figure 7* shows the calculated

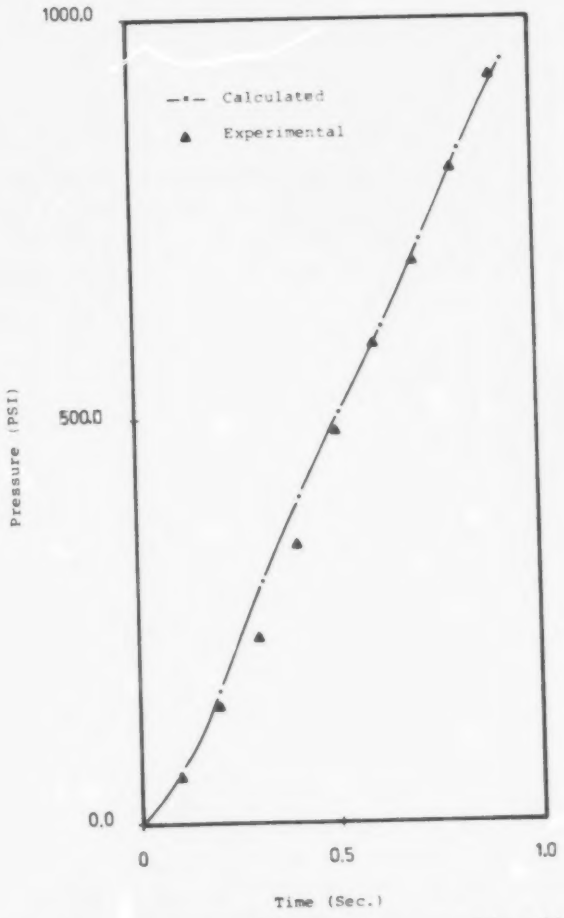


*Fig. 6 Pressure variation with time at the entrance of the mold*

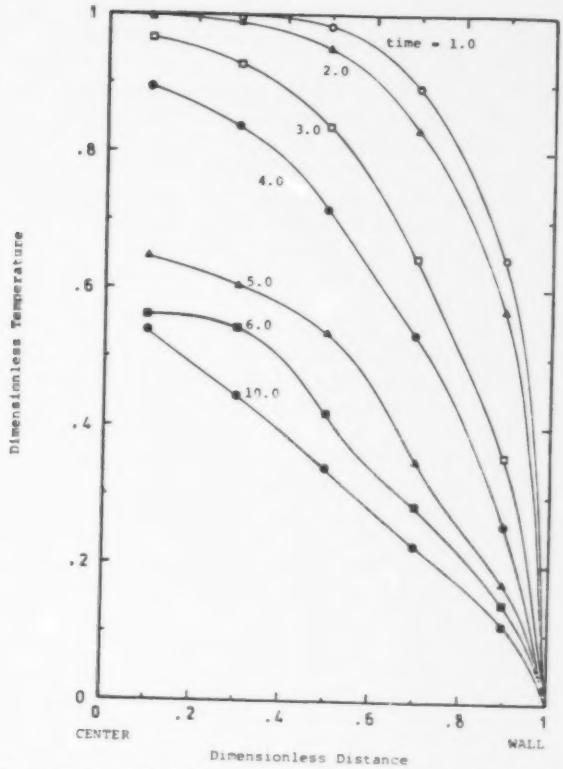


*Fig. 7. Gapwise distribution of temperature during the molding cycle at mid-plane, time in seconds.*

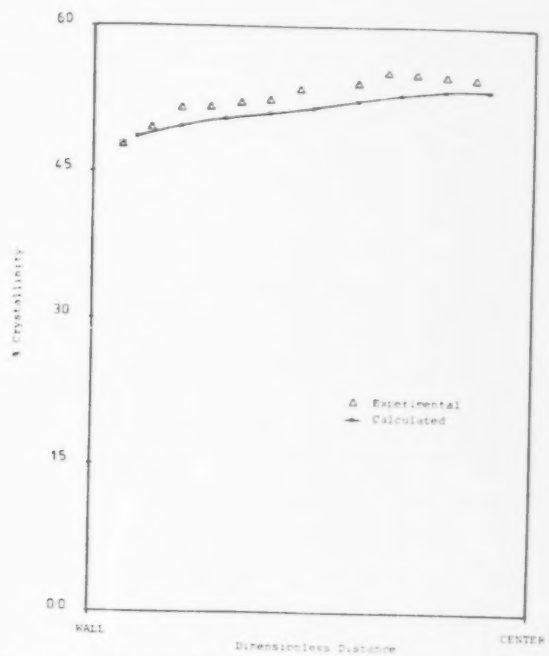


*Fig. 8. Gapwise distribution of crystallinity at the end of the process.*

temperature profiles at different times during the overall process. The filling time for this set of molding conditions was 1.1 sec. Because of this relatively short filling time and the prevailing cooling conditions, the solid layer at the end of filling was only 8 percent of the mold thickness. Comparison between the distribution of crystallinity, at the plane halfway in the mold, as obtained by D.S.C. measurements and the predicted distribution from the non-isothermal kinetics model is shown in *Fig. 8*. Good agreement between experimental and calculated profiles is evident. These results refer to the final molding.

## CONCLUSION

The processing of polymers typically includes steps involving heat transfer. Crystallization during polymer processing occurs non-isothermally and the structure formed is due to a non-isothermal crystallization under molecular orientation. Thus, the mechanical properties of a polymer are affected by processing conditions, such as the cooling history.

The model presented yields predictions of the ultimate degree of crystallinity by combining heat transfer and kinetics of crystallization models. The method is applicable to a wide variety of problems relating to the processing of crystallizable polymers.

## NOMENCLATURE

$C_i$ : Specific heat.
$\vec{g}$ : Gravitational acceleration vector.
$k(T)$: Crystallization rate constant.
$n$ : Avrami exponent.
$P$ : Pressure.
$\vec{q}$ : Energy flux vector.
$t$ : Time.
$T$ : Temperature.
$\vec{v}$ : Velocity vector.
$X(t)$ : Crystalline volume fraction.
$\eta$ : Viscosity.
$\lambda$ : Relaxation time.
$\lambda_r$ : Heat of crystallization.
$\rho$ : Density.
$\overset{=}{\tau}$ : Stress tensor.
$\overset{=}{\Delta}$ : Rate of deformation tensor.

## REFERENCES

1. Gloor, W. E., *SPE Trans.*, **3**, 270 (1963).
2. Dusinberre, G. M., "Numerical Analysis of Heat Flow," McGraw Hill, N.Y. (1949).
3. Kenig, S., and Kamal, M. R., *SPE J.*, **26**, 50 (1970).
4. Sifleet, W. L., Dinos, N., and Collier, J. R., *Polym. Eng. Sci.*, **13**, 10 (1973).
5. Dietz, W., *Polym. Eng. Sci.*, **13**, 1030 (1978).
6. White, J. L., and Metzner, A. B., *J. Appl. Polym. Sci.*, **7**, 1867 (1963).
7. Nakamura, K., Watanabe, T., Katayama, K., Amano, T., *J. Appl. Polym. Sci.*, **16**, 1077 (1972).

## DISCUSSION

*E. Mitsoulis:* Since you have solved the White-Metzner approximation of the Maxwell fluid, it seems to me that you are considering viscoelasticity. What would be the Deborah member, which is a measure of elasticity relative to viscous effects?

*M. R. Kamal:* It is slightly lower than, but not very far from, unity.

*E. Mitsoulis:* I would then like to ask which numerical method you used?

*M. R. Kamal:* Finite-difference.

*E. Mitsoulis:* So you did not have any problems with oscillations or convergence.

*M. R. Kamal:* That is right.

*M. Grmela:* I have a question regarding rheology. You have included in the White-Metzner equation changes due to the non-isothermal situation, but there will be some dependence on crystallinity. Is $X$ in the equation for the stress tensor?

*M. R. Kamal:* No, it is not. You can probably assume that, if there are any rheological effects due to crystallinity, then they are lumped into the experimental data for $\eta$ as a function of temperature. However, we did not account for the effect of crystallinity explicitly.

*L. A. Utracki:* I want to congratulate you and Mr. Lafleur for a marvelous piece of work. The agreement is rather surprising with the predictions. The question is the following. What is this two-stage Avrami equation based on? Usually people are trying to introduce crystallization kinetics based on nucleation and self-nucleation mechanisms of crystallization. The self-nucleating mechanism does not follow the Avrami equation. So why did you use this particular method of attack?

*M. R. Kamal:* Our work was carried out with two resins. We have observed that when these resins are molded, they show completely different morphological patterns, which are due to the presence of a nucleating agent in one but not in the other. Although we initially expected that different types of crystallization kinetics would be needed to describe the behavior of the two resins, early studies suggested that both resins did not deviate significantly from the Avrami model. The main deviation was noted at large crystallization times.

*P. Vangheluwe:* I was wondering about the heat flux device. Could you give me some details on it?

*P. Lafleur:* The device consists of a bunch of thermocouples that measure the difference in temperature over a very thin layer. So, using Fourier's law, the heat flux across the sensor is calculated. The device that we have used is Type 20455 supplied by the RDF Company.

*G. L. Bata:* You mentioned nucleation and self-nucleation but you mentioned that you were using high-density resins. Are there any catalyst residues in these resins that will give you nucleation anyway?

*M. R. Kamal:* That was the case for the resin that is self-nucleating. It contained a catalyst residue and not an intentional nucleating agent.

# Rheological and Heat-Transfer Considerations for the Processing of Reactive Systems

M. E. RYAN

*Department of Chemical Engineering*
*State University of New York at Buffalo*
*Amherst, New York 14260*

Thermosetting materials have found widespread use over a broad spectrum of engineering applications due to their intrinsic mechanical strength, thermal and dimensional stability, and other unique properties. Consideration is given to those aspects of reaction kinetics, rheology, fluid mechanics, and heat transfer which are of relevance for the mathematical modeling of reactive polymer processing. Particular emphasis is given to the characterization of reaction kinetics under non-isothermal conditions, the effect of fillers or reinforcing agents on the heat transfer and kinetic behavior, and the complex nature of the interactions brought about by the reactivity of these systems. In addition, the current status of the mathematical simulation of reactive polymer processing is briefly reviewed.

## INTRODUCTION

Thermosetting molding compounds are processed and utilized in a wide variety of applications owing to their advantageous physical, chemical, and mechanical properties. The characteristics which make a particular thermosetting compound attractive over a thermoplastic or even a non-polymeric material are dependent on the market and application. Typically, a combination of factors such as cost, weight, strength, and processability may result in a thermosetting material as the optimal choice for meeting the required performance of the given product. In recent years thermosetting polymers have assumed a more important role by virtue of the greater flexibility in tailoring desired ultimate properties provided by means of composite systems. In addition, the development of reaction injection molding (RIM) technology has become of particular importance for the automotive and other markets. Reactive injection molding involves the production of a finished product from monomeric or oligomeric components directly. The process has emerged relatively recently and is especially attractive from the standpoint of lower energy requirements and reduced capital investment.

The processing behavior of reactive systems is strongly dependent on their thermal and rheological properties. However, the kinetic and rheological behavior manifested by these systems in a processing situation is dependent on the particular operating conditions and processing history imposed. An understanding of these interactions is critical since very large increases in temperature and viscosity are possible. Consequently, premature solidification of an inferior part may result.

This paper is concerned with those aspects of reaction kinetics, rheology, fluid mechanics, and heat transfer which are relevant for the processing of reactive materials. A more fundamental understanding of the coupling which exists between these phenomena is necessary for a better qualitative description of processing problems, improved quantitative description of moldability criteria, more accurate mathematical simulation of the processing sequence, elucidation of structure-property relationships and optimization of product quality and performance.

## REACTION KINETICS

A wide range of experimental techniques have been employed in the study of the kinetic behavior of reactive systems. These methods include chemical analysis, calorimetry, chromatography, spectroscopy (IR, FTIR, NMR, Raman), dynamic mechanical measurements, and the monitoring of changes in various physical properties such as density, refractive index, electrical resistivity, and viscosity, among others. The latter technique implies a direct correlation between the chemical and rheological changes which occur over time. Much of the technical literature in this area is directed toward an elucidation of reaction mechanisms or pathways. However, the correlation and representation of experimental data in the form of a simple kinetic expression is of considerable importance from the standpoint of mathematical modeling. In this respect differential scanning calorimetry has been extensively used in the evaluation of rate equations and for estimation of the associated kinetic parameters.

The most commonly used commercial calorimeters can be run in either an isothermal mode or in a non-isothermal scanning mode. In the typical non-isothermal operation the temperature is pro-

grammed to vary linearly with time. Although the scanning experiments are simple and rapid, most of the kinetic characterization of reactive systems is usually conducted by means of a series of isothermal experiments. It is generally assumed that the exothermic heat evolved during the reaction is directly proportional to the extent of reaction. The data are then correlated to a kinetic expression in order to ascertain numerical values for the kinetic parameters or constants which may appear in the rate expression.

In many cases, the reactivity of thermosetting systems has been described by means of a simple $n^{th}$-order kinetic expression governed by a single Arrhenius rate constant. Thus:

$$\left(\frac{\partial \alpha}{\partial t}\right)_T = k(1 - \alpha)^n \tag{1}$$

$$k = k_0 \exp(-\Delta E_k / RT) \tag{2}$$

where $\alpha$ is some measure of the extent of reaction or degree of cure, $k$ is a rate constant, $n$ is the reaction order, $k_0$ is a constant, $\Delta E_k$ is a kinetic activation energy, $R$ is the familiar gas constant, and $T$ is absolute temperature. Integration of *Eq.* 1 yields an expression for the extent of reaction as a function of time for an isothermal or constant temperature experiment.

$$\begin{aligned} \alpha &= 1 - \exp(-kt) && \text{for } n = 1 \\ \alpha &= 1 - |(n-1)kt + 1|^{1/(1-n)} && \text{for } n \neq 1 \end{aligned} \tag{3}$$

Substitution of *Eq.* 3 into the right-hand side of *Eq.* 1 gives the following explicit expression for the reaction rate as a function of time:

$$\begin{aligned} \left(\frac{\partial \alpha}{\partial t}\right)_T &= k \exp(-kt) && \text{for } n = 1 \\ \left(\frac{\partial \alpha}{\partial t}\right)_T &= |(n-1)kt + 1|^{n/(1-n)} && \text{for } n \neq 1 \end{aligned} \tag{4}$$

*Figure* 1 shows schematically the variation of $\alpha$ and $\left(\frac{\partial \alpha}{\partial t}\right)_T$ with time for various values of $n$. It is particularly evident from the variation of the reaction rate with time that a simple $n^{th}$-order kinetic expression is unable to provide an accurate quantitative description of the entire curing process. A more general form of isothermal rate expression that has been commonly used for reactive systems is the following:

$$\left(\frac{\partial \alpha}{\partial t}\right)_T = (k_1 + k_2 \alpha^m)(1 - \alpha)^n \tag{5}$$

$k_1$ and $k_2$ are rate constants having an Arrhenius dependence on temperature and $m$ and $n$ are kinetic exponents. *Figure* 2 illustrates schematically the variation of $\alpha$ and $\left(\frac{\partial \alpha}{\partial t}\right)_T$ given by this rate equation.

It is important to note that the values of $\alpha$ or $\left(\frac{\partial \alpha}{\partial t}\right)_T$ calculated from these or other similar expressions correspond to an isothermal situation. Since the processing of reactive systems is inherently a non-isothermal process, great caution must be exercised in the application of these kinetic expressions for the determination of the extent of reaction in a production part. The isothermal rate expression must be modified in order to yield correct results for the rate of reaction or extent of cure under non-isothermal conditions. A detailed analysis for the two isothermal kinetic expressions given by *Eqs.* 1 and 5, respectively, yields (1):

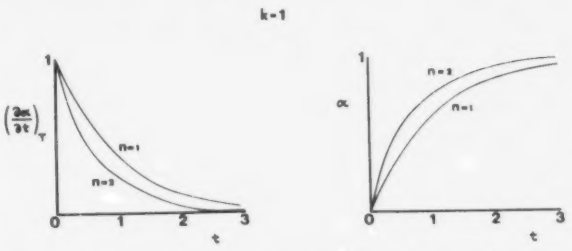


*Fig. 1. Variation of isothermal reaction rate and extent of reaction with time.*

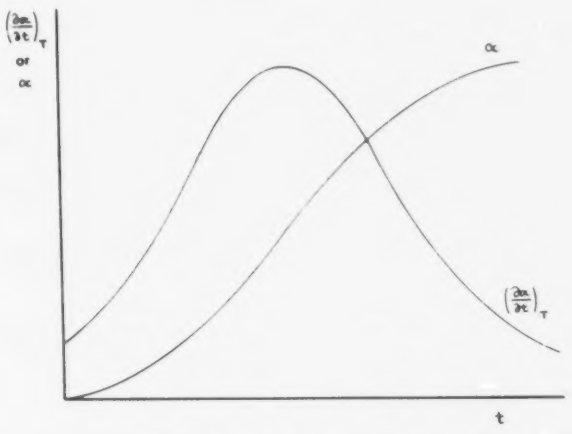


*Fig. 2. Variation of isothermal reaction rate and extent of reaction with time.*

$$\frac{d\alpha}{dt} = \left(\frac{\partial \alpha}{\partial t}\right)_T \left[1 + \frac{\beta t \Delta E_k}{RT^2}\right] \tag{6}$$

$$\frac{d\alpha}{dt} = \left(\frac{\partial \alpha}{\partial t}\right)_T \left[1 - \beta \left(\sum_{j=0}^{j=\infty} \frac{\Gamma(n+j)}{j!\Gamma(n)} \sum_{i=0}^{i=\infty} \frac{(-k_1)^i}{(k_2)^{i+1}} \cdot \left(\frac{i(\Delta E_1 - \Delta E_2) - \Delta E_2}{RT^2}\right) \frac{\alpha^{j+1-(i+1)m}}{j+1-(i+1)m}\right)\right] \tag{7}$$

where $\beta = dT/dt$ and $\Delta E_1$ and $\Delta E_2$ are the activation energies associated with the rate constants $k_1$ and $k_2$, respectively. For certain special values of $m$ and $n$ simple analytical expressions result for the dynamic rate equation given by *Eq.* 7. Clearly, predicted degree of cure distributions using *Eqs.* 6 or 7 may be markedly different from those predicted by application of the corresponding isothermal expressions given by either *Eq.* 1 or 5.

## EFFECT OF FILLERS ON REACTION KINETICS

Many thermosetting compounds contain a variety of additives and ingredients including fillers and reinforcing agents. Fillers are used for various reasons and can have a significant effect on part shrinkage, flame retardancy, and cost. An understanding of the influence of fillers on the curing kinetics is therefore of considerable interest. Dutta and Ryan (2) studied the influence of filler concentration on the kinetics of a liquid epoxy system using differential scanning calorimetry. Two different commercial-grade fillers were used, namely, a Cabot furnace-process carbon black and a surface-treated Novacite silica. The isothermal calorimetric data could be accurately correlated as a function of time, temperature, and filler content using the kinetic expression given by *Eq.* 5. The kinetic exponents ($m$ and $n$) or the reaction order of the system were found to be unaffected by the presence of the filler. However, the kinetic rate constants were found to vary with filler concentration as shown in *Figs.* 3 and 4. The dependence of the rate constants on filler concentration could be adequately described in terms of a simple third-order polynomial expression in the case of the carbon black. For the carbon black filled systems, the activation energies $\Delta E_1$ and $\Delta E_2$ were practically the same for all filler concentrations having values of 15.4 kcal/gmole and 10.9 kcal/gmole, respectively. Hsich (3) studied the crosslinking of natural rubber and also found that the carbon black loading had an insignificant effect on the activation energy of the cure reaction. However, for the liquid epoxy studied by Dutta and Ryan the silica filler was observed to have an influence on $\Delta E_1$, the activation energy associated with $k_1$.

## RHEOLOGY

The rheological characterization of reactive materials is complicated by the large number of variables on which the rheological properties depend. In addition to the obvious dependence on filler concentration and chemical formulation, the viscosity of a reactive system may be regarded as a function of pressure, temperature, deformation rate, and time. Thus:

$$\eta = \eta(P, T, \dot{\gamma}, t, \phi) \qquad (8)$$

where $P$ denotes pressure, $T$ denotes temperature, $\dot{\gamma}$ represents some suitable measure of the deformation rate, $t$ is time, and $\phi$ is the filler concentration or loading.

The principal distinguishing feature of thermosetting materials is the dramatic change of viscosity with time due to the progress of the crosslinking reaction. Some typical viscosity-time isotherms are shown schematically in *Fig.* 5. The viscosity remains essentially constant with time during the initial stages of reaction but increases rapidly until the material is transformed to an infusible rigid solid. At higher temperatures the viscosity is initially lower due to the temperature dependence of the flow characteristics. However, the crosslinking reaction proceeds at a faster rate and the viscosity rises steeply at an earlier time.

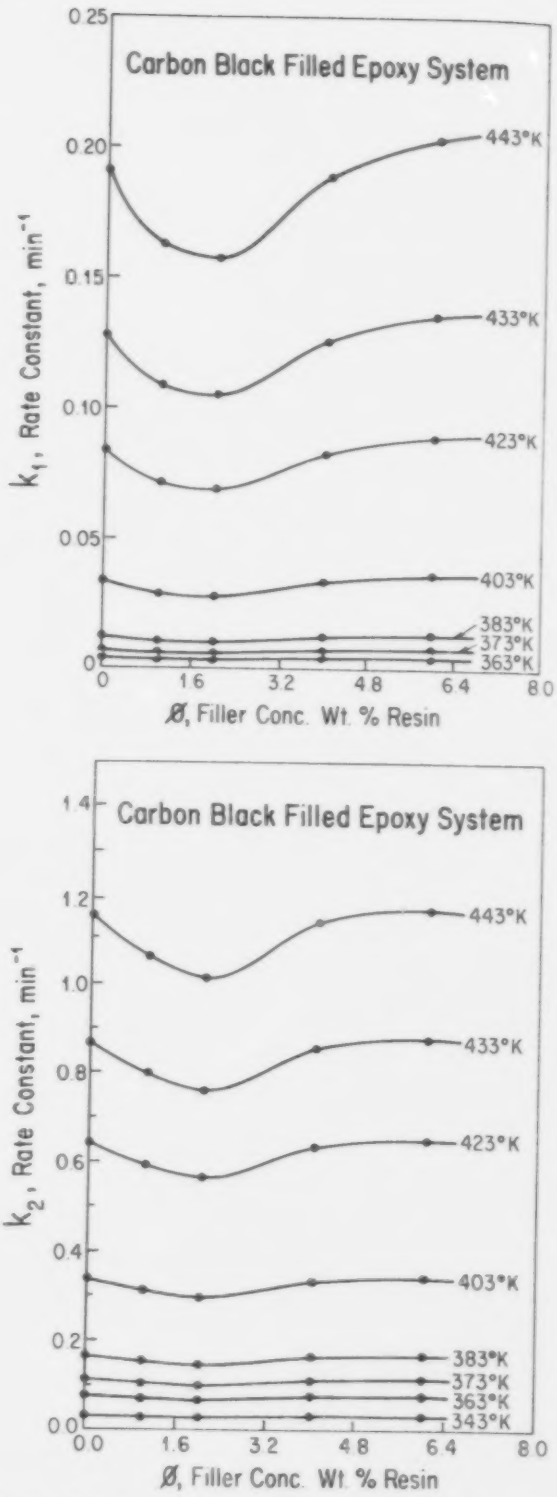


*Fig. 3. (a) Variation of rate constant $k_1$ with filler concentration. (b) Variation of rate constant $k_2$ with filler concentration.*

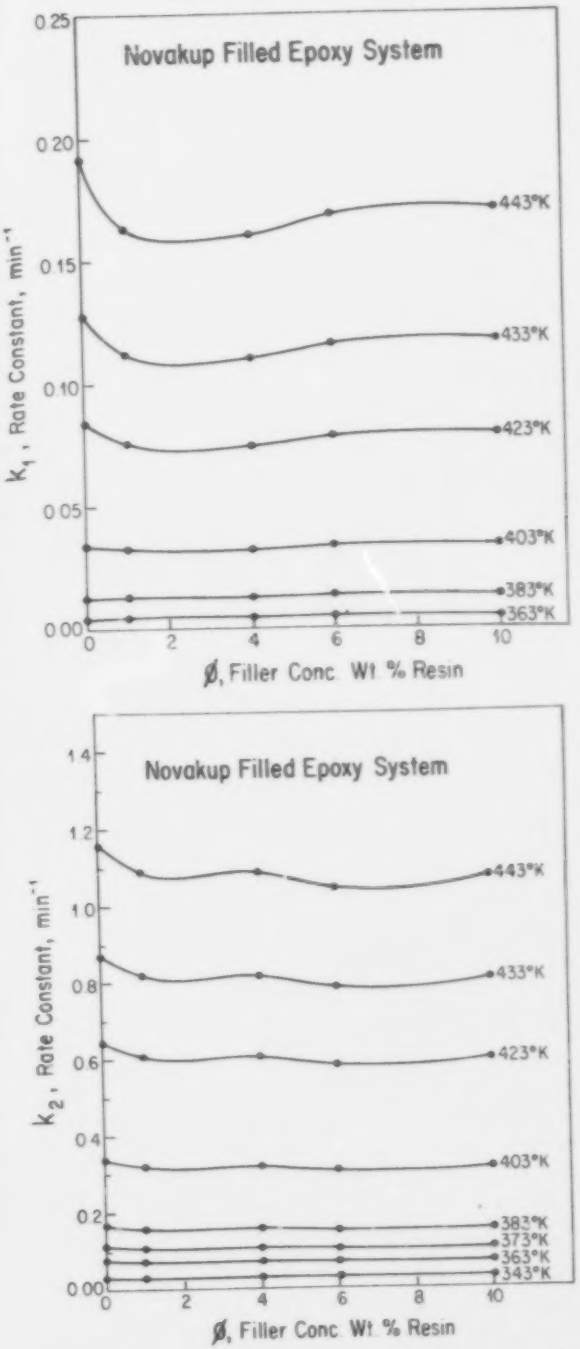


*Fig. 4. (a) Variation of rate constant $k_1$ with filler concentration. (b) Variation of rate constant $k_2$ with filler concentration.*

Several empirical correlations have been proposed to describe the time-temperature dependence of viscosity. The most prevalent relation is of the form:

$$\eta = F(P, T, \dot{\gamma}) \exp\left[Ct \exp\left(-\left(\frac{\Delta E_k}{RT}\right)\right)\right] \qquad (9)$$

where $\Delta E_k$ denotes the activation energy associated with the crosslinking reaction. This model has been successfully used by Hollands and Kalnin (4), White (5), and Roller (6). It should also be noted that many of the early experimental studies attempted to determine the flow activation energy by plotting the time or reciprocal of time required to reach a given viscosity level versus reciprocal absolute temperature (7–9). The major difficulty with this approach resides in the fact that the isoviscous state does not define the same structural or chemical composition except under isothermal conditions (10). Thus, a plot of the logarithm of viscosity as a function of reciprocal absolute temperature needs to be constructed at the same level of cure or extent of reaction in order to correctly determine the flow activation energy. This can be done by combining the experimentally measured viscosity-time isothermal data with a knowledge of the reaction kinetics of the system. Therefore, with the aid of kinetic expressions, such as the ones discussed in the previous section, the explicit time dependence of viscosity may be replaced by some measure of the progress or extent of reaction, $\alpha$. *Eq.* 8 may therefore be written as:

$$\eta = \eta(P, T, \dot{\gamma}, \alpha, \phi) \qquad (10)$$

Some attempts have been made to relate the viscosity directly to the degree of cure through the molecular weight of the system (9, 11). The dependence of melt viscosity on molecular weight is well established both theoretically and experimentally for most linear thermoplastic polymers. The success in correlating viscosity with a single structural parameter in the case of thermoplastic materials suggests that a similar approach might be employed for thermosets. Thus

$$\eta = F(P, T, \dot{\gamma})\,(a_1 + a_2 M_w + a_3 M_w^{\,b}) \qquad (11)$$

where $a_1$, $a_2$, $a_3$, and $b$ are constants and $M_w$ is a function of the extent of reaction, $\alpha$. Several theoretical treatments have been developed in order to relate molecular weight to the extent of reaction (12–20). The major practical limitation stems from

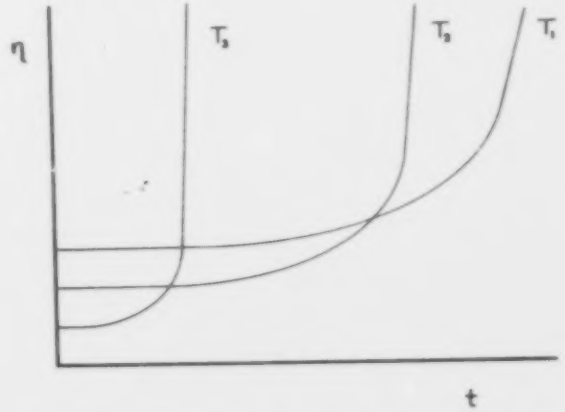


*Fig. 5. Viscosity as a function of time for various temperatures ($T_3 > T_2 > T_1$).*

the fact that many of these expressions contain molecular parameters which may be difficult to measure or estimate for a commercial material.

The dependence of viscosity on shear rate at a given extent of reaction has been studied for a number of thermosetting materials (21–24). Several of the unsaturated polyester and polyurethane RIM materials exhibit essentially Newtonian behavior over a wide range of shear rate. Molding compounds such as the epoxies, diallyl phthalates, and phenolics exhibit marked shear-thinning behavior. Simple constitutive relations, such as the power-law and Bird-Carreau models, may be used to describe the shear rate dependence of these systems with reasonable accuracy.

Very few systematic studies have been undertaken with regard to the role of fillers on the rheology of thermosetting systems. Recently, Han and Lem (25) measured the rheological properties of unsaturated polyester resins containing clay, calcium carbonate, and glass fibers. With increasing concentration of clay or glass fibers the observed rheological behavior was typical of that of suspensions, namely, pronounced shear-thinning behavior at low shear rates or shear stresses. In the case of the calcium carbonate, Newtonian behavior was observed at all concentrations. When both fillers and low-profile additives were present in combination, rather complex rheological behavior was exhibited, indicating the occurrence of some sort of interaction between the filler and the low-profile additive. Clearly there is a need for a more systematic and extensive investigation of these interactions for a variety of materials. Also, the possible influence on the rheological behavior of the reacting system by the filler through the reaction kinetics merits consideration.

## PROCESSING OF REACTIVE SYSTEMS

The optimal molding strategy for a reactive material involves a compromise between a high production rate or short cycle time on the one hand, and satisfactory ultimate properties on the other. In the case of a cyclic molding operation, such as compression or injection molding, attainment of satisfactory ultimate properties usually necessitates a relatively long curing time in comparison to the time required for flow. As a consequence, a reasonable first approximation for the mathematical analysis of a molding operation may be achieved by neglecting the complexities in the temperature and degree of cure distributions due to flow. In addition, many compression- and injection-molding operations involve thin-walled parts. Thus, a heat-transfer analysis of the process simplifies to an unsteady, one-dimensional heat conduction problem in an infinite slab. The governing conservation equation for this situation may be expressed as follows:

$$\rho c_p \frac{\partial T}{\partial t} = -\frac{\partial q}{\partial x} + \Delta H \frac{d\alpha}{dt} \tag{12}$$

$\rho$ is the density, $c_p$ is the specific heat at constant pressure, $q$ is the heat flux, $\Delta H$ is the heat of reaction, and $\frac{d\alpha}{dt}$ denotes the reaction rate. The heat flux is related to the temperature gradient by Fourier's law. Thus:

$$q = -k' \frac{\partial T}{\partial x} \tag{13}$$

where $k'$ is the thermal conductivity.

Temperature and degree of cure profiles have been computed by utilizing a simple $n^{th}$-order kinetic expression for the heat-generation term and assuming that the thermal properties were independent of temperature. Adabbo *et al.* (26) found that the temperature and degree of cure were significantly influenced by the kinetic parameters, thermal conductivity, wall temperature, and part thickness. Macosko and coworkers (27, 28) studied the non-isothermal curing of a polyurethane system in conjunction with the RIM process. Temperature profiles, gel point, and sol fraction were calculated. A similar non-isothermal analysis has been made by Progelhof and Throne (29) for reactive polyester and epoxy systems. They indicated that great care must be exercised in order to minimize the large temperature excursions which arise as a result of internal heat generation.

These theoretical analyses have also been extended for the case of composite systems (30). For composites, *Eqs. 12* and *13* must be modified in order to properly account for the thermal properties of the composite and the diluent effect of the inert filler. Thus:

$$(\rho c_p)_c \frac{\partial T}{\partial t} = -\frac{\partial q}{\partial x} + \phi_r \Delta H \left(\frac{d\alpha}{dt}\right)_c \tag{14}$$

$$q = -k'_c \frac{\partial T}{\partial x} \tag{15}$$

where the subscript "$c$" denotes the property associated with the composite and $\phi_r$ is the volume fraction of the resin. McGee (30) used a simple $n^{th}$-order kinetic expression and assumed that the presence of filler had no influence on the reaction kinetics. Time-temperature and degree of cure profiles were computed by assuming a uniform initial temperature and concentration. The thermal properties of the composite material were estimated by means of a "spherical inclusion model." Since the filler is inert, it acts as both a heat sink as well as a diluent and thereby decreases the amount of heat generated exothermally and reduces the maximum temperature rise. The progression of the cure front was found to be influenced by the filler concentration and the thickness of the slab.

Numerous experimental studies have been undertaken with regard to the flow behavior of reactive systems. Tonogai (31) employed a disk cure test in order to examine the flow and cure characteristics of phenolic and diallyl phthalate molding compounds in order to determine optimum molding conditions. Grigor (32), Heinle and Rodgers (33), and Hoffman (34) studied the effect of pressure on

the spiral flow length of a two-step phenolic. They suggested three parameters for the characterization of flow behavior, namely, flow length, flow duration, and minimum melt viscosity. Sundstrom *et al.* (35, 36) compared a variety of flow tests, such as cup close and spiral flow, for assessing the flow behavior of diallyl phthalate molding compounds. They determined that many flow problems could be solved by varying the appropriate molding conditions rather than by varying material properties. Fishberg and Longstreet (37, 38) measured flow length as a function of temperature for several phenolic resins. They observed that the variation of flow length with temperature exhibited a well-defined maximum which could be explained as the result of two competing effects, namely, the temperature dependence of viscosity and the temperature dependence of reaction rate. Barth and Robertson (39) studied the effect of molecular weight on spiral flow length for a fast-curing polybutadiene system. The spiral flow length decreased with increasing molecular weight of the base polymer. They also observed that the molecular-weight distribution had a significant effect on moldability. The rate of cure is influenced by the low-molecular-weight fraction, whereas the high-molecular-weight fraction directly affects the flow behavior. It is evident that the molecular weight is a critical parameter in achieving a balance between the processability and the ultimate mechanical properties that may be attained within a practical curing cycle. Frizelle and Norfleet (40, 41) and Beck and Golovoy (42) have discussed the importance of viscosity in relation to the mold filling behavior of thermosets. Talwar and Ashlock (43) determined the most suitable conditions for injection molding diallyl isophthalate compounds from the cure responses obtained using an oscillating disk rheometer. A similar experimental study has been made by Menges and Dalhoff (44).

The major difficulties and characteristics associated with the processing of reactive systems in general and injection molding in particular have been discussed by Biesenberger and Gogos (45) and Fleischmann (46). Kamal (47) has emphasized the necessity of thermoset characterization for moldability analysis and the interaction between material properties, molding conditions, and ultimate properties.

More rigorous and comprehensive analyses of the injection molding of reactive systems have been developed. Kamal and Ryan (48) have made a systematic experimental and theoretical study of the injection molding of an epoxy molding compound in semicircular and rectangular cavities. The dependence of viscosity on shear rate, temperature, and time was explicitly considered. The predicted pressure and temperature distributions were found to be in reasonable agreement with experimental observations. However, the experimental studies involved relatively slow filling rates in comparison with typical commercial operations.

Sidi and Kamal (49) have made a detailed experimental study of the molding behavior of a commercial unsaturated polyester resin. They used differential scanning calorimetry in order to investigate the cure distribution in the molded part. The highest cure levels were observed to occur far from the gate near the end of the mold cavity. Domine and Gogos (50, 51) developed a numerical simulation for the reactive molding of a linear condensation polymer. The rheological behavior of the system was assumed to be Newtonian but the complications arising as a result of the fountain-flow effect in the vicinity of the melt front were included. Their analysis indicated that both the filling rate and the reaction rate were important for ascertaining the time required to demold the part. A similar study for a phenolic molding compound has been give by Chung (52). Manzione (53) used a modification of the simplified marker and cell finite difference method for the simulation of cavity filling of a reactive system. A simple $n^{th}$-order kinetic expression was used to represent the rate of chemical reaction. Convective and axial conduction terms were retained in the governing equation of energy. Manzione treated the fountain-flow effect in a manner similar to the heuristic treatment of Domine and Gogos. No significant differences in the resulting temperature and conversion profiles were observed after filling indicating that inclusion of an exact treatment of the fountain-flow effect may be unnecessary.

Although considerable effort has been directed toward a more fundamental understanding of the molding behavior of reactive systems, relatively little experimental data is available for comparison purposes. In addition, a reliable quantitative description of the many complex interactions associated with reactive polymer processing requires further elucidation and development. With the exception of a few studies (54, 55), very little published information is available with regard to the behavior of reactive materials in continuous processes such as extrusion. Clearly, much additional research is required.

## CONCLUSIONS

Several points should be emphasized with respect to the mathematical modeling of reactive polymer-processing operations. Since the processing of reactive materials is inherently non-isothermal, caution must be exercised in the description of the reaction kinetics under these conditions. All previous studies have employed kinetic expressions where the kinetic parameters have been obtained from isothermal kinetic data. The effect of fillers on the kinetic and rheological behavior of thermosetting systems is not extensively known and has not been explicitly included in previous modeling efforts. Not surprisingly, a fundamental understanding of reactive processing is on a far less satisfactory basis than is the case for non-reactive systems. Only fragmentary experimental data, obtained from actual processing operations, is available in the literature. Very few definitive comparisons have been made between experimental and

theoretical results. In most cases the observations are specific to some degree and may be difficult to generalize. Despite the increased interest and technological importance of reactive processing operations, very little mathematical modeling has been undertaken.

Consequently, more systematic and comprehensive research relating to the complex interactions between kinetics, rheology, fluid mechanics, and heat transfer is clearly needed.

## NOMENCLATURE

$a_1$ = constant in *Eq* 11.
$a_2$ = constant in *Eq* 11.
$a_3$ = constant in *Eq* 11.
$b$ = constant in *Eq* 11.
$C$ = constant in *Eq* 9.
$c_p$ = specific heat at constant pressure.
$k$ = rate constant.
$k_0$ = constant in *Eq* 2.
$k_1$ = kinetic rate constant in *Eq* 5.
$k_2$ = kinetic rate constant in *Eq* 5.
$k'$ = thermal conductivity.
$k'_c$ = thermal conductivity of composite.
$M_u$ = molecular weight.
$m$ = kinetic exponent.
$n$ = kinetic exponent.
$P$ = pressure.
$q$ = heat flux.
$R$ = gas constant.
$t$ = time.
$T$ = temperature.
$x$ = spatial coordinate.
$\alpha$ = degree of cure.
$\beta$ = rate of temperature change.
$\dot{\gamma}$ = rate of deformation.
$\Delta E_k$ = kinetic activation energy.
$\Delta E_1$ = activation energy associated with rate constant $k_1$.
$\Delta E_2$ = activation energy associated with rate constant $k_2$.
$\Delta H$ = heat of reaction.
$\eta$ = viscosity.
$\rho$ = density.
$\phi$ = filler concentration.
$\phi_r$ = volume fraction of resin.

## REFERENCES


1. A. Dutta and M. E. Ryan, *Thermochimica Acta*, **33**, 87 (1979).
2. A. Dutta and M. E. Ryan, *J. Appl. Polym. Sci.*, **24**, 635 (1979).
3. H. S-Y. Hsich, *J. Appl. Polym. Sci.*, **27**, 3265 (1982).
4. K. M. Hollands and I. L. Kalnin, in H. Lee, editor, "Epoxy Resins," *Adv. Chemistry Ser.*, **92**, 60 (1970).
5. R. P. White, Jr., *Polym. Eng. Sci.*, **14**, 50 (1974).
6. M. B. Roller, *Polym. Eng. Sci.*, **15**, 406 (1975).
7. Y. Tanaka and H. Kakiuchi, *J. Appl. Polym. Sci.*, **7**, 1063 (1963).
8. Y. Tanaka and H. Kakiuchi, *J. Appl. Polym. Sci.*, **7**, 1951 (1963).
9. F. G. Mussatti and C. W. Macosko, *Polym. Eng. Sci.*, **13**, 236 (1973).
10. M. R. Kamal, S. Sourour, and M. Ryan, *SPE ANTEC Tech. Papers*, **19**, 187 (1973).
11. M. E. Ryan, M. Eng. Thesis, McGill University, Montreal, Canada (1973).
12. P. J. Flory, "Principles of Polymer Chemistry," Cornell University Press, Ithaca, New York (1953).
13. W. H. Stockmayer, *J. Chem. Phys.*, **11**, 45 (1943).
14. W. H. Stockmayer, *J. Chem. Phys.*, **12**, 125 (1944).
15. W. H. Stockmayer, *J. Polym. Sci.*, **9**, 69 (1952).
16. W. H. Stockmayer, *J. Polym. Sci.*, **11**, 424 (1953).
17. J. K. Beasley, *J. Am. Chem. Soc.*, **75**, 6123 (1953).
18. R. A. Jackson, P. A. Small, and K. S. Whiteley, *J. Polym. Sci.*, **11**, 1781 (1973).
19. W. W. Graessley and E. S. Shinbach, *J. Polym. Sci.*, **12**, 2047 (1974).
20. C. W. Macosko and D. R. Miller, *Macromolecules*, **9**, 199 (1976).
21. R. Slysh and K. E. Guyler, *Polym. Eng. Sci.*, **10**, 607 (1978).
22. D. W. Sundstrom and M. F. English, *Polym. Eng. Sci.*, **18**, 728 (1978).
23. D. W. Sundstrom and S. J. Burkert, *Polym. Eng. Sci.*, **21**, 1108 (1981).
24. M. D. Hartley and H. L. Williams, *Polym. Eng. Sci.*, **21**, 135 (1981).
25. C. D. Han and K-W. Lem, *J. Appl. Polym. Sci.*, **28**, 743 (1983).
26. H. E. Adabbo, A. J. Rojas, and R. J. J. Williams, *Polym. Eng. Sci.*, **19**, 835 (1979).
27. E. B. Broyer and C. W. Macosko, *AIChE J.*, **22**, 268 (1976).
28. L. J. Lee and C. W. Macosko, *SPE ANTEC Tech. Papers*, **24**, 155 (1978).
29. R. C. Progelhof and J. L. Throne, *Polym. Eng. Sci.*, **15**, 690 (1975).
30. S. H. McGee, *Polym. Eng. Sci.*, **22**, 484 (1982).
31. S. Tonogai, *SPE ANTEC Tech. Papers*, **20**, 568 (1974).
32. J. M. Grigor, Jr., *SPE J.*, **24**, 1, 63 (1968).
33. P. J. Heinle and M. A. Rodgers, *SPE J.*, **25**, 6, 56 (1969).
34. K. R. Hoffman, *Mod. Plast.*, **44**, 131 (1967).
35. D. W. Sundstrom, L. A. Walters, and C. S. Goff, *Mod. Plast.*, **46**, 3, (1969).
36. D. W. Sundstrom and L. A. Walters, *SPE J.*, **27**, 4, 58 (1971).
37. L. D. Fishberg and D. C. Longstreet, *Mod. Plast.* **46**, 6, (1969).
38. L. D. Fishberg and D. C. Longstreet, *Mod. Plast.* **48**, 10, (1971).
39. H. J. Barth and J. J Robertson, *Mod. Plast.*, **47**, 11, (1970).
40. W. G. Frizelle and J. S. Norfleet, *SPE ANTEC Tech. Papers*, **17**, 397 (1971).
41. W. G. Frizelle and J. S. Norfleet, *SPE ANTEC Tech. Papers*, **19**, 538 (1973).
42. R. H. Beck, Jr. and A. Golovoy, *SPE ANTEC Tech. Papers*, **18**, 87 (1972).
43. B. L. Talwar and L. T. Ashlock, *SPE J.*, **26**, 9, 42 (1970).
44. G. Menges and W. Dalhoff, *Kunststoffe*, **59**, 584 (1969).
45. J. A. Biesenberger and C. G. Gogos, *Polym. Eng. Sci.*, **20**, 838 (1980).
46. J. J. Fleischmann, *Polym. Eng. Sci.*, **16**, 235 (1976).
47. M. R. Kamal, *Polym. Eng. Sci.*, **14**, 231 (1974).
48. M. R. Kamal and M. E. Ryan, *Polym. Eng. Sci.*, **20**, 859 (1980).
49. S. Sidi and M. R. Kamal, *Polym. Eng. Sci.*, **22**, 349 (1982).
50. J. D. Domine and C. G. Gogos, *SPE ANTEC Tech. Papers*, **22**, 274 (1976).
51. J. D. Domine and C. G. Gogos, *Polym. Eng. Sci.*, **20**, 847 (1980).
52. T-S. Chung, Ph.D. Thesis, State University of New York at Buffalo, Amherst, New York (1980).
53. L. T. Manzione, *Polym. Eng. Sci.*, **21**, 1234 (1981).
54. J. T. Lindt, *Polym. Eng. Sci.*, **21**, 424 (1981).
55. B. Siadat, M. Malone, and S. Middleman, *Polym. Eng. Sci.*, **19**, 787 (1979).


## DISCUSSION

*M. R. Kamal:* Have you been able to invert the non-isothermal kinetic equation to give isothermal kinetics? Suppose that all I can obtain is non-isothermal kinetic results. Would I be able to determine the isothermal kinetics? Some people have claimed in the past that this can be done for the situation

that you have described using the Kamal-Sourour kinetic expression. Is it possible to calculate the rate constants and the kinetic exponents $m$ and $n$? I'll tell you the reason for my question. In my view, the most important industrial problems at the present time are those situations involving thermosets with very fast cure rates under processing conditions. In particular, our group is working with some of these systems. One is a phenolic and the other is an SMC compound. Both of these cure typically in a matter of a few seconds. It is very difficult to obtain DSC isothermal data on these systems. It is much easier to obtain scanning data and so it would be advantageous to start with the non-isothermal kinetic results and deduce the isothermal results. I'll add one more question. Can you recommend other techniques for studying these very fast curing systems? We haven't been able to find a reasonable technique to study systems that cure within a couple of seconds.

*M. E. Ryan:* Let me first try to answer the first couple of questions relating to the determination of the isothermal kinetic constants from a dynamic or scanning experiment. Although we have not actually done this, in principle I don't see any reason why this could not be done. All that would be required is to use the dynamic form of the rate equation that I have shown which has the isothermal kinetic constants and exponents embedded in it. By directly correlating the scanning data to the dynamic expression it should be possible to obtain the isothermal kinetic parameters. It would be of interest to see what sort of agreement could be obtained with actual isothermal measurements. With regard to your other question relating to the fast curing systems, there are a variety of techniques that may be used to characterize fast curing systems but in general they have not been directed toward obtaining the kind of parameters or information that I have been discussing in the context of calorimetric measurements. FTIR might be one possibility. I can perhaps provide you with some detailed references so that you can look into these techniques more completely.

*M. R. Kamal:* Also, from our experience with the DSC it is impossible to obtain a DSC trace that does not possess a maximum. You always start from the baseline, go up, and then come down. It is inherent in the nature of the measurement and we got stuck on that concept earlier on since it was a real effect that had to be dealt with. However, in some of these fast reactions we are finding that we must eliminate that portion of the curve which is strictly associated with the nature of the operation of the instrument. If we do this we find that these reactions may be characterized as first order or simple nth order reactions. Of course these are not excluded by the kinetic model that you have described. I think that one must be careful in thinking that all reactive systems must start at zero rate, go through a maximum, and then decrease. Would you agree with this statement?

*M. E. Ryan:* Yes, if you have a fast curing system such as you describe in the order of 1 or 2 seconds, the response time of the differential scanning calorimeter is on that time scale so that you will miss or not be able to properly interpret a significant portion of the data or DSC trace. In that sense I would definitely agree with the comments that you have made. The calorimeter possesses that inherent limitation, at least the Perkin-Elmer DSC instruments that we are talking about, in terms of the response time or time delay associated with the introduction of a sample into that type of instrument. For the fast curing systems the appearance of a maximum could be an instrument artifact and I would therefore agree with your statement.

*A. Kallos:* Along the same lines as Prof. Kamal's question, have you ever encountered a system in which the value of $k_2$ was essentially zero and in which case you would have a typical nth order reaction? What kind of DSC results would you get in this case?

*M. E. Ryan:* None of the systems that we have studied exhibited that particular type of behavior in which the value of $k_2$ was found to be zero. All of the systems that we have studied were chosen to some extent on the basis that they had been fairly widely understood and discussed in the literature. We chose similar systems for the experimental investigation of the effect of fillers on the reaction kinetics. These systems all exhibited a non-zero value for $k_2$. We have not encountered the type of situation or behavior that you describe but we were not actually looking for that kind of system. In fact we expressly wanted to avoid the very fast curing systems so that we could reliably measure the changes in reaction rate. Our motivation was somewhat different from the real problems that you are facing in having to work with a particular fast curing system.

*A. Kallos:* I would like to ask another unrelated question. How are the values of $k_1$, $k_2$, $m$, and $n$ actually determined?

*M. E. Ryan:* There is generally a preferred sequence or order by which the regression is done. The kinetic rate constant $k_1$ can usually be obtained directly from the DSC trace since it is equal to the initial rate at time zero. For the epoxy system the remaining kinetic parameters were obtained by fitting the experimental data with the kinetic expression using a non-linear least-squares estimation procedure. The rate constants were found to correlate with temperature according to an Arrhenius relation. Using the correlated values of $k_1$ and $k_2$ the exponents $m$ and $n$ were again determined. These exponents can generally be taken as constant or vary linearly with temperature. More explicit details can be found in my PhD. thesis.

*L. A. Utracki:* I would like to make a comment with regard to your introduction. According to the market review to the year 2000 the production or market share for thermosets is going to be reduced

by 50 percent. Thus it appears that it is not a highly developing technology.

*M. R. Kamal:* I would like to comment on that. I shouldn't show my age but 25 years ago I got involved in the plastics business and worked for a company whose business activity was entirely in the thermoset field and every year the projections for thermosets were to lose a share of the market. However, every year since then, except perhaps for a recession, this was not the case. The technology of processing thermosets and of operating with them in a fashion similar to thermoplastics has made them move ahead. Of course, SMC, RIM, and so on are new frontiers which represent major applications for thermosets which did not exist before. This is not to justify our involvements in this field but rather the real fact that this industry has been more dynamic than people give it credit for.

*L. A. Utracki:* However the market share doesn't increase.

*M. R. Kamal:* Yes, but bear in mind that thermoplastics have grown at a substantial rate.

*M. E. Ryan:* I didn't mean to suggest or imply some misleading market forecast for the consumption or use of thermosets. As I said, the variety of applications in which thermosets are used will broaden. How this will be reflected in terms of market share is another question and I agree that the commodity polymers will most probably continue to expand their share of the overall market.

# Numerical Simulation of Entry and Exit Flows in Slit Dies

E. MITSOULIS,* J. VLACHOPOULOS* *and* F. A. MIRZA**

* *Department of Chemical Engineering*
** *Department of Civil Engineering*
*McMaster University*
*Hamilton, Ontario, Canada L8S 4L7*

A general-purpose finite element program has been used to simulate the flow of Newtonian, power-law, and viscoelastic fluids in the entry and exit regions of a slit die. It was found that shear-thinning increases the entrance correction while it decreases the exit correction. Shear-thinning reduces the size of the small corner vortex that forms in the entry flow of a Newtonian fluid. The swelling ratio had a value of 1.196 for Newtonian fluids and decreased as the value of the power-law index decreased. Viscoelastic calculations were performed using the Criminale-Ericksen-Filbey (CEF) constitutive equation. Convergence of the iterative scheme was unattainable for Deborah numbers above 1.0. The results showed a decrease of the entrance correction and an increase of the exit correction with elasticity. Extrudate swell first decreased slightly and further increased with the Deborah number.

## INTRODUCTION

The numerical simulation of polymeric liquid flows has been the object of many investigations over the last ten years. Both finite difference and finite element methods have been used. The emphasis has been shifted progressively towards finite element methods, because of their ability to incorporate complicated geometrical boundaries. The major conclusions of these research efforts are summarized by Mitsoulis *et al.* (1), Crochet and Walters (2) and Crochet and Keunings (3). Most authors agree that there are no special problems associated with the application of the finite element method for Newtonian and shear-thinning fluids. However, considerable difficulties are encountered in the application of finite element (and finite difference) methods to viscoelastic fluid models. The main difficulty from the computational point of view is the lack of convergence of the iterative scheme required for the non-linear solutions at moderate to high elasticity levels.

The elasticity level is assessed in terms of one of the following dimensionless groups:

(a) Deborah number defined by

$$De = \lambda \dot{\gamma}_w \tag{1}$$

where $\lambda$ is a characteristic fluid time and $\dot{\gamma}_w$ a characteristic shear rate usually evaluated at the wall.

(b) Weissenberg number defined by

$$We = \lambda \frac{V}{H} \tag{2}$$

where $\lambda$ is a characteristic time, $V$ a characteristic velocity, and $H$ a characteristic length.

(c) Recoverable shear or stress ratio defined by

$$S_R = \frac{(N_1)_w}{2\tau_w} \tag{3}$$

where $(N_1)_w$ is the first normal stress difference and $\tau_w$ the shear stress both evaluated at the wall.

The above definitions are equivalent under certain conditions as discussed by Astarita and Marrucci (4). However, the definition of Deborah and Weissenberg numbers are often used interchangeably and there is often confusion when results from different research groups are compared.

In addition to the numerical difficulties associated with the viscoelastic fluid models there is always the question as to whether a given viscoelastic model describes reasonably well the behavior of a real polymer solution or melt. Many researchers devoted a large amount of effort for the convected Maxwell fluid, with a constant viscosity $\eta$ and a single relaxation time $\lambda$. It is easy to show that the Maxwell model gives an infinite elongational viscosity at a finite elongation rate. The finite element calculations predict an extrudate swell at the die exit first decreasing and then increasing with elasticity for Deborah numbers up to 1.25. The entrance pressure calculations in a sudden contraction are in disagreement with well-accepted experimental data (1). It is known that whenever a molten polymer enters from a reservoir into a die and then emerges from the die into the atmosphere, excess pressure drops are required over and above the fully developed losses. These pressure drops are usually referred to as entrance and exit pressure losses and the corresponding total correction to Poiseuille flow in the die is referred to as the end correction (also known as Couette correction for Newtonian fluids and Bagley correction for viscoelastic fluids). The origin and the significance of

end correction in dies has been examined by many investigators (5–12) and has been the object of controversy (13–16). Most publications have dealt with flow in axisymmetric (capillary) dies.

For slit dies we may write

$$\tau_w = \frac{P_{res}}{2\left(\frac{L}{2H} + n_B\right)} \tag{4}$$

where $\tau_w$ is the shear stress at the wall for fully developed flow in the die, $P_{res}$ is the gage pressure in the reservoir, $L$ the die length, $2H$ the die gap and $n_B$ the end correction. The end correction is due to excess pressure drops in the entry and exit. Thus, we have

$$n_B = n_{en} + n_{ex} \tag{5}$$

where

$$n_{en} = \frac{\Delta P_{en}}{2\tau_w} \tag{6}$$

$$n_{ex} = \frac{\Delta P_{ex}}{2\tau_w} \tag{7}$$

While experiments suggest that $n_{en}$ increases with $S_R$, the numerical calculations with Maxwell, second-order and Oldroyd-B models predict the opposite.

Recently, Keunings (17) presented a finite element solution for a Phan Thien-Tanner model (18, 19) that shows an increase of $n_{en}$ with $S_R$ for high elasticity levels.

In the present paper we present the results of finite element calculations for slit die entry and exit flows using purely viscous models (Newtonian, power-law) as well as a viscoelastic model known as the Criminale-Ericksen-Filbey (CEF) equation (1).

The calculations were performed using the MACVIP finite element program (20) developed at McMaster University for viscoelastic flows.

## CONSERVATION AND CONSTITUTIVE EQUATIONS

For two-dimensional incompressible flow, the continuity equation can be written as

$$\frac{\partial v_x}{\partial x} + \frac{\partial v_y}{\partial y} = 0 \tag{8}$$

The equation of conservation of momentum for creeping flow ($Re \ll 1$) simplifies to

$$0 = -\frac{\partial p}{\partial x} + \frac{\partial \tau_{xx}}{\partial x} + \frac{\partial \tau_{yx}}{\partial y} \tag{9}$$

$$0 = -\frac{\partial p}{\partial y} + \frac{\partial \tau_{xy}}{\partial x} + \frac{\partial \tau_{yy}}{\partial y} \tag{10}$$

and the equation of conservation of energy yields

$$\rho C_p \left(v_x \frac{\partial T}{\partial x} + v_y \frac{\partial T}{\partial y}\right) = k\left(\frac{\partial^2 T}{\partial x^2} + \frac{\partial^2 T}{\partial y^2}\right) + \tau_{xx}\frac{\partial v_x}{\partial x} + \tau_{xy}\frac{\partial v_x}{\partial y} + \tau_{yx}\frac{\partial v_y}{\partial x} + \tau_{yy}\frac{\partial v_y}{\partial y} \tag{11}$$

It should be noted that because of the symmetry of the stress tensor, $\tau_{xy} = \tau_{yx}$. Thus, only three stress components are needed for two-dimensional flow. This simplifies the finite element formulation by using a stress vector ($\tau_{xx}$, $\tau_{yy}$, $\tau_{xy}$) and a corresponding rate of strain vector ($\dot\gamma_{xx}$, $\dot\gamma_{yy}$, $\dot\gamma_{xy}$).

For two-dimensional flow, the Newtonian constitutive equation gives

$$\tau_{xx} = 2\eta \frac{\partial v_x}{\partial x} \tag{12}$$

$$\tau_{yy} = 2\eta \frac{\partial v_y}{\partial y} \tag{13}$$

$$\tau_{xy} = \eta\left(\frac{\partial v_y}{\partial x} + \frac{\partial v_x}{\partial y}\right) \tag{14}$$

For the power-law fluid model, we have

$$\eta(\dot\gamma) = m\left(\frac{1}{2} I_2\right)^{\frac{n-1}{2}} = m\left[\frac{1}{2}\left(\dot\gamma_{xx}^2 + \dot\gamma_{yy}^2 + 2\dot\gamma_{xy}^2\right)\right]^{\frac{n-1}{2}} \tag{15}$$

The CEF equation (1, 21) for steady two-dimensional flow gives

$$\tau_{xx} = 2\eta\frac{\partial v_x}{\partial x} + \left(\frac{1}{2}\Psi_1 + \Psi_2\right)\left(\dot\gamma_{xx}^2 + \dot\gamma_{xy}^2\right) - \frac{1}{2}\Psi_1\left[\left(v_x\frac{\partial \dot\gamma_{xx}}{\partial x} + v_y\frac{\partial \dot\gamma_{xx}}{\partial y}\right) - \dot\gamma_{xy}\left(\frac{\partial v_x}{\partial y} - \frac{\partial v_y}{\partial x}\right)\right] \tag{16}$$

$$\tau_{yy} = 2\eta\frac{\partial v_y}{\partial y} + \left(\frac{1}{2}\Psi_1 + \Psi_2\right)\left(\dot\gamma_{yy}^2 + \dot\gamma_{xy}^2\right) - \frac{1}{2}\Psi_1\left[\left(v_x\frac{\partial \dot\gamma_{yy}}{\partial x} + v_y\frac{\partial \dot\gamma_{yy}}{\partial y}\right) + \dot\gamma_{xy}\left(\frac{\partial v_x}{\partial y} - \frac{\partial v_y}{\partial x}\right)\right] \tag{17}$$

$$\tau_{xy} = \eta\left(\frac{\partial v_y}{\partial x} + \frac{\partial v_x}{\partial y}\right) + \left(\frac{1}{2}\Psi_1 + \Psi_2\right)\left[\dot\gamma_{xy}\left(\dot\gamma_{xx} + \dot\gamma_{yy}\right)\right] - \frac{1}{2}\Psi_1\left[\left(v_x\frac{\partial \dot\gamma_{xy}}{\partial x} + v_y\frac{\partial \dot\gamma_{xy}}{\partial y}\right) + \frac{1}{2}\left(\dot\gamma_{xx} - \dot\gamma_{yy}\right)\left(\frac{\partial v_x}{\partial y} - \frac{\partial v_y}{\partial x}\right)\right] \tag{18}$$

where

$$\dot\gamma_{xx} = 2\frac{\partial v_x}{\partial x}, \quad \dot\gamma_{yy} = 2\frac{\partial v_y}{\partial y} \quad \text{and} \quad \dot\gamma_{xy} = \frac{\partial v_y}{\partial x} + \frac{\partial v_x}{\partial y} \tag{19}$$

In the above expressions $\eta$, $\Psi_1$, $\Psi_2$ are the viscosity, the first and second normal stress coefficients, respectively. These are functions of the magnitude of the rate of strain tensor

$$|\dot{\gamma}| = \left[\frac{1}{2} I_2\right]^{1/2} = \left[\frac{1}{2} \{\dot{\gamma}:\dot{\gamma}\}\right]^{1/2} = \left[\sum_i \sum_j \dot{\gamma}_{ij}\dot{\gamma}_{ji}\right]^{1/2} \tag{20}$$

## THE FINITE ELEMENT METHOD

The finite element formulation was developed using the primitive variable approach (velocities $v_x$, $v_y$ and pressure $p$) and was based on the principle of virtual work (1, 22, 23).

The differential equation for conservation of momentum was written in an integral form as:

$$\int_\Omega \sigma_{ij}(\delta\dot{\gamma}_{ij})d\Omega - \int_\Omega b_i(\delta v_i)d\Omega - \int_{\Gamma_t} \bar{T}_i(\delta v_i)d\Gamma = 0 \tag{21}$$

where $\sigma_{ij}$ is the total stress tensor, $\sigma_{ij} = -p\delta_{ij} + \tau_{ij}$, $\delta_{ij}$ is the Kronecker delta and $\tau_{ij}$ is the extra stress tensor. $\dot{\gamma}_{ij}$ is the rate of strain tensor, $\delta\dot{\gamma}_{ij}$ is the virtual rate of strain tensor, $v_i$ is the velocity vector, $\delta v_i$ is the virtual velocity vector, $b_i$ are the body forces, $\Omega$ is the volume, and $\bar{T}_i$ are the surface tractions applied on part of the boundary $\Gamma_t$.

A second virtual work equation is required to incorporate incompressibility (continuity equation) and is of the following form:

$$\int_\Omega (\delta p)\frac{\partial v_i}{\partial x_i} d\Omega = 0 \tag{22}$$

where $\delta p$ is the virtual pressure.

Another virtual work equation was written for energy conservation (1). The flow domain was discretized into triangular elements with six nodes for the velocities and three nodes for pressure. Each velocity-pressure triangle was subdivided into four temperature triangles. Quadratic interpolation functions for velocity and linear interpolation functions for pressure and temperature were used. The resulting algebraic equations were solved by the Choleski decomposition method. The non-linear problems were solved by using successive iterations (Picard method).

Once the velocity field is known, the vorticity $\omega$ can be obtained from the definition

$$\omega = \frac{\partial v_y}{\partial x} - \frac{\partial v_x}{\partial y} \tag{23}$$

A finite element program is used to solve the Poisson equation for the streamlines $\Psi$

$$\nabla^2\Psi = -\omega \tag{24}$$

where each velocity-pressure triangle is subdivided into four streamline triangles.

## RESULTS AND DISCUSSION

### Die Entry Flow

The isothermal version of our MACVIP finite element program (20) was used for simulation of entry flow in slit dies at very low Reynolds numbers ($Re < 10^{-3}$). While several entry geometries have been examined, the results presented in this paper are for a 10 to 1 planar contraction. For such a contraction ratio the reservoir pressure drop is negligible. It can thus be assumed that such results are also reasonably good approximations for entry flow from an infinite reservoir. The die shape and dimensions are shown in *Fig. 1* (inset).

Most finite element investigations for entry flow have been carried out for a 4 to 1 axisymmetric contraction. It was found that the finite element mesh had some influence on convergence limits and on the accuracy of the results. An elaborate mesh developed by Caswell (24) is known to improve convergence. In the present investigation we used the finite element grid shown in *Fig. 1*. It consists of 200 elements, 459 nodes, and 881 degrees of freedom. The Newtonian problem requires 200 CPU seconds in McMaster's CDC 6400/CYBER 170. A mesh generation subroutine was developed in order to investigate other finite element layouts. The results presented here are virtually free from mesh influence. The 200 element grid shown in

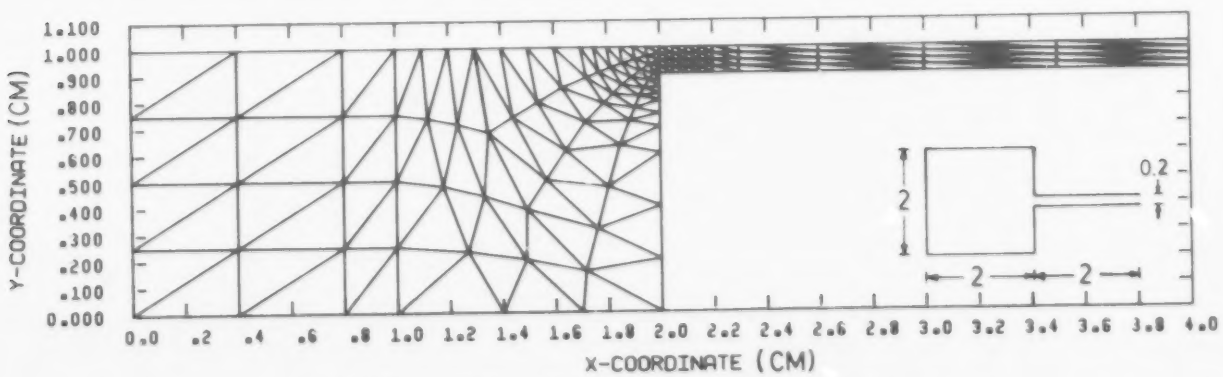


*Fig. 1. Finite element grid for die entry flow and die dimensions (inset).*

*Fig. 1* is our best compromise between accuracy and economy of calculation.

Calculations were performed for Newtonian and power-law fluids in order to examine the effect of the power-law index $n$ on the entrance correction $n_{en}$. *Figure 2* shows the flow field for a Newtonian fluid. A small and weak vortex appears in the reservoir corner in qualitative agreement with other numerical investigations (24, 25) for axisymmetric entry flow and careful experimental observations by Nguyen and Boger (26). The value of the ratio $X = L_v/2H_{res}$, where $L_v$ is the detachment length of the vortex and $2H_{res}$ the reservoir width, was found to be 0.15. Nguyen and Boger (26) found experimentally $X = 0.175$ for the axisymmetric case and quoted predicted values between 0.14 and 0.18. The flow field for a power-law fluid with $m = 9500$ Pa.s$^n$ and $n = 0.38$ are shown in *Fig. 3*. It can be seen that shear-thinning reduces the vortex size and intensity.

*Figure 4* shows the entrance correction $n_{en} = \Delta P_{en}/2\tau_w$ as a function of the power-law index $n$. The entrance correction increases as the power-law index decreases and it is always lower for slit dies than for capillary dies. For the Newtonian fluid we have $n_{en} = 0.407$, which is somewhat lower than the asymptotic value of 0.43 obtained by Adachi and Yoshioka (27) who used a variational method. The differences between the two methods are apparently due to the inadequate trial velocity field used in the variational method (7). These differences exhibit the same trends as in the comparison of the capillary entrance correction calculations of Duda and Vrentas (8) and Boger *et al.* (7).

Finite element calculations were also carried out for a CEF fluid with constant coefficients $\eta$, $\Psi_1$ and $\Psi_2$. In such a case the CEF constitutive equation reduces to that of a second-order fluid. The normal stress coefficients $\Psi_1$ and $\Psi_2$ for viscometric flows with a shear rate $\dot{\gamma}$ are related to the first and second normal stress differences by the expressions

$$\tau_{xx} - \tau_{yy} = \Psi_1 \dot{\gamma}^2 \tag{25}$$

$$\tau_{yy} - \tau_{zz} = \Psi_2 \dot{\gamma}^2 \tag{26}$$

There are no reliable correlations for the second normal stress difference. A reasonable approximation was taken to be

$$\Psi_2 = -0.15\Psi_1 \tag{27}$$

We were able to achieve monotonic convergence up to $De = 0.75$ and marginal convergence for $De = 1.0$. Here, the Deborah number was defined as

$$De = \frac{(\tau_{xx} - \tau_{yy})_w}{(2\tau_{xy})_w} = \frac{\Psi_1 \dot{\gamma}_w^2}{2\eta\dot{\gamma}_w} = \frac{\Psi_1}{2\eta}\dot{\gamma}_w = \lambda\dot{\gamma}_w \tag{28}$$

where $\dot{\gamma}_w$ is the shear rate at the wall.

The entrance correction for $De = 0.5$ was found to be $n_{en} = 0.369$ and for $De = 1.0$, $n_{en} = 0.290$. It can be seen that elasticity decreases the entrance correction (Newtonian $n_{en} = 0.407$). This result is in agreement with Black and Denn (28), Viriyayuthakorn and Caswell (24) and Crochet (29) for

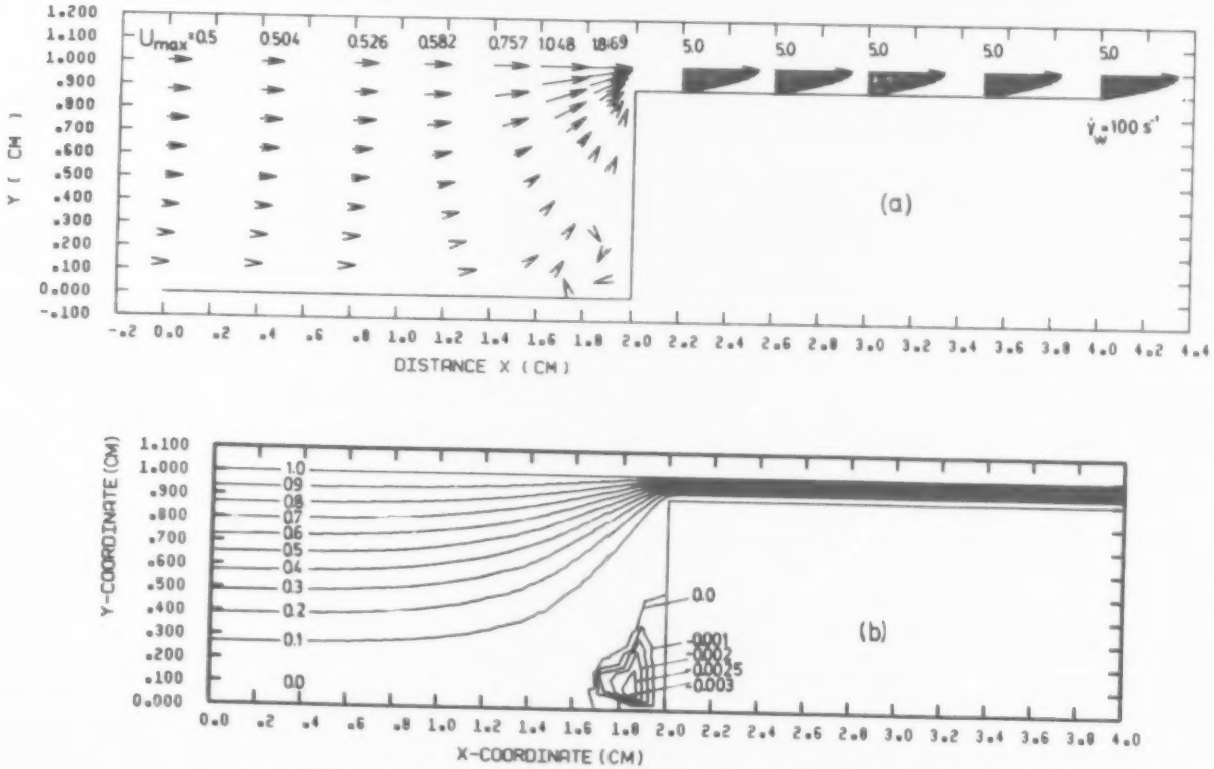


*Fig. 2. (a) Velocity field for a Newtonian fluid in a 10:1 planar contraction. (b) Streamlines.*

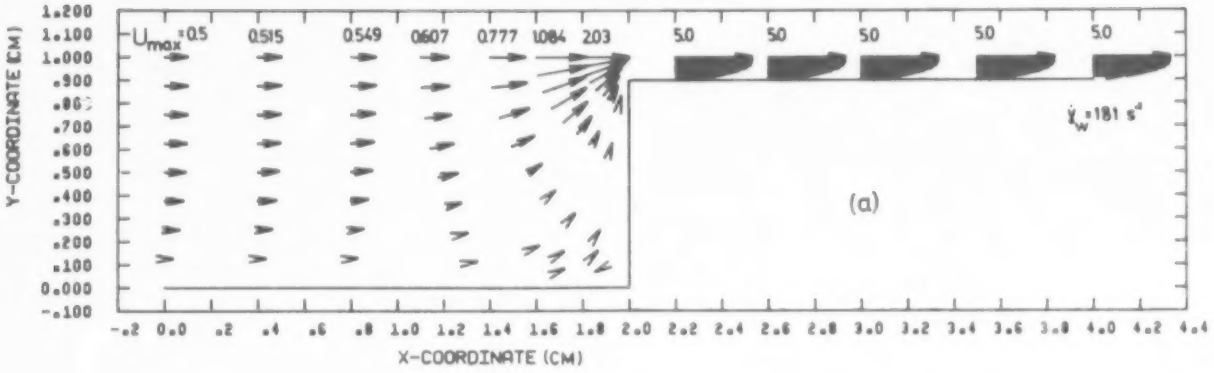


*Fig. 3. (a) Velocity field for a power-law fluid in a 10:1 planar contraction ($m$ = 9500 Pa $s^n$, $n$ = 0.38). (b) Streamlines.*

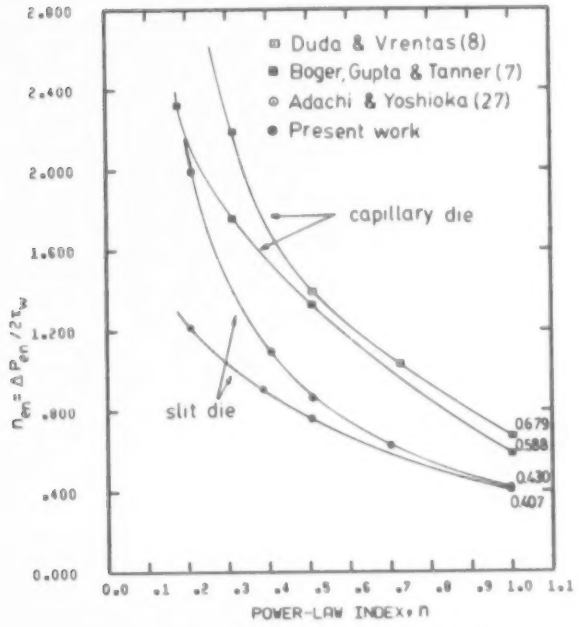


*Fig. 4. Entrance correction for power-law fluids.*

axisymmetric flow, as well as our earlier calculations for a tapered die entry (1). Nevertheless, it is contrary to the well-accepted interpretation of entry pressure drops that was proposed by Bagley (5, 12). The present calculations did not show any enlargement of the weak corner vortex as has been observed experimentally (26, 30).

Some calculations were carried out for $\eta$, $\Psi_1$, and $\Psi_2$ dependent on $\dot{\gamma}$. While the computational procedure became more complicated the results were qualitatively the same as those for $\eta$, $\Psi_1$ and $\Psi_2$ constant.

## Die Exit Flow

It is well known that die exit flow of polymeric liquids is accompanied by considerable swelling of the emerging jet. Consequently, the finite element mesh must be allowed to take the shape of the extrudate. Crochet and Keunings (31, 32) have examined the influence of finite element method, grid layout, and die and extrudate lengths on swelling ratio determination. Taking into account these studies we developed a mesh consisting of 184 triangular elements with 423 nodes and 859 degrees of freedom as shown in *Fig. 5(a)*. The die and extrudate lengths were equal to eight times the die gap width. The free surface is determined iteratively by constructing a streamline using the most recently computed velocity field as proposed by Nickell, Tanner and Caswell (33). Usually 4 to 5 iterations on the free surface were sufficient for inelastic fluids.

For a Newtonian fluid the swelling ratio was found to be 19.6 percent. The deformed mesh and the velocity field are shown in *Fig. 5*. The exact shape of the surface is plotted in *Fig. 6* ($n$ = 1). It

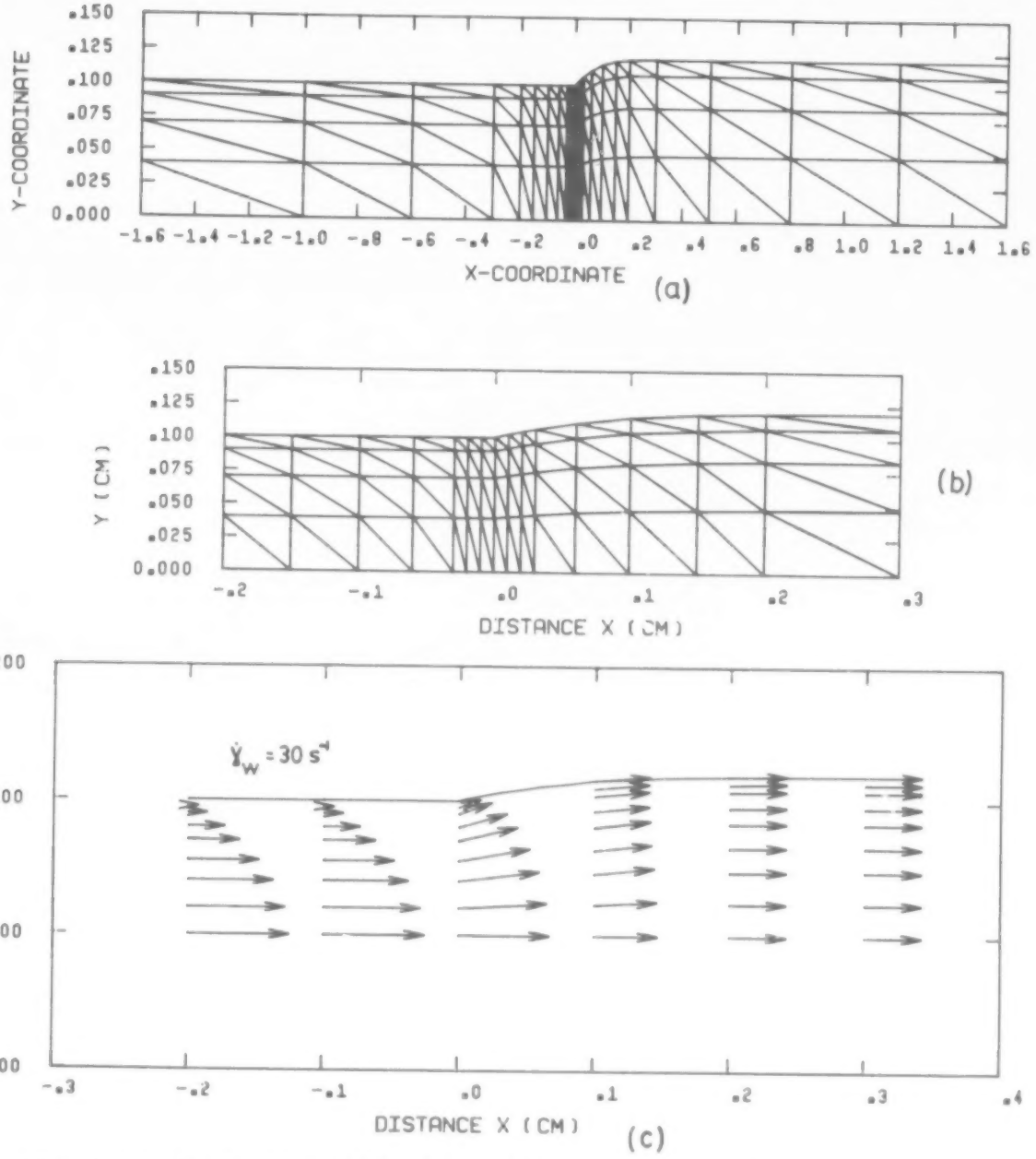


*Fig. 5. (a) Finite element grid for die exit flow. (b) Enlarged section of the grid near the exit. (c) Velocity field for a Newtonian fluid*

can be seen that our estimate is somewhat higher than that of Crochet and Keunings (34). However, in a more recent publication (31) these authors give asymptotic swelling ratios of 20.0 percent and 19.6 percent with two refined meshes. These results are fully in agreement with Coleman (35, 36) and Reddy and Tanner (37).

Shear-thinning was found to reduce the degree of swelling in agreement with the calculations of Boger *et al.* (7), for round extrudates and those of Coleman (35) for plane extruded sheets. *Figure 6* also shows the extrudate shape for a power-law fluid with $n = 0.5$ and $n = 0.38$. A small contraction appears immediately after the exit for these values of $n$. It is not clear whether this contraction represents the real behavior of highly shear-thinning fluids or merely a numerical artifact.

The pressure distribution along the centerline and along the die wall is shown in *Fig. 7*. In the vicinity of the die exit the wall pressure exhibits a disturbance due to the singularity at the exit corner, while the centerline pressure drops smoothly. The exit pressure correction is defined as

$$n_{ex} = \frac{P_o - \Delta P_s}{2\tau_w} \tag{29}$$

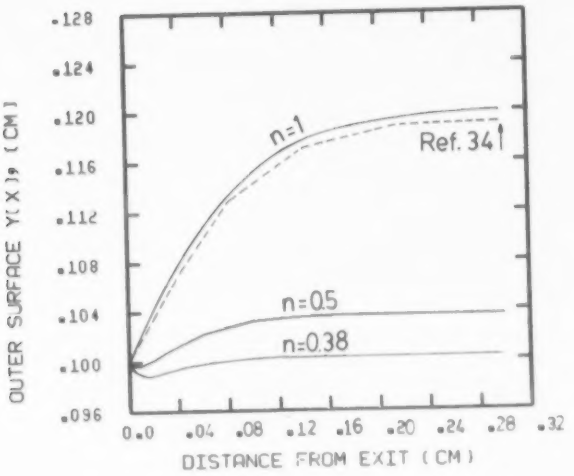


*Fig. 6. Shape of free surface for power-law fluids*

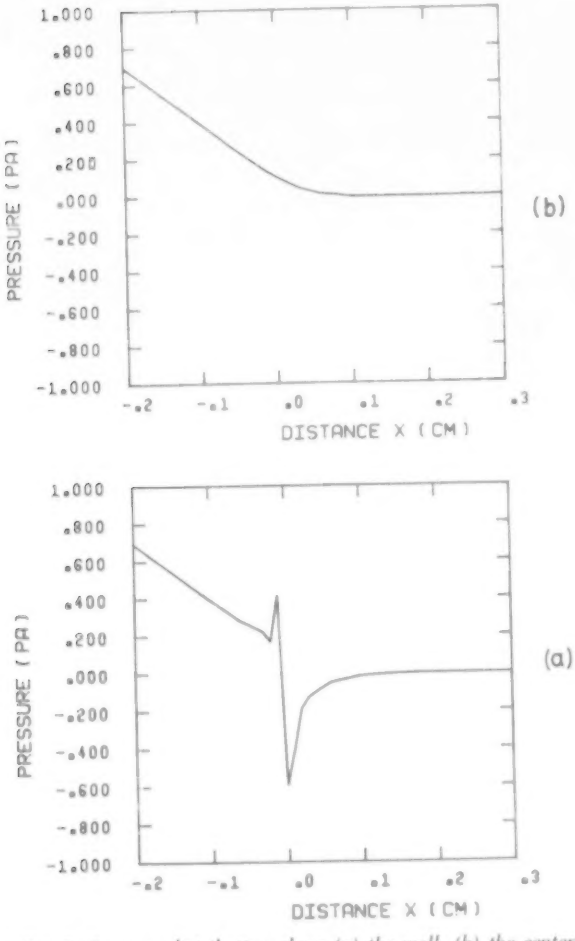


*Fig. 7. Pressure distribution along (a) the wall, (b) the centerline for a Newtonian fluid ($\eta$ = 1 Pa·s).*

where $P_o$ is equal to $(p - \tau_{yy})$ at the inlet wall, $\Delta P_s$ the pressure drop for fully developed flow in the slit and $\tau_w$ the shear stress at the wall. For Newtonian flow we found $n_{ex} = 0.153$, fully in agreement with Crochet and Keunings (31) and Reddy and Tanner (37). Shear-thinning reduces the value of exit pressure correction as shown in *Table 1*. This result is in disagreement with the calculations of Boger *et al.* (7) for axisymmetric flow. It should be noted, however, that the above authors reported deviations as large as 4.2 percent between wall and centerline pressures for fully developed flow while in the present calculations the largest deviation was less than 0.1 percent. At $n = 0$ we expect the exit correction to be zero while the entrance correction would become infinite.

Calculations were also performed for a second-order fluid, i.e. the CEF model with $\eta$, $\Psi_1$, and $\Psi_2$ constant. Convergence of the iterative scheme was obtained for Deborah numbers up to about 0.75. The results are shown in *Table 2*. Swelling first decreases slightly with elasticity and then it increases for *De* higher than 0.5, fully in agreement with other numerical and theoretical predictions (31, 36, 37, 38). The exit correction increases with elasticity and is in reasonable agreement with Reddy and Tanner's (37) equation

$$n_{ex} = 0.26\ De + 0.155 \qquad (30)$$

*Figure 8* shows the entrance, exit, and end or Bagley correction as a function of Deborah number. For this range of elasticity levels the end correction increases slightly [see also (39) for axisymmetric flows] but not as much as expected from experimental observations. It is possible that the dramatic increase of end correction occurs at much higher elasticity levels. However, numerical calculations with Maxwell and Oldroyd-B fluids (24, 29) that converged for high Deborah numbers (up to *De* = 4), showed a decrease of the end correction with elasticity. This was due to the fact that the entrance correction decreases much more rapidly with elasticity than the exit correction increases. These results suggest that the above simple constitutive models (second-order, Maxwell, Oldroyd-B) give

**Table 1. Entrance, exit correction and extrudate swell for power-law fluids in slit dies.**

| Power-law Index $n$ | Entrance Correction $n_{en}$ | Exit Correction $n_{ex}$ | End Correction $n_B$ | Extrudate Swell $h/H$ |
|---|---|---|---|---|
| 1.00 | 0.407 | 0.153 | 0.560 | 1.196 |
| 0.50 | 0.764 | 0.135 | 0.899 | 1.036 |
| 0.38 | 0.931 | 0.113 | 1.044 | 1.003 |
| 0.20 | 1.22 | — | — | — |

**Table 2. Entrance, exit correction and extrudate swell for second-order fluids in slit dies.**

| Deborah Number $De$ | Entrance Correction $n_{en}$ | Exit Correction $n_{ex}$ | End Correction $n_B$ | Extrudate Swell $h/H$ |
|---|---|---|---|---|
| 0.00 | 0.407 | 0.153 | 0.560 | 1.196 |
| 0.25 | 0.396 | 0.207 | 0.603 | 1.184 |
| 0.50 | 0.369 | 0.258 | 0.627 | 1.172 |
| 0.75 | 0.333 | 0.306 | 0.639 | (1.23) |
| 1.00 | [illegible]30 | (0.360) | (0.650) | — |